Climate Change and Copepod Size Distribution: Comparison of Two Coastal Long-Term Series in the Western Mediterranean Sea

Thesis

UNRESTRICTED

ARC: **Stazione Zoologica Anton Dohrn**

Collab. Estab.: **Laboratoire d'Océanographie de Villefranche sur Mer**

The Open University of London

Climate change and copepod size distribution:

Comparison of two coastal long-term series in the Western Mediterranean Sea

Carmen Garcia-Comas Rubio

Licenciada en Biología por la Universidad de Oviedo
Rama Ambiental

Date of Submission: 16 October 2009
Date of Award: 1 July 2010

Thesis for the degree of Doctor of Philosophy

October 2009

ProQuest LLC.
789 East Eisenhower Parkway
P.O. Box 1346
Ann Arbor, MI 48106 – 1346

Director of studies:

Dr. Maria Grazia Mazzocchi

Supervisors:

Dr. Maurizio Ribera d'Alcalá

Dr. Euan Brown

Stazione Zoologica Anton Dohrn
Villa Comunale
80121 Napoli, Italy

¡El que la sigue la consigue!

Spanish saying: 'He who follows it attains it'

(If at first you don't succeed, try, try again!)

Acknowledgements

I would like to express my thanks to the people who made possible this thesis:

First of all, I am very grateful to *Grazia Mazzocchi* and *Lars Stemmann* for supporting and teaching me during these years. Thank you for your patience, your time and your good advices. I have learnt a lot from you.

To *Maurizio Ribera d'Alcalá* and *Gabriel Gorsky* for hosting me in their very dynamic teams. Their enthusiasm and great knowledge of pelagic systems has been very inspiring to me.

I would also like to thank *Gregory Beaugrand* for his enthusiasm at the beginning of this project, and for his spatial PCA on SST of the western Mediterranean. To *Euan Brown* for his helpful comments while I was writing this thesis.

To all the colleagues that helped me with the analyses, or provided me with additional data. To the crews of the vessels involved in sampling at both stations, and to the people involved in sample treatment. To Somlit. Thank you, *Federico Corato* and *Ornella Passafuime* for your availability while validating the hydrological datasets from both stations. To *Diana Sarno* and *Adriana Zingone* for providing their phytoplankton taxonomic counts and cell size of the MC time series. To Grazia Mazzocchi and *Iole Di Capua* for their copepod taxonomic counts of the MC time series. To Iole Di Capua, *Frank Predjer* and *Elvire Antajan* for checking the manual identification. Elvire Antajan introduced me in supervised-learning methodology, thank you very much for your time and patience. Thanks to *Stéphane Gasparini* for developing Plankton Identifier and for his advices. To *Paul Nival* and *Louis Legendre* for their availability and interest on the students' research. I am very grateful to the undergraduate students, *Oceane Dahan*, *Fanny Chenillat* and *Marine Gouzeo* and to *Corinne Desnos* who processed part of the samples with the ZooScan. With Oceane I shared the beginning of the analyses of the Point B time series; thanks for your commitment and accuracy. Very special thanks to *Marc Picheral* for his continuous assistance with the ZooScan, for suffering my impatience and for his friendship and great dinners!

To *Philip Reid* and *Adrianna Ianora* for accepting examining me. Thanks for your insightful suggestions and corrections which really improved this manuscript.

To *Laurent Dubroca*, *Lionel Guidi* and Lars Stemmann for introducing me to programming, and for their advices on statistical analyses; I have learnt a lot from you! Thanks also to *Léo Berline* and *Anne Goarant*, who arrived latter but who were always

available to discuss about statistics. But most important, thanks for your friendship and support, guys! Thank you, *Frederic Ibañez*, for being always available for me and the rest of students, for your matlab programs of PCA, Escoufier and EWMA, and for your humour and enthusiasm. Thank you also to *Giuseppe Bianco* for our continuous exchange of knowledge on programming, statistics, ecology and many other topics. Thanks for the wonderful 'caffè' that kept me awake! Thanks also to *Pieter Vandromme* and *Baptiste Romagnan* for making a 'ZooScan team' to help ourselves out when needed. To the *secretaries* and to the *staff of the canteen* for their logistics support.

To the *many good friends* of the lab for sharing our joys and defeats. First of all, thanks to the 'Wagram' and 'Belle Donne' for sheltering us in our moments of euphoria or desperation! Thanks to Gueorgui, Margaux, Agostina, Fanny, Thomas, Enzo, Luisa, Alina & Yoann, Pierre, Anne, Amelie & Charles, Ceci, Andrea, Laurent, François, Baptiste, Francis, Giuseppe, Benedetto, Lio, Alex & Amandine, Iole, Anita, Fanny T. & Jerem, Dorris, Lauriane, Raffaele, Tristan & Elise, Simona, Aldine, Laurent G., Yannick, Julia, Mathilde, Atsushi, Marie, Raffaela, Isabella. I will really miss you all, and wish you the best for the future! Thanks to Francis, for his open-mind, his stories, jokes, availability to fix things and for letting me seeing the mountains from above the clouds! To Charles for showing me the sea from below! To Enzo and Pierre & Marianne for their gastronomic hospitality! Special thanks go also to the ones that sheltered me anytime I needed during these years, the primary 'coloc': Gueorgui, Pierre, Thomas and Atsushi; and Ceci, Agos, Luisa, Evoula and BB. The most stressful moments were shared with Margo 'McGyver', George 'my fake brother', Fannita 'down with procrastination!', Tomasiño 'the train traveller', Agos 'la rossa', Dorris and Ceci. Thanks for supporting and suffering me! I am also very grateful to Marco, who endured most part of my moments of frustration, and who was always optimistic and showed me the fun of learning every day, and the greatness of always trying to do better. I also want to thank the friends that stayed behind during these years, for their patience and encouragement. Thanks Rebe, Marta, Covi, Bibi and Carmen among many others.

Finally, last but by no means least, to my family for their enthusiasm and optimism. To Alfredo, for his advices and for his quick answers on my request of papers! Very special thanks to my parents for giving me education, for their unconditional encouragement and for suffering me! Thanks to Isa and Fer, my siblings, for their company and support. To Gon, my godson, that was born with this thesis.

This project was supported by the European FP6 SESAME integrated project under contract no. GOCE-036949 and the EU NoE EUROCEANS data rescue program.

Exchanges between researchers from the SZN and LOV were partly funded by a CNR/CNRS collaboration program.

Carmen García-Comas Rubio was financially supported by a P.h.D. fellowship from *Eur-Oceans* network of excellence under contract no. WP4-SYSMS-1070.

Abstract

This thesis was aimed at investigating long-term dynamics of zooplankton communities in relation to climate change. It represents a pioneer study in comparing Mediterranean time series with a standardised methodology, i.e., the ZooScan, a digital imaging system for counting and sizing mesozooplankton from preserved samples. This study has proven that copepod size spectra (i.e., histogram of organisms arranged by size classes) obtained with the ZooScan is a powerful synthetic index to monitor changes in the pelagic system.

Copepod abundance and size spectra were analyzed in the zooplankton time series conducted at stn MC (Gulf of Naples, Tyrrhenian Sea) and Point B (Villefranche Bay, Ligurian Sea) for the years 1986-2005 and 1974-2003, respectively. In both time series, the proportion of large individuals in the copepod community increased over the years, with a shift in the early 1990s at stn MC and in 1987 at Point B. In both cases, the 1990s copepod reproduction might have decreased due to earlier and stronger stratification driven by rising temperature. At stn MC, the shift to dominance of small phytoplankton cells in the 1990s seemed to be the direct cause. At Point B, in addition to the detrimental effect of earlier stratification in the 1990s, the 1980s seemed to be very productive due to strong winter convection driven by cool salty winters. High salinity was related to low winter atmospheric pressure linked to the North Atlantic Oscillation (+ winter NAO). In both locations, the frequency of occurrence of typical offshore species increased over the years, suggesting changes in coastal-offshore interactions.

Mechanisms controlling the copepod communities in both sites seem to be different. Stn MC has a more coastal character than Point B and thus the former is more affected by local conditions as terrestrial nutrient inputs. At Point B, stratification-destratification dynamics seem to control production.

Contents

List of tables

List of figures

Chapter 1. Introduction

Climate change is altering marine ecosystems, and therefore the current scientific community is focused on identifying the mechanisms involved to try to predict and mitigate future changes (e.g., Drinkwater et al. 2010; Ottersen et al. 2010). Plankton have been appointed as suitable indicators of climate change for their rapid population dynamics, their non-economical exploitation and for amplification of subtle changes by non-linear responses (Taylor et al. 2002; Hays et al. 2005). Plankton long time series are a key tool to detect changes related to climate, and to try to elucidate the mechanisms linking both (Perry et al. 2004). To better understand the processes linking climate variability with plankton ecosystems and thus to be able to predict future changes, Mackas and Beaugrand (2010) have recently proposed parallel time series analyses, as the comparative method is the available alternative to experimental studies (Alheit and Bakun 2010). A key issue in the comparison of time series is the standardisation and intercalibration of their methods (Perry et al. 2004).

In the Mediterranean Sea, in contrast with the Atlantic and Pacific oceans, there are very few long-term studies on zooplankton. In this thesis, the two longest zooplankton time-series in the western Mediterranean Sea: (1) Station (stn) MC in the Gulf of Naples (Tyrrhenian Sea) (sampled from 1984), and (2) Point B in the Bay of Villefranche (Ligurian Sea) (sampled from 1966) are analysed. A comparative study is carried out between these two time series after parallel analyses of the MC time series from 1986 to 2005, and the Point B time series from 1974 to 2003. The comparison is possible due to harmonization of the two time series with the ZooScan digital imaging system (Grosjean et al. 2004; Gorsky et al. 2010). The ZooScan enables one to rapidly count and size mesoplankton. Analyses focus on the abundance and size distribution of copepod assemblages, which constitute the bulk of zooplankton biomass in the oceans

(Verity and Smetacek 1996). Size is considered in theoretical ecology as an intrinsic characteristic that links through metabolism an individual organism to population, community and ecosystem functionality by prey-predator interactions and trophic-web organisation (Rodriguez 1994). The copepod-community size structure is used in this thesis as a synthetic index for detecting pelagic-ecosystem changes related to climate change.

Main goals of this thesis

The ultimate goal of the present thesis is to detect long term changes and to propose mechanisms liking climate change and plankton, in the two western Mediterranean coastal sites, by analysing copepod size spectra. We test the utility of using size as a fast and sensitive indicator of changes in community structure. This study is also intended to broaden knowledge of size distribution in coastal zooplankton communities, which thrive in complex environments that are far from the steady-state conditions many mathematical models assume. The study is applied to the comparison of the standardized zooplankton time series at stn MC and Point B because they represent typical Mediterranean coastal communities and because they provide large and consistent datasets encompassing decadal time scales.

The manuscript is organised in chapters to tackle the main goals of this thesis, presented here as four questions to be answered:

1 – *Can copepod total abundance and size distribution be automatically estimated with the ZooScan imaging system?*

In this thesis, samples are analysed with the ZooScan prototype. Automatic recognition based on supervised-learning analysis is set up to obtain copepod total

abundance and body size. Section 3.4, and chapter 4 deal with methodological aspects of the automatic and semi-automatic construction and validation of copepod datasets.

2 - *Can plankton communities be monitored by indicators based on size spectrum?*

From the data provided by the ZooScan, monthly copepod total abundance and size distribution are analysed from MC time series, for the period 1986-2005 (Chapter 5), and from Point B time series, from 1974 to 2003 (Chapter 6). Size is expected to indicate complementary information to taxonomic composition in order to detect changes in copepod variability in both time series. Size distribution varies as a response to changes in species composition, population dynamics and prey-predator interactions.

3 - *Has climate change affected copepod communities in both studied sites?*

Previous published results of long-time series analyses from Point B (Molinero et al. 2005a; Molinero et al. 2008b) and stn MC (Mazzocchi and Ribera d'Alcalà 1995; Ribera d'Alcalà et al. 2004; Mazzocchi et al. 2010) reported substantial changes in the abundance of a few copepod species. In the case of Point B, changes were related to local environmental conditions that were linked to large-scale atmospheric changes in the North Atlantic. In the case of stn MC, changes were less marked at the species level. Nevertheless, phytoplankton was reported to have undergone pronounced changes between the 1980s and the 1990s (Ribera d'Alcalà et al. 2004; Zingone et al. 2009). In this thesis (Chapters 5 and 6), we seek to verify the reported changes obtained with different approaches, and to investigate other aspects of the variability in the structure of the copepod communities. Copepod size distribution and local environmental conditions are analysed in order to detect changes and any synchronies among them. The results obtained from those analyses are interpreted to formulate possible scenarios of change.

4 - *Are the mechanisms linking climate and the copepod communities similar in both studied sites, and do local changes reflect changes at a larger scale?*

In chapter 7 a combination of the results obtained from the parallel analyses of the copepod community at stn MC and at Point B is attempted, to have an overall view of the changes and mechanisms involved. Overlapping periods are compared, and similarities and differences discussed to have a wider vision of the effect of climate change on Mediterranean coastal ecosystems. This study was motivated by previous studies showing synchronies in zooplankton community changes from different regions, related to global warming (reviewed in Richardson 2008; Alheit and Bakun 2010).

Chapter 2. Background

2.1 Marine ecosystems and climate change

Global ocean temperature rose 0.31 °C between the 1950s and 1990s in the top 300 m, and the increase has been steeper since the early 1980s (Levitus et al. 2000). In the last decade, the scientific community has focused on the amplitude of global climate change, as well as on the identification of factors and mechanisms involved (IPCC 2007). Progress has been achieved in understanding the consequences of climate forcing on the biosphere, such as ecosystem health, and water and food availability. One of the major challenges is to be able to propose scenarios of changes and to foresee the variations that ecosystems will experience in the future (Stenseth et al. 2002; Durant et al. 2005; Walther et al. 2005). Climate can affect marine ecosystems at a variety of temporal and spatial scales, its effect on a population or a community may be direct or indirect, and the consequent response may be linear or non-linear (Ottersen et al. 2010). Understanding the effect of climate changes on Mediterranean mesozooplanktonic systems (biodiversity and size structure) is at the core of the present work. Mesozooplankton are a key component of the trophodynamics of pelagic ecosystems. They represent a central link in the transfer of matter and energy from phytoplankton to fish, and also play a substantial role in biogeochemical cycles (Reynolds 2001; Buitenhuis et al. 2006). Fish yields have been affected by direct effect of climate on physiology and by indirect effect on their prey (i.e., mesozooplankton) and hydrology (Perry et al. 2005).

Plankton are good indicators of climate change for several reasons. Most species are not being commercially exploited, and the long-term changes observed in their stocks can therefore be attributed to changes in environmental conditions (Hays et al. 2005). As passive drifting organisms, they are good indicators of features and dynamics

of water masses. In addition, they have a short life span that helps to relate population size to environmental conditions. Finally, plankton, with their non-linear responses to environmental changes, can amplify subtle environmental perturbations that otherwise would not be perceived (Taylor et al. 2002).

The level of response to environmental changes differs throughout the species composing a plankton community, and can lead to a mismatch among trophic levels and functional groups (Edwards and Richardson 2004). Species phenology (i.e., timing of the seasonal cycle) can vary due to temperature changes resulting in a disruption of prey-predator seasonal succession (Costello et al. 2006; Mackas et al. 1998; Parmesan and Yohe 2003; Richardson and Schoeman 2004; Sydeman and Bograd 2009). Also, latitudinal shifts of species distribution have been reported due to changes in water temperature and hydrology, and those shifts affect trophic interactions (Beaugrand and Ibanez 2004; Beaugrand et al. 2002a; Beaugrand et al. 2009; Crame 1993; Johns et al. 2001; Lindley and Daykin 2005; Perry et al. 2005; Southward et al. 1995).

Because species differ in their response to hydro-climatic changes, the structure and composition of plankton communities has been altered (reviewed in Bertram et al. 2001; Perry et al. 2004; Hays et al. 2005; Richardson 2008). Changes in the plankton community resulting from climate forcing are difficult to forecast due to the complex trophic webs that they form. Non-linear relationships, synergies and feedbacks complicate defining the mechanisms linking climate change and plankton. For example, Kirby and Beaugrand (2009) showed by causal statistical modelling how temperature had directly and indirectly affected several compartments of the pelagic system, from phytoplankton to fish, in the North Sea. Direct effect of temperature might be due to physiological constraints at species level, whereas indirect effects are related to changes in the trophic dynamics such as prey-predator and competitor interactions. In addition, a

reverse in the sign of correlations between pairs of pelagic compartments occurred at the beginning of the 1980s. The reverse was synchronous with an increase of the water-column temperature. These results reflect the trophic amplification of a climate signal (i.e., warming) and the sudden reorganization of a pelagic system due to overcoming of an ecological threshold (i.e., regime shift), which may be difficult to predict.

2.1.1 Bottom-up control, top-down control, trophic cascades and wasp-waist control in marine ecosystems

Subtle hydro-climate variations can be amplified by their effects on the trophic relationships of a community. The structure of marine ecosystems may be affected by climate by two main mechanisms of trophic control, the bottom-up control (resource-limited) (Fig.2.1A) and the top-down control (predation-driven) (Fig.2.1B). Trophic cascades can take place when top-predators in a food web decrease the abundance of their prey, releasing the lower trophic level from predation, and so forth across the following trophic levels. A third, less reported, mechanism is the wasp-waist control (Fig.2.1C), which occurs when in a trophic web an intermediate trophic level is represented by a single species. Climate change effect on that single species may alter the whole trophic web by predator-prey interactions. Wasp-waist control has been described in up-welling ecosystems, where a few species can sequester most of the energy flux between plankton and top-predators (Bakun 2006; Cury et al. 2000).

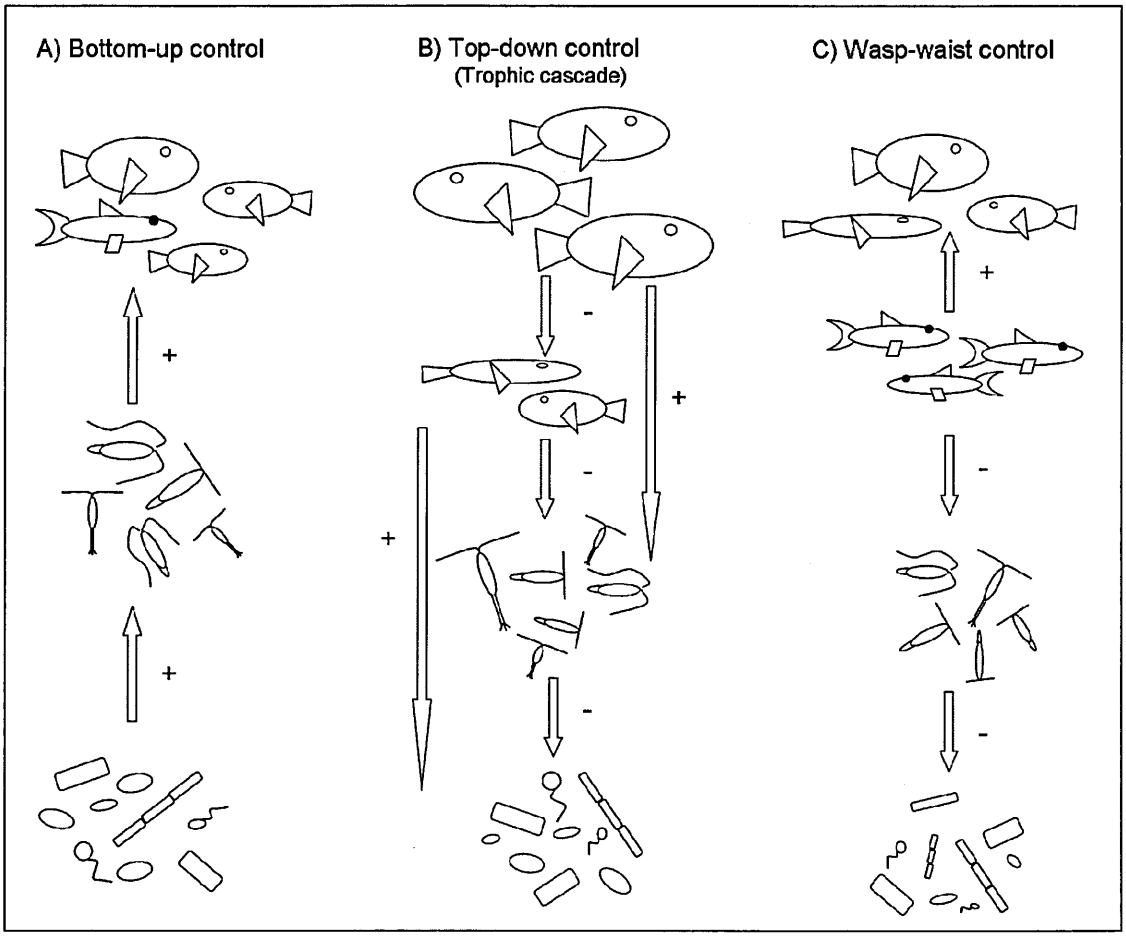

Figure 2.1 - Main trophic controls found in marine ecosystems. Signs indicate the sign of correlation between two trophic levels.

Bottom-up control is the classical pathway by which a trophic web is altered due to changes in prey availability, limited by the nutrients in an ecosystem. Thus, phytoplankton biomass would be regulated by nutrients, zooplankton would be regulated by phytoplankton, and fish by zooplankton biomass. Several bottom-up control effects, triggered by climate change, have been reported in pelagic ecosystems (e.g., Aebischer et al. 1990; Alheit et al. 2005; Frederiksen et al. 2006; Richardson and Schoeman 2004). Global warming is predicted to increase the strength and duration of seasonal stratification enhancing nutrient depletion in the photic zone (Sarmiento et al. 2004a; Sarmiento et al. 2004b). Ocean net phytoplankton primary productivity (NPP) has been reported to decrease since the late 1990s due to stronger stratification; both NPP and stratification were shown to be well correlated (r^2~0.7) (Behrenfeld et al.

2006). It has been predicted that, due to nutrient depletion, global warming might cause a shift to dominance of prokaryotes in the phytoplankton community (Karl et al., 2001). Furthermore, zooplankton abundance has been found to decrease in relation to stronger stratification (Roemmich and Mcgowan 1995). Richardson and Schoeman (2004), by performing a meta-analysis on plankton samples covering the Northeast Atlantic for the period from 1953 to 2002, found that bottom-up control regulated by temperature was the mechanism controlling standing stocks from phytoplankton to carnivorous zooplankton. The study showed that while in the cooler regions sea surface warming was accompanied by increasing phytoplankton abundance, in the warmer regions it was accompanied by decreasing phytoplankton abundance. Cod recruitment has been reported to increase with warming in the northern region of the Northeast Atlantic, while in the southern region warmer temperatures are detrimental for cod recruitment (O'brien et al. 2000). These results suggest that whereas in mid-latitude ecosystems warming entails increasing strength and duration of stratification and thus less productivity, in high latitudes warming benefits productivity maybe by means of metabolic enhancement. Mesozooplankton biomass, dominated by copepods, is the nutritional basis for many fish larvae. Beaugrand et al. (2003) showed how a trend of rising temperature modified the mesozooplankton community structure, and how this modification affected cod recruitment in the North Sea.

Top-down control has been traditionally related to fisheries removal of a top-predator species or a whole functional group in the case of non-selective fishing (Baum and Worm 2009). Top-down effects of climate change are related to changes in hydrology, water temperature and variability of temperature tolerance and preference by predators and prey. For example, in the California Current System, hake distribution changed due to water temperature changes and this had an impact on populations of fish

and shrimps due to predation relaxation (Field et al. 2006). A special case of top-down control is the predator to prey loop (Bakun and Weeks 2006), in which adults of a species control predators of their juveniles by feeding on them. For example, Atlantic cod populations are recovering very slowly from their fisheries collapse in the early 1990s due to low recruitment related to intense egg predation. The main predators of cod eggs, as herring and mackerel, are abundant due to predation relaxation from cod caused by fisheries (Swain and Sinclair 2000). Climate change, by rising water temperature, has been predicted to favour population outbreaks of gelatinous zooplankton due to related stronger and/or longer stratification, due to related metabolic enhancement, and to their asexual reproduction (Richardson 2008), although a global coherent pattern of jellyfish response to rising temperature has not been found (Purcell et al. 2007). In the Bering Sea, jellyfish abundance has increased since the early 1990s while Pollock abundance has decreased (Brodeur et al. 2002). It seems that jellyfish populations were favoured by a climate shift entailing warming, more stable water column and more primary production. Pollock populations may have decreased due to enhanced competition with jellyfish for zooplankton, related to the higher reproduction rates of jellyfish in those beneficial conditions.

A big controversy has been generated between the bottom-up control and top-down control supporters. The predominant view is that marine ecosystems are naturally structured from the bottom-up, and that top-down control may be dampened due to the prevalence of omnivory, ontogenetic diet shifts, high connectance among species and functional redundancy (Link 2002; Persson 1999; Strong 1992). Nevertheless, some studies highlight the strong selection that predation exerts to shape morphological and behavioural characteristics of plankton populations (Kiørboe 1998; Ohman 1988; Verity and Smetacek 1996). Recently, it has been suggested to study ecosystem changes as the

product of the interplay between bottom-up and top-down controls due to two main sources of perturbation, climate variability and fisheries removals (Frank et al. 2007; Hunt and Mckinnell 2006; Scheffer et al. 2005; Worm et al. 2002). Hunt and McKinnell (2006) propose to seek evidence for where each mechanism is likely to dominate rather than to demonstrate that one or the other control is the main mechanism occurring in overly confounded ecosystems.

The openness of the studied system could play a role on the dominance of top-down control over bottom-up control. In lakes, top-down control is found more often than in oceanic ecosystems. Ohman (1988) proposed hydrological complexity as the main factor preventing top-down control by providing refuge to prey populations. The author suggested that whereas in closed systems as small lakes an entire population was exposed to intensive predation pressure, in open systems such as oceanic environments and great lakes, physical heterogeneity would alter spatial overlap of predators and prey and thus part of a prey population could escape from predation. Another possible explanation for top-down control to be more present in lakes could be the usually lower species diversity in lakes than in marine ecosystems. Thus, with simpler trophic chains occurring in small lakes, the effect of climate change on a single species could lead to a trophic cascade (Finke and Denno 2004). Supporting this hypothesis, Frank et al (2007) found top-down control to dominate in the northern coastal shelf of the North Atlantic, characterised by poor species diversity and cold waters, whereas bottom-up control tended to dominate in the southern areas, where species diversity was high and water was warmer. Nevertheless, in that study, temperature could not be dissociated from species diversity to explain the dominance of top-down and bottom-up controls.

Recently, it has been suggested that the dominance of top-down and bottom-up control would temporally oscillate in a given ecosystem (Hunt et al. 2002; Litzow and

Ciannelli 2007). Hunt et al (2002) proposed that the pelagic ecosystem in the Bering Sea would be regulated by bottom-up control during cold periods (i.e., zooplankton biomass limits fish larvae survival), and by top-down control during warm periods (i.e., larger fish stocks keep zooplankton stocks small). Litzow and Ciannelli (2007) highlighted that the dominance of one control or the other was dependent on the proportion of prey at the beginning of the transition period (i.e., from cold to warm regime, zooplankton increase allowing a fast increase of fish recruitment). Thus the initial conditions, after the ecosystem equilibrium has been lost, may lead to a top-down controlled ecosystem or a bottom-up controlled ecosystem.

2.1.2 Ecosystem regime shifts and climate teleconnections

An ecosystem regime shift has been defined as an abrupt (i.e., catastrophic) decadal-scale change from one dynamic regime to another (Scheffer, 2001). The reorganization of an ecosystem might occur when the compartments of a food web are not equally altered by one or several forcing factors, at such a level that provokes loss of equilibrium and an abrupt shift to a new stable state. The magnitude of disturbance an ecosystem can endure without shifting to another stable state is called resilience (Holling 1973). The resilience of an ecosystem may increase with diversity (Folke et al. 2004). The more species constitute an ecosystem, the more functions and functional redundancy will be represented (Worm and Duffy 2003). Therefore, high diversity increases the ecosystem buffering of perturbations provoked by external forcing such as climate change, decreasing the possibility of a regime shift to occur (Loreau et al. 2001). Once a regime shift has occurred, reestablishment of the previous environmental conditions does not entail reestablishment of the previous community (Scheffer et al. 2001).

Detection of regime shifts and their relationships to climate change has been possible due to the existence of long standardised time series. Perry et al. (2004) stressed the importance of standardised time series and intercalibration of methods to be able to detect trends and shifts in plankton communities, and to relate them to climate variability. For instance, in the Atlantic Ocean and the North Sea, the Continuous Plankton Recorder (CPR) survey has allowed the creation of coherent time series from 1931 (Reid et al. 2003a).

There is evidence suggesting that regime shifts might be synchronous in marine ecosystems located far from each other in a basin, and even in different ocean basins (Alheit and Bakun 2010; deYoung et al. 2008; Richardson 2008). While the effect of climate on a variety of ecological processes operates through local climatic components and their interactions, very often local, climate variations are coupled over large geographic areas due to atmospheric teleconnections (Glantz et al. 1991; Stenseth et al. 2002). The most well-known teleconnections are monitored with the following hydro-climatic indexes: El Niño/Southern Oscillation (ENSO), the Pacific Decadal Oscillation (PDO) and the North Atlantic Oscillation (NAO) (Fig.2.2). Several ecosystem regime shifts have been reported to be related to shifts in any of those indexes.

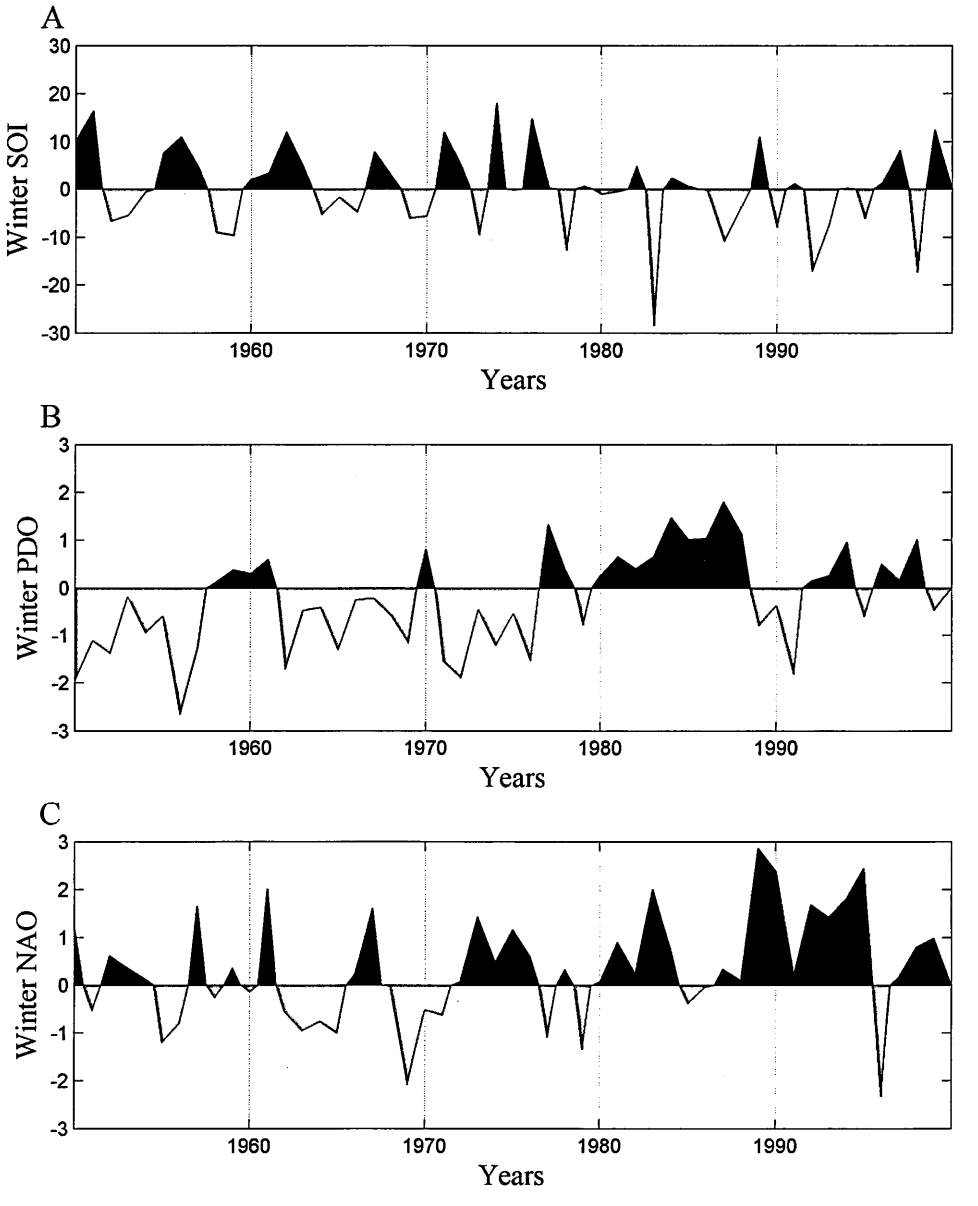

Figure 2.2 – Annual values from 1950 to 2000 of hydroclimatic indexes to monitor teleconnections in the Pacific and Atlantic oceans. A) the Southern Oscillation Index (SOI) (source of data: www.bom.gov.au) , B) the Pacific Decadal Oscillation (PDO) (source of data: http://jisao.washington.edu) and C) the North Atlantic Oscillation (NAO) (source of data: www.cru.uea.ac.uk).

El Niño/ Southern Oscillation (ENSO)

El Niño refers to 3-7 year oscillations in the sea surface temperature of the tropical Pacific. During an El Niño event, equatorial surface water temperature warms over the eastern margin of the ocean (western coast of South America). The Southern Oscillation is the atmospheric component linked to this phenomenon (Fig.2.2A). It

consists of high atmospheric pressure over the western Pacific during an El Niño phase. When the atmospheric pressure over the western Pacific is low, sea surface temperature is cold along the western coast of South America. This phase is called la Niña.

The most striking ecosystem change related to ENSO variability is the alternation of sardine and anchovy regimes and associated restructuring of the ecosystem from phytoplankton to top predators (i.e., seals) in the Humboldt current, along the Peruvian and Chilean coasts (Alheit and Niquen 2004). Seven distinct populations are found along the Humboldt Current, and all the stocks have shown synchronous changes. The main turning points of the observed regime shifts occurred in 1969-1971, when the Peruvian anchovy stock started to collapse and warm sea surface temperature (SST) increased due to the approach of warm subtropical oceanic waters; and in 1985-1988 when SST cooled down due to the retreat of subtropical oceanic waters, while the anchovy regime was restored to the detriment of sardine populations. Alheit and Bakun (2010) have summarized all the ecosystem changes reported for the two periods. In 1969, zooplankton started to decrease, and the relative abundance of fish larvae changed. The abundance of anchovy larvae diminished. Contemporarily, salinity increased and Subtropical Surface Water (SSW) approached the coast. The following year, SST started to increase and also turbulence. Sardine spawning and the relative abundance of horse mackerel increased, whereas bonito and hake catches decreased. In 1971 anchovy recruitment, biomass and catches started a decreasing period, and the following two years were characterised by El Niño, which enhanced the decrease. Anchovy populations continued to decrease until reaching their lowest stocks ever in 1983, an El Niño year, to then starting to recover from 1984 in relation to lower SST and lower salinity. In the following years, sardine catches decreased while anchovy, phytoplankton and zooplankton biomasses increased. It seems that the approach or

retreat of the SSW favours sardine or anchovy feeding conditions, respectively. Sardine prefers feeding on smaller particles than anchovy (Louw et al. 1998). During the 1970s, SST got warmer, the thermocline deepened, mixing increased and coastal upwelling was not possible. Thus, mesozooplankton decreased to the detriment of anchovy populations. In addition, anchovy is a coastal species, whereas sardine has a more oceanic distribution. The variation of SSW distance to the coast could also play a role in the population dynamics of both species.

Pacific Decadal Oscillation (PDO)

The Pacific Decadal Oscillation (PDO) index is defined as the first principal component of monthly sea surface temperature above the 20° North latitude (Mantua et al. 1997). The PDO is usually referred to the winter months, and represents inter-decadal variations of winter climate over the Pacific Ocean (Fig.2.2B). Its spatial dynamics are similar to the ENSO index. During the positive phase of PDO, winter storms over the Pacific are more frequent, the eastern margin (coast of North America) gets warmer and moister, and the central Pacific cools down. During the negative phase, the pattern reverses and the western coast of America cools down.

Due to the PDO, in the North Pacific, there have been reported regime shifts between a cool-high productivity system and a warm-low productivity one, with the changes dated on 1925, 1947, 1977, 1989 and 1998 (Mantua et al. 1997, Hare and Mantua 2000; Peterson and Schwing 2003; Mackas et al. 2007). Mantua et al. (1997) found that Alaskan salmon abundance showed interdecadal oscillations similar to those of the PDO. While the PDO shifted from a positive to a negative phase in 1947, to then enter a positive phase in 1977, salmon catches were above the long-term average before and after 1947-1977, and below the average in the negative phase, which corresponds to a cool-high productivity system. The authors suggested that the system would be

regulated by bottom-up control from phytoplankton availability up to salmon populations due to stratification-nutrient supply processes. Mackas et al. (2007) highlighted the relevance of variations in seasonality and advection patterns due to the thermal and atmospheric decadal oscillations. Phenological mismatches and changes in the flow of the main currents affected zooplankton composition in the eastern Pacific and thus the food available for salmon.

North Atlantic Oscillation (NAO)

The North Atlantic Oscillation (NAO) index is the dominant mode of climatic variability in the North Atlantic region. It is measured as the difference of atmospheric pressure between the subtropical high-pressure centre, usually located over the Azores, and the Arctic low-pressure centre, typically located over Iceland. It gives an average estimate of the strength of the westerly winds blowing across the North Atlantic Ocean (40°-60° latitude), which determine regional temperature, precipitation, storm occurrence and wind regimes over Europe (Hurrell 1995). The NAO affects the ocean through changes in heat content, gyre circulations, mixed layer depth, salinity, high latitude deep water formation and sea ice cover (Hurrell and Deser 2010).Usually, the NAO index refers to the winter NAO index, which is the average of the monthly values from December to February, and presents inter-decadal variability as the PDO. The winter NAO index changed in the late 1980s to a very positive phase (predominance of anomalies above +1) (Fig.2.2C). Global warming together with stronger winter irradiance and reduced ozone layer have been predicted to move the winter NAO into a stronger positive phase (Osborn 2004). High NAO values indicate stronger-than-average westerly winds over the middle latitudes. Generally, high values of the winter NAO entail enhanced storm activity, milder temperatures and increased precipitation in northern Europe and a modest decrease of winter storms, cooler temperature and less

precipitation to the south (e.g., the northern Mediterranean Sea) (Hurrell 1995; Hurrell and Deser 2010). Thus, over much of central and southern Europe, the Mediterranean and parts of the Middle East evaporation exceeds precipitation during years of high NAO index, while in northern Europe occurs the opposite occurs.

Contemporary to the NAO shift to a positive phase in the late 1980s, water temperature increased in the North Sea, the Central Baltic and the northwestern Mediterranean, and in all locations ecosystem regime shifts were reported.

In the Atlantic Ocean and the North Sea, the CPR datasets allowed phenological and latitudinal-spatial distribution shifts that led to trophic mismatches to be detected (Beaugrand et al. 2002b; Beaugrand et al. 2003; Edwards and Richardson 2004). Phytoplankton Colour, a visual index for chlorophyll in the CPR samples, was monitored in the North Sea and Northeast Atlantic during the period from 1948 and 1995 (Reid et al. 1998). In the mid-1980s, a step-wise increase of Phytoplankton Colour, due to extended season of high values, was observed in the central Northeast Atlantic and North Sea. This increase was synchronous with a SST increase related to increasing winter NAO values. Interestingly, the opposite trend was observed in the north part of the Northeast Atlantic where SST got colder. In the North Sea, the increase of Phytoplankton Colour in the mid-1980s was accompanied by an increase of zooplankton abundance and horse mackerel catches (Reid et al. 2001). The authors related these increases to the higher winter NAO values by means of warmer winter and spring SST which would have enhanced the water column stratification, and by oceanic inflow which would have increased the nutrient input in the basin. Horse mackerel experienced also a northward migration, and plankton species distribution changed. Further studies showed that the North Sea regime shift, in circa 1988, involved a shift from cold to warm zooplankton biotopes (Reid et al. 2003b; Beaugrand 2004), and that

phytoplankton composition had shifted to a community with a trend of decreasing dominance of diatoms and thus a higher proportion of dinoflagellates and flagellates (Edwards et al. 2006). Due to milder temperatures, the phenology of dinoflagellates, copepods, other holoplankton and meroplankton presented earlier seasonal peaks from 1988 (Edwards and Richardson 2004). Diatom phenology did not change much, probably because light rather than temperature was acting as a limiting factor for growth. Phenological change could be one of the main factors to provoke the ecosystem regime shift due to trophic mismatches. Cod recruitment decreased since 1988 due to less favourable prey for larvae. Prey conditions changed due to a decrease of the mean size of copepods, to less euphasiid abundance, and to the substitution of *Calanus finmarchicus* by *Calanus helgolandicus* (Beaugrand et al. 2003). *C.helgolandicus* presented a later phenology than *C.finmarchicus*, entailing trophic mismatch with cod larvae, and also had less lipid content. The substitution trend of the typical Artic copepod *Calanus finmarchicus* by the more temperate *Calanus helgolandicus* in the North Atlantic and North Sea (Fromentin and Planque 1996; Planque and Fromentin 1996) is occurring due to a temperature increase in the northern regions, which accelerates metabolism and increases water column stability to the detriment of nutrient concentration and oxygen (Helaouet and Beaugrand 2007). In the Northeast Atlantic, the CPR datasets have shown a northward shift of calanoid species associations (from temperate to subartic assemblages) related to SST warming, which was in turn correlated with Northern Hemisphere Temperature (NHT) and the NAO (Beaugrand et al. 2002b).

In the Baltic Sea, in the late 1980s temperature increased above the permanent halocline, spring vertical mixing reduced inducing earlier stratification onset, river run-off increased due to increased precipitation, and the frequency of winter intrusion of

water from the North Sea decreased (Alheit et al. 2005). Less inflow provoked stagnation in the central Baltic Sea and thus decreases of deep water salinity and oxygen levels (Fonselius and Valderrama 2003). Nutrients availability increased in that period due to organic matter degradation in the bottom sediments (Mollmann et al. 2009). As a result of all these changes, phytoplankton biomass increased and the growing season extended, but diatom biomass dropped in 1988, while dinoflagellate biomass showed a steady increasing trend from then on (Wasmund et al. 1998). The diatom decrease was probably due to less vertical mixing in spring. The abundance of the spring copepods, *Acartia* spp. and *Temora longicornis*, increased from 1988 as dinoflagellates dominated phytoplankton biomass and the temperature increase benefited hatching of resting eggs in the sediment. On the other hand, *Pseoudocalanus* ssp. abundances were above the long-term average in the 1970s to then decrease to the 1960s average levels (Alheit et al. 2005). Responding to the temperature increase, salinity decrease and changes in prey availability, the spawning stock biomasses of cod and herring decreased, whereas sprat biomass increased in the late 1980s (Mollmann et al. 2009). Different physiological requirements and competition feedbacks would have result in the observed changes, but the ultimate mechanism in the reorganization of the Baltic Sea was bottom-up control as was the case for the North Sea ecosystem change (Alheit et al. 2005).

In the northwestern Maditerranean Sea relevant ecosystem changes took place in the late 1980s. In the region of Calvi (northwestern Corsica coast), the phytoplankton winter-spring bloom was high from 1979 to 1986 to then decrease from 1988, due to less nutrient input in the photic zone related with warming, an overall decrease of salinity and stronger stratification (Goffart et al. 2002). Gomez and Gorsky (2003), by compiling information of single-year studies on the spring-peak amplitude in the Bay of Villefranche, showed that the spring peak was high from 1985 to 1988, whereas it was

low in all the seven non-consecutive years of study from 1988 to 1999. Copepods, jellyfish and chaetognaths showed also a shift in their abundances around 1988 at the Bay of Villefranche (Molinero et al. 2005a; Molinero et al. 2008a; Molinero et al. 2008c). Jellyfish seemed to dominate the zooplankton community from the early 1980s due to increasing temperature and longer stratification. In all these studies, the authors related the reported changes to the shift of the winter NAO index to a positive phase. Also analyses of a coastal time series in the Balears isle showed significant relationships between the copepod community and local climate with the NAO and atmospheric variability in the North Atlantic sector (Fernandez de Puelles and Molinero 2007; 2008).

The results presented above indicate intra-basin and inter-basin synchronies of changes. Bottom-up control seems to be the main process taking place in the reorganization of the studied pelagic ecosystems, although the mechanisms linking climate and trophic levels can be very different depending on the environmental and community basal conditions (Alheit and Bakun 2010). Nevertheless, from these studies it can be concluded that diatoms are negatively affected by global warming and that temperature and water-column stability may be the environmental factors which affect trophic webs the most.

2.2 The Mediterranean Sea and climate change

The Mediterranean Basin has been suggested as a suitable model to study climate change and anthropogenic effects on marine ecosystems (Duarte et al 1999; Turley 1999), and to have a relevant role in Atlantic Ocean circulation (Reid 1994; Rixen et al. 2005). The Mediterranean Basin, with its deep bathymetry, its open-water oligotrophic and some coastal mesotrophic conditions, deep water formation and mesoscale circulation features, can be considered as a model for climate change effect on the oceans (Bethoux et al. 1999). It is a semi-enclosed basin, with Atlantic water

entering by the narrow Gibraltar Strait and is modified along the continental slope by a counterclockwise circulation (Millot 2005) (Fig.2.3). Modified Atlantic Water is vertically mixed all along its transport route with Mediterranean waters, and exits the Mediterranean Sea, below 200 m depth, warmer and saltier than it entered it at the surface. Its thermohaline signal can be traced out into the North Atlantic at about 1100 m depth, and could have a key role in deep water formation in the Greenland Sea and the Labrador Sea (Reid 1979), although the relevance of its role is arguable (Lozier and Sindlinger 2009; Mccartney and Mauritzen 2001). The Mediterranean outflow helps to maintain high salinity levels in the Norwegian Sea.

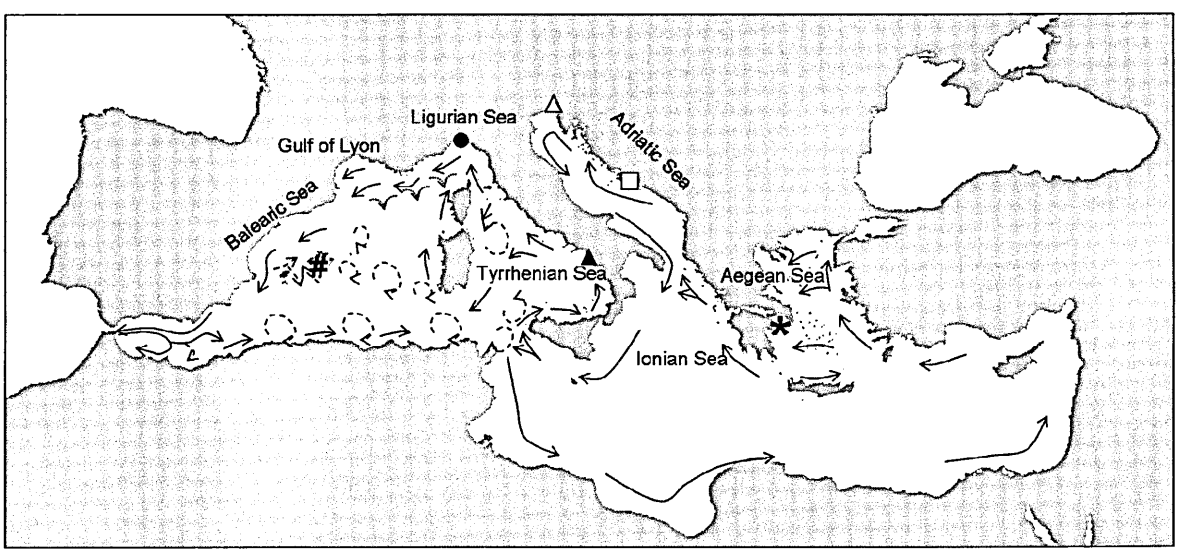

Figure 2.3 - The Mediterranean Sea with its permanent surface circulation (black arrows). Mesoscale currents and wind-induced mesoscale eddies (dashed line arrows) are indicated in the western basin. Location of sampling sites of zooplankton long time series is indicated: the stn MC (▲) and Point B (●) are the time series studied in this thesis; others are Baleares Station (#), Station C1 in Trieste (Δ), Stoncica sampling station (□) and Station S11 in Athens (*).

2.2.1 Environmental changes

Several studies indicate long-term changes in the hydro-meteorological conditions of the Mediterranean Sea, such as water warming, less rainfall and lower

wind speed trends from the early 1980s to the late 1990s (Bethoux et al. 1990; Trigo et al. 2000; Vargas-Yáñez et al. 2008).

One of the most striking hydrological changes occurred in the late 1980s. The deep and intermediate circulation in the eastern basin experienced relevant modifications, named the Eastern Mediterranean Transient (EMT) (Roether et al. 1996). The EMT was a transformation of the Eastern Mediterranean thermohaline system from a stationary state to a transient state. Comparison, between 1987 and 1995, of the thermohaline circulation in the eastern Mediterranean basin revealed that while in the 1980s deep water formation occurred in the south Adriatic Sea, in the 1990s ~20 % of the deep water formation occurred in the Aegean Sea (Lascaratos et al. 1999). This change was due to increasing density of waters in the Cretan Sea, firstly driven by salinity increases from 1987 to 1992 and then enhanced by a following cooling. The consequent strong deep outflow from the Aegean Sea was already recorded by Tsimplis et al. (1997) in 1989; thus, the EMT might have started anytime between 1987 and 1989. Due to the EMT, deep waters formed in the eastern basin have become saltier and warmer and the western basin seems to have been affected (Millot et al. 2006). Historical data from the 1960s to the 1980s show that most water out-flowing through the Gibraltar Strait (i.e., Modified Atlantic Water or MAW) was dense water formed in the western basin (i.e., Western Mediterranean Deep Water or WMDW). Nevertheless, in the mid-1990s the outflow became saltier and warmer, and in the mid-2000s much of the outflow belonged to Tyrrhenian dense water, which is formed mostly by dense water from the eastern basin and in a lower rate by transformed WMDW.

In the Mediterranean Sea, water warming has been accompanied by a salinity increase in the whole basin (Rixen et al. 2005). Bethoux et al. (1998) estimated temperature and salinity to have increased 0.13 °C and 0.04 psu, respectively, from

1959 to 1997, and the observed variations have modified water circulation and dense water formation (Herbaut et al. 1997; Samuel et al. 1999; Astraldi et al. 2002). Salinity levels have increased in relation to increased evaporation due to water warming, and to a reduced freshwater budget due to lower precipitation and river damming (Bethoux and Gentili 1999). As a result, in the Mediterranean Basin, the sea level has been decreasing at rates up to -1.3 mm yr^{-1} since the 1960s to the late 1990s (Tsimplis and Baker 2000), which is opposite to the general trend of sea level rise due to global warming (IPCC 2007). The sea level has been decreasing due to an increased evaporation-precipitation ratio, but also due to a rising trend of atmospheric pressure (Tsimplis and Baker 2000). The NAO has been linked to the local atmospheric changes involved in salinity and temperature changes (Vignudelli et al. 1999; Trigo et al 2000, Tsimplis and Baker 2000; Tsimplis and Josey 2001; Rixen et al. 2005).

The positive trend of the winter NAO since the 1970s, and more intense in the 1990s, seems to have provoked a decrease of winter rainfall in most parts of the Mediterranean Sea, driven by the coupled ocean-atmospheric circulation in the North Atlantic (Mariotti et al. 2002). Trigo et al (2000) analysed precipitation records between October and March (the wettest period), from 1956 to 1996, for an area covering the whole Mediterranean Basin except for the southern part of the eastern sub-basin. The authors reported a precipitation decrease that they related to a poleward shift of the zonal storm tracks in the North Atlantic, which reduced the intensity of the deepest Mediterranean cyclones. In addition, Vignudelli et al (1999) showed that negative values of the winter NAO were associated with intense heat loss in the Gulf of Lions which intensified the flow of the Northern Current within the Ligurian Sea. The heat loss anomaly in the Gulf of Lions and the winter NAO were correlated in a similar way to the correlation between the winter NAO and the heat loss in the North Atlantic

(Rixen et al. 2005). The wind pattern over the basin seems to be also affected by the NAO. Vargas Yáñez et al (2008) found that the NAO index explained 50% of the variance of Ux wind component (the east-west component) in a coastal area of the south of Spain. A change in the wind pattern, concomitant with the winter NAO change in the late 1980s was appointed to have had a role in the occurrence of the EMT (Samuel et al. 1999). The Mistral wind weakened whereas wind stress intensified over the Aegean and Levantine Basin in the late 1880s with respect to the early 1980s. Consequently, the Levantine Intermediate Water (LIW) changed its path across the eastern basin. In the new LIW circulation pattern, the Aegean Sea received more LIW than in the early 1980s, favouring deep water formation in this area. In 1987 the path to the Adriatic Sea would have been interrupted, and thus there would have been a salinity deficit which might have complicated deep water formation in this area. In addition, winters cooled down at a higher rate in the Aegean than in the Adriatic Sea, contributing to denser waters in the former. The results presented by Samuel et al (1999) reflect how large-scale forcing by atmospheric teleconnections does not affect the whole Mediterranean Basin in the same way.

Regionalization of the Mediterranean Basin according to the response to environmental forcing

The response of local environmental conditions to large-scale environmental forcing is not homogeneous throughout the Mediterranean Basin. For example, Tsimplis and Josey (2001) compared environmental conditions during the ten most extreme positive winter NAO years with the ten most negative in the last four decades, and showed a longitudinal gradient in related changes of sea level pressure, and a latitudinal gradient in precipitation changes. Winter sea level pressure increased during extreme positive values of the winter NAO, but increases were stronger from east to west (Fig. 3A in Tsimplis and Josey 2001). Winter precipitation records decreased in the northern

part of the basin, and increased in the southern part, when the winter NAO increased (Fig. 3C in Tsimplis and Josey 2001). As a result of evaporation-precipitation ratio changes, the winter sea level average for the period 1990-1993 (+ winter NAO period) was lower than the average for the period 1960-1964 (- winter NAO period) in most parts of the Mediterranean Sea. The strongest sea level decrease was of 2.5 cm and occurred in the northern coast of the western Mediterranean (Fig.3E in Tsimplis and Josey 2001).

Water warming has not been homogeneous throughout the Mediterranean Basin (Bethoux et al. 1998). A recent standardized spatial Principal Component Analysis performed by Beaugrand (Pers. Comm.) on gridded temperature annual time series from 1960 to 2005 of the whole western and part of the eastern basins, available in the International Comprehensive Ocean-Atmosphere Data Set (ICOADS), showed that although the whole area presented a common warming trend since the early 1980s (Fig.2.4 A and B), the 2nd Principal Component (2nd PC) revealed a divergence of interannual temperature variability between the eastern and the western basins (Fig.2.4 C and D). As indicated by the correlation colour maps (Fig.2.4 A and C), while all grids were positively correlated with the 1st PC which represented most of the common variability (73%), only the eastern area was positively correlated with the 2nd PC (11% of common interannual variability), which might indicate that from 1988 the warming trend in the eastern basin was steeper than in the rest of the Mediterranean Basin. This year is considered to be the period in which the Eastern Mediterranean Transient (EMT) took place (Roether et al. 1996). Regarding the two time series studied in this thesis, Point B was not related with this event, while stn MC was at the boundary, in the area of low positive weightings.

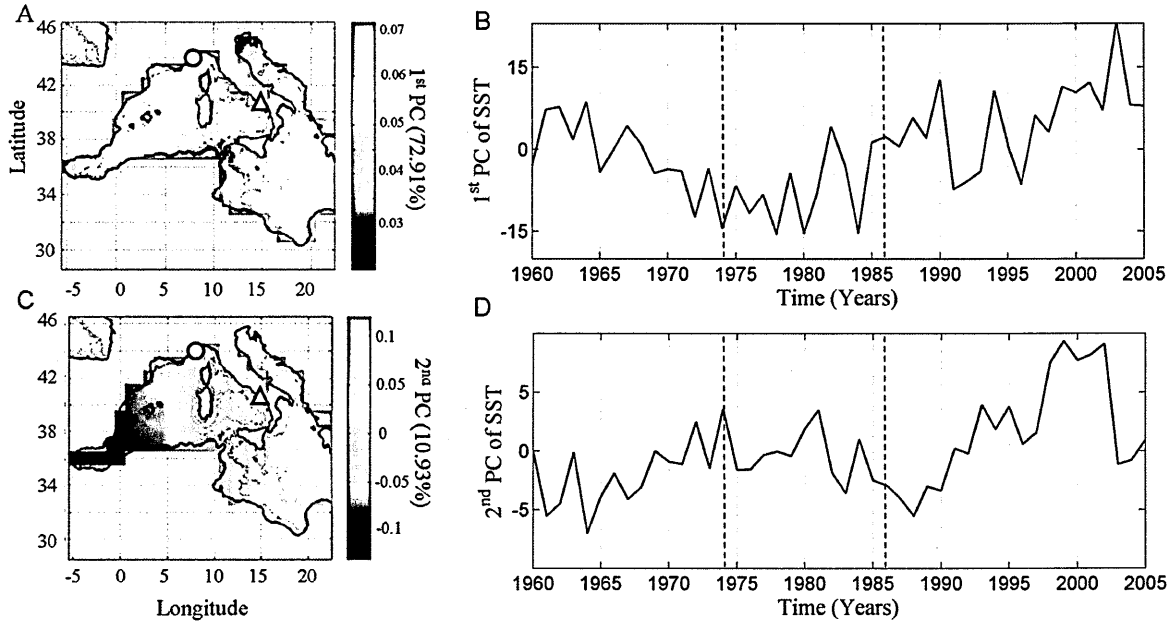

Figure 2.4 – A) Map of the western Mediterranean Basin in which the colour shading represents the weighting of each gridded temporal variability on the 1st PC of SST; stn MC and Point B locations are represented by a triangle and a circle respectively; B) Interannual time series of the 1st PC of SST; dashed vertical lines indicate first years of MC (1986) and Point B (1974) time series C) same as in A but for the gridded weightings on the 2nd PC of SST; D) same as in B but for the 2nd PC of SST.

Recently, D'Ortenzio and Ribera d'Alcalà (2009) classified the Mediterranean Basin into seven classes depending on the chlorophyll a (chl *a*) seasonal cycle inferred from satellite datasets. The seven classes obtained by cluster analysis appeared grouped in quite homogenous regions. These original regions were then reduced to four general regions depending on the position and height of the annual maximum in the clusters' centres. The four regions were named 1) blooming, 2) intermediate-blooming, 3) non-blooming, and 4) coastal. The authors stressed the similarity between the regions detected with their method and the trophic regimes determined by Longhurst (1998). The blooming region was very similar to the model proposed by Longhurst for the North-Atlantic-like dynamics, and it was located in an area covering most of the northwestern sub-basin. According to this study, the Ligurian Sea (where Point B is located) is more similar to the North-Atlantic-like dynamics, while the Tyrrhenian Sea (stn MC) is more similar to the south-eastern Mediterranean Basin. The authors

proposed that the Mediterranean Sea would be located on the boundary between a sub-tropical regime characterised by the non-blooming regions (i.e., Tyrrhenian Sea), and the northern area (mostly, the northwestern sub-basin) characterised by the blooming and intermittent-blooming regions. In this northern area, North Atlantic bloom-like events could happen depending on the hydroclimatic conditions.

Regionalization depending on SST trends presented here, as well as that related to the winter NAO conditions (Tsimplis and Josey 2001) and the one depending on the trophic conditions of the system (D'Ortenzio and Ribera d'Alcalà 2009) show similar complementary patterns. Combining results from the three studies, two gradients are found in the Mediterranean Sea, an east to west gradient and a south to north one. The northwestern area (i.e., Ligurian Sea) would be more affected by atmospheric changes forced by the winter NAO (i.e., precipitation regime changes) and thus its seasonal cycle can be similar to that of North Atlantic areas, whereas the Tyrrhenian Sea would present sub-tropical conditions more similar to the eastern than to the western Mediterranean Basin. Stn MC seems to be at the boundary between the eastern and western hydro-meteorological conditions, as reflected in the 2nd PC of SST and the sea level pressure difference between positive and negative NAO conditions.

2.2.2 Zooplankton changes

Parallel to the warming trend of the Mediterranean Sea, population establishment of warm-water benthic and nekton species has been reported in the northern sectors of the western basin (Astraldi et al. 1995; Bianchi and Morri 2000; Francour et al. 1994). Bombace (2001) reported catches of several fish species from the eastern and southern areas of the Mediterranean Basin in the northern 'cold biota', and a reduction of relatively abundant 'cold species' in these northern areas (i.e., sprat in the North Adriatic Sea and Gulf of Lions). Since the mid-1980s, the presence of warm-

water species in the Ligurian Sea has greatly increased, suggesting establishment of stable populations (Bianchi and Morri 2000; Bianchi 2007).

Regarding zooplankton, despite the availability of fewer and shorter time series (see their location in Fig.2.3) than in the adjacent Atlantic Ocean, in the last decades, relevant changes have been recorded in Mediterranean marine ecosystems as a response to climate forcing. Studies performed on data from the Baleares Station (Balearic Sea; # location in Fig.2.3), covering the period from 1994 to 1999 and then expanding their analyses to 2003, showed that zooplankton was more abundant during cooler and more saline years than the long-term average, when the influence of northern waters was stronger (Fernandez de Puelles et al. 2007; Fernandez de Puelles et al. 2004). In that coastal station, copepods were significantly positively correlated with salinity and negatively with temperature, and also nitrate concentration increased from 1998 according to a temperature decrease and an increasing trend in salinity. Positive correlations of copepod abundance with salinity have also been described in the western and eastern parts of the Mediterranean basin (Christou 1998; Kouwenberg and Razouls 1990) and related with upwelling and/or offshore waters intrusion. In the case of the Baleares station, salinity enhancement was interpreted as an indicator of intrusion of the Northern Current which is richer than the nutrient-depleted Atlantic waters entering the area by the south. Fernandez de Puelles and Molinero (2007) proposed that the spreading of the Northern Current into the Balearic Sea was related to the atmospheric variability over the North Atlantic. A monthly correlation was found, for the period from 1950 to 2005, between the 1st PC of several indicators of the North Atlantic climate and the 1st PC of several meteorological variables representing the Balearic Climate. Moreover, annual average values of copepod abundance were correlated to the winter NAO, although the relationship was not strong because of the availability of just

10 values and only one year showing a clear negative winter NAO. Similar analyses carried out on data from the Bay of Villefranche (Point B location indicated by a • in Fig.2.3) showed that much of the variability in local climate and zooplankton abundance from 1967 to 1993 was governed by the pattern of changes in the winter NAO (Molinero et al. 2005a). Studies on different components of the plankton communities at Point B highlighted the correspondence between changes in the abundance and/or composition of some key species and the shift in the NAO index that occurred in the late 1980s (Molinero et al. 2005a; Molinero et al. 2008b). In those studies jellyfish seemed to outcompete chaetognaths and to be detrimental to copepods, which abundance dropped from the late 1980s. The authors proposed a trophic reorganization due to oligotrophication related to increasing stratification driven by water warming in the 1990s. According to this, phytoplankton blooms were reported to decrease from 1988 in the Bay of Calvi (northern Corsica, Ligurian Sea), but this decrease was rather related to a salinity decrease which was appointed to entail less nutrient replenishment by vertical mixing due to water density reduction. At stn MC (Gulf of Naples, ▲ in Fig.2.3) chl *a* and phytoplankton cell size decreased in the second part of the time series (from 1995 on with respect to the period 1984-1991), but zooplankton abundance and biomass did not show such clear trends (Ribera D'alcalà et al. 2004). Nevertheless, in that study some rare copepod species were reported to disappear and others to appear in the sampling station, and those diversity changes were considered to indicate possible relevant environmental changes affecting that area. Also in the Gulf of Trieste (Adriatic Sea, Δ in Fig.2.3) some rare species appeared and others disappeared during 30 years of study (Kamburska and Fonda-Umani 2006; Conversi et al. 2009). Some cold-water species showed a strong decrease while other species that previously had a more southern distribution increased their numbers in the late 1980s. After 1987, in the Gulf of Trieste, copepod abundance doubled, phenological changes

were recorded in some species, and small copepods belonging to *Oithona* spp. and *Oncaea* spp. groups increased their dominance in the copepod assemblages. The authors explained those changes with anticipated phenology due to temperature increases in the gulf, and with circulation changes related to the Eastern Mediterranean Transient (EMT). According to them, the change of location of the main source of deep water in the eastern basin would have altered the input of Atlantic water in the gulf favoring the entrance of southern species. Also Mazzocchi et al. (2003) related changes in zooplankton vertical distribution in the Ionian Sea to the EMT, by means of a transformation of the Ionian Anticyclone into a cyclonic gyre. This change may have caused the zooplankton in 1999 to be concentrated in lower layers than in 1992 due to the presence of highly oligotrophic surface waters in 1999, and also that in 1999 the western and eastern sides of the cyclone presented different composition and biomass levels due to differences in the depth of the nutricline. Data from another time series in the Adriatic Sea (Stoncica sampling station, □ location in Fig.2.3) showed that from 1965 to 1985 there was an increasing trend of primary production that the authors related to increasing entrance of Mediterranean Water in the gulf, indicated by a trend in salinity increase (Marasović et al. 1995). Pressure differences between the northern and southern waters of the Adriatic Sea would drive the entrance of Mediterranean waters rich in nutrients. Recently, phytoplankton counts from 1962 to 2005 in the same location showed a decadal oscillation, with phytoplankton decreasing again in the 1990s and a correlation with the NAO that was explained by its link with atmospheric conditions ruling precipitation and irradiance in the area (Gladan et al. 2010).

The several studies conducted on the effect of climate change on Mediterranean ecosystems are independent. Recently, the six zooplankton time series of the Mediterranean Sea (Fig.2.3) have been compared for the first time (Berline et al. 2010).

Despite the different sampling techniques and time span, some patterns could be depicted. The authors stressed the dominance of the coastal-offshore gradient over the east-west gradient to sort locations. They also observed correlations of temperature in Villefranche sur Mer, Naples and Trieste, and a common temperature shift in 1987. In the three stations, the plankton community suffered changes between the 1980s and the 1990s.

2.3 Size as an ecological descriptor of pelagic ecosystems

The interest of ecologists in body size as a characteristic for the community organisation has been intermittent since the beginning of the 20th century. Elton (1927) was the first to write about biomass regularity with size. He attempted to find general features to simplify ecosystem complexity, interpreting communities as food chains in which the largest organisms are at the top, and size decreases to the bottom while abundance increases. Current research still focuses on the use of body size as an aggregative descriptor of the ecosystem, and as a mean to calculate rates at individual and population levels. A brief history of reseach on size as an ecological descriptor is given below.

Allometry is the study of scaling with size and was firstly presented by Huxley (1932). It is used to express the different relationships between metabolic rates and body size by the following simple equation:

$$Y = a\, M^{b}$$

where Y is the metabolic rate, a is a normalization constant, M the body size, and the exponent b scales as a quarter power (multiples of ¼) (Peters 1983; Calder 1984; Schmidt-Nielsen 1984). The study of these relationships (Fenchel 1974) and the definition of a ¾ scaling of basal metabolism with respect to body size (Kleiber 1932)

highly contributed to setting theories of body size as an organisational parameter of the structure of ecosystems.

In the mid-twentieth century, the study of community size distribution slowed down due to the appearance of the trophic level concept (Lindeman 1942) and the controversy of using such a simple parameter as body size to describe such a complicated entity as ecosystems. It was half a century later that body size became even more relevant by the arrival of new theories and ideas based on energy flow and thermodynamics to explain ecosystems functioning, as well as the need to understand ecosystem structure (Margalef 1961; Margalef 1963). The pioneer of such ideas was Odum (1956) who later postulated that a general trend to increasing production rates and increasing body size occurred with succession. This assertion was corroborated by observations in plankton dynamics (Margalef 1963; Peters 1976). The size-efficiency hypothesis (Brooks and Dodson 1965; Hall 1976) was developed based on plankton population studies and tried to explain the size distribution of a community by means of predation and competition, constrained by individual size. Based on these theories, some models were proposed, where organisms were arranged in size spectrums, i.e., each organism belongs to a size class into which range its dimensions fall.

The first models were those of Kerr (1974) and Sheldon et al. (1977). They proposed that in a logarithmic scale biomass was constant along size classes. The model of Platt and Denman (1977) proposed that biomass was slightly decreasing among size classes as energy was flowing through the spectrum (Fig.2.5). The model was based on a continuous flux of energy from small to large organisms. Loss of energy from one step to another would be due to metabolism and unassimilation (constant loss rate in the turn over), and so would be dependent on body size by allometry. Size classes of the Platt and Denman size spectrum were not of the same width but presented a geometrical

progression (i.e., increasing octave-scale). The authors normalised the distribution by dividing each size-class biomass by its width. This is the Normalised Biomass Size Spectrum (NB-S Spectrum), and it is still the most common used in size spectrum research.

The spectrum of Platt and Denman is defined by the following equations:

$$B_w = b_w / \Delta(W)$$

$$B_w = aW^b$$

$$\log_2 (B_w) = a + b \log_2 (W)$$

where B_w is the normalised biomass, bw is the biomass contained in a size class and $\Delta(W)$ the width of the size class or bin. The normalised biomass (B_w) has an allometric relationship with size, W, defined by two constants, *a* and *b*. This allometric relationship is dependent on the allometric equations for growth and respiration (Fig.2.5). Platt and Denman assigned the value -1.22 to the coefficient *b*, the slope of the logarithmic relationship.

Contemporary to Platt and Denman' model, Silvert and Platt (1978) improved it by taking into account time for representing the flow of energy along the biomass spectrum. They calculated the derivate of biomass with time, by a loss function due to respiration and incorporation to higher size classes, and a gain function from smaller size classes determined by growth, but also by predation. Since these first models, many others have been developed (e.g., Cousins 1987; Dickie et al. 1987; Rodriguez et al. 1987; Boudreau et al. 1991; Zhou and Huntley 1997; Zhou 2006).

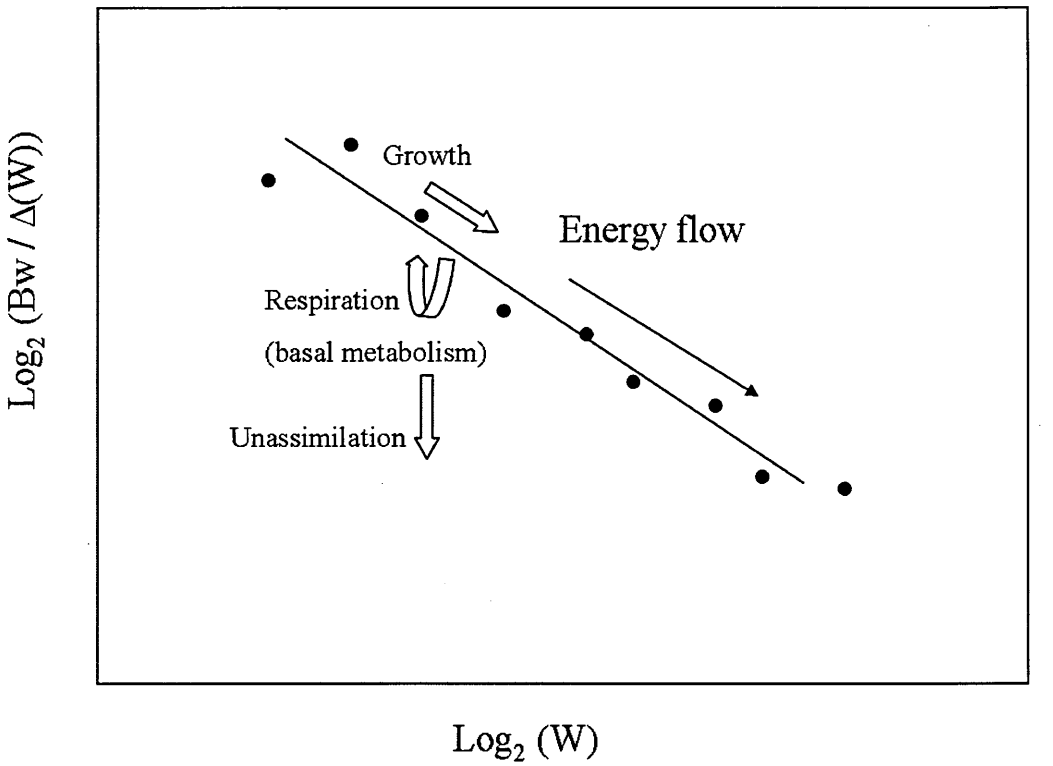

Figure 2.5 - Schematic diagram of Platt and Denman's model on the size structure of marine ecosystems. On the X axis, the size classes defined by nominal size, W, are reported. On the Y axis, the biomass in each size class normalised by the width of the size class is reported. Both axes are in 2-base-logarithmic scale. The linear relationship represents a continuous flow of energy along with increasing size, defined by growth, and a loss of energy from one step to another due to unassimilation and respiration.

Recently, a macroecological theory has been stated to explain ecosystem functioning and structure solely by metabolism (Brown 2004 and references therein). The Metabolic Theory relates the ecosystem dynamics and composition to the individual metabolic rate, which is constrained by body size, temperature and stoichiometry. Food web dynamics would be explained by relating standing stocks of biomass, rate of flux, production of energy and turnover rates to body mass and temperature. The theory is able to make quantitative predictions on how size, temperature and stoichiometry affect the pools and fluxes of biomass and energy among trophic levels. Planktonic communities seem to adapt to climate change by adjusting their diversity and size of organisms. Macro-ecological empirical relationships between

size of organisms, diversity and water temperature have been recently documented (Beaugrand et al. 2002a; Irigoien et al. 2004). Variations in size and diversity can then impact the functioning of the ecosystem, by altering prey-predator relationships, and can ultimately influence regional carbon cycling (Karl et al. 2001). The coupled study of taxonomic and size-base approach in ecosystem studies could help in understanding ecosystem organization and functioning (Gaedke 1995; Brucet et al. 2006).

With the proliferation of models based on plankton size spectrum from the 1980s, a need for automated systems to furnish large datasets arose. The Coulter Counter (Coulter 1953) was already available for counting and sizing small particles and cells, but could not distinguish between organisms and detritus. In the early 1970s, flow cytometry started to develop. By this method, pico and nanoplankton cell size is measured and cells can be automatically recognised by fluorescence. Net plankton was firstly automatically measured by silhouette photography (Ortner et al. 1979). Then, in the late 1980s, *in situ* imaging systems such as the Optical Plankton Counter (OPC) and the Underwater Video Profiler (UVP) (Herman 1988; Gorsky et al. 1992) were created, among others, to characterize plankton community structure and to estimate the export of carbon to the deep oceans (Benfield et al. 2007). Preserved samples of micro and mesoplankton can be also treated by automated systems such as the FlowCAM (i.e., a flow cytometer adapted to microplankton) and the ZooScan (i.e., a scanning system adapted to water samples of mesozooplankton) among others (Sieracki et al. 1998; Grosjean et al. 2004; Gorsky et al 2010).

Since the creation of automated systems, the resulting datasets have allowed the creation of inverse mathematical models to estimate population dynamics from size spectra (i.e., Heath 1995; Edvardsen et al. 2002), and the theories and models formulated in the 1980s have started to be tested (e.g., Lopez-Urrutia et al. 2006;

Maranon et al. 2007). The Platt and Denman model has been validated by size spectra from steady-state ecosystems such as the oligotrophic North Pacific Central Gyre (Rodriguez and Mullin 1986), the North Atlantic Gyre (San Martin et al. 2006) and the Northwest Atlantic and Sargasso Sea in summer (Quinones et al. 2003). Also in lakes regular patterns have been described in the size structure of pelagic communities (e.g., Sprules et al. 1988; Echevarria et al. 1990; Sprules and Goyke 1994; Gaedke and Kamjunke 2006; Sprules 2008).

In coastal Mediterranean ecosystems, biomass size distribution has been reported to be less regular than in more oligotrophic systems, but still a pattern is found (Rodriguez et al. 1987; Jimenez et al. 1989). Although the slope is the most used descriptor of size spectra, the Shannon diversity Index (H) of the size classes can also be used as synthetic indicator that reflects how evenly organisms are distributed in the size classes (Parsons 1969; Ruiz 1994; Brucet et al. 2006). The maximum value of H is obtained when organisms distribute equally among all the size classes; if the system is dominated by one or few size classes (i.e., small organisms), the value of H will be low. Ruiz (1994) recommends it for systems other than the oligotrophic ocean, due to spatial and temporal variability that affect spectra linearity and make difficult to use the slope as an allometric model in those cases.

Empirical studies with automated systems have contributed new insights into plankton size structure. For example, the biomass size spectrum can be used as a descriptor of the trophic conditions of a community. In eutrophic environments more variability in the size spectra slopes is expected, while oligotrophic systems are more stable (Quinones et al. 2003). Kimmel et al. (2006) reported that in eutrophic lakes the normalised biomass size spectrum slope of the whole mesozooplankton community with detritus was less negative than in oligotrophic ones, and thus there would be

increasing relative biomass of large size classes with increasing nutrient availability. This was assessed by Boudreau and Dickie (1992) by fertilizing the Great Central Lake and observing a much less steep negative slope afterwards. Rodriguez et al. (1987), by inverted microscopy and scanning of net-samples from a Mediterranean coastal station, reported the dominance of nanoplankton in oligotrophic stable environments whilst net-plankton dominated in fluctuating systems. This would likely be due to the direct relationship between nutrient storage capability and cell size, which allows survival of large organisms in case of discontinuous nutrient inputs.

D'Elbèe (2001) identified, in the Gulf of Biscay, a coastal/offshore gradient in copepod size with small species characterizing the coastal community (e.g. *Acartia* spp., *Oithona* spp., and *Oncaea* spp.) and larger species as *Candacia* spp., *Anamalocera* spp. and *Calanus* spp. mainly present in offshore waters. By using a lab-OPC, Sourisseau and Carlotti (2006a) found this coastal/offshore gradient in size distribution in several transects performed over two successive springs along the French continental slope of the Bay of Biscay. The coastal zone was characterised by the highest densities of organisms and highest slopes, i.e., small zooplankton dominated the communities. Also Mackas and Coyle (2005) found this pattern of larger copepods in offshore waters than in the coastal shelf of the subartic regions of the East Pacific.

Chapter 3. Material and Methods

3.1 Sampling sites and zooplankton sample collection

3.1.1 Stn MC (Gulf of Naples, South Tyrrhenian Sea, western Mediterranean)

The Tyrrhenian Sea is situated between Sardinia and Sicily and the south-west coast of Italy. Its northern and central parts are influenced by western winds blowing through the Bonifacio Strait (Astraldi 1994). The Thyrrhenian Sea with its topography plays a major role in the connection between the north and south western Mediterranean sub-basins. In winter, Modified Atlantic Water (MAW) flows northward along the Italian coast to reach the Ligurian Sea where it becomes the Ligurian Current (Astraldi 1994; Millot 1999). Decadal variability of the flow through the Corsica Channel is related to climatic forcing (Astraldi and Gasparini 1992; Astraldi 1994; Astraldi et al. 1995).

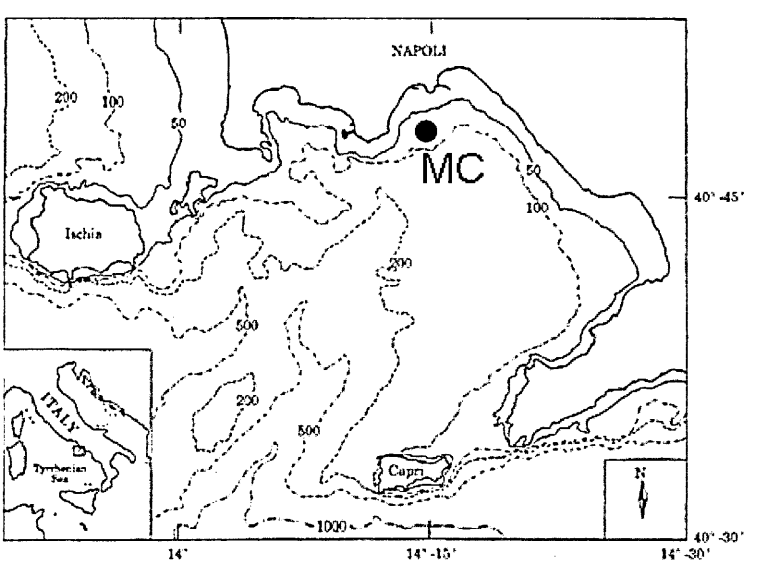

Figure 3.1 - Sampling location (stn MC) in the Gulf of Naples (Tyrrhenian Sea).

The stn MC sampling site is located in the inner part of the Gulf of Naples, two nautical miles from the coastline (40°48.5'N, 14°15'E; ~80 m depth), in the boundary region between the offshore and coastal systems (Fig.3.1). In the Gulf of Naples, the littoral area is strongly influenced by land runoff from a densely populated region;

however, due to the general physiography and bottom topography, the inner shelf area is strongly coupled with the offshore waters of the Tyrrhenian Sea (Ribera d'Alcalà et al. 2004).

The *Mare Chiara* (MC) time series for the study of the planktonic system is ongoing since 1984, with a major interruption from August 1991 to February 1995 due to the loss of the sampling vessel due to a shipwreck. From 2006, this time series has been part of the International network: Long Term Ecological Research (I-LTER). Sampling was fortnightly before the interruption, and has been weekly since 1995. Zooplankton samples have been collected by a vertical haul from 50 m depth to the surface with a Nansen net (200 μm mesh, 1.13 m mouth diameter) and fixed with buffered formaldehyde at ~2-4% final concentration (for more details see Ribera d'Alcalà et al. 2004). In the present work, years with more than 3 months missing were discarded. Thus, analyses were performed on samples from 1986 to 1990 and from 1995 to 2005 (16 years).

3.1.2 Point B (Villefranche Bay, Ligurian Sea, north-western Mediterranean)

The Ligurian Sea is enclosed by the French and Italian Riviera on the north, and by the Island of Corsica to the south. It is characterised by a permanent cyclonic circulation of MAW flowing south-westward along the Riviera and forming the Ligurian Current. The Ligurian Current is a component of the Northern Mediterranean Current, which transports less saline Atlantic Water from Italy towards Spain (Prieur et al. 1983; Millot 1999). Transport in the upper 200 m depth layer has a marked seasonal variability because, in addition to the permanent contribution of the Western Corsica Current, there is a strong seasonality in the contribution of flow from the Tyrrhenian Sea through the Corsica Channel, with maximum records in January and minimum in September (Bethoux et al. 1982; Béranger et al. 2005). The southern edge of the current

is separated from the central water of the Ligurian Basin by a permanent thermohaline front.

Point B station (Fig.3.2) is located at the entrance of Villefranche Bay (43°41'10''N, 7°19'00''E; ~80 m depth). The site is affected by hydro-climatic variability such as the Ligurian Current flow, wind patterns and by open sea conditions due to a narrow continental shelf and the presence of a submarine canyon (~2000 m depth) in front of the bay.

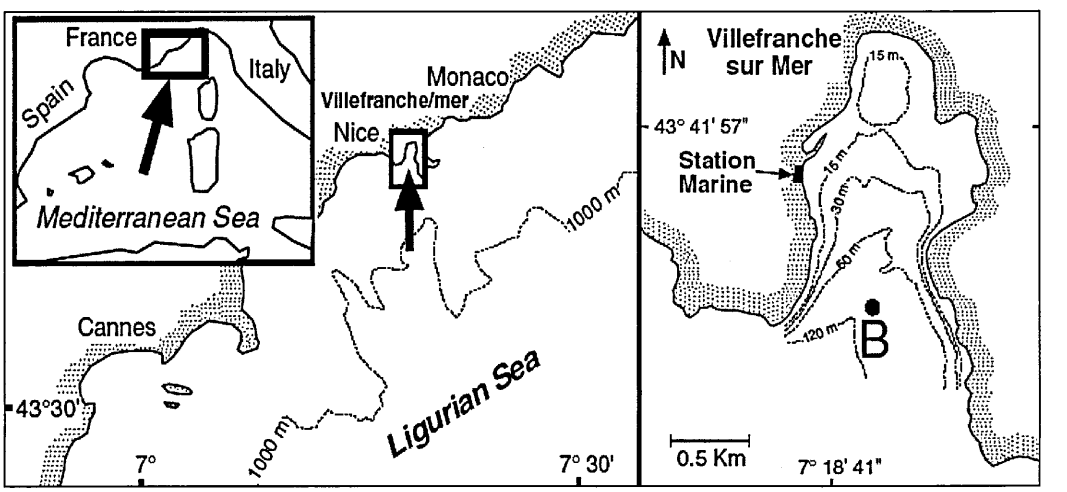

Figure 3.2 - Sampling location (Point B) in Villefranche Bay (Ligurian Sea).

Zooplankton sampling at Point B has been performed since 1966, often on a daily basis. Zooplankton has been collected by two vertical hauls from 75 m depth to the surface, one haul with a Juday-Bogorov net (330 μm mesh, 0.5 m mouth diameter) and the other haul with a Regent net (680 μm mesh, 1 m mouth diameter). Samples have been preserved by formol fixation (2.5%) buffered with borax (Sodium Borate) until saturation. Daily samples from each week were pooled in a single beaker to reduce variability due to small-scale spatial patchiness. In the present work, analyses were performed on samples obtained with the Juday-Bogorov net for the period 1974 to 2003 (30 years).

3.2 Environmental datasets

3.2.1 Stn MC

For the time series in the Gulf of Naples, water temperature, salinity and chlorophyll *a* (chl *a*) were analysed. During the whole studied period (1986-1990; 1995-2005), temperature and salinity were measured at 0.5, 2, 5, 10, 20, 30, 40, 50, 60 and 70 m depth. Before 1995, samples were taken with 5 L Niskin bottles and reversing thermometers. From 1995 a SBE911 CTD was installed on a Rosette sampler equipped with ten 12 L Niskin bottles. Chl *a* was determined, in samples collected at selected depths (0.5, 2, 5, 10, 20, 40 and 60 m), with a spectrophotometer until 1991 (Strickland and Parsons 1972) and from 1995 onwards with a spectrofluorometer (Holm-Hansen et al. 1965; Neveux and Panouse 1987). No information is available on methodological intercalibration. Chl *a* measurements at 40 and 60 m depths were integrated to obtain Chl *a* concentration at 50 m depth for homogenisation with temperature and salinity measurements.

3.2.2 Point B

The environmental data considered for analysis are listed in Table 3.1. Water temperature, salinity, chl *a* and nitrates (NO_3) were measured, once a week, at 0, 10, 20, 30, 50 and 75 m depth. Before 1991, temperature was measured with a reversing thermometer whilst salinity was estimated with an induction salinometer (details in Etienne et al. 1991). Since 1991, these parameters were recorded with a Seabird SBE25 CTD. Sampling methods were intercalibrated for both parameters. Chl *a* and NO_3 measurements started in 1991. Water was sampled with Niskin bottles and filtered onto 47-mm GF/F Whatman fiber filters. From 1991 to 2002, chl *a* was estimated with a spectrophotometer (Parsons and Strickland 1963) and since 2002 with a fluorimeter

(Lorenzen 1966) without any intercalibration between the two methods. NO_3 concentration was estimated using standard colourimetric techniques.

Local meteorology was provided by Meteo France. Atmospheric pressure, irradiance and precipitation were recorded daily at a station next to Nice airport (43°39'12"N, 7°12'00"E; 4 m above sea level; ~15 km from Point B). In the frame of the present work, wind measured at this station was detected to be biased by a change in the position of the anemometer in 1989. The bias consisted of stronger and more frequent north-western winds at the new location. Thus, measurements from the Cap Ferrat semaphore station (43°41'00"N, 7°19'42"E; 138 m above sea level; ~800 m from Point B) were analysed. Data from the Cap Ferrat semaphore station were interrupted from August 1991 until December 1996. Missing data for wind speed were estimated by Reduced Major Axis regression (i.e., model II regression) between the two independent variables, i.e., wind speed recorded at Nice airport from 1989 (after the anemometer relocation) and the one registered at Cap Ferrat (Fig.3.3). Both wind speed series which were obtained at different heights (u_h) were previously recalculated for a 10 m height above sea level (u_{10}) by applying the following formula proposed in engineering (Heier 2005):

$$u_h = u_{10}\left(\frac{h}{10}\right)^{0.11}$$

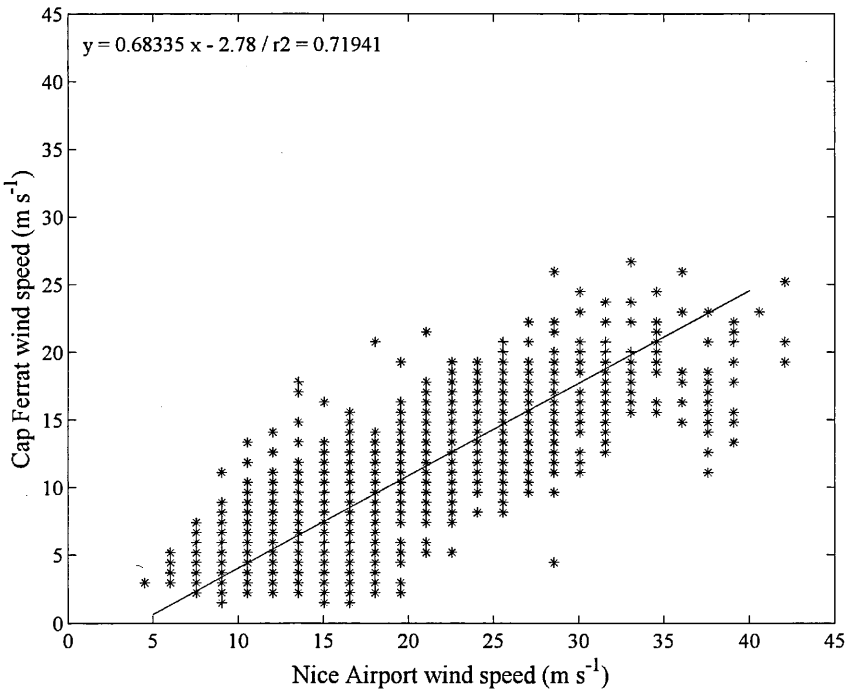

Figure 3.3 - Linear relationship (Reduced Major Axis regression, 5478 daily observations from 1989) between daily-maximal wind speed at Nice airport station (x-axis) and Cap Ferrat station (y-axis).

After the gap was filled, the Ekman depth was calculated from wind speed using the formula described by Cushman-Roisin (1994). The Ekman depth corresponds to the surface layer of the ocean set in motion by wind. It is not easy to determine as currents decrease exponentially with depth and the dispersion of wind energy depends on several variables including wind speed and persistence, and water density. To compute the Ekman depth, a different weight is given to the wind depending on its speed (u_{10}) using the drag coefficient (C_D) (Dupuis 1997):

$$u_{10} \leq 5 \text{ m s}^{-1} \rightarrow C_D = (11.7\, u_{10}^{-2} + 0.668)\, 10^{-3}$$

$$5 \text{ m s}^{-1} \leq u_{10} \leq 9 \text{ m s}^{-1} \rightarrow C_D = (0.019\, u_{10} + 0.978)\, 10^{-3}$$

$$u_{10} \geq 9 \text{ m s}^{-1} \rightarrow C_D = (0.07\, u_{10} + 0.600)\, 10^{-3}$$

Wind stress (τ) is estimated by the weighted speed including the air density (ρ= 1.22 kg m^{-3}):

$$\tau=\rho_a C_D u_{10}^2 \ (\text{Kg m}^{-1}\ \text{s}^{-2})$$

The Ekman depth includes wind stress, water density and the Coriolis force ($fcor = 10^{-4}(s^{-1})$) by the following formula:

$$E_D=0.4\left(\sqrt{\sqrt{\tau}\,\rho_a}\,/\,fcor\right)$$

Intercalibration of wind direction recorded at both sampling sites is not possible due to the different orographic condition of Nice. The airport area has an intense thermal wind which blows from south to north (i.e., from sea to land) during the day and in the opposite direction at night. Therefore, the 5-year gap remained in the wind-direction time series.

Point B station is mainly affected by easterly and westerly winds. Easterly winds accelerate the normal circulation which consists of a branch of the Ligurian Current entering the bay on its east side and exiting at a deeper depth on the west side. Westerly winds cause a reverse of this circulation pattern (Hentch 1959; Nival and Corre 1976). Instead of using the common approach of frequency of wind direction, which implies defining a speed floor and degree windows for each direction, in this work the approach used is the one applied by Licandro and Ibanez (2000) to estimate the East-West component of water currents. The parameter is estimated as follows:

$$\text{Wind Pattern} = \alpha \sin(\beta)$$

where α is the wind speed and β the direction. Wind Pattern weights wind speed by its direction, so that only very strong winds of North-South component are retained. The weak winds with directions close to 90 and 270 degrees (East and West winds respectively) were also erased. Wind pattern is driven by winds close to 90 or 270 degrees or by very strong winds, the main winds affecting Point B. To study the predominance of easterly or westerly winds, the monthly frequency of the (+) easterly component and of the (-) westerly component were calculated separately. To avoid taking into account the weakest winds, (-) values considered were below the first quartile of total wind pattern data (-4.4945), which corresponded to 59% of all – wind pattern values, and (+) values were above the third quartile (6.5712), constituting 43% of all + values.

Table 3.1 - Variables considered to depict the environmental conditions at Point B.

Variables	*Units*	*Frequency*	*Sampling site*
Temperature	°C	weekly	Point B
Salinity	_	weekly	Point B
NO_3	mg m^{-3}	weekly	Point B
Chl *a*	mg m^{-3}	weekly	Point B
Atm.Pressure	hpa	daily	Nice Airport
Precipitation	mm	daily	Nice Airport
Irradiance	minutes	daily	Nice Airport
Ekman depth	m s^{-1}	daily	Cap Ferrat
Wind pattern	m	daily	Cap Ferrat

3.2.3 North Atlantic Oscillation

The winter NAO (December-March mean value) is generally used to represent atmospheric perturbations in the Atlantic Ocean (see section 2.1.2 in chapter 2 for detailed information), and was also used in this thesis. Datasets were downloaded from www.cru.uea.ac.uk following previous work in the Mediterranean Sea (Molinero et al. 2005a; Fernandez de Puelles and Molinero 2007).

3.3 Phyto- and mesozooplankton microscopic counts from stn MC time series

Data on species composition and abundance from microscopic counts were available for the entire studied period only in the case of stn MC (e.g., Ribera d'Alcalà et al. 2004; Zingone et al. 2009; Mazzocchi et al. 2010). Identification and counts of zooplankton specimens were performed by Grazia Mazzocchi and Iole Di Capua at a

dissecting microscope on aliquots ranging from ¼ to $1/_{32}$, according to sample density. Subsamples were taken by using the Huntsman beaker subsampling technique (Van Guelpen et al. 1982) or, more recently, by using a large-bore graduated pipette. In these aliquots, all zooplankters were identified and counted, while the rest of the sample was checked for the presence of rare species. Copepods were generally identified to the species level and separated into females, males, and juveniles for the most abundant species (mainly copepodites III-V were retained by the 200 µm mesh). For *Clausocalanus*, *Oithona*, and *Oncaea*, all juveniles were attributed to genus, since it was arduous to distinguish copepodites among the numerous congener species occurring in the samples. For this thesis, 45 copepod taxa were considered for the studied period, 34 of them corresponding to species. All other zooplankton taxa were identified at the phyla, class, or order levels (i.e., chaetognaths, jellyfish, siphonophores, doliolids, salps, appendicularians, decapod larvae, ostracods and echinoderm larvae), and only the cladocerans *Penilia avirostris*, *Evadne* spp. and *Podon* spp. were identified at the genus or species level.

Phytoplankton samples were collected from the subsurface (0.5 m Niskin bottle). Samples were fixed with neutralized formaldehyde (0.8–1.6% final concentration). Phytoplankton microscopic counts were provided by Diana Sarno and Adriana Zingone. Cell counts were performed under an inverted microscope after sedimentation of variable sample volumes (1–100 ml), depending on cell concentration (Utermöhl 1958), on two transects representing ca 1/30 of the whole bottom area of the sedimentation chamber, at ×400 magnification. For selected species, the identification was checked under the electron microscope. Cells smaller than 2 µm, unless very abundant, were not counted. Species were gathered in four main groups, diatoms, coccolithophores, dinoflagellates and small phytoflagellates. To calculate the mean cell size of each group,

linear measurements were routinely taken on phytoplankton cells over 1 year of sampling and afterwards, occasionally, on selected samples for species that were rare or variable in size. A mean equivalent spherical diameter (ESD) was allocated to each species, and by multiplying each species ESD by its estimated abundance, a mean ESD was obtained for each of the four main groups.

3.4 The ZooScan mesozooplankton datasets: Data acquisition and processing

3.4.1 Image processing

For this thesis, zooplankton samples from both time series were analysed using the ZooScan. In the case of MC time series, monthly samples from 1984 to 1996 and from 2002 to 2005 were scanned by Carmen Garcia-Comas, and the period from 1997 to 2001 was scanned by Corinne Desnos. The Point B samples were scanned by four operators: from 1974 to 1983 samples were scanned by Océane Dahan; from 1983 to 1995 by Carmen Garcia-Comas; from 1996 to 2000 by Marine Gouezo; and from 2001 to 2003 by Fanny Chenillat. The operators' work was supervised by the author of this work, Carmen Garcia-Comas. The ZooScan is a digital imaging system recently developed in the Laboratoire d'Océanographie de Villefranche sur Mer (LOV) under the supervision of Dr. Gabriel Gorsky (Grosjean et al. 2004; Gorsky et al 2010). It provides standardised measurements of body size and abundance of several taxonomic groups contained in preserved zooplankton samples.

In this study, samples were analysed with the ZooScan prototype (Fig.3.4A). Since 2006 there is a new version (Fig.3.4B), it is commercialised by Hydroptic, and 30 machines are already in use in several laboratories around the world. Two of them are placed at LOV in Villefranche-sur-Mer and one at SZN in Naples.

The ZooScan system was conceived to achieve the construction of homogeneous, permanent and secure image data-banks that will allow global comparison of zooplankton series. Standardisation of image quality allows time series harmonisation, a key issue for monitoring plankton communities and understanding their responses to climate changes (Perry et al. 2004).

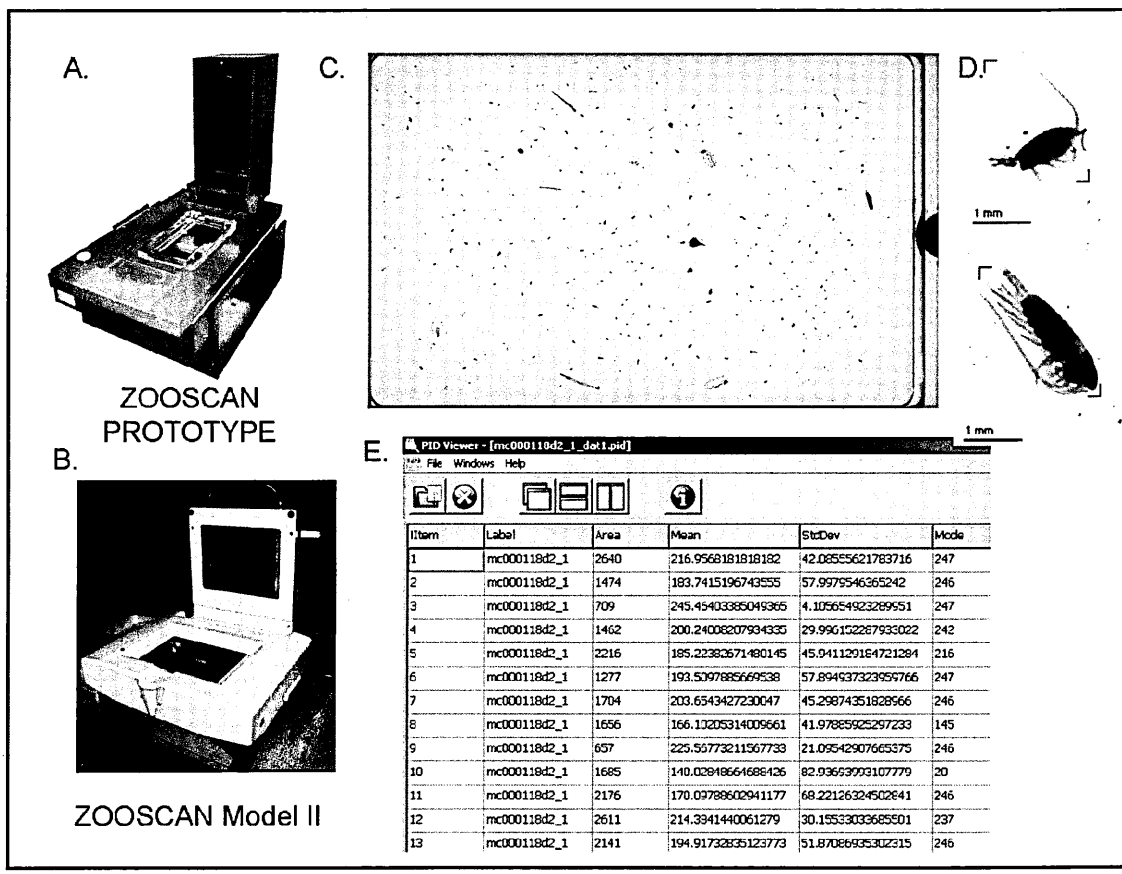

!Item	Label	Area	Mean	StdDev	Mode
1	mc000118d2_1	2640	216.9568181818182	42.08555621783716	247
2	mc000118d2_1	1474	183.7415196743555	57.9975546365242	246
3	mc000118d2_1	709	245.45403385049365	4.105654923289551	247
4	mc000118d2_1	1462	200.24008207934335	29.996152267933022	242
5	mc000118d2_1	2216	185.22382671480145	45.941129184721284	216
6	mc000118d2_1	1277	193.5097885669538	57.894937323956766	247
7	mc000118d2_1	1704	203.6543427230047	45.29874351828966	246
8	mc000118d2_1	1656	166.13205314009661	41.97885925297233	145
9	mc000118d2_1	657	225.55773211567733	21.09542907665375	246
10	mc000118d2_1	1685	140.02848664688426	82.93693993107779	20
11	mc000118d2_1	2176	170.09788602941177	68.22126324502841	246
12	mc000118d2_1	2611	214.3941440061279	30.155330336855501	237
13	mc000118d2_1	2141	194.91732835123773	51.870869353023315	246

Figure 3.4 - ZooScan and image process components: (A) The ZooScan prototype used in this work; (B) The new ZooScan model; (C) Raw image of a zooplankton sample scanned with the ZooScan; (D) Thumbnails of two copepods from the sample; (E) Pid file containing information on sample processing and all the objects' measured in the sample.

To check image quality and to achieve homogenisation of the images, parameterisation of scans is done using the *Vuescan* software, which allows different configuration files to be uploaded and keeps track of the configuration procedure applied to each image. Scanning information is kept in the header of the output file (the *pid file*) (Fig.3.4E). Scans are made at 8 bits (256 grey level values), image resolution is

of 2400 dpi (i.e., dots per inch) and thus each pixel is equivalent to 10.58 μm (1 pixel = 25.4 mm/resolution; being 1 inch equal to 25.4 mm).

Zooprocess software controls the whole ZooScan processing, from the image scanning to the acquisition of the data matrix. *Zooprocess* has been created at LOV using the *Image J* macro language. It includes multiple tools for image processing, which are summarised in Table 3.2. More information on the ZooScan can be found on the website http://www.zooscan.com/.

Table 3.2 - List of principal Zooprocess functions.

ZOOPROCESS main functions
Scanning and storing images
Converting images for calibration
Scanning and processing an image
Processing images in batch mode
Computing basic statistics on the variables
Outlines for object delimitation and separation process of organisms touching
Objects selection by size or taxonomical criteria for thumbnail extraction

Almost one sample per month (the closest to the 15th day) was analysed for each time series. The stn MC original time series consisted of 192 samples covering 190 months for the periods 1984-1990 and 1995-2005. Only 6 and 4 months were scanned for 1984 and 1985, respectively, because some samples were not available anymore, and annual peaks were missed in both years. Thus, the dataset utilized in this thesis for MC time series starts in 1986 instead of 1984. In the case of Point B, 359 samples were scanned, covering 345 months of the 1974-2003 period. For 15 discontinuous months

no samples were available for scanning, and for some months more than one sample was scanned to validate outlier values.

Before scanning, to avoid underestimation of large organisms which are much rarer than the small ones, each sample was sieved with a 500 μm sieve. As a result, 2 size-fractions named d1 (with organisms > 500 μm) and d2 (with organisms between 200-500 μm) were obtained. Each size-fraction was split several times with a Motoda-box (Motoda 1959) until the subsample was diluted enough to allow separation of all the organisms in the scanning tray. This is a critical step to obtain reliable size measurements and taxonomic identification. When objects are too numerous in the scanning tray, they can touch or overlap and be detected as a single object, creating a bias in the size spectrum and/or taxonomic recognition. As the sample is split in two fractions, two images (Fig.3.4C) were processed separately for each date.

From the process of each image, a *pid* file was created. The *pid* file (Fig.3.4E) is an ascii file that contains: 1) a header, consisiting of the metadata with all the information on the scanning parameters and sample processing as well as the log file of sampling at sea, and 2) a table, with rows that correspond to the enumerated objects of the scan, and 32 columns; the first two columns represent the unique label of an object which are the number in the original image and the name of the image, and the other columns correspond to the variables computed by *Zooprocess* to describe each object. They refer to the position of the object in the tray, its size and shape, and to the grey level distribution in the object (see Table 1 in Appendix I for list of parameters).

3.4.2 Taxonomic automatic recognition

Both time series datasets sum up around 1000 raw images with about 500-1000 objects per image. An automatic classifier to facilitate the object recognition process was set up following a supervised-learning methodology. By the supervised-learning (steps outlined in Fig.3.5) it was possible to study both copepod time series, in terms of abundance and size, gathering a large amount of data in a much shorter time than with traditional microscopy methods, and in a standardised fashion.

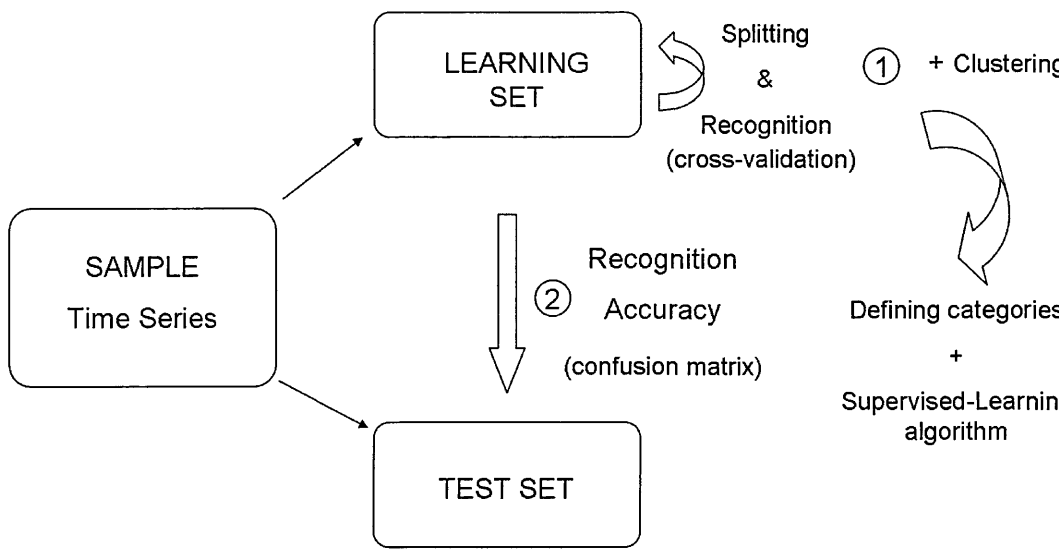

Figure 3.5 - Flow chart representing the supervised-learning recognition process. A two-step process was carried out. Firstly, a learning set was used to create the model (e.g. category definition and algorithm choice), and then the model was tested with an independent test set which represented the sample.

Creation and development of the automatic classifier was done with *Plankton Identifier*, an interface created by Dr. Gasparini that uses functions of the free data mining software Tanagra (Rakotomalala 2005), and that incorporates some new variables (Table 2 in Appendix I) based on the original ones computed by *Zooprocess*. In total, 28 variables are available for the classification of the objects; 12 are based on grey level measurements, 10 on size and six provide information on the shape of the object.

Step 1. Learning set: Defining categories and supervised-learning algorithm

In supervised-learning mode, a learning set, which is a collection of object thumbnails (Fig.3.4D) arranged in different categories, acts as a reference. The automatic classifier sorts an object (i.e., organism or detritus) into a certain category (e.g., copepod) depending on the values of the parameters describing the object, and on the distribution of those parameters in each category represented in the learning set. The learning set used for this study was composed of 13,100 objects randomly picked from 8 non-consecutive years of the Point B time series. All years and months were equally represented to avoid biases due to temporal changes of the zooplankton community. The learning set accuracy was similar when tested on Point B and MC samples, and thus it was not necessary to build another learning set with MC samples. The original classification of the learning set consisted of 45 categories, 8 of which described different types of detritus, as these were very abundant and diverse.

To obtain a good supervised-learning model, the learning set must be a random sub-sample of the studied sample, in this case the time series, and categories must be balanced in terms of abundance (Kotsiantis 2007). A random zooplankton learning set as the one here created is always unbalanced. Organisms have very different concentrations in nature and many of them follow a seasonal pattern. Usually copepods dominate marine zooplankton, although in certain months they can be outnumbered by other categories that have very high seasonal peaks, such as the cladoceran *Penilia avirostris* in August in both studied time series. In an unbalanced learning set as the one used here, dominant taxa can usually be well recognised due to proper representation of their intra-category variability, and due to the relative low abundance of similar categories that could be misidentified as part of the dominant category. On the contrary, the abundance of rare categories tends to be overestimated due to contamination by

similar wrongly identified objects of a more abundant category. In addition, rare objects can be easily misidentified if the category has high intra-category variability that is not fully represented by the few objects represented in the learning set.

The learning set recognition accuracy can be improved by merging original categories that present high cross-contamination in their classification. The recognition accuracy varies also depending on the algorithm used for classification. Seven supervised-learning algorithms are available in *Plankton Identifier*: k-nearest neighbour, linear and RBF Support Vector Machine (C-SVC), random forest, Decision Tree C 4.5, Multinomial Logistic Regression with a Ridge estimator, and Multilayer Percertron neural network. All supervised-learning algorithms were tested on several clusters of the original 45 categories. Categories were iteratively associated according to the results of confusion matrix and Hierarchical Cluster Analysis performed on the categories. At each step of clustering, performances of the supervised-learning algorithms were compared, and the ecological significance of the categories was taken into account before merging.

The confusion matrix (Fig.3.6) is a contingency table in which rows refer to manual classification (observation, Y) and columns refer to the automatic classification (supervised-learning prediction, $\hat{Y}$) and thus it provides information on the performance of the applied algorithm and also on the similarity (by mixing) of the categories. It was issued from a cross-validation (2 folds, 5 trials) applied on the learning set. One fold of the learning set recognized the objects of the other fold, the operation was repeated 5 times, and recognition results were summed up and represented in the confusion matrix.

F=False; T=True

Y=Observation

$\hat{Y}$=Prediction

N+ = category objects

N-=other objects

Y \ $\hat{Y}$	+	-	Total
+	T^+	F^-	N^+
-	F^+	T^-	N-
	$T^+ + F^+$	$T^- + F^-$	N

Accuracy rate= $(T^+ + T^-)/N$

Error rate= 1-AR= $(F^+ + F^-)/N$

Recall= TPR= T^+/N^+

FPR= F^+/N^-

Precision= $T^+/ T^+ + F^+$

Figure 3.6 - Example of a confusion matrix of just 2 categories (to be part of the category +, or others -), with observations (Y) versus predictions ($\hat{Y}$).

From the confusion matrix, one can calculate accuracy rate and error rate, but both of them are dependent on the proportion of organisms representing a category with respect to the total objects constituting the learning set (N+ / N). Two independent accuracy metrics were considered to rate the classifier: recall and 1-precision. Recall (true positive rate) is the rate of objects correctly classified in a category among the objects which actually belong to that given category. The 1-precision value is the rate of objects wrongly classified among objects which are assigned to that given category (i.e., rate of contamination).

The process to improve the learning set was terminated when the best trade-off between the number of distinct categories and error rates was reached. The final classifier consisted of 26 categories, and the algorithm showing the best performance was the Random Forest algorithm. This algorithm has already been tested and proved to be efficient for zooplankton image recognition (Grosjean et al. 2004; Bell and Hopcroft 2008). The Random Forest algorithm (Breiman 2001) consists of performing several random trees, in this case 100, where every knot is a question on the value of a variable (descriptor), and every branch is a batch (category or class to belong to). These random trees are not pruned (e.g. all the branches are relevant), and each of them is computed

by using just a random subsample of the learning set by bagging (bootstrap aggregating) and a random part of the total descriptors. The decision of the category to which an object belongs depends on the mode of the 100 replicates. The algorithm 'decides' the most probable category to belong to depending on the times the object was classified in that category during the whole batch of trials.

The original learning set (45 categories) presented a total error rate of 0.41 (see Table 3 in Appendix I) while the error of the definitive learning set (26 categories) was reduced to 0.23. Of the 26 definitive categories, 15 referred to taxonomic groups, and for some of them the recognition performance was quite high (Table 4 in Appendix I, top-ten categories in Table 3.3). The 'Copepoda' category gathered all the copepods and had a very high recognition rate. This good performance was due to the fact that the category is quite homogeneous in terms of grey level, size and shape and that its proportion in the learning set was very high (41% of the total learning set, Table 4 in Appendix I).

Table 3.3 - Top-ten recognised categories with their respective accuracy rates, as well as the number of objects, in the final learning set of 26 categories classified with the Random Forest algorithm.

Categories	Recall	1-Precision	Abundance
Copepoda	0.96	0.19	26840
Appendicularia	0.87	0.22	4861
Appendicularian tail	0.85	0.08	530
Pteropod *Cavolinia* spp.	0.81	0.18	870
Gelatinous Zooplankton	0.81	0.25	4210
Chaetognatha	0.77	0.12	1020
Cladoceran *Penilia*	0.71	0.29	1475
Cladocera (others)	0.66	0.38	1850
Jellyfish *Aglaura hemistoma*	0.64	0.19	450
Decapod larvae	0.48	0.31	2590

Step 2. Test set: Validation of recognition accuracy

Accuracy rates on the learning set alone tend to overestimate the true recognition performance on the whole time series. This is due to misrepresentation of the whole natural variability of some categories. Therefore, to validate and to quantify the recognition accuracy of the classifier, a test set was created. A test set must be a random independent subset of objects from the sample, in this case the time series (Dundar et al. 2004), and must be different from the learning set (data not shown) and representative of the whole time series. To check if there were recognition biases produced by temporal changes of the zooplankton community, four test sets were built (each of them with about 600 objects). The test sets represented all the months of different years. One of these test sets was produced with objects of a year belonging to the MC time series. Objects were sorted in the same 26 categories defined in the learning set. The recognition accuracy of the classifier was very different on the four test sets for all categories except copepods (Table 3.4). This was mainly due to low representation of some categories which generates statistical weakness because of unbalanced abundances and high intra-category variability. Consequently, it was not possible to assert a percentage of recognition that would account for the whole time series. To reduce the possible statistical weakness due to low representation of some categories in the test sets, a final test set was created by summing up all the single sets (named here super test set). It consisted of 2500 thumbnails sorted into the 26 categories.

Table 3.4 - Performance of the learning set on the several test sets.

	PointB_Test1			PointB_Test2			PointB_Test3			MC_Test set			Super Test Set		
	Recall	1-Precision	Abundance	Recall	1-Precision	Abundance	Recall	1-Precision	Abundance	Recall	1-Precision	Abundance	Recall	1-Precision	Abundance
Copepod	0.95	0.12	239	0.90	0.19	264	0.90	0.17	303	0.97	0.18	380	0.96	0.18	1186
Appendicularia	0.68	0.24	20	0.30	0.50	11	1.00	0.71	5	0.69	0.62	17	0.77	0.55	53
Appendicularia tail	0.89	0.11	8	0.90	0.18	10	0.00	1.00	0	0.85	0.21	13	0.94	0.31	31
Chaetognatha	0.71	0.58	7	0.92	0.19	23	0.50	0.57	6	0.61	0.21	18	0.75	0.37	54
Pteropoda Cavolinia	0.50	0.89	2	0.00	1.00	0	0.75	0.57	4	0.00	1.00	0	0.83	0.84	6
Gelatinous Zooplankton	0.42	0.69	12	0.67	0.50	14	0.78	0.56	6	0.53	0.67	19	0.65	0.70	51
Cladocera Penilia	0.00	1.00	0	1.00	0.80	1	0.56	0.25	17	0.35	0.33	17	0.54	0.47	35
Cladocera	1.00	0.50	3	0.25	0.50	4	0.47	0.47	20	1.00	0.43	8	0.74	0.54	35
Jellyfish A. hemistoma	1.00	0.75	1	0.00	1.00	0	1.00	0.00	2	1.00	0.33	2	1.00	0.17	5
Decapoda	0.00	1.00	5	0.42	0.41	31	0.33	0.60	6	0.53	0.32	49	0.48	0.46	91
Total (26 groups)			530			621			623			750			2524

From the confusion matrix of the learning set versus the test set, it was observed that the Random Forest recognition accuracy was very satisfactory for copepods; 96% of copepods were recognised (recall) although 18% (1-precision) of the category was actually contamination. Accuracy was less good for the other categories (Table 5 in Appendix I, recognition rates of top-10 classified categories in Table 3.4). Therefore, copepods were automatically recognised in the monthly samples, while some other zooplankton categories were sorted by semi-automatic recognition.

3.4.3 Taxonomic semi-automatic recognition

Semi-automatic recognition consists of manually sorting objects after a fast pre-sorting by automatic recognition. The five other sorted categories were large copepods, chaetognaths, jellyfish, siphonophores and decapod larvae. Large copepods were sorted to check if changes in the copepod size distribution could be due to changes in the proportion of typical offshore species, usually rare and with large body size. The interannual variability in the other zooplankton groups can help in the ecological interpretation of copepod temporal patterns in the time series. Furthermore, these groups were not very abundant and so their semi-automatic sorting was feasible. To avoid revisiting all the thumbnails of all the objects of the two long time series, a size-

threshold, above which objects could belong to any of the target groups, was determined. Only thumbnails above the 0.32 mm^3 of ellipsoidal volume were checked and re-sorted if classification was wrong. This size threshold corresponds to copepods about 1.5 mm long. In the case of colonial siphonophores, only the first bell was taken into account and considered as a single individual.

A parallel time series of microscope taxonomic counts exists only for the MC time series. To help in the interpretation of the results of the Point B time series obtained with the ZooScan, all organisms from samples in 1979, 1985, 1995-1997 and 2003 years were semi-automatically identified. These years were selected according to the hypotheses formulated after detecting changes in abundance, size of copepods and environmental conditions. Copepods were classified into 7 groups: *Oithona spp.*, Poecilostomatoida (i.e., oncaeids, corycaeids, *Farranula*), *Centropages* spp., *Temora stylifera*, *Acartia* spp., other Calanoida (most of them *Paracalanus* spp. and *Clausocalanus* spp.) and offshore calanoids (i.e., genera belonging to the following families (Mazzocchi, pers.com.): Aetideidae, Augaptilidae, Calanidae, Candaciidae, Eucalanidae, Euchaetidae, Heterorhabdidae, Lucicutiidae, Scolecithricidae). Other zooplankton groups considered were: Appendicularia (i.e., *Oikopleura* spp. and *Fritillaria* spp.), *Penilia avirostris*, and other Cladocera (i.e., *Podon* spp. and *Evadne* spp.). In addition, the calanoid copepod *Calanus helgolandicus* was sorted from all the samples of the Point B time series.

3.4.4 State of the art of the ZooScan

The data presented herein were fully produced with the ZooScan prototype, and related software (i.e., Zooprocess and Plankton Identifier). Both the instrument and software were improved during the course of this project. The methodological results obtained in this thesis helped to their development, and continuous feedbacks were

exchanged, with the members of the LOV dedicated to the ZooScan, to implement an integrated system. Images of the new ZooScan version are of better quality, and the image treatment is more complete and user-friendly.

Imaging technology in zooplankton research is still under development. With the new ZooScan, automatic recognition performance has already been improved for several taxonomic groups due to better image quality and the addition of new variables to better describe and so differentiate the zooplankton groups. These new features are: the coarseness and the cumulative histogram of the grey level of an object as texture descriptors, and the convexity, symmetry and thickness as shape descriptors (Santos Filho et al. in preparation). Although efforts to automate plankton identification have been undertaken since decades (Benfield et al. 2007), the automated methods show relatively low zooplankton classification efficiency (Bell and Hopcroft 2008; Fernandes et al. 2009). The huge intra-category variability and high imbalance of abundances in natural samples continues to limit the fully automatic classification of zooplankton samples, and thus validation by semi-automatic recognition is highly recommended (Gorsky et al. 2010).

Currently, ZooScan is commercialised by Hydroptic (www.hydroptic.com) for a price of 18,000 euros. The ZooScan is already used in 27 laboratories around the world, and the basis for a standardised methodology has been stated (Gorsky et al. 2010). In the ZooScan website (www.zooscan.com) users can find all the free programs, research advances and a complete ZooScan manual. In addition, under the framework of this project, a user-friendly manual was produced (Appendix II) and can be downloaded by anyone from the ZooScan website. The manual was produced as an output of this PhD project to help beginners to use the ZooScan independently, following the protocol stated at the LOV (Gorsky et al. 2010). With this working protocol, currently around 20

digital images are produced and fully validated (i.e. abundance and size of ~ 15-30 taxonomic groups) by a single person during a 5-day work (~35 hours) in the laboratory of Villefranche-sur-Mer.

3.4.5 Size Structure Analysis

Once copepods were sorted, their size distribution, which represents the core of this thesis, was explored. Three size variables were retained: the area of the object, and the major and minor axes of the best fitting ellipse. These size variables were previously transformed from pixels to millimetres (1 pixel = 10.58 μm). The sample dataset also incorporates another vector containing the automatic recognition of the objects.

The major axis of a copepod can be taken as the total copepod length (a one-dimension descriptor) that can be converted to prosome length, which is generally used by taxonomists in species description. The length does not represent accurately the real size of copepods, because species differ in length: width ratios. Thus length alone does not provide a proper estimate of copepods in terms of energy source and prey-predator interactions. To have an estimate of plankton productivity, ecologists use plankton biomass or biovolume as currency.

Zooplankton biomass or biovolume can be determined by numerous methods. There are conventional methods such as the settling volume, displacement volume, wet and dry mass, and free-ash dry mass. In addition, there are biochemical methods, such as the organic carbon measurement to quantify the organic biomass, and the ATP quantification as an approach for energy content. Conversion equations have been defined by several authors to relate results from these very different approaches (Harris et al. 2000). Copepod biovolume could be transformed into biomass by conversion factors between zooplankton volume and carbon content (Wiebe 1975; Wiebe 1988; Alcaraz et al. 2003; Cushing et al. 1958). Recently, relationships between copepod

body size measured on the ZooScan images and C and N body content have been formulated (Gorsky et al 2010).

In size structure research, any object is generally described as a sphere of equal volume to be able to relate objects of different shapes by the diameter of the computed sphere (Jennings and Parlslow 1988). This diameter is called the equivalent spherical diameter (ESD) and it can be computed from a sphere with a projected cross sectional area (CSA) equal to the measured area of the object. Then, assuming the object to be a sphere, volume is computed as $4/3\pi(ESD/2)^3$. For copepods, which are mostly elongated with a shape better represented as a spheroid than as a sphere (Herman 1992), the computed volume by ESD is overestimated due to a higher ratio volume: CSA for spheres than for other shapes (Sprules et al. 1998; Beaulieu et al. 1999). Therefore, in this study the major (M) and minor (m) axes were used to calculate copepod biovolume following the formula for a prolate spheroid, an ellipsoid with equal equatorial radii (m):

$$\text{Ellipsoidal Biovolume} = 4/3\pi\ (M/2)\ (m/2)^2$$

When comparing ESD volume and ellipsoidal volume estimates, it appears that copepod volume is overestimated by ~ 30% when considered a sphere (slope of 0.7 between ESD and ellipsoidal volume datasets) (Fig.3.7). Sprules et al. (1998), in their calibration of an optical plankton counter for fresh water systems, found a relationship between equivalent circular diameter (ECD) volume and ellipsoidal volume of 44%. The difference between the two measures was higher than in our work probably because in their study it was calculated not only on copepods but on the total zooplankton of a lake, meaning a wider range of shapes and sizes. Regarding the relationship of these two measures on the copepods analysed with the ZooScan, there is a progressive higher deviation from the linear relationship as copepods are larger (Fig.3.7). A bias due to the

increasing relevance of appendages (e.g. antennulae and legs) in the body volume estimate with increasing body size, as well as contamination by overlapping copepods or other misidentified large objects could explain this larger residual at greater copepod size. In those cases, the shape of the object may not be properly represented by a spheroid as is the case for a regular copepod. Yet, large objects are rare when considering the whole copepod bulk. In the studied time series, only 0.09% of copepods were larger than 2 mm^3.

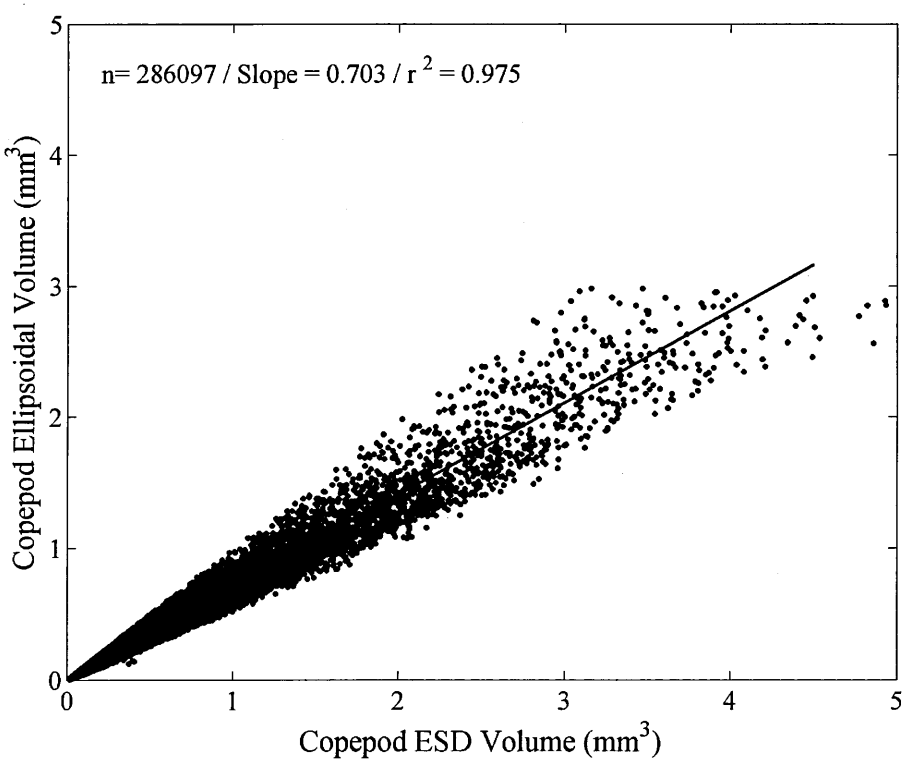

Figure 3.7 – The ESD volume (mm^3) and ellipsoidal volume (mm^3) relationship for the whole ZooScan dataset (286,097 copepods belonging to both time series).

Copepod size distribution is skewed to the left in both time series (Fig.3.8) due to a progressive increase in abundance with body size decrease (e.g., inverse allometric relationship, Elton 1927). Yet, the mode is a bit less skewed to the left due to abundance underestimation of copepods smaller than the net mesh size (i.e., net capture bias). This feature was taken into account later when computing synthetic variables describing the size distribution. The peak of the Point B dataset is slightly more skewed to the right as the net used in this sampling station is of 330 μm mesh size whereas for stn MC it is of 200 μm.

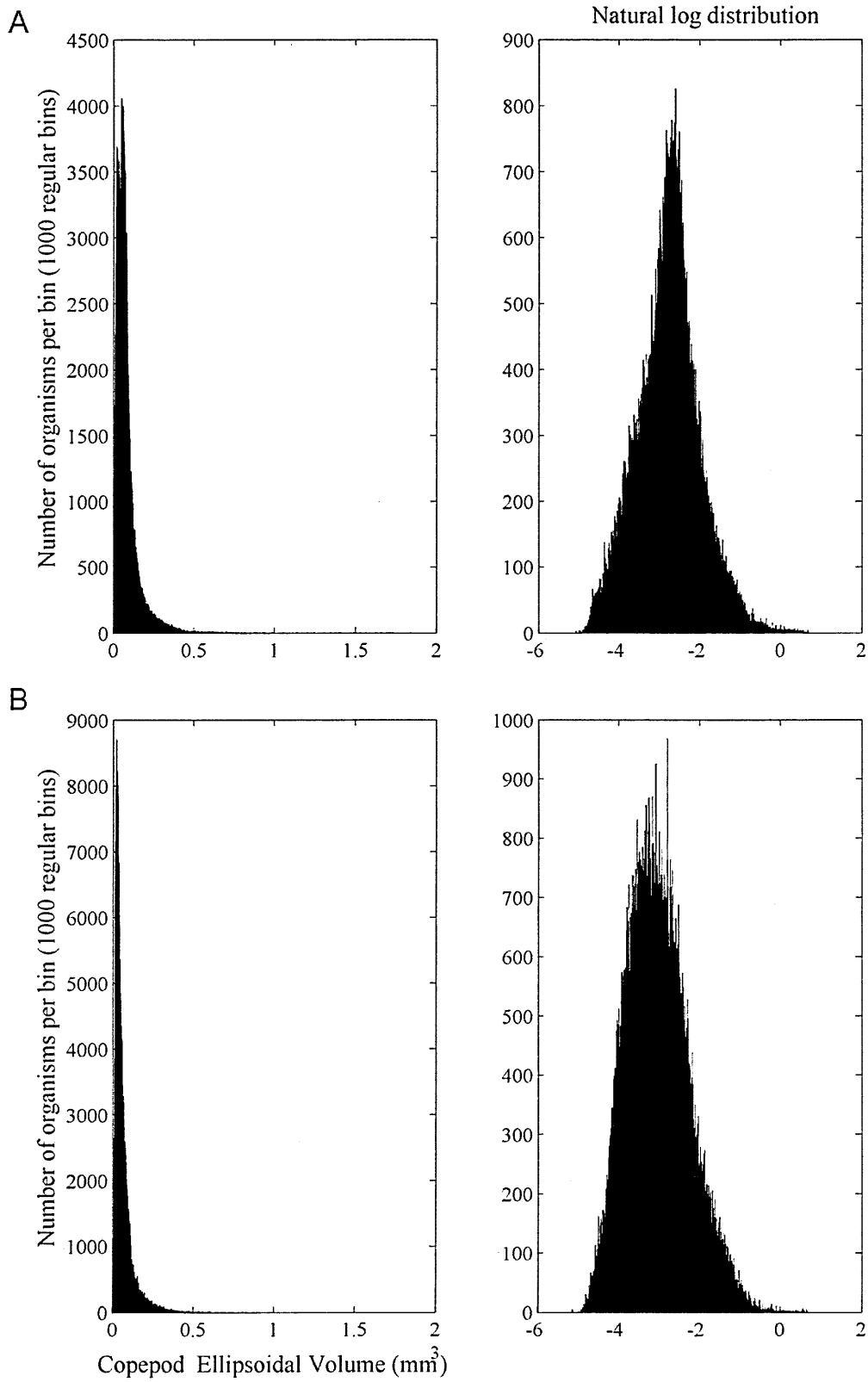

Figure 3.8 - Copepod size distribution (ellipsoidal biovolume) of (A) Point B time series (359 dates) and (B) stn MC time series (192 dates). Both histograms are cut at 2 mm^3 upper level (99% of copepod community) to zoom on the dense part of the size distribution. On the x-axis the individual biovolume (1000 size classes), and on the y-axis abundance. Left panels represent the time series histograms, whereas right panels represent them at a natural logarithmic scale.

From the individual copepod ellipsoidal biovolume, the copepod community could be monitored by computing its mean body size as a synthetic descriptor. Yet, despite being very useful for the detection of changes, it cannot provide information on the internal variations in the copepod size distribution. The same mean value could represent very different size distributions. A mean size change could be driven by very few individuals (extreme values) or by the majority of copepods (the dense part of the distribution). To monitor temporal changes of the copepod size distribution in both time series, data were arranged in the form of comparable size spectra.

How to build a size spectrum

Acquisition of size data from nature is performed in a discrete way, which leads to a discrete function constituted of individual sizes (Blanco 1994). To overcome this sampling limitation, a size spectrum is built by sorting the organisms into size classes that have been previously defined. As a result of this clustering by size classes, a histogram representing the number of organisms belonging to each size class is obtained (Fig.3.8). The histogram can be studied as a continuum in its linear logarithmic form.

The above histograms contain 1000 size classes (Fig.3.8), too many to be able to interpret their changes. Determining the size classes plays a major role in the shape and interpretation of size spectra. A size spectrum formed by size classes of equal width presents a progressive increasing variability towards larger size classes (Fig.3.9). This effect is due to the intrinsic community size-distribution. The deviation from the mean size of a size class is proportional to it, thus large copepods have wider size variability than small ones. In other words, the larger the organisms are the wider a size class must be to have a proper representation of those organisms (Blanco 1994). For this reason, it is recommended to build a spectrum of geometrical scale, which means that each size class is proportionally wider than the previous one. In particle size-spectrum analysis an

octave-scale (a geometric 2^n series) has been applied since the first description of particle-size distribution in the ocean (Sheldon et al. 1972). This scale allows size classes to be defined by the entire base of the logarithmical scale, and the width of a size class corresponds to its lower limit (Blanco 1994).

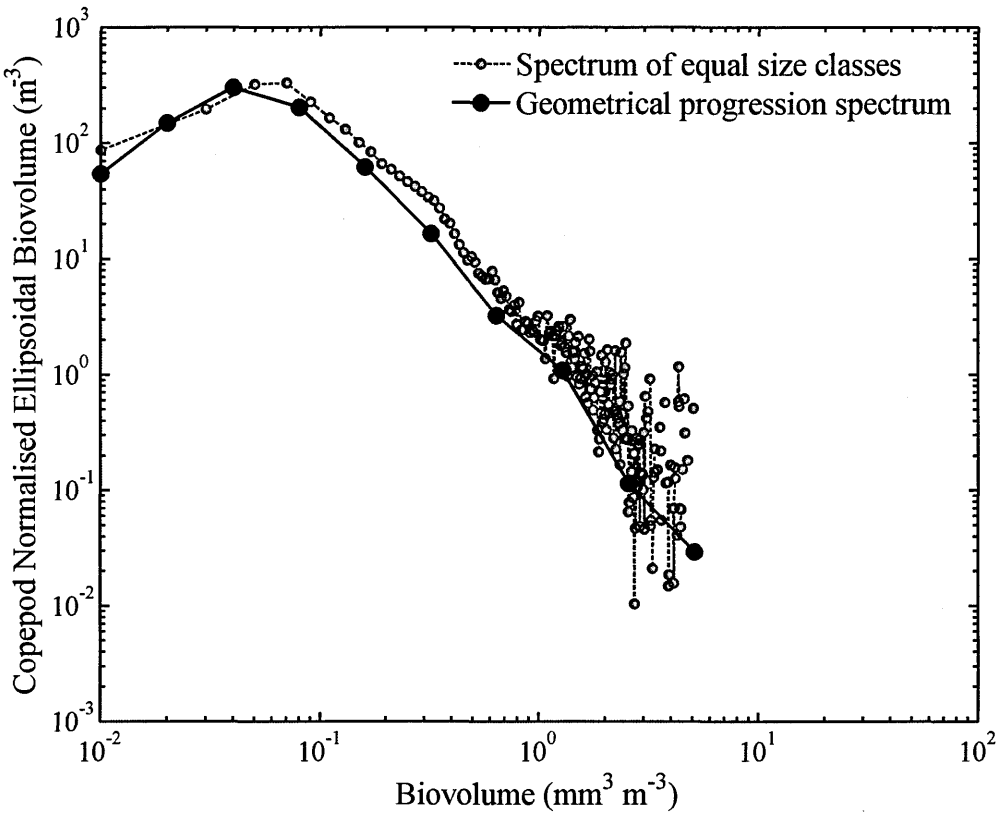

Figure 3.9 - Mean size spectra of the Point B copepod time series. A spectrum of equal size classes (0.02 mm^3 width) (grey dotted line) and an octave-scale spectrum (black line). Both spectra are normalised by the width of the size-classes and represented on a logarithmical scale.

Size spectra of the present study were built by arranging ellipsoidal volume in size classes of octave-scale amplitude. From the preliminary exploration of both datasets (Fig.3.8), the lowest limit was established at 0.01 mm^3, which roughly corresponds to small copepods of ~ 450-µm length, and from this lowest limit size classes were progressively wider (x2) up to the uppermost limit of 10.24 mm^3 volume, which corresponds to a ~ 4.5-mm length copepod (Fig.3.10). The equivalent limits in

prosome length were calculated by transformation from the 2.3 major : minor ratio (mode value) of all copepods measured (size class lower limits in Table 3.5).

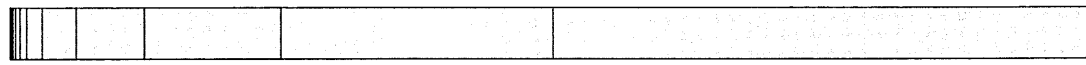

Figure 3.10 - Biovolume spectrum of octave-scale progression built to arrange the copepod-volume data of both time series. The lowest limit is 0.01 mm^3 and the highest limit is 10.24 mm^3.

Copepod ellipsoidal-biovolume spectra were normalised by multiplying the number of copepods in a size class by its nominal size (i.e., the size representing each size class) and then dividing the resulting biovolume by the width of the size class (Platt and Denman 1977). Copepods belonging to a certain size class are assumed to have the same size, the nominal size, which has to be defined. Depending on the choice of nominal size, the height of the size spectrum slightly varies. The nominal size can be the lower limit of the size class, its geometric or the arithmetic mean size as well as the size to best fit the continuous function of the spectrum. The last option has been proved to be the best choice (Blanco 1994). Yet, in the present work, the nominal size was the geometric mean of the size class (third column in Table 3.5), assuming that copepods in each size class had a Gaussian size distribution. The geometric mean was chosen for its simple calculation and its wide-spread use in size spectrum analysis. The normalization procedure of dividing the biovolume contained in a size class by its width resulted in comparable biovolume among the size classes. Furthermore, the equality of width and lower limit of each size class made the spectra very similar to the corresponding abundance size spectra (Platt and Denman 1977). Spectra built in this work by following the above procedures are named Normalised Biovolume Size Spectra (NB-S Spectra).

Building the spectra following Platt and Denman' methodology allows results from other studies to be compared (Boudreau et al. 1991; Kimmel et al. 2006; Sourisseau and Carlotti 2006a). And, although spectra based on carbon are somewhat steeper than those based on biovolume (Quinones et al. 2003), estimates of the C content corresponding to each nominal biovolume of the size spectra were calculated for further comparisons with other studies. Carbon body content was estimated from a linear regression equation obtained from a comparison of the ellipsoidal biovolume of fixed sample images with the C content in the same fresh samples, and successive transformation to C content in fixed samples. Zooplankton samples used in this study came from the western Mediterranean and contained mostly copepods (65% of copepods in total samples, regression calculated in the <5mm size fraction) (Cushing et al. 1958; Wiebe 1975; Wiebe 1988; Alcaraz et al. 2003).

Normalised Biovolume Size Spectra (NB-S Spectra) mode position due to net capture bias

The spectra analysed in this work show a dome-like pattern due to net capture bias of the small-size fraction. The size class from which net capture is unbiased was determined by calculating the mode of the maximum volume in each time series spectra. Biovolume of size classes above it, on the right of the mode, are well estimated, whereas size classes below the mode, on the left, are underestimated due to a strainer effect (i.e., organisms passing through the net mesh). The mode is situated mostly on the 3rd bin (lower limit = 0.04 mm^3) of the Point B NB-S spectra, whereas, in the case of MC time series, it is distributed between the 2nd and the 3rd size classes (Fig.3.11). This difference between the two time series is due to the smaller mesh size used at stn MC. A single mode was chosen, i.e., the 3rd size class for both time series, to keep homogeneity between time series.

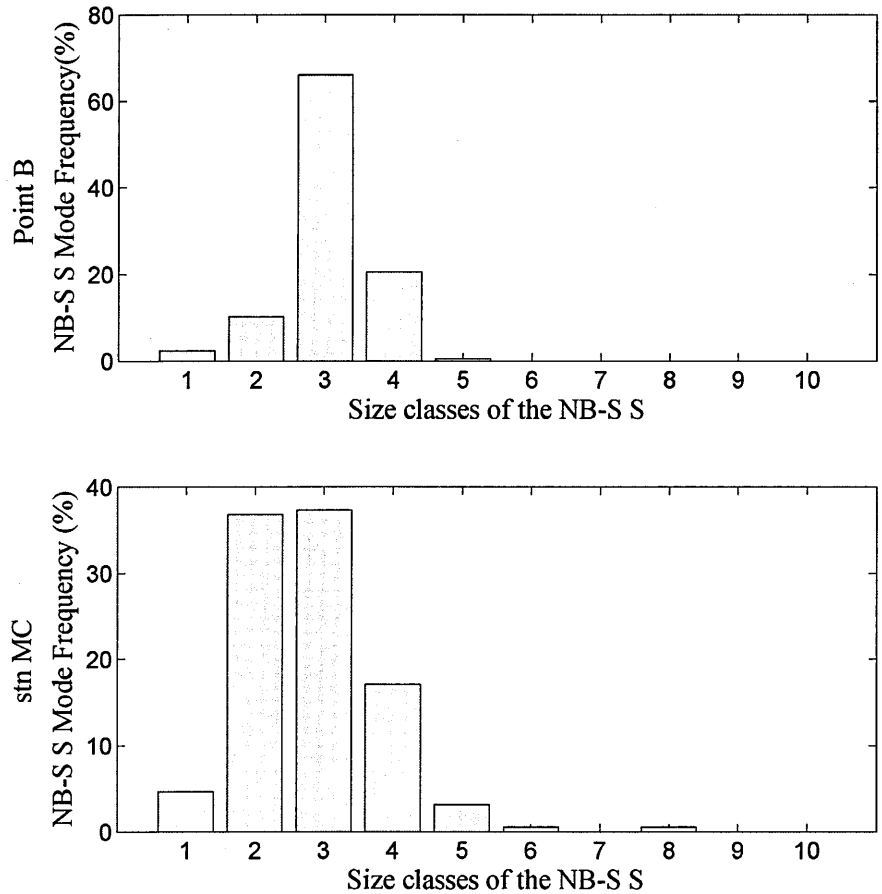

Figure 3.11 - Frequency of mode position (y-axes) in the size classes (x-axes) of Point B (upper panel) and MC (lower panel) time series.

Synthetic descriptors of the NB-S spectra

Slope of the NB-S spectrum

The slope that defines the linear relationship (type I regression) between the logarithm of the normalised biovolume and the logarithm of the size classes is the most used index to characterize size spectra, and is expected to be close to -1 (Platt and Denman 1977; Platt 1978; Rodriguez and Mullin 1986; Duarte et al. 1987; Blanco et al. 1994; Huntley et al. 1995; Quinones et al. 2003; Zhou 2006). The slope represents the flux of energy along the size classes. A system characterised by steeper (more negative) slopes will be a less efficient system in terms of energy transfer (Platt and Denman 1977; Platt 1978).

Despite its wide acceptance, this index presents some limitations. Two communities could show the same slope and yet have a different production. In the case of equal slope the production of the system is reflected by the height of the regression y-intercept (Sprules and Munawar 1986; Quinones et al. 2003). Moreover, the slope tends to be mostly modified by its extreme values, the minimum and maximum size classes. The smallest organisms have more peaks and troughs in their abundance, due to seasonal reproduction peaks, while the largest copepods are rare and their occasional occurrence can modify the slope in unpredictable ways. In addition, contrary to the linearity assumption of the model, usually spectra are not linear, and therefore the slope is not the best representation of them. Instead, some authors have proposed probability density functions to characterise the spectra (Vidondo et al. 1997; Brucet et al. 2006; Quintana et al. 2008), but the output variables of these functions are difficult to ecologically interpret. Non-linearity can arise from a system far from equilibrium (Sourisseau and Carlotti 2006a), can result from the propagation of a peak of biomass or energy through the system, or it can simply be due to methodological artefacts (Garcia et al. 1994; Sourisseau and Carlotti 2006b).

Although the slope calculation would be more exact from the mode (Garcia et al. 1994), in this thesis it was considered that abundance underestimation below the mode is constant and so changes in those size classes would have followed similar trends to changes in the sea (qualitative data). Therefore, to avoid any loss of information on the first size classes the slope was computed on the whole spectrum.

Size-spectrum diversity index

Due to the limitations of the linear model (the slope) to fully represent the NB-S S, another index was calculated to describe the normalised biovolume size spectra. This is the Shannon-Wiener index (Shannon and Weaver 1948) applied to define the diversity of the size classes constituting a spectrum (Parsons 1969; Ruiz 1994). This index is based on information theory and measures the entropy of the distribution:

$$H' = \sum_{i}^{S} p_i \log_2 p_i$$

where H' is the Shannon index, and p_i is the probability that an organism belongs to a certain size class (e.g., the frequency of each size class). The higher the index is the more equilibrated the size classes are. This index does not respect the size-class sequence; instead its calculation is made on the frequencies of each size class. The two first size classes do not reach their natural environment abundances (the highest of the spectrum) in the net samples, and thus their contribution to the Shannon index is biased. Therefore, the two first size classes of the spectra (i.e., copepods with body size smaller than the spectra mode) were not considered to compute the size-spectrum diversity in order to avoid misinterpretation of results due to the net capture bias. Size-spectrum diversity increases can be interpreted as an increasing proportion of large copepods in the community.

Hierarchical Clustering of the NB-S spectra

The slope and the size diversity synthetic indexes have both positive properties as well as limitations describing size spectra. A complementary approach was performed to analyse the shape of the whole spectrum, including the small size classes, by computing a hierarchical clustering on the time series spectra according to the

Kolmogorov cumulative-classes' distance (D). Firstly, the cumulative sum of size class frequencies for each spectrum k (val_k), where n_i is the number of copepods in the size class i and x is the total number of size classes in a spectrum, was computed:

$$val_k = \sum_{i=1}^{x} \left(\frac{n_i}{\sum_{i=1}^{x} n_i} \right)$$

Then, the maximum distance between the cumulative sums by pair of samples (D) was calculated:

$$D = 100 \max\left(\left|val_k - val_{k+1}\right|\right)$$

$$D = 100 \max\left(\left|val_k - val_{k+1}\right|\right)$$

According to D value, samples were clustered obtaining the distribution of size spectra shapes along the time series. Clustering was done following the Ward's minimum variance method (Ward 1963). At each interaction, clustering was performed to minimize the square error. Therefore, at each step, the 2 spectra, or clusters of spectra that merged were those that would have increased at a lower level the sum of the squared distances of all the objects with respect to their cluster centroids.

Small (< 0.02 mm^3) and large (> 0.32 mm^3) copepod abundances

In this work, the Shannon index of the size classes above the mode (i.e., size-spectrum diversity or size diversity) was the main synthetic index used to detect changes in the copepod-community size distribution. Although this index is, as the slope, more influenced by the ends of the spectra (smallest and largest size classes considered), the size diversity index is also shaped by the rest of the size classes, giving a better insight into changes in the whole community. As size diversity does not take into account the smallest size classes of the spectra, the cluster analysis of the whole

spectra was presented to depict shape changes. Then, abundances of copepods constituting the first and last size classes (1^{st}-2^{nd} size classes and 6^{th}-11^{th} size classes respectively) of the spectra were separately analysed to give complementary insights on the observed changes in the size diversity index and in the spectra shapes.

Table 3.5 - NB-S S size classes. The first four columns of the table represent the size classes limits and transformation of these limits in copepod length and C content. The slightly shaded boxes correspond to the position of the spectrum mode. The last four columns illustrate by shaded boxes the size classes taken into account to compute each index.

Size class lower limits (mm^3)	Equivalent Total length (mm)	Nominal Biovolume (mm^3)	C content Fixed samples (µg)	Small Copepods	Large Copepods	Slope and Cluster	Size Diversity
0.01	0.463	0.015	45.5				
0.02	0.584	0.030	46.4				
0.04	0.735	0.060	48.3				
0.08	0.927	0.12	52.2				
0.16	1.167	0.24	59.8				
0.32	1.471	0.48	75.1				
0.64	1.853	0.96	105.7				
1.28	2.335	1.92	166.9				
2.56	2.942	3.84	289.2				
5.12	3.706	7.68	533.9				
10.24	4.670	empty					

3.5 Database organization

Sample images and all scanned objects were stored in databases, one for each time series. Data arrangement and treatment was performed with Matlab® 7.0 (The Mathworks, Inc., Natick, MA). The database consists of a structure variable in Matlab in which each branch is a sample named by its date and size-fraction, d1 or d2. For each sample there is information on the sampling processing (e.g. net dimensions and

performance, net tows if samples were pooled, aliquot of the original sample that was scanned, etc.) and there is the object size information stored in vectors.

The Point B ZooScan database is available in two free data networks: Publishing Network for Geoscientific and Environmental Data (PANGEA, http://doi.pangaea.de/10.1594/PANGAEA.724540), and Coastal & Oceanic Plankton Ecology, Production and Observation Database (COPEPOD, http://www.st.nmfs.noaa.gov/plankton/time-series-methods/).

3.6 Time series statistical methods

For both time series, a quality check was performed on all the environmental and zooplankton parameters. In the case of MC time series, only one sample was discarded (May of 2004). For Point B, five samples were discarded (April of 1987 and 1988, May of 1999, and February and April of 2000) due to suspicious values issued from improper sample treatment. Time series were regularised by monthly mean, except for the Point B wind pattern that was already represented at a monthly frequency. In this section the main statistical analyses performed in this thesis are presented.

3.6.1 Principal Component Analysis (PCA)

To depict the general pattern of observed changes in several related variables, the PCA multivariate statistical method (for its computation see Legendre and Legendre 1979; Jollife 2002) was applied on annual average values. The PCA is a very widespread method in numerical ecology.

Datasets were previously standardised due to their different nature. Then, new synthetic variables (principal components, i.e. PCs) were created by minimisation of the Euclidian distances among the original variables in each new projected space. In other words, new axes (PCs) were created in the multispace of n original variables. The first

PC is the one minimizing most of the distance between variables, i.e. it accounts for as much of the variability in the data as possible. The following new axes are orthogonal (independent) to one another and ordered by minimization of distances with the original variables. This method enabled the maximal common interannual variability among the studied variables to be obtained and the depiction of the relationships among the variables.

3.6.2 Prediction of missing values by the Eigen Vector Filtering method (EVF)

After time series regularisation, a few months were missing in the time series. In the case of the ZooScan datasets, missing values were 10 months out of 192 in the MC time series, and 19 months out of 360 in the Point B time series. In order to fill the gaps of missing values with predicted values, the Eigen vector filtering method (EVF) was applied (Colebrook 1978; Ibanez 1991; Ibanez and Etienne 1992). The method is based on the construction of a matrix in which the first column corresponds to the original series, and the successive columns correspond to several copies of it, lagged by one time unit. The missing values (MD) are coded, and a Principal Component Analysis (PCA) adapted to missing values is then performed on this matrix (see equations in Ibanez and Conversi 2002). The principal components are calculated on an autocovariance matrix (based on the constructed matrix), instead of being calculated, as for a common PCA, on the variance matrix derived from several original variables. The steps of this interactive method are summed up in the following diagram (Fig.3.12).

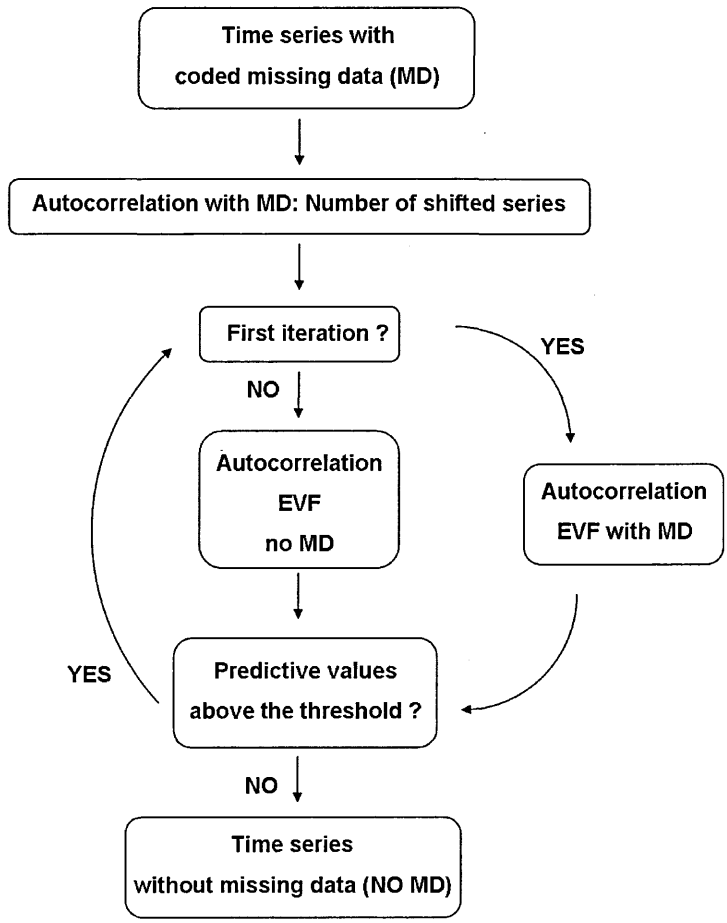

Figure 3.12 - Flow diagram summarizing the steps of prediction of missing values by the EVF method, reproduced from Ibanez and Conversi (2002).

The first step is to determine the number of lags (p) of the original time series (z) with MD. It is calculated by detection of the number of lags p at which the autocorrelation of the original time series first goes to zero. Values separated by p interval are independent. Then from the constructed matrix of original and lagged series, an autocovariance matrix is calculated. Only pairs of data ($z_t + z_{t+k}$) without MD are taken into account for the first interaction. A PCA is calculated on this matrix by extraction of eigen values and eigen vectors. The principal components retained (n PCs) sum up at least 80% of the total variance. The prediction of MD is then done from the matrix product of the n PCs with the n first eigen vectors. The same process is then repeated, several interactions, each time on the new series with the predicted MD ($\hat{z}_t$),

until the last two time series with predicted MD differ less than 1/100 of the original time series standard deviation ($\sigma_{\hat{z}t-1,\hat{z}t} < 0.01\sigma_z$).

3.6.3 Escoufier method

A stepwise statistical method was applied to synthesize temperature, salinity and Chl *a* information in all depth layers without missing the main pattern of temporal changes. For each variable, depth temporal profiles, and their combinations, were rated depending on their correlation with the first principal component (1st PC) of the sampled depth profiles (Fig.3.13).

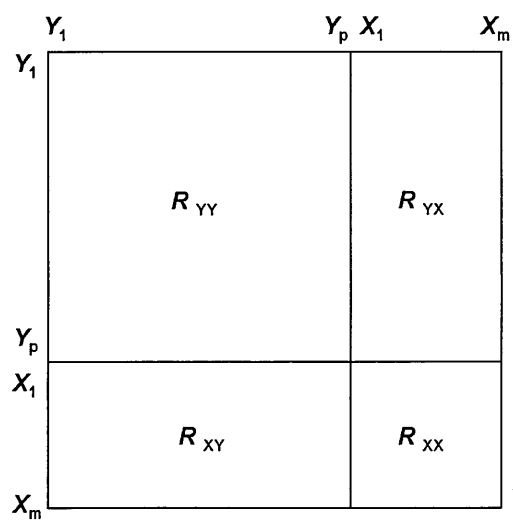

Figure 3.13 - Correlation matrix between the original matrix with all depth profiles (Y) and x profiles (X).

Correlation was established by calculating the RV-coefficient (Escoufier 1973; Robert and Escoufier 1976) between the 1st PC of the depth-profile combination matrix (X) and the 1st PC of the matrix containing all the depth profiles together (Y):

$$RV(X,Y) = \frac{TR(R_{YX}R_{XY})}{\left[TR(R^2{}_{YY})TR(R^2{}_{XX})\right]^{1/2}}$$

The RV-coefficient varies between 0 and 1 correlation. It is equal to 1 when both first PCs are proportional (same direction). Interactively, a new depth temporal profile was added to the depth profiles previously ranked (e.g., m-1 +1 depth of the remainder, until m = p, number of total profiles) according to the maximum RV-coefficient obtained between the 1st PC of Y and 1st PC of X. The number of depths retained for analysis was selected by the saturation of the curve representing the cumulated sum of the maximum RV-coefficient at each step. In the case of Point B, the temporal depth-profiles retained were 20 m and 50 m, whereas for stn MC, they were the 10 m and 50 m depth-profiles. In both cases, they represent the surface and deep layers of the water column respectively.

3.6.4 Normalised anomalies

Interannual changes of each studied variable were represented by annual normalised anomalies (deviations from the mean) (A_i). Annual mean values of each variable were calculated ($\overline{Y}_i$), the mean of these annual values was subtracted to them ($\overline{Y}$), and the obtained anomalies were normalised by the standard deviation of the annual mean values ($\sigma(\sum_{i=1}^{n}\overline{Y}_i)$), to allow intercomparison with other variables.

$$A_i = \frac{\overline{Y}_i - \overline{Y}}{\sigma(\sum_{i=1}^{n}\overline{Y}_i)}$$

3.6.5 Cumulative sum (cusum)

To distinguish the main periods in the interannual changes of a variable, the cumulative sum (cusum) of the deviations from the mean (without normalisation) was depicted (Ibanez et al. 1993). Deviations were successively added to the previous ones. Periods were individualised taking into account the turning points of the resulting curve. By this method, the sign and steepness of the slopes reflect the direction and range of deviation of a period from the mean value of a time series. The slope of a given period added to the long term mean value indicates the local mean value for that period.

3.6.6 Moving Average (MA) and Exponentially Weighted Moving Average (EWMA) filtering

To filter a signal, in this case the monthly changes of each variable of the studied time series (x), the moving average (MA) method was used. As its name indicates, this is a method based on calculating the mean value of contiguous data points in a window of p values. Each time, the window moves one data point forward. In this case, the window contained 13 data points (~ a year window) and therefore, the resulting filtered curve missed 6 values at both of its ends ($(p-1)/2$). Here is its formulation:

$$ma_t = \frac{1}{p} \sum_{j=t-(p-1)/2}^{t+(p-1)/2} x_j$$

The exponential weighted moving average (EWMA) is a variant of the MA method and is usually applied in industrial production for quality control by stepwise forecasting. Observations out of predetermined confidence intervals are considered out of control and they indicate a change in the time series trajectory. This method was used to determine if an observed trend could be considered a regime shift.

The EWMA presents the same stepwise calculation as the moving average, but the computed value is not the middle of the window but its last observation, and the

window increases one observation ahead at a time. In addition, each value in the window is multiplied by a weight which increases exponentially the more the value is close to the last observation:

$$\hat{z}_t = \lambda x_t + \lambda(1-\lambda)x_{t-1} + \lambda(1-\lambda)^2 x_{t-2} + \lambda(1-\lambda)^3 x_{t-3} + \ldots + \lambda(1-\lambda)^t x_0$$

Out of control limits (confidence intervals) are calculated from a constant, i.e., L= 1.96 and two parameters, μ and σ:

$$\mu_{z_t} = \mu_{x_t} \qquad \sigma_{z_t} = \sigma_{x_t}\sqrt{(\frac{\lambda}{2-\lambda})}$$

Being the confidence intervals:

$$\mu_{z_t} \pm L\sigma_{z_t} = \mu_{x_t} \pm L\sigma_{x_t}\sqrt{\left(\frac{\lambda}{2-\lambda}\right)}$$

The value λ is determined from the interval 0.01-0.1 by simulations. From these simulations, the average run length (ARL) (i.e., number of observations/number of observations out control in the simulation) and the sum of squares of deviations of the original time series from the model (SCE) are calculated. The chosen value λ is the one at the breaking point of the curve relating both measures. The new time series will show a regime shift if it passes from a state of - out of confidence points to a new state of + out of confident points, or *vice versa.*

Chapter 4. Data validation

The ZooScan copepod datasets were validated by a stepwise protocol. Firstly, sampling biases were considered. They could arise from bad preservation of organisms in formaldehyde or from changes in the sampling collection, or during analysis. Time series of sample treatment (i.e., sample fractionation, number of objects in the scanning tray, number of net tows for Point B) were depicted to check for possible methodological changes in the studied period. Secondly, copepod abundance estimated by supervised-learning was compared to copepod abundance in the samples ('true abundance'). Thirdly, contamination by other categories of each size-class in the copepod spectra was depicted, and size-spectra shapes were compared between the automatic and true copepod spectra. Finally, the sensitivity of the size-spectrum diversity index to contamination was tested.

4.1 Quality control of sampling methodology

Because copepod size distribution was the main issue of this thesis, the effect of formalin fixation on shrinking copepod bodies was taken into account. Fixation can cause shrinking, swelling or even complete degradation of certain bodies. Nevertheless, the rate of modification as well as its clear effects on body structure is still controversial (Quinones et al. 2003). Copepods are much less affected than gelatinous zooplankton (Omori 1978). In a study of copepod size distribution using an Optical Plankton Counter (OPC), Wieland et al. (1997) compared measurements after catch with replicates after 3 months of fixation and did not find significant changes. Shrinkage due to formaldehyde starts 10-15 minutes after fixation and the most pronounced change in biovolume occurs within the first day. The process slows down 3 to 7 days later. Thus, it is recommended that volume determination takes place not earlier than 3 days after preservation (Ahlstrom and Thrailkill 1962). Stability is reached between a month and 1

or 2 years after preservation (Harris et al. 2000). All the samples analysed in this thesis were scanned after several years of conservation. Consequently, the shrinking effect was already stabilised. In addition, to my knowledge, no major changes in the fixation protocol occurred in the course of any of the time series analyzed. To be sure that there was no shrinkage of copepods in the samples, the size of 4,869 individuals of *Centropages typicus* was measured from samples belonging to the years 1979, 1985, 1995-1997 and 2003 from Point B. There was no evidence for a decreasing trend in body size with time (data not shown).

While scanning was standardised, not all samples were processed by the same person. The time series at Point B was processed by four different operators. I scanned samples from 1984 to 1995, whereas 3 other operators scanned periods from 1974-1983, 1996-2000 and 2001-2003 respectively. I processed also samples from 10 years of the MC time series, except the 1997-2001 period, which was processed by another operator. Although a protocol was set up, sampling processing varied depending on the operator. For instance, for the period 2001-2003 of Point B and the period 1997-2001 of the MC time series, d1-d2 splitting was not carried out correctly. For those periods, both d1 and d2 represented the whole size distribution of copepods in the samples. Splitting (i.e., subsampling rate) of the d1-fraction in both cases was much higher than for the rest of both time series, while the number of objects in the scanning tray was similar (see figures in Appendix III). Less effort in separation of d1 and d2 caused more splitting of the d1 fraction and therefore a possible underestimate of the rare large copepod contribution to the size spectra. However, a lower concentration of large copepods was not recorded in those periods (see chapters 4 and 5), suggesting that there was no sampling bias, or that natural changes overcame the possible bias.

In the case of Point B, each sample was an amalgam of all the net tows performed during a week. Over the 30-year time series, the weekly frequency of net tows was not constant (Fig.4.1), especially in the 1970s, when fewer tows were performed per week. The number of tows contained in a sample play a role in smoothing short term (i.e., diel) variability by averaging the community structure of all the single samples (e.g., replicates) representing a week. However, very intense peaks or large troughs were not observed during those first years of the time series, in which the tows per week were less frequent. In addition, the appearance of *Calanus helgolandicus,* which is a rare species at Point B, was independent from the weekly tow number according to a test by general linear model (glm).

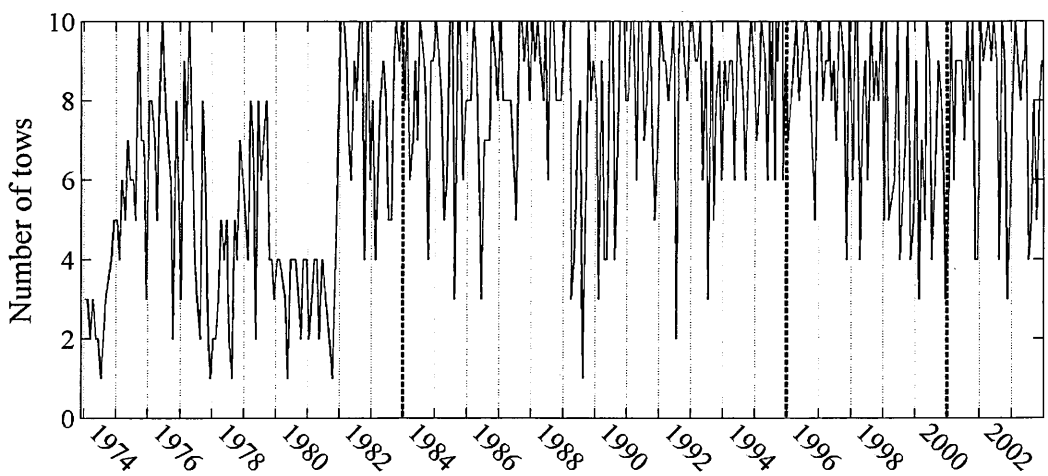

Figure 4.1 - Number of tows performed to constitute each sample of Point B time series.

In this work, possible sources of methodological biases, described above, were taken into account, when analyzing temporal changes, to avoid misinterpretation of results.

4.2 Copepod abundance estimates

To confirm the accuracy of copepod automatic recognition, in the case of the MC time series, ZooScan counts were compared with independent microscope counts performed many years before (i.e., from the same sample but not the same subsample;

189 pairs of data). In the case of Point B, due to a lack of microscopic counts, samples from five years (1979, 1985, 1996, 1997, 2003) were semi-automatically recognised, and a comparison was made between automatic and true copepod abundance in the scans of those samples (60 pairs of data).

For the MC time series, ZooScan estimates of copepod abundance agreed with traditional microscopic counts on different subsamples of the same dates (Fig.4.2). Therefore, interannual changes in the copepod abundance at stn MC can be followed with the ZooScan methodology. Data dispersion was slightly high because the pairs of counts did not correspond to the same subsamples.

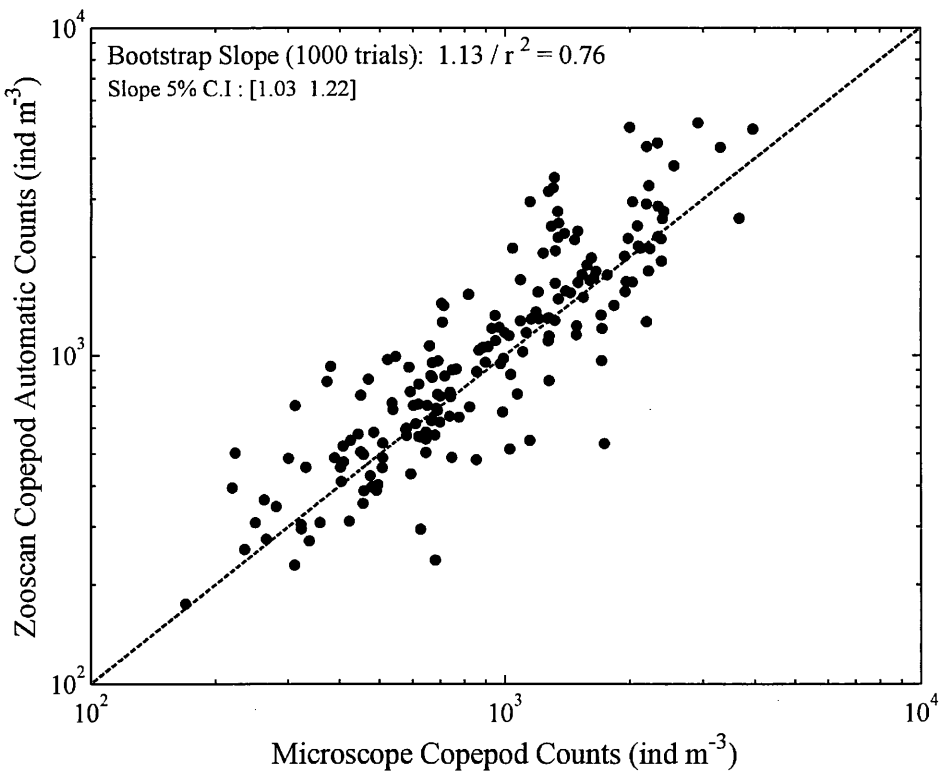

Figure 4.2 - Linear relationship by logarithmical scale between copepod abundance estimated with ZooScan and by microscopy for the whole stn MC time series. The 1:1 relationship is depicted for reference (dashed line).

For Point B datasets, the close fit between automatic estimates and true copepod abundance in the scanning tray for five non-continuous years (Fig.4.3), suggests that the

98% recall value estimated with the test set can be extended to the whole time series. Copepod abundance was slightly overestimated by the ZooScan methodology (most data above the 1:1 fit) because contamination by other groups (on average, 17% of objects recognised as copepods were not copepods) overcame the abundance underestimation by misrecognition of true copepods (1-r = 2% of copepods were not recognised as copepods).

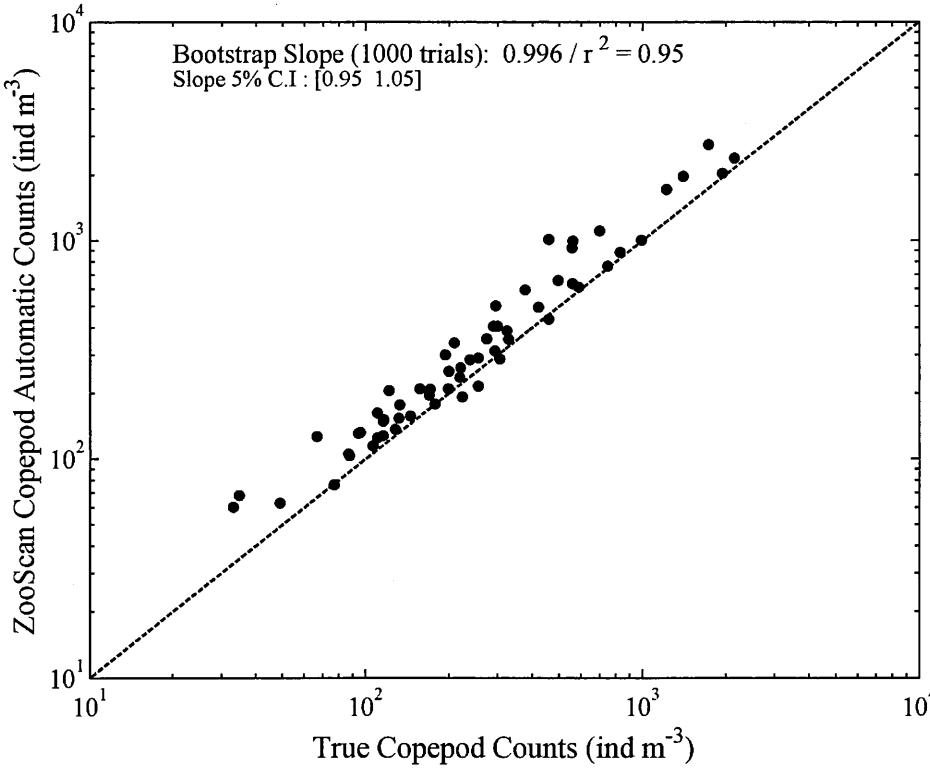

Figure 4.3 - Linear relationship at logarithmical scale between the copepod abundance estimated by automatic recognition and the true abundance in 5-year scans of the Point B time series. The 1:1 relationship is depicted for reference (dashed line).

Despite contamination, the above results demonstrate that copepod abundance can be monitored by ZooScan automatic recognition.

4.3 Contamination effect on the copepod size-spectrum shape

Although the ZooScan automatic estimates fitted well the true copepod abundance in the samples, there was a slight overestimation due to contamination by other misrecognized categories. In this section, tests to see if contamination could bias the copepod size spectra are outlined. Analyses were carried out on the 5-year semi-automatic recognition datasets of Point B time series.

Contamination consisted mainly of detritus, cladocerans, copepod pieces and copepod aggregates (Fig.4.4). Although contamination was very variable among samples, it constituted a very low proportion of the total copepod spectrum. High copepod recognition and a low proportion of contamination in the spectra resulted in a close match of the annual average spectrum of true copepods in the samples (Real Cop.), the spectrum of the true copepods composing the automatic-recognition spectrum (T+ Cop.) (i.e., automatic-recognition spectrum after taking out contaminant objects) and the annual average spectrum issued from automatic-recognition (Autorec. Cop.) (Fig.4.5).

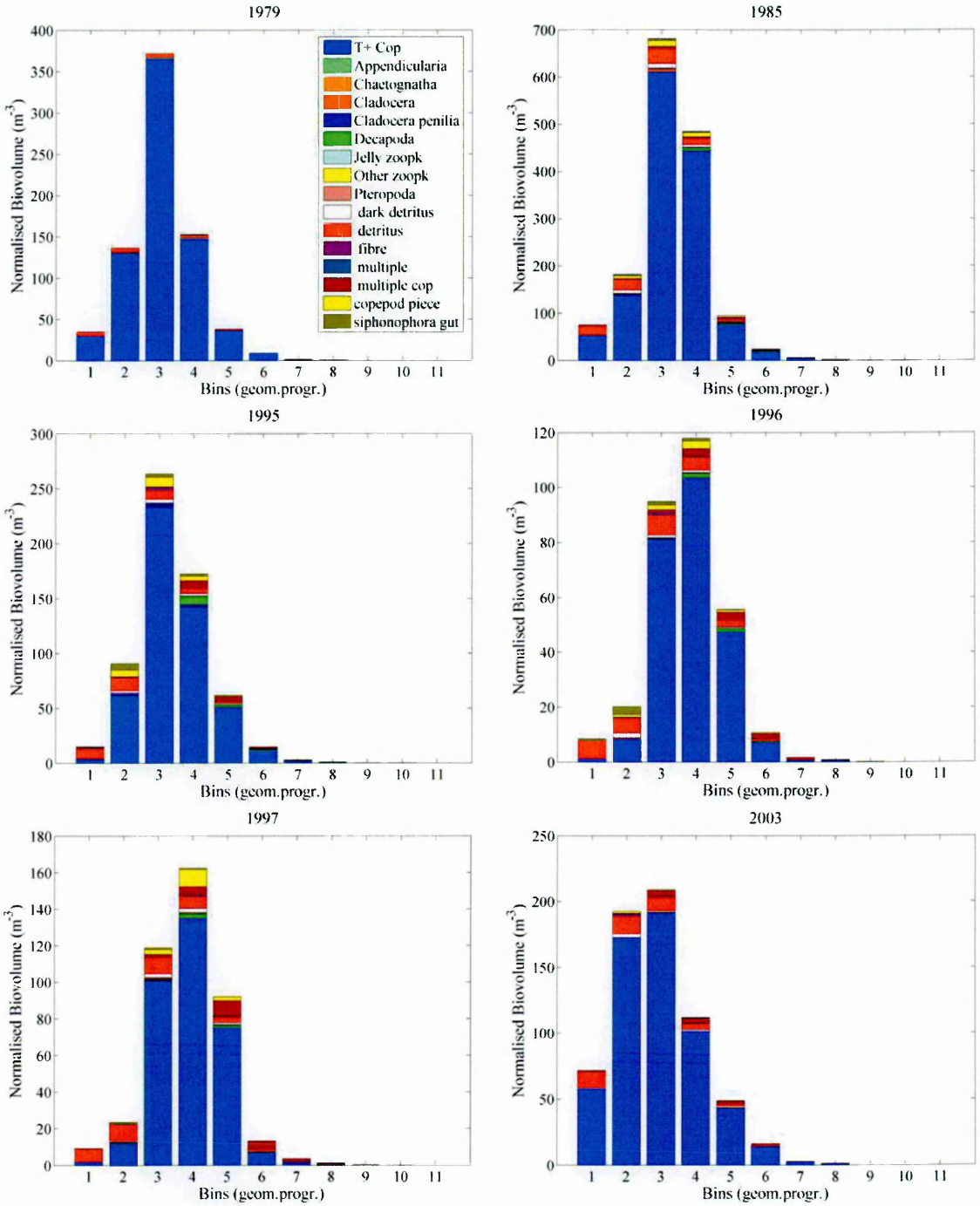

Figure 4.4 - Annual average normalised-biovolume size spectra (NB-S spectra). True copepods in the size spectrum (T+ copepods) are in blue; other colours correspond to different categories contaminating the copepod category (F+, contamination).

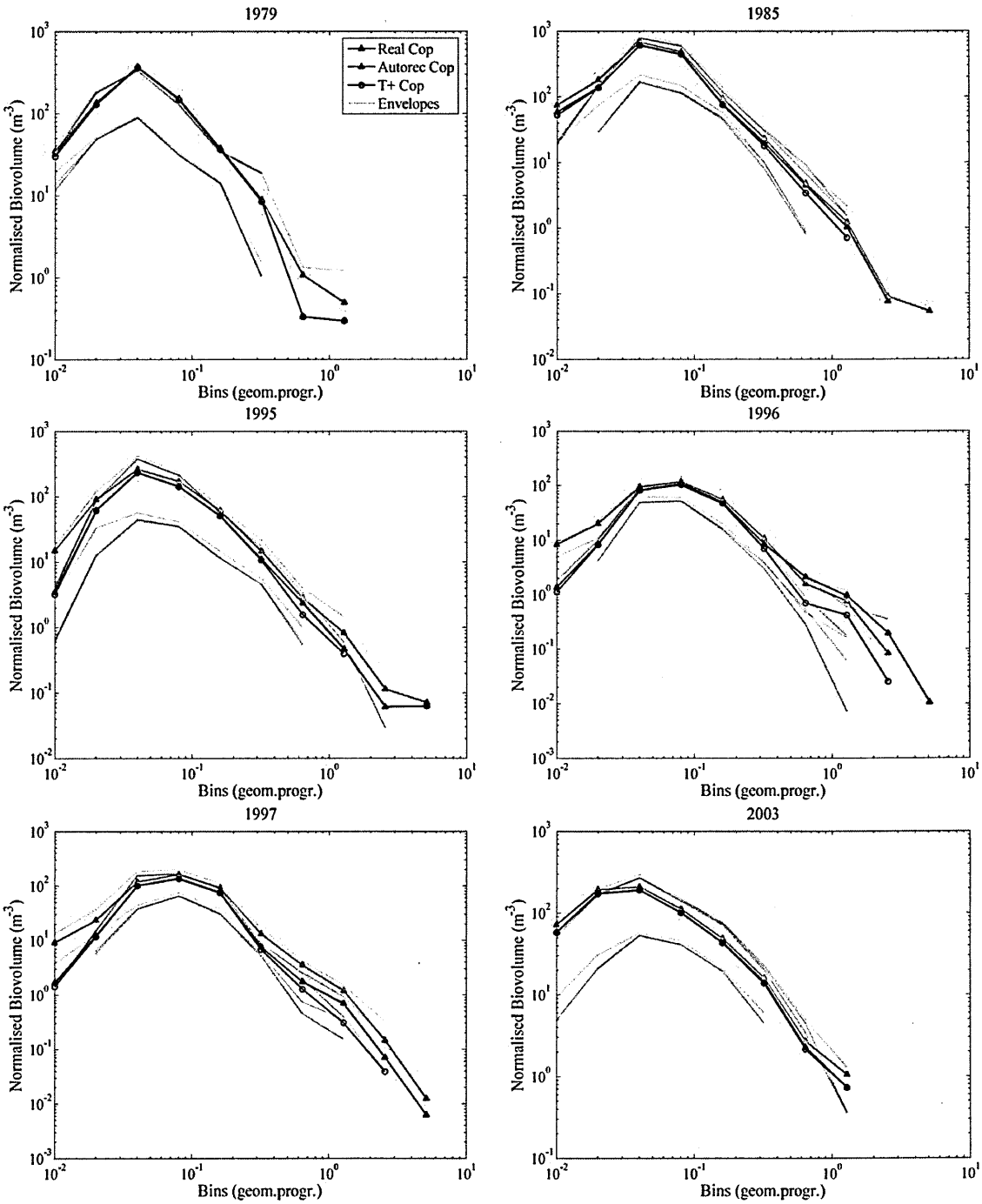

Figure 4.5 - Each-year mean copepod NB-S spectra. True copepod (blue line), automatic-recognition copepod (red line), and T+ copepod (black line) are depicted for comparison. Dashed lines represent the envelopes of the first and third quartiles.

To test if the observed contamination varied seasonally or between years, a Friedman test was run on recall (% of copepods well recognised) and 1-precision (% of contamination) recognition metrics. The test was run twice; once on samples previously clustered by seasons, and then on samples clustered by years. The Friedman test is a non-parametric statistical test similar to a two way analysis of variance (ANOVA) but

grouping raw data in ranks. The test performed on the 4 seasons determined independence from seasonality for both, recall ($p = 0.8012$) and 1-precision ($p=0.3916$). The same test performed on by-year clusters produced p-values of 0.015 for the recall, and 0.0513 for the 1-precision. Depending on the confidence interval (5% or 1%) annual values were significantly different or not. These differences could be partly due to: a different operator treating the samples or changes in the zooplankton community structure. Nevertheless, ranges were small, ~0.91-0.99 for the recall and ~0.1-0.2 for the 1-precision value, and no interannual trend was observed for any of the 2 metrics between the five discontinuous years.

4.4 Size-spectrum diversity sensitivity to contamination

The close relationship between true:automatic copepod NB-S spectra was reflected in their size-spectrum diversity index (Fig.4.6). The size-spectrum diversity index calculated on the automatic-recognition spectra was not significantly different from the one calculated on the true copepods, as reflected by the bootstrap test. The goodness of fit ($r^2 = 0.8$) assures that temporal trends observed in this index are highly related to the size-spectrum diversity index calculated on the true-copepod spectra.

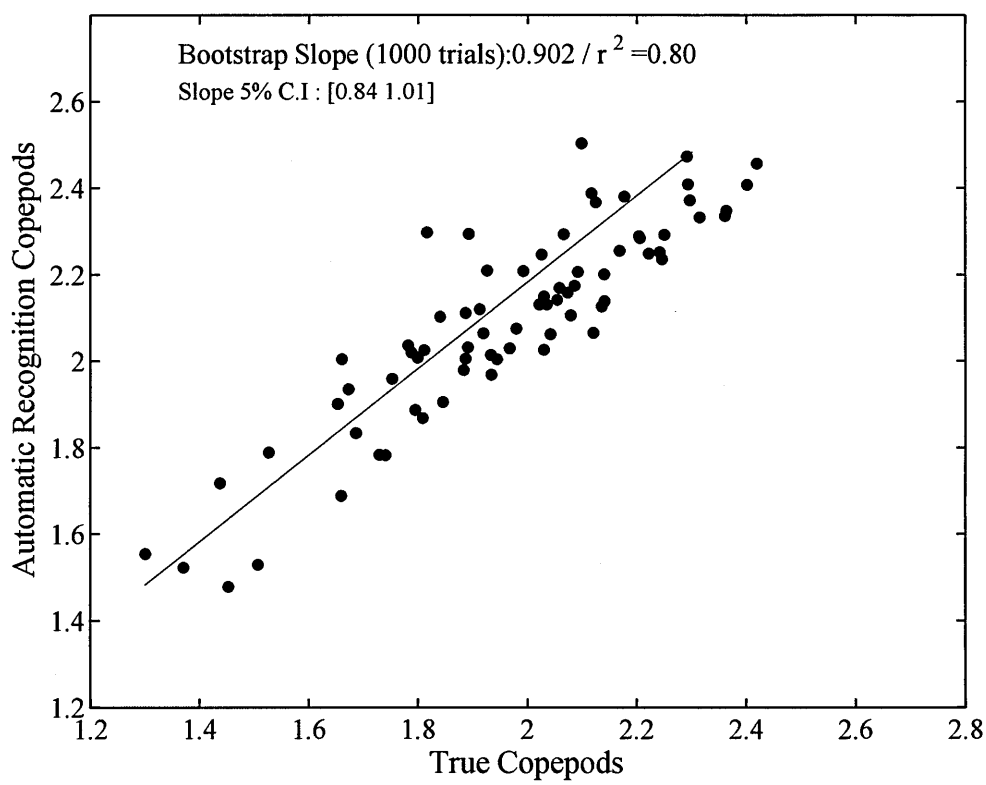

Figure 4.6 – Size spectrum diversity calculated on the NB-S spectra of true copepods (x-axis) versus automatic copepods (y-axis).

From the results presented in this chapter it is concluded that copepod automatic counts from ZooScan images are a good proxy to study temporal changes in copepod abundance and size distribution.

Chapter 5. MC time series

5.1 Introduction

Previous studies on plankton variability at stn MC have already shown considerable temporal evolution and given some insight to the possible mechanisms taking place at this coastal station. Small-cell species have been reported to increase their presence and to dominate phytoplankton assemblages from 1995 (Ribera d'Alcalà et al. 2004). Furthermore, in a study based on winter phytoplankton assemblages, small phytoflagellate abundance was reported to increase and the abundance of large diatoms to decreased after the 1980s (Zingone et al. 2009). In the case of copepods, long-term changes in their species assemblages have not been so marked (Mazzocchi and Ribera d'Alcalà 1995; Ribera d'Alcalà et al. 2004). They seem to cope well with environmental changes reported in this location (Mazzocchi et al. 2010). Although total zooplankton biomass was higher in the first part of the time series than in the second part, and some signs of changes, such as the replacement of some rare copepod species, have been described, it has been difficult to detect a common pattern of variation in the copepod community (Mazzocchi and Ribera d'Alcalà 1995; Ribera d'Alcalà et al. 2004).

In this chapter, the copepod size distribution was used as a synthetic index to try to detect changes in the copepod community that would indicate a response to the reported changes, between the first and second period of study, in the phytoplankton community. Local environmental conditions were also analysed to attempt link the changes to possible environmental forcing. In addition, the available microscopic taxonomic counts allowed the relationships between copepod size distribution and community composition to be established. Small copepods were compared to copepodite concentrations and large copepods to the presence of typical offshore

species, which often present large body sizes. Finally, a comparison was made between the size-spectrum diversity and species diversity of copepods.

5.2 Results

5.2.1 Environmental variability

Temperature at stn MC, for the studied period, generally ranged from 13-14 °C (winter minima to 25-26 °C, summer maxima 20-22 °C at 50 m depth, Fig.5.1 A, B). From 1999 to 2003, most of the annual mean temperatures were warmer than the long-term average (Fig.5.1C).

The classical seasonal pattern of temperate zones was recorded (Fig.5.1 D, E). Thermocline formation started in April-May, and the water column remained stratified until November. As indicated by the 19 °C isoline at 10 m depth, it is evident that in the second part of the time series the onset of stratification generally started a month earlier than in the 1980s.

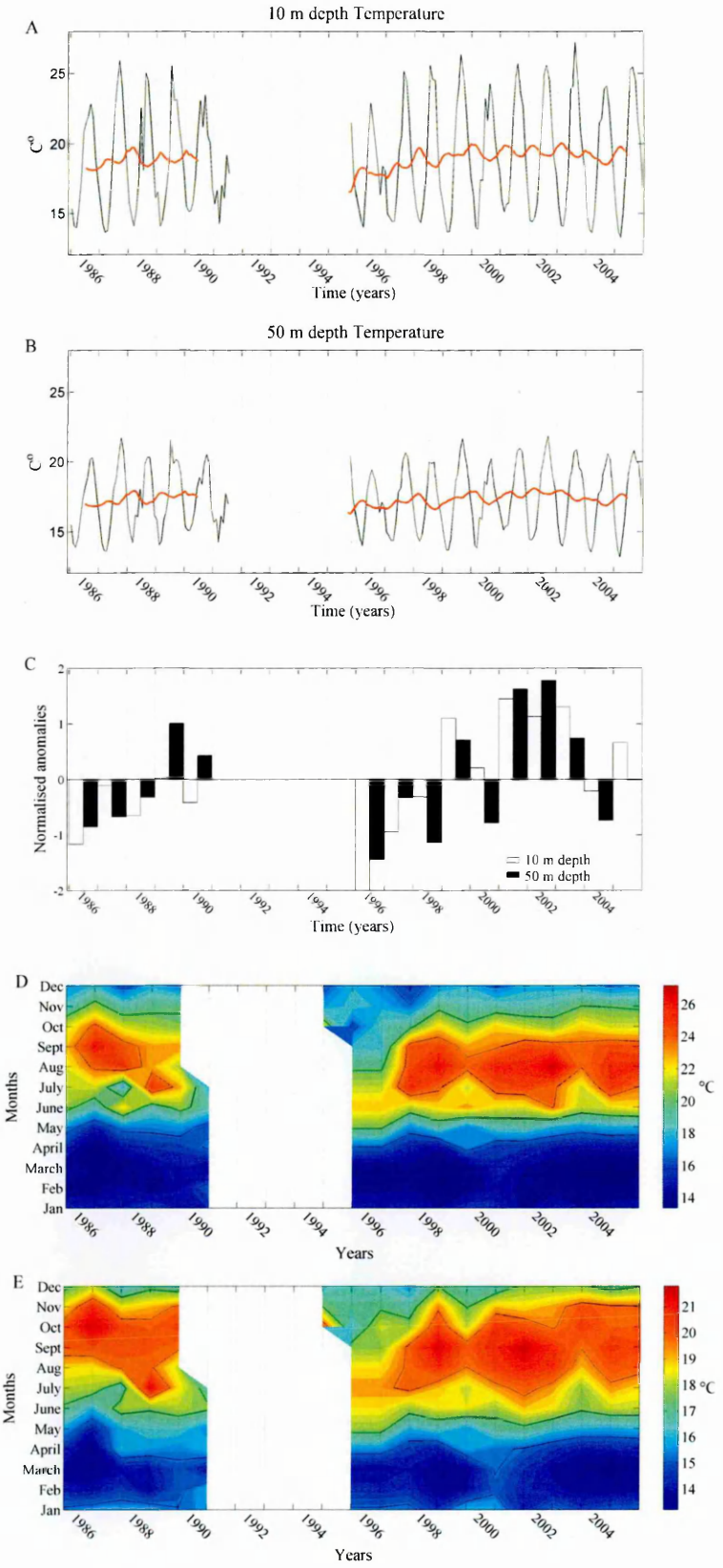

Figure 5.1 - Water temperature at stn MC. A) Monthly time series (black line) and an annual (i.e., 12 points window) moving average to smooth the seasonal signal (red line) for values recorded at 10 m depth; B) same as in A for values at 50 m depth; C) annual normalised anomalies at 20 m (white) and 50 m (black) depths; D) seasonal and interannual variability at 10 m depth; E) same as in D for values at 50 m depth.

The amplitude of ranges of salinity was wider than that of temperature. Minimal annual records ranged between 37.35 and 37.9, and maximal annual records were in the 37.9-38.2 range (Fig.5.2 A, B). Annual mean values were above the long-term average during the 1987-1990 and 2000-2003 periods (Fig.5.2C).

A clear seasonal pattern was depicted, with lowest annual values usually recorded between April and June. Interannual changes of salinity occurred due to concomitant changes in the four seasons (Fig.5.2 D, E).

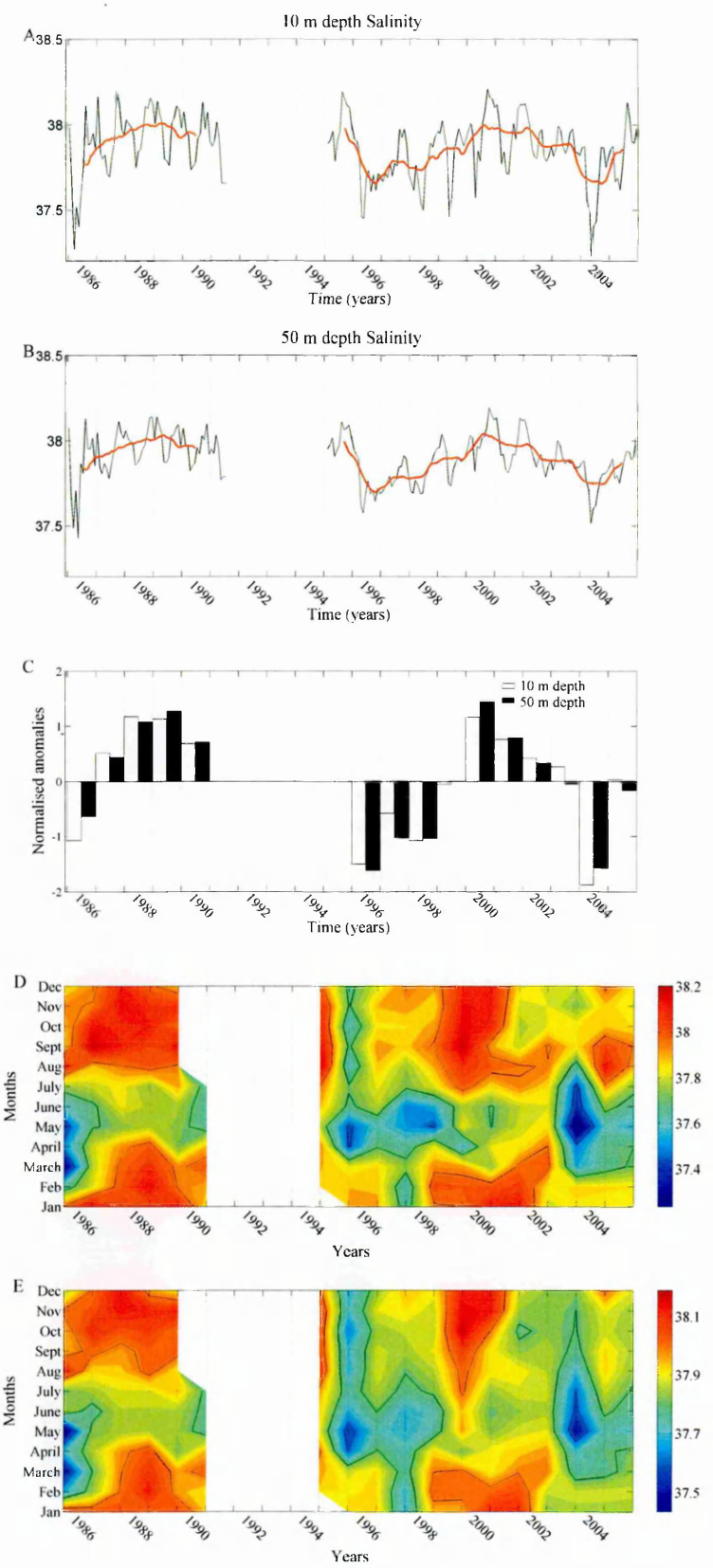

Figure 5.2 - Salinity at stn MC. A) Monthly time series (black line) and an annual (i.e., 12 points window) moving average to smooth the seasonal signal (red line) for values recorded at 10 m depth; B) same as in A for values at 50 m depth; C) annual normalised anomalies at 20 m (white) and 50 m (black) depths; D) seasonal and interannual variability at 10 m depth; E) same as in D for values at 50 m depth.

Water-column stability was calculated by computing the density difference between 50 and 10 m depths (Lacroix and Nival 1998). Water density was calculated from salinity, temperature and sampling depth (Millero et al. 1980; Fofonoff and Millard Jr. 1983). Stratification onset (i.e., water-column stability increase) occurred one month earlier in the second part of the time series (Fig.5.3), and stability was higher during those summers than during the summers of the 1980s.

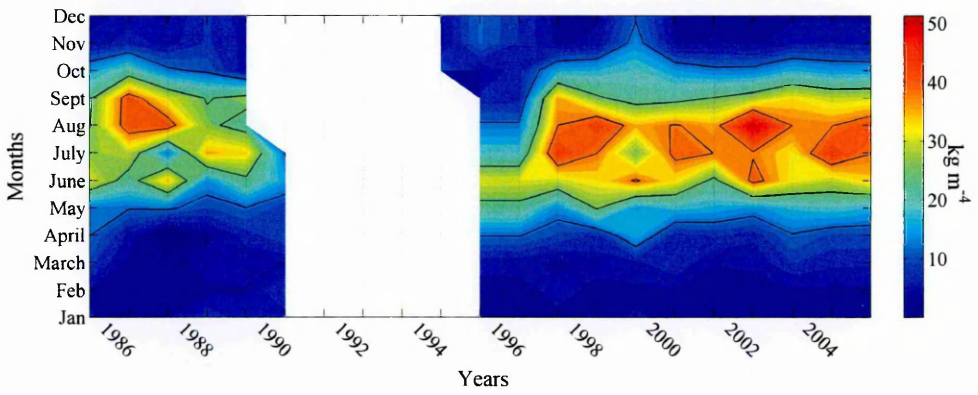

Figure 5.3 - Seasonality of the water column stability, indicated by the difference between water density at 10 m and 50 m depth.

5.2.2 Phytoplankton variability

Chlorophyll *a* (chl *a*) concentration varied from 0.5-1 mg m^{-3} minimal records to very variable annual maximal values in the 0.5-4 mg m^{-3} range (0.5-2 mg m^{-3} at 50 m depth) (Fig.5.4 A, B). Annual amplitude was higher in the 1980s than in the second period of the time series. From 1996 to 2003, annual mean chl *a* concentration was below the long-term average (Fig.5.4C). The highest annual mean values were recorded at the beginning of the time series, and the lowest in 2001-2002.

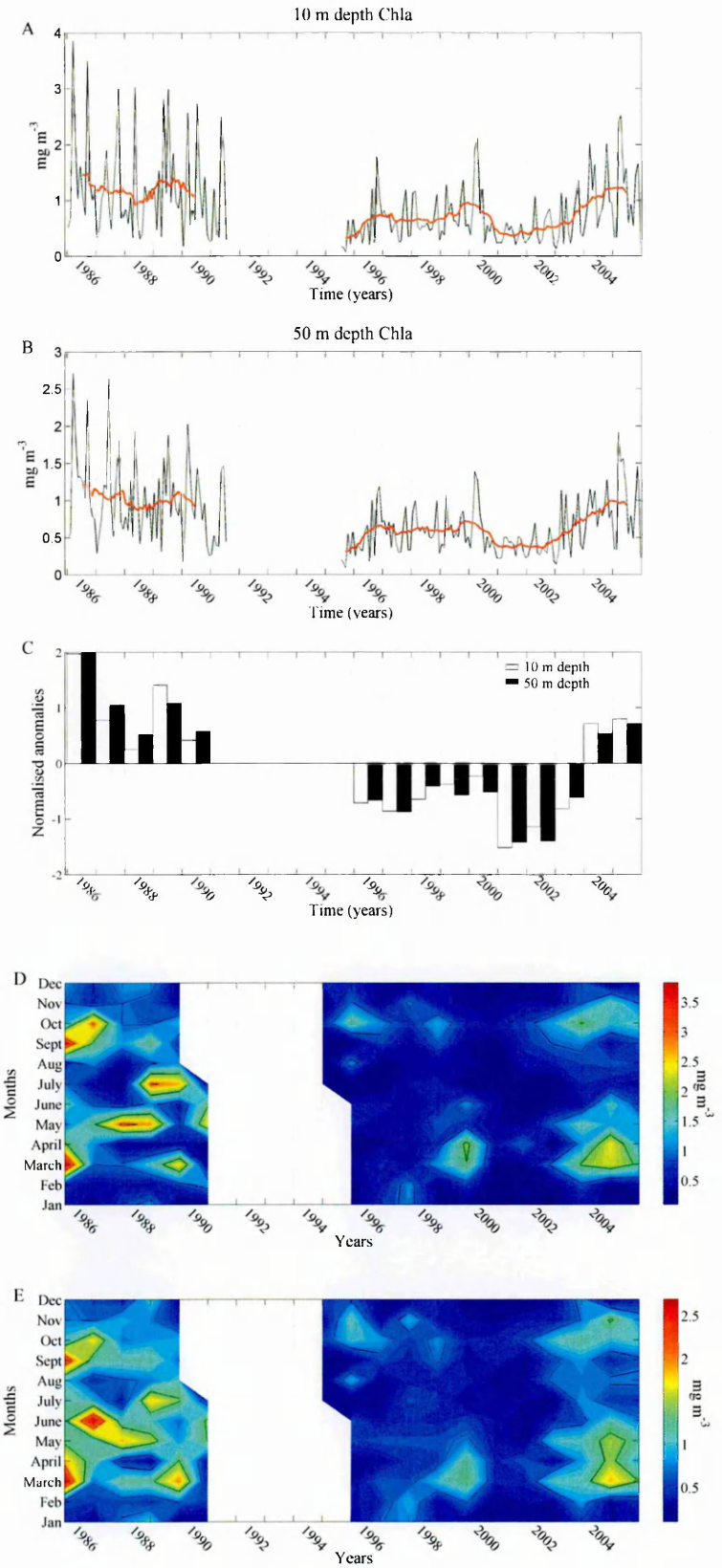

Figure 5.4 - Chl *a* concentration at stn MC. A) Monthly time series (black line) and an annual (i.e., 12 points window) moving average to smooth the seasonal signal (red line) for values recorded at 10 m depth; B) same as in A for values at 50 m depth; C) annual normalised anomalies at 20 m (white) and 50 m (black) depths; D) seasonal and interannual variability of log (mg m^3+1) at 10 m depth; E) same as in D for values at 50 m depth.

A main spring peak and a secondary autumn peak were depicted for most of the years of the studied period (Fig.5.4 D, E). Nevertheless, at stn MC, chl *a* seasonal patterns showed notable interannual variability. In the first part of the time series, several peaks were observed between March and October, whereas in the second period only the autumn and/or the spring peaks occurred.

Four major groups of phytoplankton have been considered in this study, i.e. diatoms, dinoflagellates, coccolithophores and small phytoplagellates. Small phytoflagellates represented on average 50% of the total phytoplankton abundance, followed by diatoms (40%), coccolithophores (6%) and dinoflagellates (3%). Diatom and small phytoflagellate abundance ratios were highly anticorrelated (720 pairs of data; non-parametric Spearman correlation coefficient $\rho = -0.89$; p-value <0.00001).

The autumn abundance of coccolithophores increased from 1997 (Fig.5.5A). In the second part of the time series, dinoflagellate (Fig.5.5B), small phytoflagellate (Fig.5.5C) and diatom (Fig.5.5D) abundances started to increase in the water column around March instead of April. The dinoflagellate annual peak, around June, was lower in the second part of the time series. The period of high concentrations of diatoms and small phytoflagellates lasted longer in the second part of the time series (i.e., until September-October) than in the 1980s (i.e., until July-August). In the second part of the time series, small phytoflagellates tended to dominate more often in phytoplankton assemblages, replacing diatoms in those cases (data not shown).

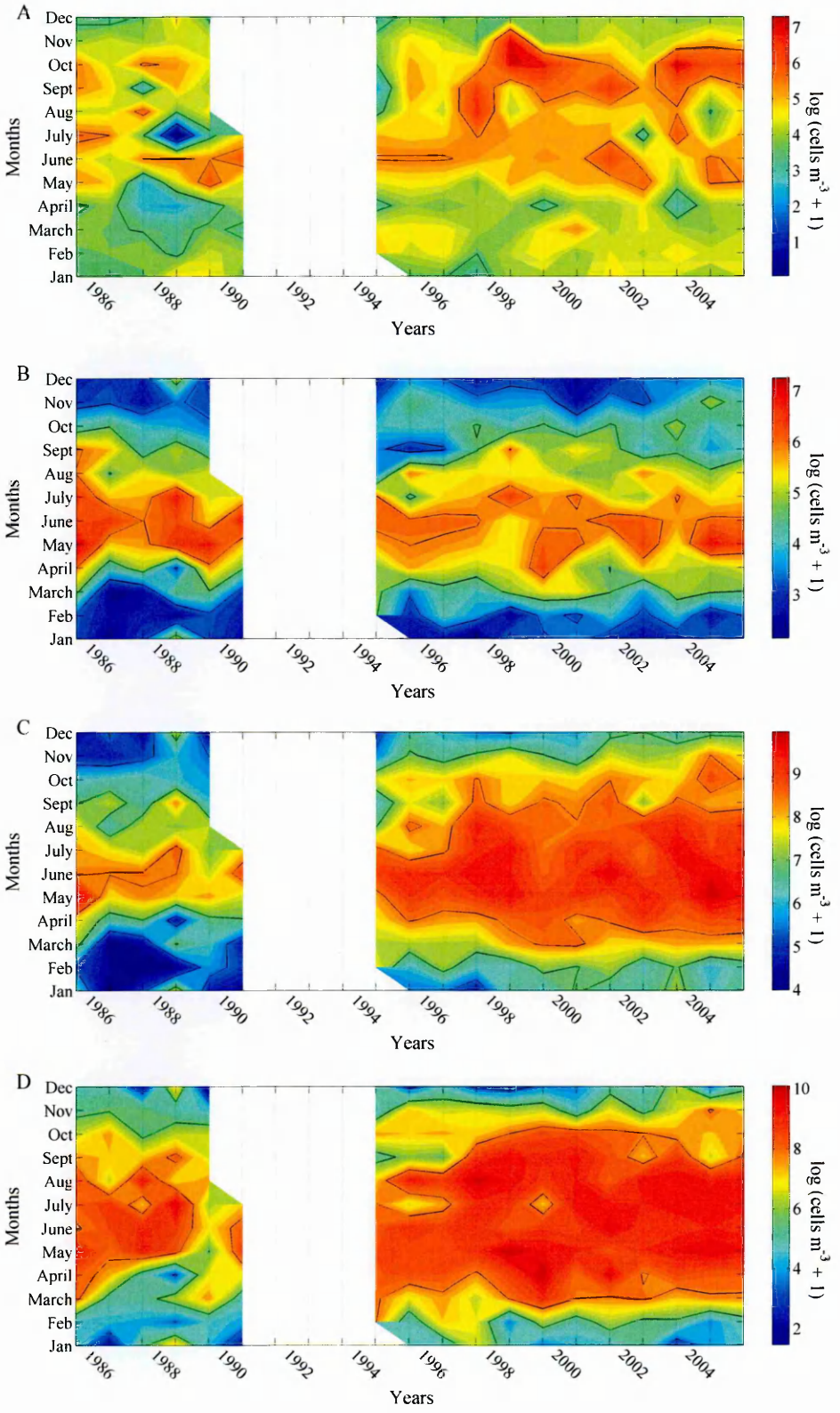

Figure 5.5 – Seasonal and interannual variability in the concentrations (log(cells m^{-3} +1)) of (A) coccolithophores, (B) dinoflagellates, (C) small phytoflagellates and (D) diatoms.

The mean cell size of phytoplankton varied between the 1980s and the second part of the time series, when all groups but coccolithophores presented an increased proportion of small-cell species. This fact together with changes in the dominance of the four groups led to a change in cell-size (Fig.5.6). While in the first period of the time series only 20 % of the samples presented a mean phytoplankton ESD < 5 μm (black line), in the second part, ~70% of the samples had mean cell-sizes below that size threshold.

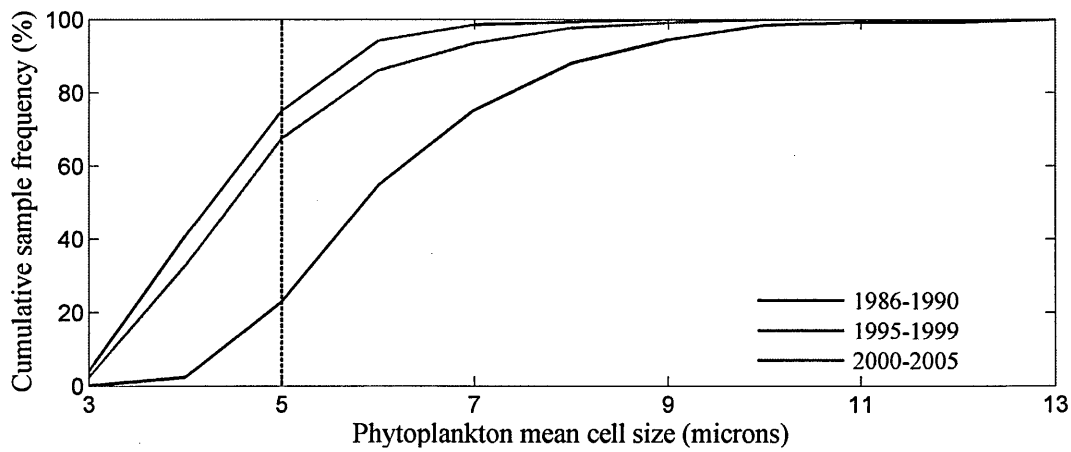

Figure 5.6 - Cumulative sum of the sample percentage presenting a certain phytoplankton mean cell size (μm ESD), for three periods (~5 years each) of the MC time series.

Phytoplankton biovolume was computed from abundance and size. Diatoms contributed most to the average total phytoplankton biovolume with a mean interannual value of 64%. They were followed by dinoflagellates (18%), small phytoflagellates (6%) and coccolithophores (6%). Total biovolume did not present any trend, yet the contribution of each phytoplankton group to total biovolume varied during the studied period. The most notable interannual changes of the annual mean contribution of each group to total phytoplankton biovolume were an increase in the small phytoflagellate group and the concomitant decrease in the contribution of dinoflagellate in the second part of the time series (Fig.5.7).

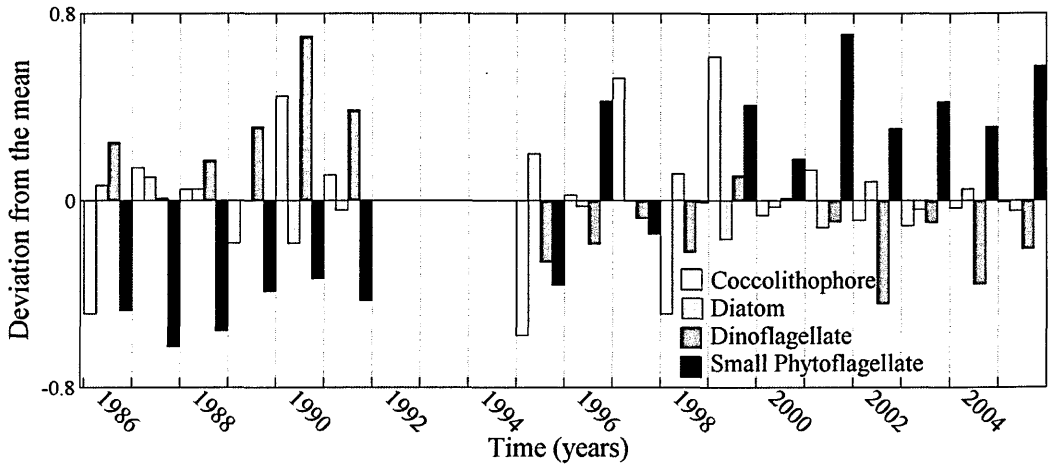

Figure 5.7 - Standardised deviation from the mean contribution of each group to the total phytoplankton biovolume at stn MC.

5.2.3 Zooplankton general patterns

The PCA (see section 2.6.4 for explanation on the method) performed on the annual mean abundances of the 13 major zooplankton groups, sorted under the microscope, at stn MC (i.e., copepods, chaetognaths, jellyfish, siphonophores, doliolids, salps, appendicularians, the cladocerans *Penilia avirostris*, *Evadne* spp. and *Podon* spp., decapod larvae, ostracods and echinoderm larvae) revealed similarities in the interannual changes of some of them. The 1st PC accounted for 36% of the total common variability compared to 21% for the 2nd PC. Although, both PCs together represent only half of the total variability, the contribution of the zooplankton groups to the construction of these two new axes revealed some relevant patterns (Fig.5.8).

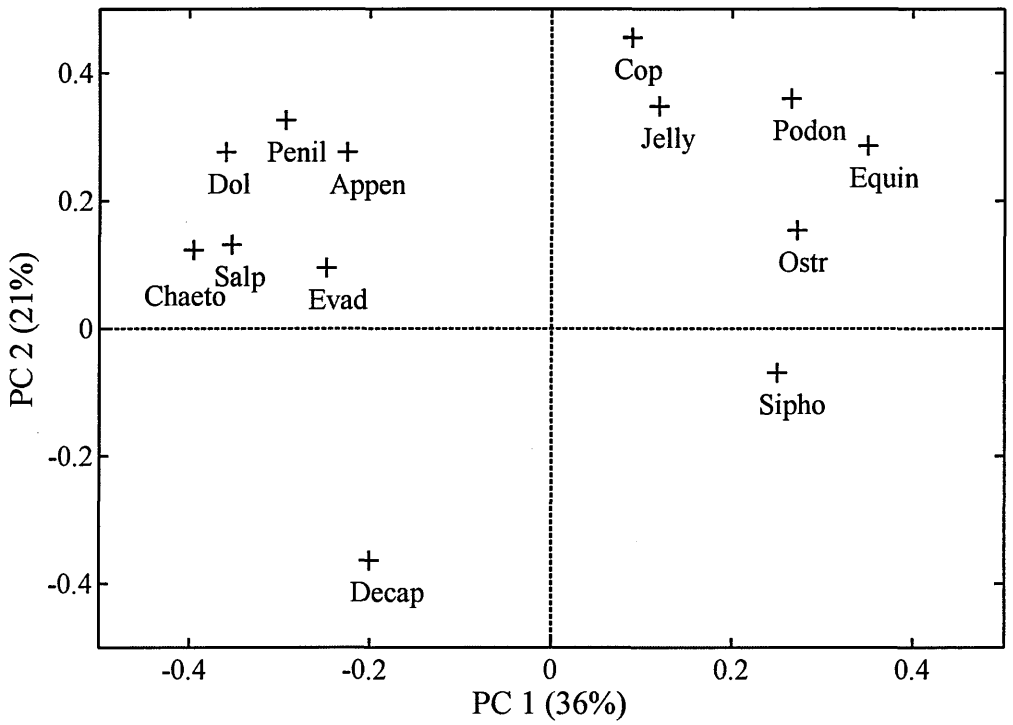

Figure 5.8 - Saturation space of the 1st and 2nd PCs and the position of the several zooplankton groups in this space.

All zooplankton groups placed in the first quadrant of the saturation space of these two PCs (i.e., chaetognaths, appendicularians, doliolids, salps and cladocerans *Penilia avirostris* and *Evadne* spp.) presented their maximal annual abundances in the second half of the year, between July and November (Fig.5.9 A-F). All these groups, except the carnivorous chaetognaths, are very efficient filter feeders. Chaetognath abundance increased, and appendicularia, salps and doliolids tended to increase their presence in the water column in the second period of the time series, whereas cladocerans seemed to be mainly controlled by physiological constraints, reflected by ~2-year cyclical outbursts.

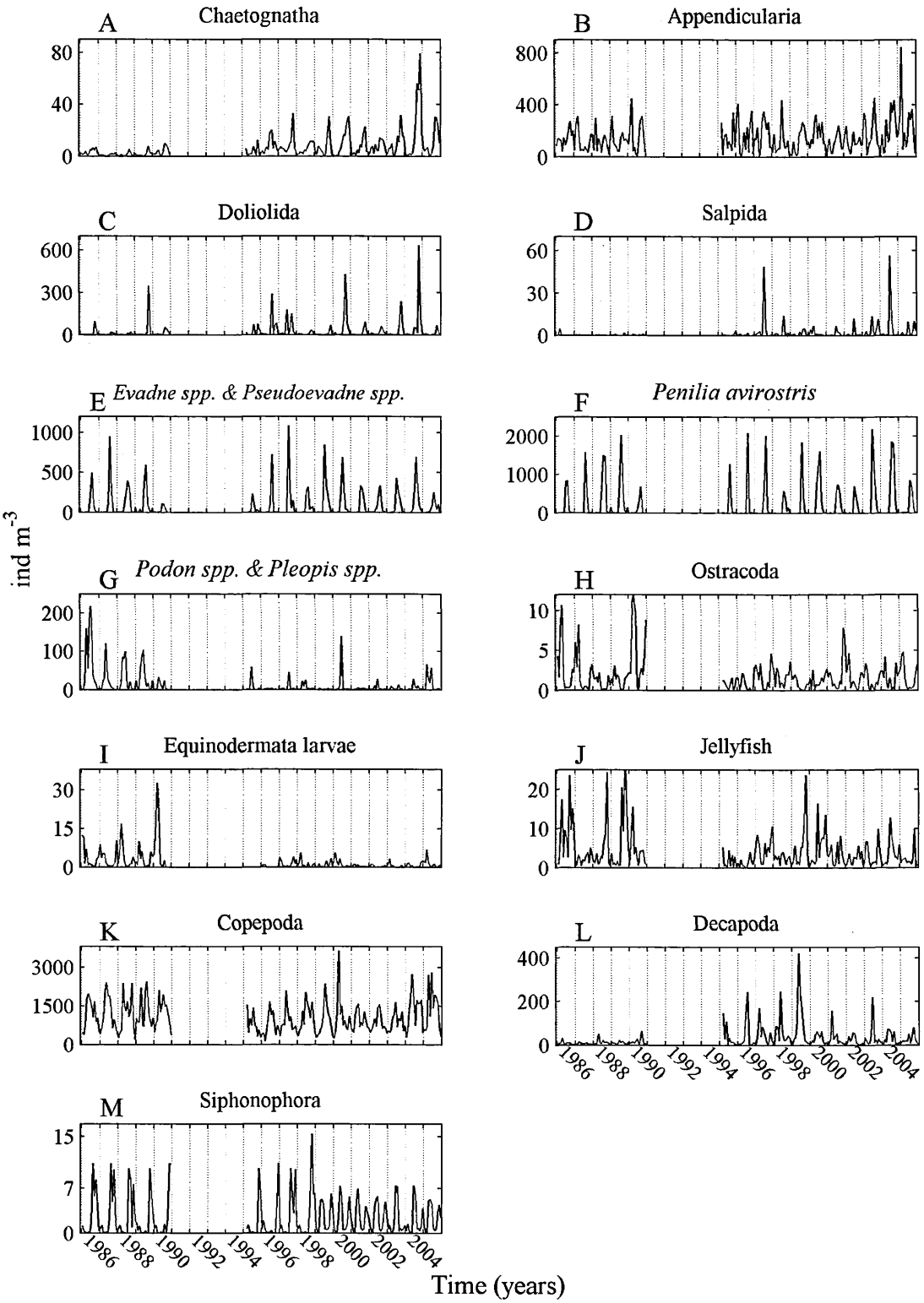

Figure 5.9 - Monthly time series of the 13 zooplankton groups sorted under the microscope. The order of the groups follows their position in the saturation space of the 1st PC and 2nd PC obtained from the PCA performed on their average annual abundances.

In the second quadrant of the space defined by the two PCs, *Podon* spp., echinoderm larvae and ostracoda were grouped, all presenting their annual peaks in the first part of the year, between winter and early summer, and with lower abundance records in the second part of the time series (Fig.5.9 G-I), in contrast to the previous long-term pattern (Fig.5.9 A-D). Abundance of the cladoceran *Podon* spp. was correlated to dinoflagellate abundance (Bravais-Pearson correlation, $r = 0.56$; $p<0.0001$). Copepods were mostly positively related to the 2nd PC.

The 1st PC reflected higher abundances in the first period of the time series than later (Fig.5.10A). The 2nd PC showed a similar pattern, although less marked, and it also reflected the increase of copepod abundance after 2002 (Fig.5.10B, Fig.5.9K).

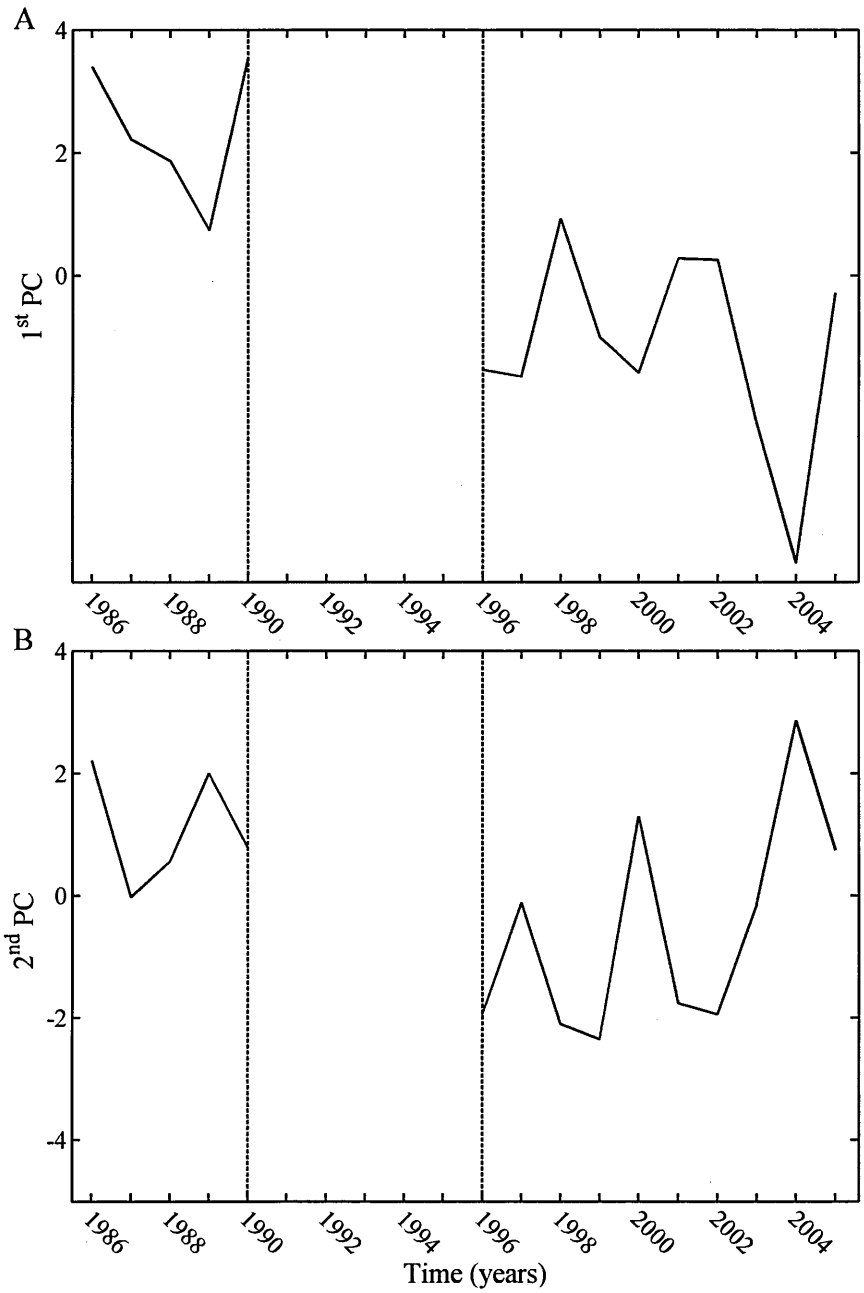

Figure 5.10 - Temporal variability of the 1st PC (A) and 2nd PC (B) of the annual mean abundance of zooplankton groups.

5.2.4 Copepod abundance and size distribution

Total copepod abundance (adults and copepodites), inferred using the ZooScan, varied from minimal annual concentrations of 100-500 individuals m^{-3} to maximal values of 2000-5000 individuals m^{-3} (Fig.5.11A). Years from 1997 to 2001 were characterised by annual mean abundances below the long-term average (Fig.5.11B).

Maximal annual abundance was generally between April and October, while minimal abundances were recorded between December and February (Fig.5.11C). In 2003, the autumn copepod community was more abundant than the seasonal average, following a high peak in August. The following years, three high peaks were recorded in spring, summer and autumn.

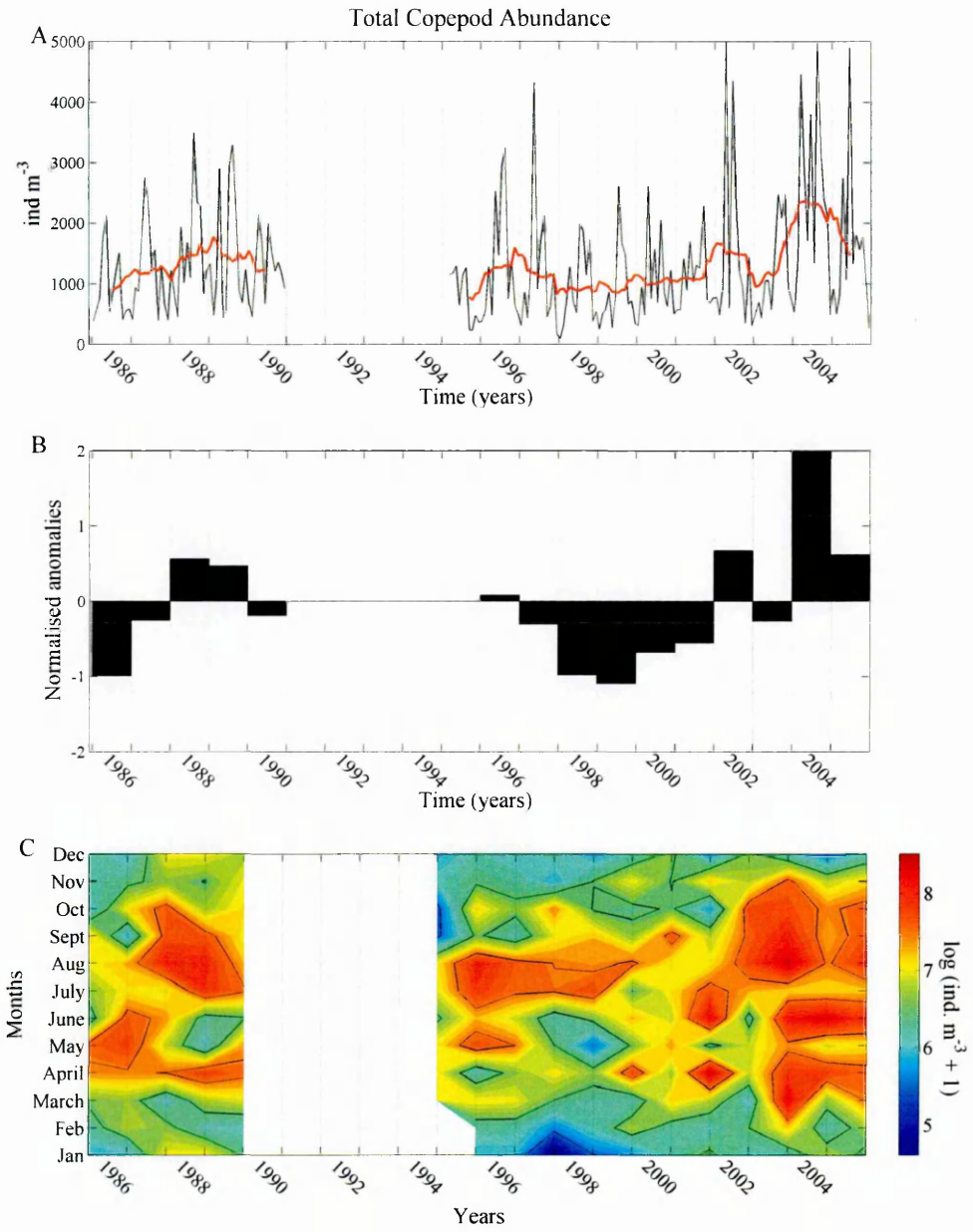

Figure 5.11 - Copepod abundance at stn MC. A) Monthly time series (black line) and an annual (i.e., 12 points window) moving average to smooth the seasonal signal (red line); B) annual normalised anomalies; C) seasonal and interannual variability of log (abundance+1).

Minimal and maximal annual values of copepod size-spectrum diversity were below the long-term average at the beginning of the time series (Fig.5.12A). The annual mean size diversity was below the long-term average during the first period, whereas from 1996 to 2001 the annual mean was constantly above the average, and from 2002 it slightly decreased (Fig.5.12B). Rather similar patterns were found in mean copepod body size and spectrum slope indexes (figures in Appendix IV).

Lowest annual size diversity was usually recorded in summer (Fig.5.12C). In the 1980s a single annual peak was recorded in spring, in 1990 and the mid-1990s size diversity was also high in autumn-winter.

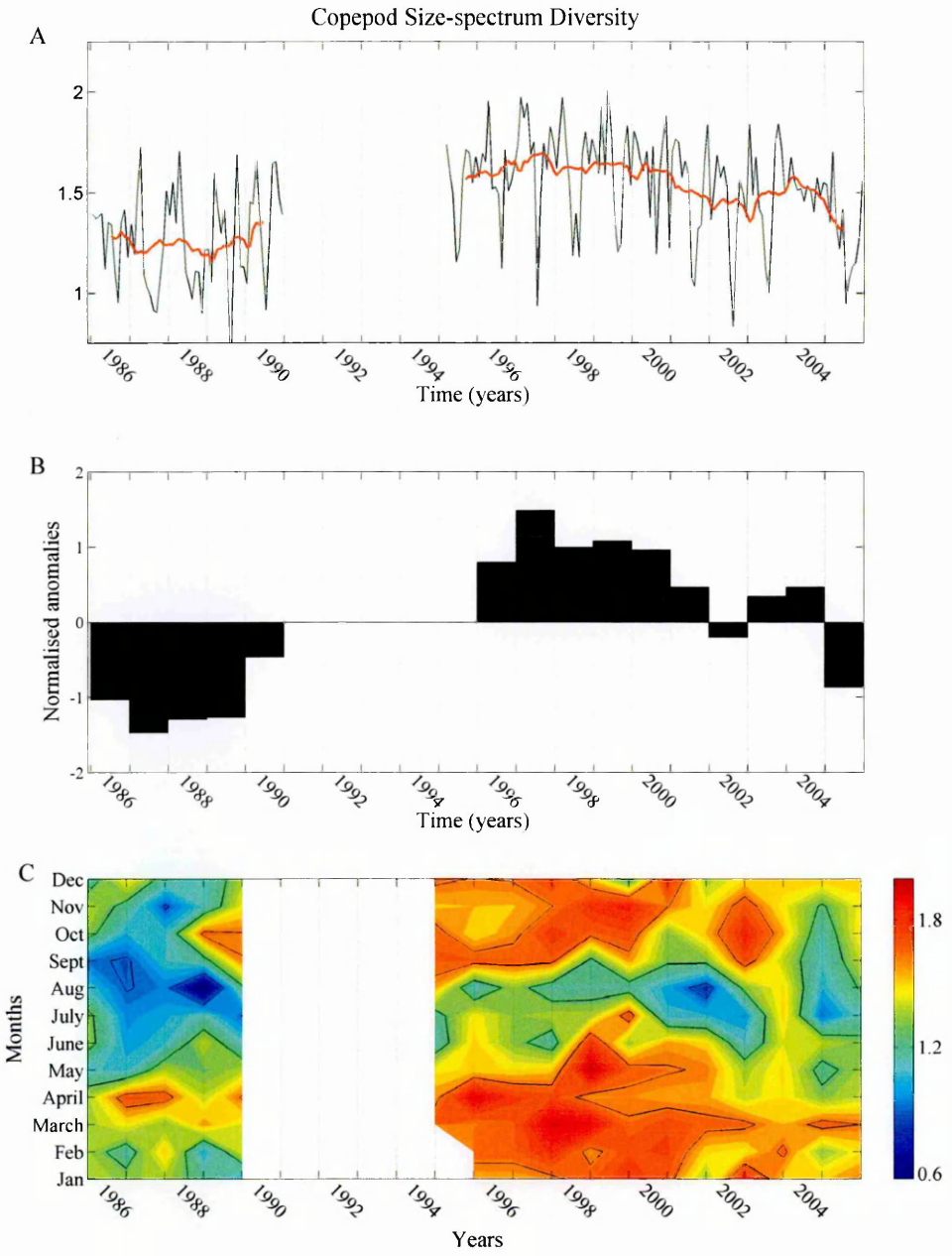

Figure 5.12 - Copepod size-spectrum diversity at stn MC. A) Monthly time series (black line) and an annual (i.e., 12 points window) moving average to smooth the seasonal signal (red line); B) annual normalised anomalies; C) seasonal and interannual variability.

To classify the size spectra by their shape, a cluster analysis was performed on the Kolmogorov distances of the size classes of each spectrum. The resulting dendogram (Fig.5.13) was cut at a distance of 40 to obtain five groups of spectra. The groups differed mainly in the position and width of the spectra mode, and in the presence of large copepods (Fig.5.14). Spectra belonging to group 1 were the steepest, with the narrowest mode and lacked copepods representing the large size classes. Spectra of group 5 were the flattest, with the widest mode and highest presence of large copepods.

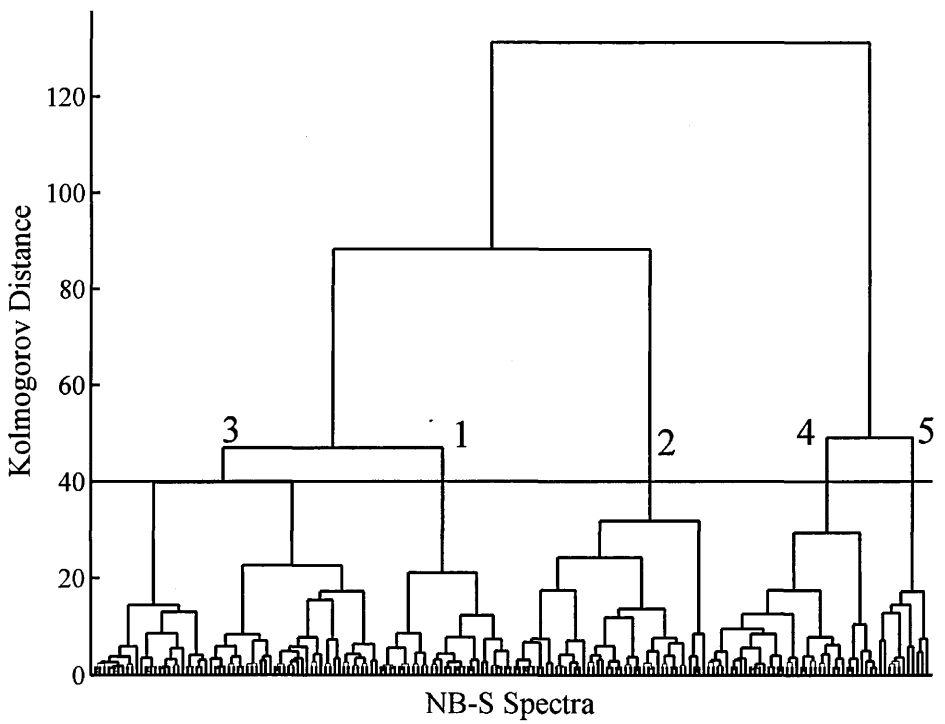

Figure 5.13 - Dendrogram obtained from the hierarchical cluster analysis performed on the Kolmogorov distances of the cumulative sum of the MC NB-S spectra size classes. Hierarchical (cut-off) level at 40 highlighted 5 groups.

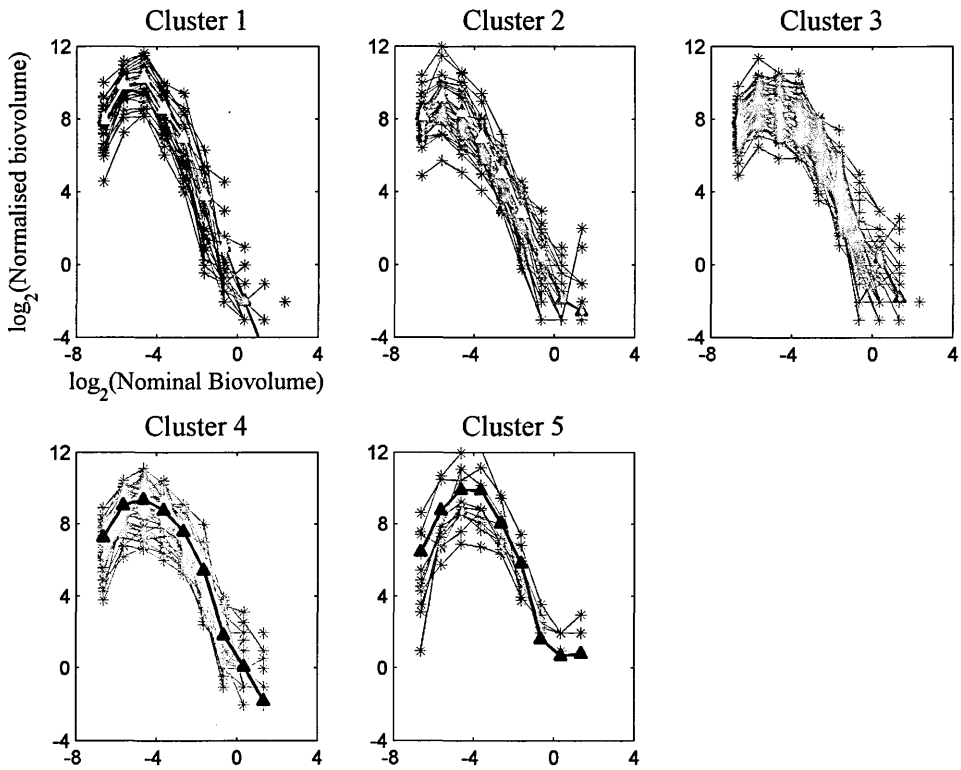

Figure 5.14 – MC Spectra constituting each of the five clusters with the average spectrum of each cluster superposed (bold line with triangle marks).

In the first part of the time series, only 7% of the spectra belonged to group 4 and none of the spectra was classified as part of group 5 (Fig.5.15). In the 1990s, 39% of the spectra belonged to group 3, and 25% to group 4. In group 5, ten out of the eleven spectra occurred in the 1997-2000 period. Finally, from 2002 to 2005, 50% of the spectra belonged to groups 3 and 4. Seasonality was not very marked. Yet, summer was usually the season presenting the steepest annual spectra.

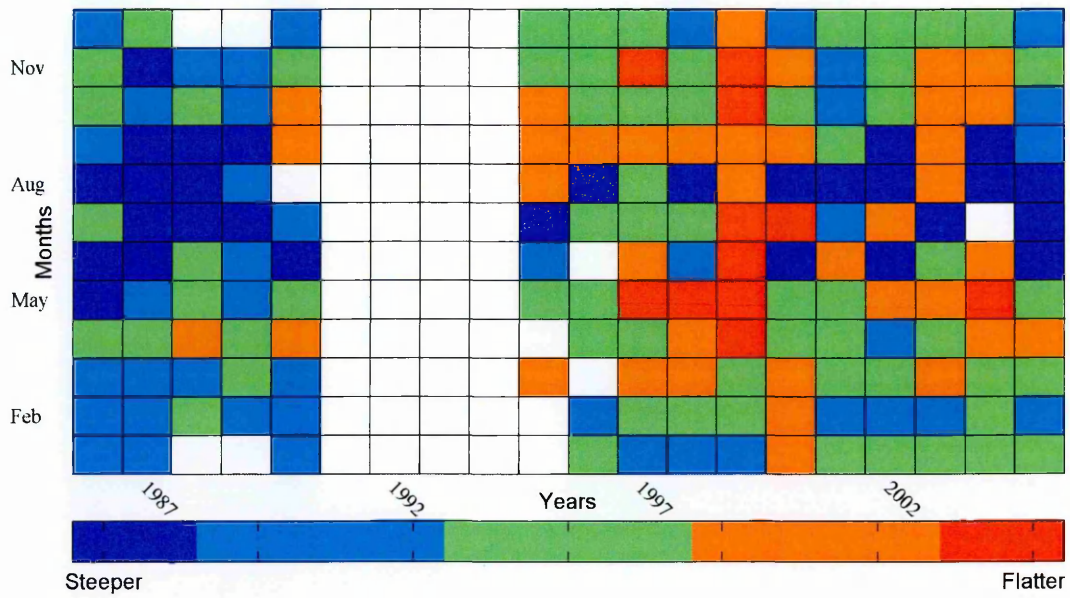

Figure 5.15 - Seasonality and interannual variability of the MC spectra shape. Colour codes are the same as in Fig. 4.13; Group 1 gathers the steepest spectra and group 5 the flattest.

From the cluster analysis, it can be observed that the small size fraction of the spectra decreased throughout the years, while the large size fraction seemed to increase. To have a better insight of these changes, the abundance of the first two size classes (small) and the last six classes (large) of the spectra were explored separately.

The size fraction containing copepods smaller than 0.04 mm^3 (~ < 700 μm length) corresponded on average to 50% of the whole copepod abundance. The amplitude of the signal was high, with the lowest annual values ranging from 50 to 300 individuals m^{-3}, and peaks between 500 and 3500 ind. m^{-3} (Fig.5.16A). Annual mean values were below the long-term average from 1996 to 2001 (Fig.5.16B). Indeed, the average annual amplitude (i.e., the average difference between annual minimum and maximum values) of the ratio between small copepod abundance and total copepod abundance in the samples presented a shift during the interruption of the time series. It was 35-73% for the first years of the time series, to then decrease to 25-60% in the second period, from 1996 to 2005.

Seasonality of small copepods was not very marked; punctual peaks occurred between early spring and autumn, and the lowest records occurred in winter (Fig.5.16C).

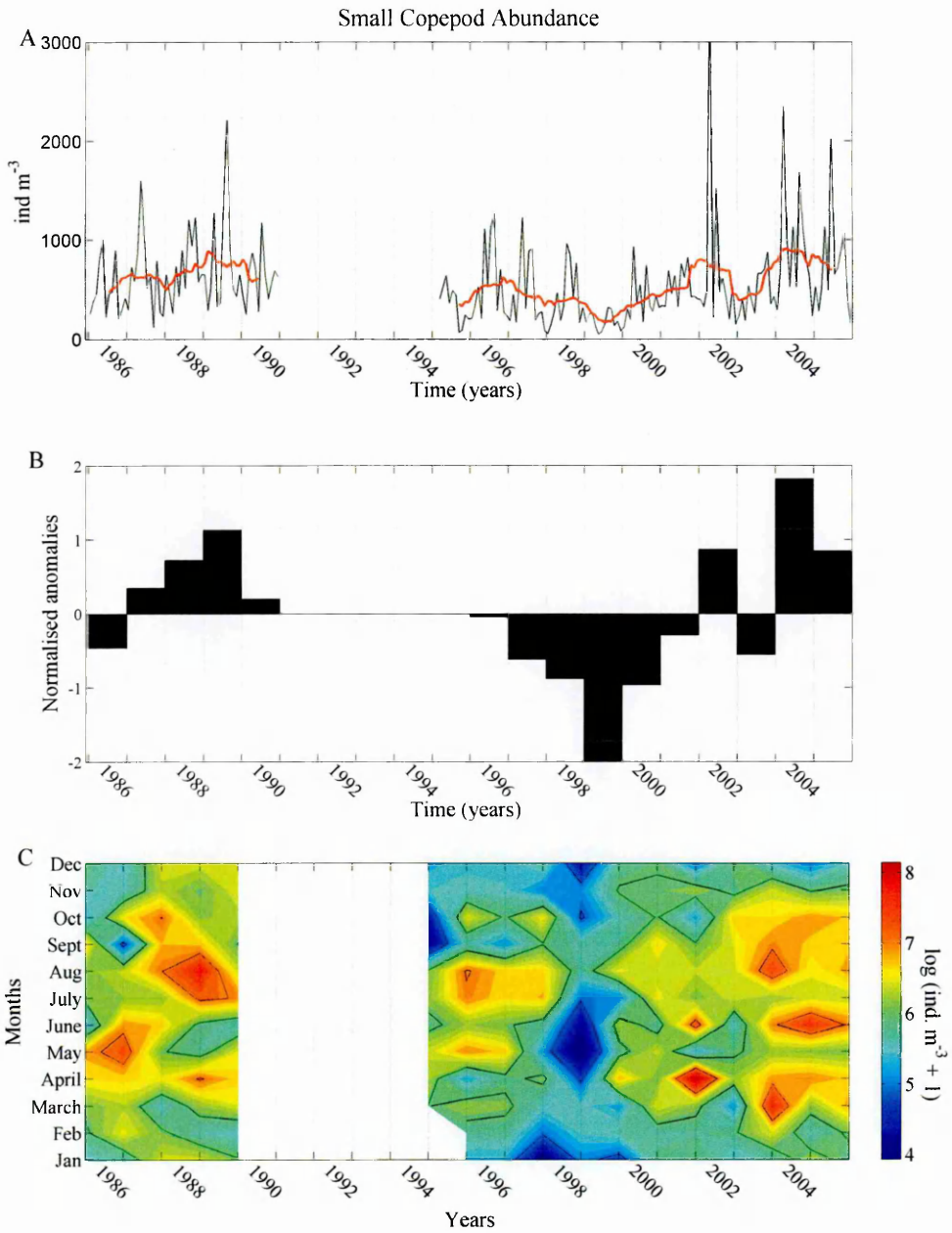

Figure 5.16 - Abundance of copepods smaller than 0.04 mm^3 at stn MC. A) Monthly time series (black line) and an annual (i.e., 12 points window) moving average to smooth the seasonal signal (red line); B) annual normalised anomalies; C) seasonal and interannual variability of log (abundance+1).

The large size fraction of the spectra (> 0.32 mm^3 ~ 1.5 µm length) accounted on average only for 2% of the whole copepod abundance. Large copepod annual abundance ranged from a few individuals to 50-100 individuals m^{-3} (Fig.5.17A). Annual mean values were below the long-term average from 1986 to 1990, and generally above the average from 1996 to the end of the time series (Fig.5.17B). In agreement to this, the average annual amplitude of the ratio between large copepod and total copepod abundances increased from 0.05-0.38% for the first years of the time series to 2-5% in the second part of the time series.

During the first period, the abundance of large copepods peaked in spring (Fig.5.17C). In 1990 and after the interruption, they were generally most abundant in autumn. From 2002, the early spring peak disappeared.

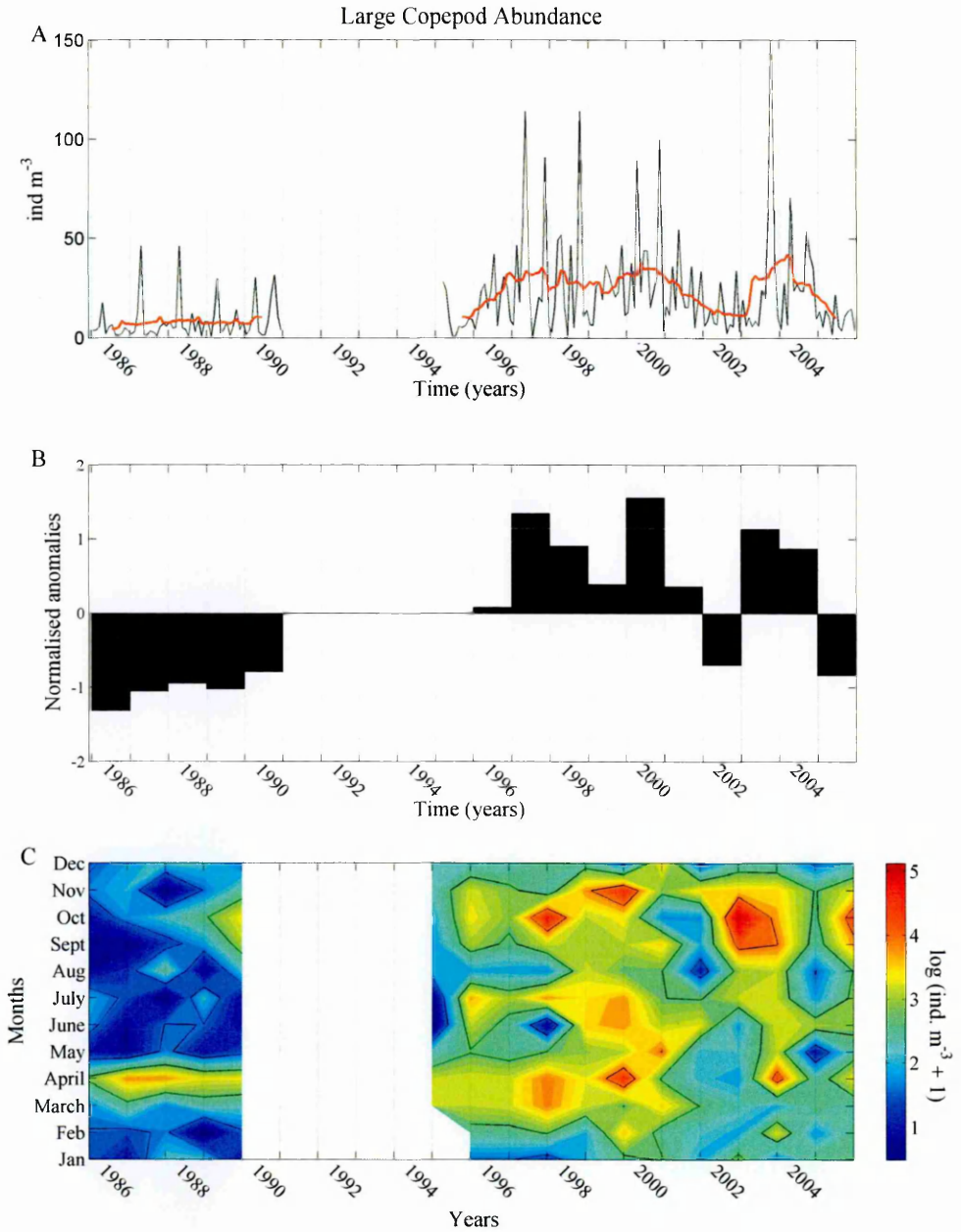

Figure 5.17 - Abundance of copepods larger than 0.32 mm^3 at stn MC. A) Monthly time series (black line) and an annual (i.e., 12 points window) moving average to smooth the seasonal signal (red line); B) annual normalised anomalies; C) seasonal and interannual variability of log (abundance+1).

5.2.5 Copepod size distribution and copepod community composition

Copepodites belonging to 35 copepod taxonomic groups were sorted under the microscope. Five copepod groups contributed to 92% of the whole copepodite abundance. *Clausocalanus* spp. and *Paracalanus* spp. copepodites constituted a single group and, on average, they accounted for 48.6% of the total copepodite abundance.

Acartia clausi copepodites accounted for 13.6%, *Centropages typicus* for 11.7%, *Temora stylifera* for 9.6% and *Oithona* spp. accounted for 8.6% of the total copepodite abundance.

Small copepod abundance (abundance of copepods smaller than *0.04* mm^3) reflected well changes in total copepodite abundance (Fig.5.18). Both abundances (single dates; previously log transformed) were highly linearly correlated (185 pairs of data; Bravais-Pearson correlation, r = 0.75; p<0.0001).

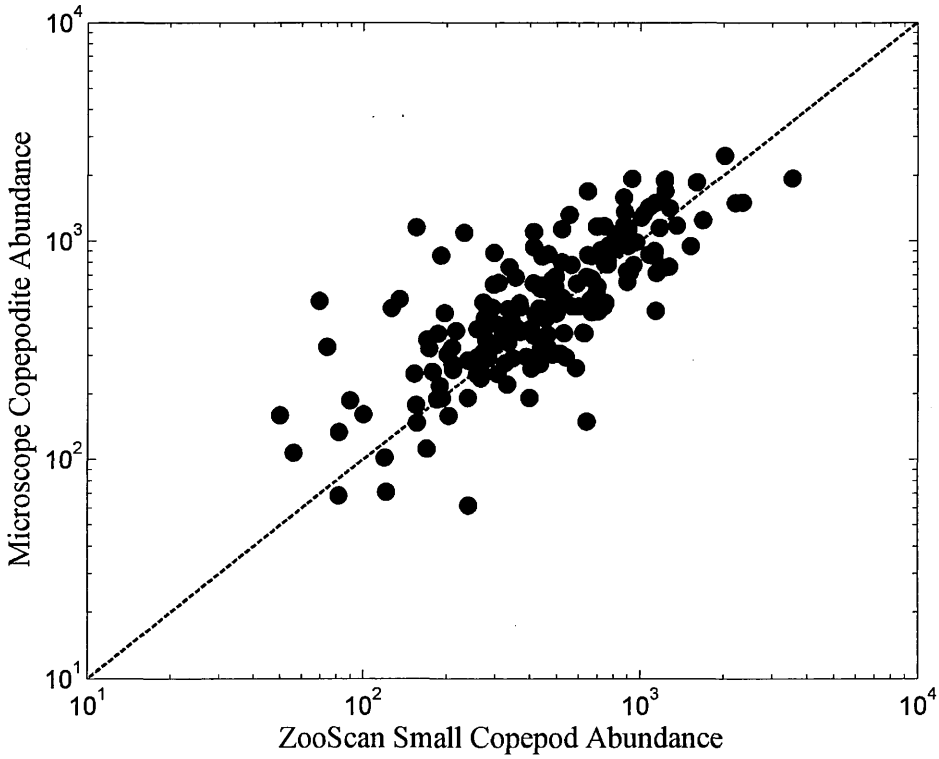

Figure 5.18 - Correlation between small copepod abundance and copepodite abundance at stn MC (185 pairs of data; Bravais-Pearson correlation r = 0.75; p-value <0.00001). The dashed line corresponds to the 1:1 relationship to act as a reference.

Copepodite abundance considerably decreased from 1995 to 2003. Depending on the interannual period, spring, summer and/or autumn peaks were recorded. Winter was the season with less copepodites throughout the time series (Fig.5.19).

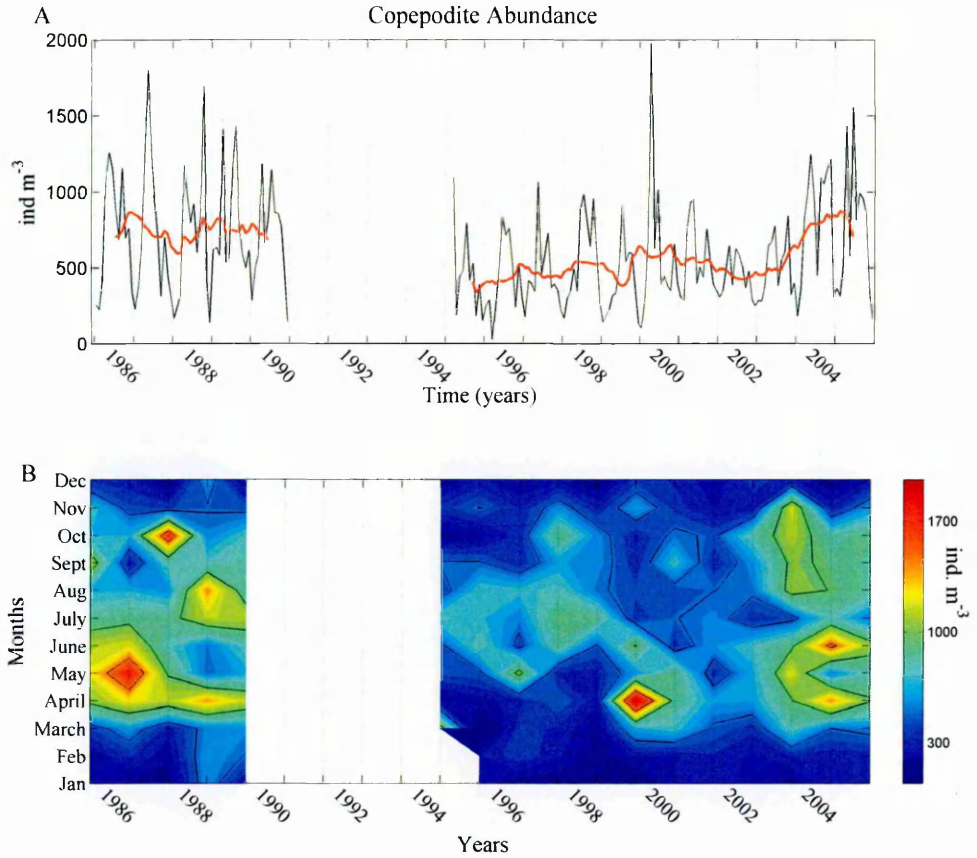

Figure 5.19 - Copepodite abundance at stn MC obtained by sorting under the microscope. A) Monthly time series (black line) and an annual (i.e., 12 points window) moving average to smooth the seasonal signal (red line); B) seasonal and interannual variability of abundance.

At genera or species level, groups showed diverse patterns. While *Temora stylifera* did not present any clear interannual pattern, *Centropages typicus* did present higher copepodite abundance in the first part of the time series than afterwards, as well as *Acartia clausi* that presented peaks that lasted longer in the 1980s (Fig.5.20). Both, *Centropages typicus* and *Acartia clausi* present similar seasonal patterns, with their peaks in spring-early summer. The group of copepodites belonging to *Clausocalanus* spp. and *Paracalanus* spp. and to *Oithona* spp. presented lowest concentrations in the 1995-1999 period. The highest concentrations of *Oithona* spp. occurred in the last part of the time series.

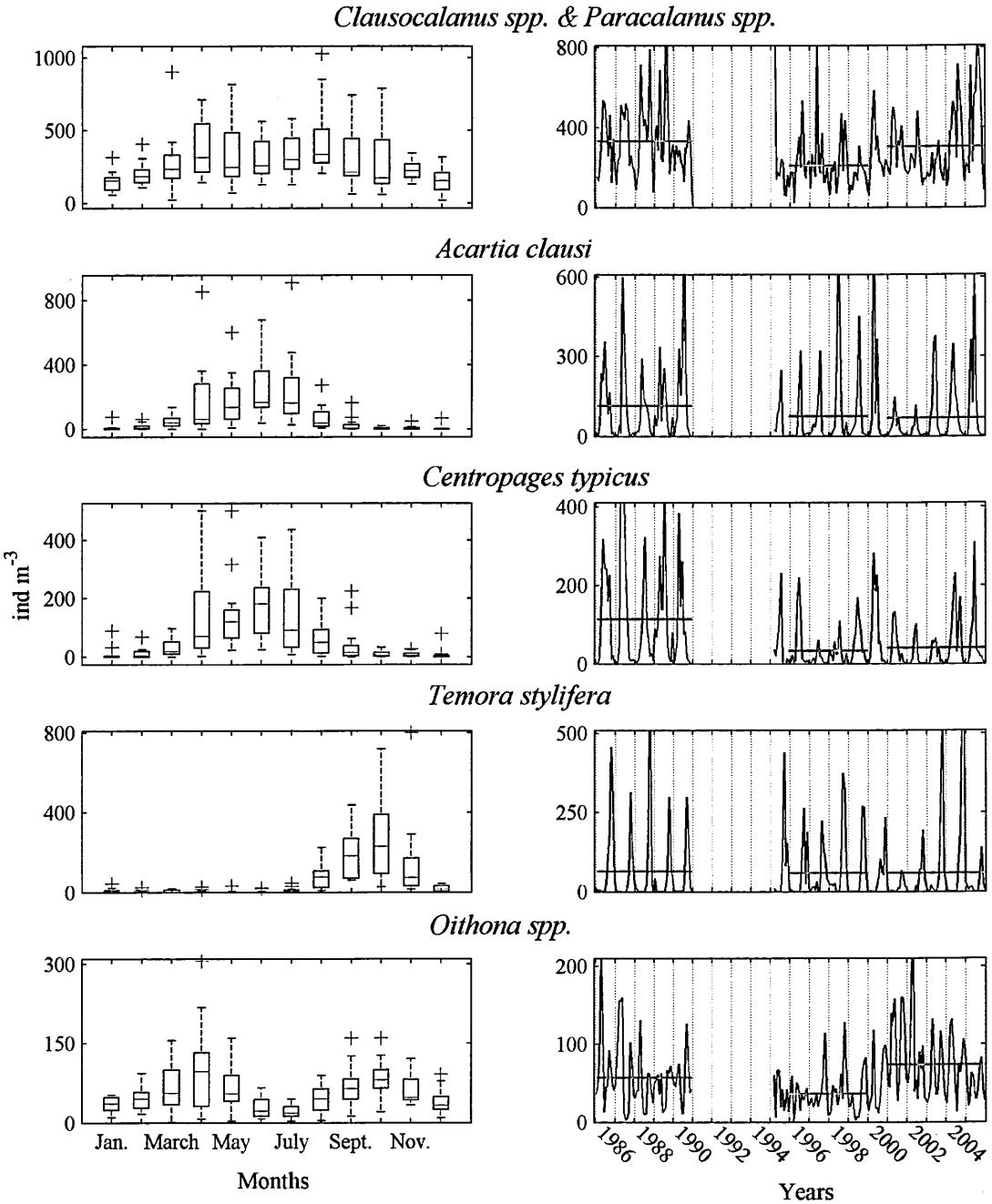

Figure 5.20 - Copepodite abundance of the top five taxonomic groups contributing most to total copepodite abundance at stn MC. Left panels depict boxplots of their seasonal cycles (red lines indicate the median of each month's distribution, whiskers are 1.5 time the interquartile range, and outliers are indicated by the red crosses), while right panels correspond to their long term changes (red lines correspond to the mean values of each five-year periods).

Offshore copepods (see section 3.4.3 for list of species) were correlated to the large copepod fraction (copepods larger than 0.32 mm^3) of the size spectra (single dates; both previously log transformed, 185 pairs of data; Bravais-Pearson correlation after correction for autocorrelation, $r = 0.46$; $p<0.0001$) (Fig.5.21).

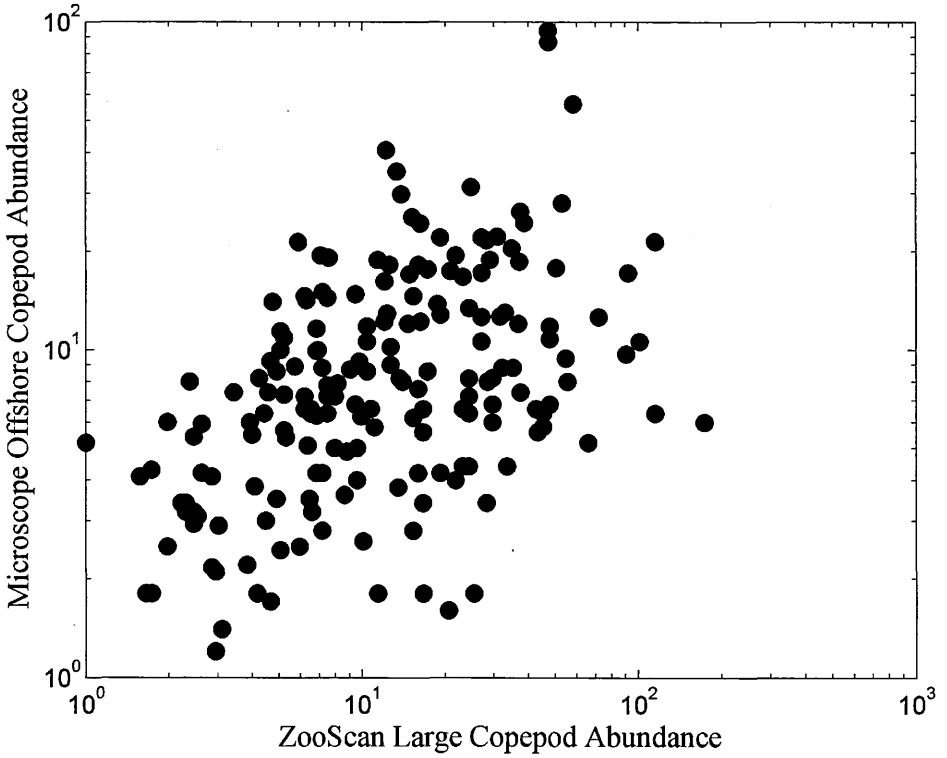

Figure 5.21 - Correlation between large copepod abundance and offshore copepod abundance at stn MC (185 pairs of data; Bravais-Pearson correlation $r = 0.46$; $p<0.00001$).

Offshore copepods occurred in low numbers with concentrations usually oscillating between 1 and 20 ind. m^{-3} per month. From 1997 to 2000, the annual mean abundance was above the long-term average (Fig.5.22). In the first part of the time series a single annual peak occurred in spring, whereas after the major interruption other peaks were recorded between August and February.

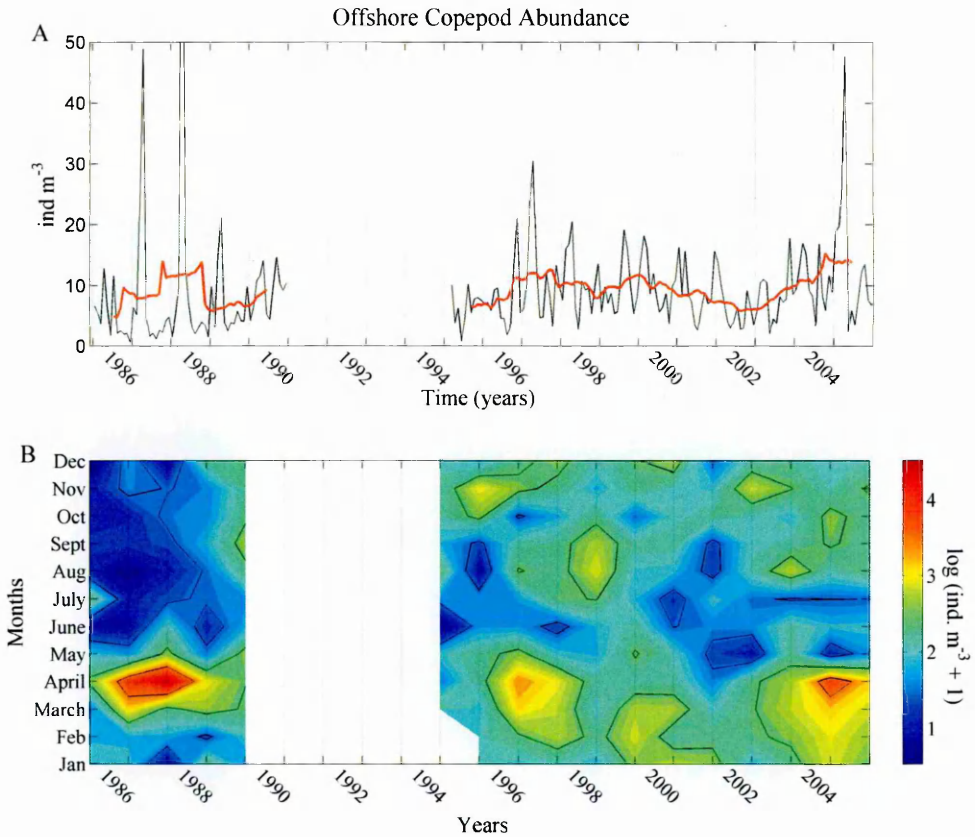

Figure 5.22 - Offshore copepod abundance (microscope counts) at stn MC. A) Monthly time series (black line) and an annual (i.e., 12 points window) moving average to smooth the seasonal signal (red line); B) seasonal and interannual variability of log(abundance+1).

The Shannon Index computed on the adult abundance of 45 copepod groups (species and genera) was compared to size diversity. Both indexes were normalised by the maximum possible value of each series, log(S), where S is the number of species and number of size classes, 45 and 11 respectively (Pielou 1975). Species diversity was significantly correlated with size diversity (185 pairs of data; Bravais-Pearson correlation accounting for the reduction of degrees of freedom due to autocorrelation, $r = 0.56$; p-value<0.00001) (Fig.5.23).

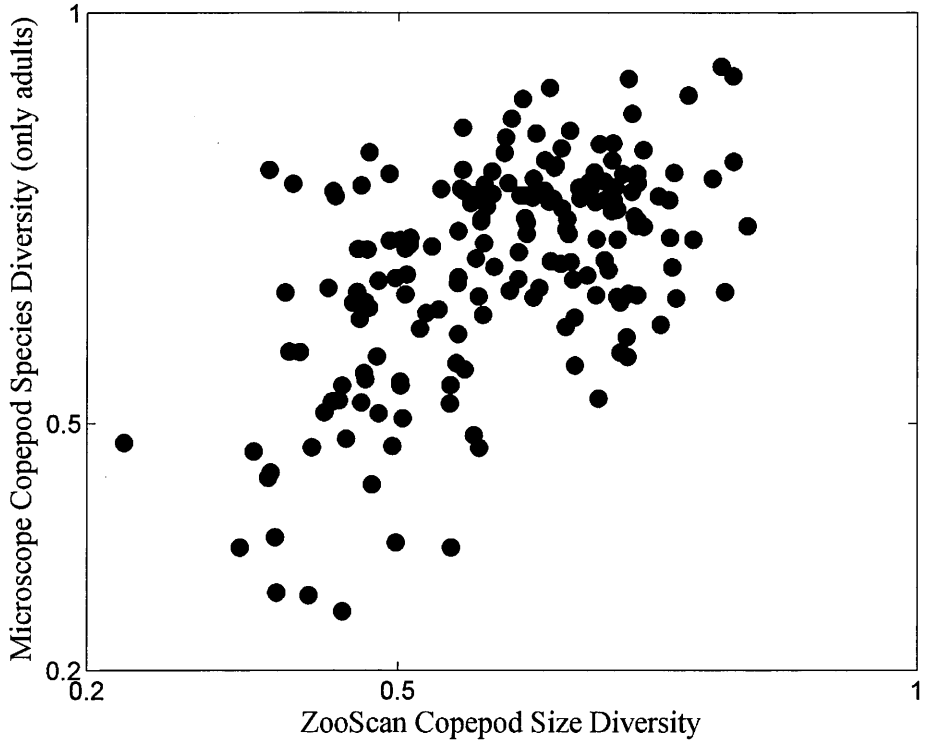

Figure 5.23 - Correlation between species diversity (only adult abundances considered) and size diversity at stn MC (185 pairs of data; Bravais-Pearson correlation r = 0.56; p-value<0.00001).

Species diversity varied from 1 to 4 throughout the time series (Fig.5.24). Annual mean values were mainly above the long-term average from 1996 to 2002. The season that presented the lowest species diversity was summer, and highest annual values occurred usually in winter.

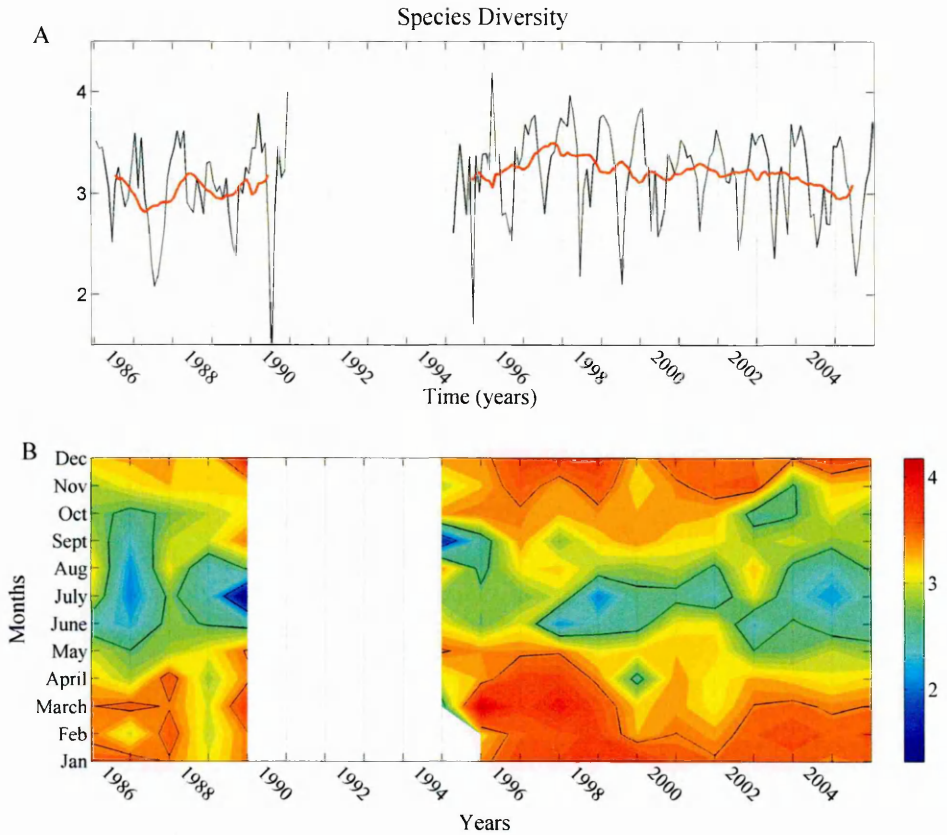

Figure 5.24 - Shannon Index computed on 35 copepod taxonomic groups from stn MC sorted under the microscope. A) Monthly time series (black line) and an annual (i.e., 12 points window) moving average to smooth the seasonal signal (red line); B) seasonal and interannual variability.

5.2.6 Phytoplankton and copepod size distribution

Chl *a* annual mean concentration and annual mean copepod size-spectrum diversity were highly anticorrelated (16 pairs of data; Bravais-Pearson after correction for autocorrelation, $r = -0.69$, p-value < 0.05). At the seasonal level (i.e., three-month mean value, winter starting from December), significant anticorrelation was only found in spring (16 pairs of data; $r = -0.76$, p-value < 0.05) and autumn (16 pairs of data; $r = -0.6$, p-value<0.05). Copepod size diversity was weakly but significantly correlated to the small phytoflagellate abundance ratio measured one month earlier (185 pairs of data; Bravais-Pearson after correction for autocorrelation, $r = 0.24$, p-value < 0.01). The same correlation was found between phytoplankton mean-cell size and copepodite

concentration a month later (185 pairs of data; Bravais-Pearson after correction for autocorrelation, r = 0.28, p-value = 0.0001) (Fig.5.25).

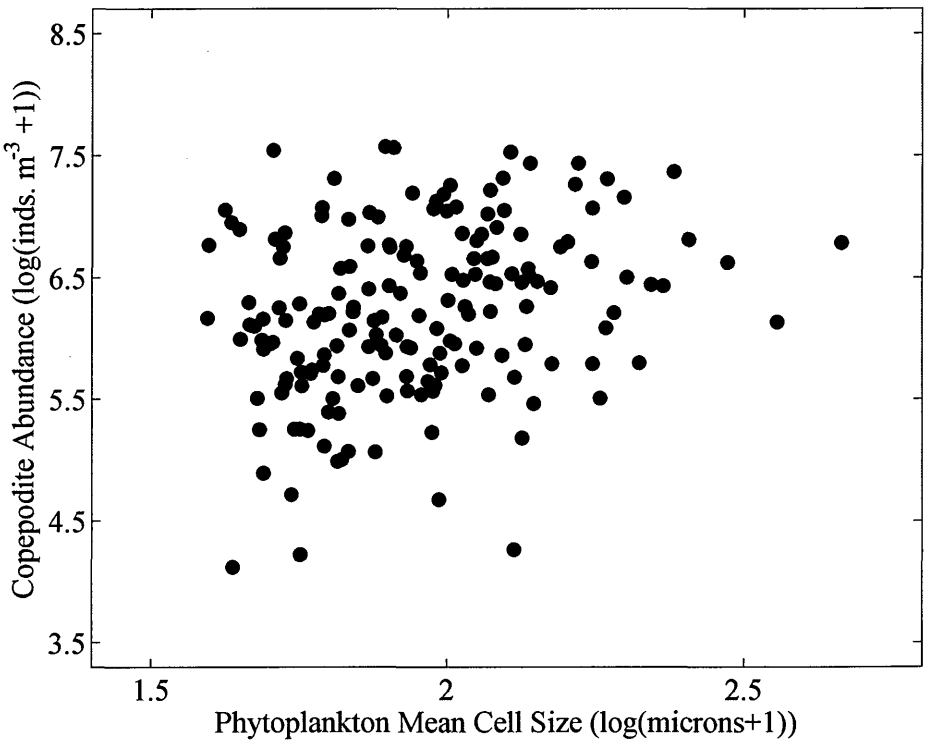

Figure 5.25 - Correlation between phytoplankton mean cell size (μm ESD) and copepodite abundance a month later at stn MC (both measure log transformed) (185 pairs of data; Spearman rank $\rho = 0.28$; p-value = 0.0001).

5.3 Discussion

5.3.1 Phytoplankton changes related to earlier and enhanced stratification

Diatom, small phytoflagellate and dinoflagellate phenological changes tightly reflected the observed changes in the water-column stability, which were mainly driven by increasing temperatures. It seems that in response to an earlier onset of stratification and to stronger summer stability in the second period of the time series, the concentration of the most abundant phytoplankton groups (e.g., diatoms and phytoflagellates < 10 μm) in the water column occurred earlier in the year, and that high concentrations lasted longer. In other words, the winter season, characterised by a mixed water-column and low phytoplankton concentrations, was shorter in the second part of the time series. This change was accompanied by a notable decrease of chl *a* concentration that was likely due to the more intense occurrence of small flagellates and small diatoms (Ribera d'Alcalà et al. 2004). These results at stn MC are in accordance with the general observations and predictions for marine primary production due to global warming (IPCC 2007).

The annual primary production in the global ocean decreased by 6.3% when comparing ocean-colour derived values of the CZCS (1979-1986) period to the SeaWiFS (1997-2002) period; this decrease was accompanied by a 0.2 °C thermal increase (Gregg et al. 2003). Increasing temperature enhances stratification in temperate areas, and thus causes nutrient depletion by reducing nutrient input from deeper waters (Kamykowski and Zentara 1986; Sarmiento et al. 1998). Also the comparison of ocean-colour derived values of the CZCS (1979-1986) period to the SeaWiFS (1997-2002) period in the Mediterranean basin resulted in lower chl *a* in the second period, although this decrease was not quantified (Barale et al. 2008). At stn MC, nutrients are seldom depleted. Although a clear decreasing trend of nutrient concentration was not observed

for the period 1984-2000 (Ribera d'Alcalà et al. 2004), nitrates presented low values more often, and phosphates presented a clear decrease. Usually, nitrogen is considered to characterise the nutritional status of marine systems, neglecting phosphorus. Yet, in some parts of the Mediterranean Sea the nitrate:phosphate ratio is below Redfield (Krom et al. 1991). Moreover, a study on summer production, conducted at the entrance of Villefranche Bay, indicated that bacteria and phytoplankton growth were limited by phosphates rather than by nitrates during the stratification period (Thingstad et al. 1998). The authors stressed that the results were not related to fresh water input.

Coinciding with stratification enhancement, in the second part of the time series small phytoflagellates increased their numbers and relative biovolume in the water column, outnumbering diatoms more often than in the first period. The increase of small phytoflagellate abundance was probably favoured by a decrease of trophism related to stronger stratification. The group of small phytoflagellates at stn MC includes mainly autotrophic but also heterotrophic cells, although the two categories are not separately quantified. The heterotrophic flagellates are the main grazers of low productive ecosystems, where prokaryotes and picoplankton dominate primary producers (Calbet 2008 and references therein). Dinoflagellate abundance and biovolume decreased in the second period. Heterotrophic dinoflagellates are typical of coastal areas and other productive systems; their high biomass during blooms of large diatom chains suggests a role as main grazers of diatoms (Sherr and Sherr 2007). At stn MC, the shift in predominance of large diatoms vs small diatoms, together with the increased concentration of small phytoflagellates was reflected in the higher frequency of samples with mean cell-size < 5 μm ESD during the second part of the time series with respect to the 1980s.

The changes reported above match predictions on the effect of stratification enhancement on phytoplankton assemblages. Further stratification due to global warming would affect pelagic food webs, by favouring the microbial loop based on nitrogen regeneration over the classical food web based on diatoms (Karl et al. 2001). In a recent model, Bopp et al. (2005) predicted that stratification enhancement in the surface layers of temperate oceans would cause the decrease of diatom relative abundance, and would favour small phytoplankton, due to the lower half-saturation rates and sinking speeds of the latter. It seems that similar changes might have occurred at stn MC during the early 1990s, with small cells dominating the phytoplankton communities, likely as a response to climate forcing.

5.3.2 Copepod changes related to phytoplankton changes

Previous studies that focused on copepod species revealed strong seasonal patterns but not major interannual changes at stn MC (Mazzocchi and Ribera d'Alcalà 1995; Ribera d'Alcalà et al. 2004; Mazzocchi et al. 2010). However, in the present study, differences in the interannual variability of total copepod abundance and size distribution were detected, which seemed to be related to the phytoplankton changes.

Total copepod abundance presented lower annual peaks between 1997 and 2001 at the same time as a decrease in chl *a* at stn MC. Copepod size-spectrum diversity showed an increasing trend that was opposite to the decreasing trend of chl *a* concentration. Annual mean values of chl *a* and copepod size-spectrum diversity were highly anticorrelated. In addition, copepod size-spectrum diversity was correlated with small phytoflagellate relative abundance one month earlier. These results seem to point to a negative effect of the phytoplankton-assemblage changes on the copepod community. Phytoplankton were more abundant, but composed of smaller cells in the second period of the time series. Small phytoflagellates alternate with diatoms as the

dominant group of phytoplankton assemblages at stn MC (Ribera d'Alcalà et al. 2004). Both abundances were highly anticorrelated, and in the second part of the time series small phytoflagellates tended to dominate over diatoms. This could have represented a detrimental change to grazer copepods in terms of the quantity and quality of potential food availability.

The structure of phytoplankton assemblages plays a key role in copepod food limitation (Dam and Peterson 1991), and changes in potential-prey composition may significantly affect copepod growth and fecundity (Hirst and Lampitt 1998 and references therein). Nevertheless, the effect of prey composition on copepod populations is not clear yet due to contradictory results on nutritional value and toxicity, mainly of diatoms and dinoflagellates (e.g., Kleppel 1993; Irigoien et al. 2002; Broglio et al. 2003; Ianora et al. 2003; Jones and Flynn 2005; Paffenhöfer et al. 2005).

Spectra clustering showed that copepod size distribution shifted to spectra with lower contributions of small copepods, a wider mode, and a greater contribution of large copepods in the second period of the time series. The negative anomalies observed in the small copepod abundance, from 1995 to 2003, reflected lower copepodite abundance in that period than in the rest of the time series. It should be noted that copepodite abundance was found to be correlated with phytoplankton mean cell size a month earlier. According to these results, it is hypothesized that copepod reproduction success could have decreased in the 1990s due to detrimental effects of small cells dominating phytoplankton assemblages. It is assumed that copepodites were less abundant due to lower fecundity because fecundity has shown a stronger dependency on nutrient availability than copepodite developmental rates and growth, and because in the case of nauplii growth no nutrient dependency has been found (Kiørboe 1998; Hirst and Bunker 2003). Kiørboe (1998) observed a variability of 116% in situ measurements of

copepod fecundity, 62% in the case of copepodite growth rate and 47% for nauplii, all results reported at 15 °C, and he related this variability to the limitation of food for each stage. An increase in mortality might have played an important role too. Nevertheless, the strong changes found in phytoplankton, and the significant correlations between those changes and copepods, suggest that food is likely to have played a key role in the copepodite reduction reported here.

5.3.3 Proposed scenario of changes at stn MC

The new results on the MC time series presented in this chapter suggest a mechanism that might explain, at least partially, the decrease in copepodite abundance observed at stn MC. Copepod production might have decreased, in the second part of the time series, due to the phytoplankton shift to smaller cell-size species that was induced by earlier and stronger annual stratification. In the second part of the time series, encounter rates between copepods and prey probably increased due to more abundant phytoplankton. Yet, capture efficiency and biomass per cell captured decreased due to the dominance of small cells. This hypothesis can be tested in the future by examining a more extensive dataset of field observations and laboratory experiments acquired at stn MC, such as: (1) the results of grazing experiments recently conducted at stn MC in different seasonal periods with the most abundant calanoid species fed on natural particle assemblages (Mazzocchi et al., unpublished data), and (2) a decadal time series of egg production and viability of the abundant species *Centropages typicus* (Ianora, unpublished data).

Experimental studies have stated that copepod ingestion rates depend on cell size (Frost 1972; Frost 1977; Paffenhöfer 1984; Paffenhöfer 1988). In a study on variations of *in situ* ingestion rates and body size of *Temora longicornis* with respect to seasonal variation of chl *a* size-fractions, the authors concluded that food-limitation was more

severe following the onset of stratification in the water column, because net phytoplankton abundance was low (Dam and Peterson 1991). Ingestion rates decreased when the >20 μm or >10 μm size fraction of phytoplankton decreased. When the relative abundance of small cells (e.g., small phytoflagellates) is high, copepods tend to increase the time allocated to filter feeding rather than ambush feeding (Jonsson and Tiselius 1990; Kiørboe et al. 1996). This is in accordance with the optimal foraging theory (Lehman 1976) which predicts that predators tend to select prey with the optimum energy gain:energy expenditure. By grazing on the most abundant small cells, copepod capture efficiency would decrease and energy and time spent on filter feeding increase. Under this scenario, copepods might have had less time for mating and less energy for egg production in the 1990s.

Supporting the proposed scenario, it was reported here that while in the first period only ~20% of samples presented <5 μm mean cell size, in the second part of the time series ~70% of samples presented mean cell size below that threshold. 5-10 μm ESD seems to be the sensitivity threshold for cells to be individually perceived by adult calanoid copepods (Price et al. 1983). Below this threshold, particle retention efficiency of copepods decreases (Berggreen et al. 1988). In the western Mediterranean grazing experiments, on *in situ* phytoplankton assemblages of one-year monthly samples, reported negative selection of five common copepod genera on <5 μm phytoplankton (Broglio et al. 2004). Selectivity was calculated by Chesson's method which removes the effect of relative abundance on ingestion rates. Thus, negative selection reported by Chesson's method could also have been due to low relative ingestion rates related to low capture efficiency when the small-size cells were dominating the assemblages. In the same study, for some experiments, cladocerans were found to select this small size fraction of phytoplankton.

Lower trophic conditions resulting from longer and stronger stratification are expected to favour cladocerans, appendicularians and thaliaceans (e.g., doliolids and salps) over copepods as the former taxa are very efficient filter feeders, and also have high individual and population growth rates induced by temperature increases (Gorsky and Fenaux 1998; Richardson 2008). At stn MC, these three groups, except the cladoceran *Podon* spp., did not shown the general pattern of abundance decrease in the 1990s, as reflected by their relationship with the 1st PC of the zooplankton PCA. The decrease of the cladoceran *Podon* spp. after the 1980s seemed to be related to a reduction in dinoflagellate abundance. The two groups presented strong seasonality, with their peaks in spring.

The scenario proposed above is based on a simplistic mechanism issued from the patterns observed in the synthetic index represented by copepod size-spectrum diversity. Nevertheless, the mechanisms and patterns that govern the structure and dynamics of plankton communities are far from being simple, particularly in the coastal ecosystems that are affected by high variability of both natural and anthropogenic forcing. Various biological interactions and physical factors affect individuals and communities at different time scales. For instance, despite a total copepodite abundance decrease, at species level this was not observed in all of them. Although the spring-summer copepods *Centropages typicus* and *Acartia clausii* had less juveniles in the second part of the time series, *Centropages typicus* presented a much clearer pattern of reduction. The autumn copepod *Temora stylifera* did not show any trend, but it had low abundances in 2001-2002, coinciding with the lowest concentrations of chl *a*. In that period, also *Centropages typicus* and *Acartia clausii* showed their lowest copepodite abundances, but not *Clausocalanus* spp./*Paracalanus* spp. and *Oithona* spp. These two groups showed similar patterns, with 1995-2000 being the period of lowest abundances.

Sommer (1996), in his review on plankton ecology, suggests that the debate about bottom-up control versus top-down control to explain plankton changes is just a product of the scale in which those changes are considered. At a large-scale, like this study (i.e., study of broad groups), bottom-up control may be the main mechanism shaping populations. Yet, regarding single populations, top-down control can be the main forcing, as shown by an Individual Based Model applied to *Temora stylifera* at stn MC (Mazzocchi et al. 2006).

Finally, the reported increase of large copepod abundance after the 1980s pointed to an increasing presence of typical offshore species in the bay after the 1980s. In the first part of the time series, they had a single peak in spring and after they also presented sporadic peaks in autumn-winter. Their arrival in the different seasons might be related to specific behavioural features (i.e., vertical migration), related to a certain moment of their biological cycle, in such a way to provide them with trophic advantages. This hypothesis is supported by the fact that this group is mainly represented by juveniles at stn MC (Mazzocchi et al. 2010). Nevertheless, their increasing presence in winter might be due to more regular coupling between open Tyrrhenian Sea and the Gulf of Naples during that season (Pierini and Simioli 1998). Thus the increasing presence of offshore species at stn MC might be pointing to hydrological changes. Advection, vertical migration and possible swarming are sources of patchiness (Mackas and Boyd 1979; Mackas et al. 1985) that can play a key role in the observed changes at a fixed sampling station. Studies of the on-offshore coupling between water masses in the Gulf of Naples need to be conducted to improve understanding of of the occurrence of offshore species in these coastal waters.

The scenario here proposed points to a direct link, by means of feeding constraints, between copepodite abundance and phytoplankton cell size. These biological changes might have occurred due to climate forcing on stratification dynamics. In the 1990s, stratification started earlier and was stronger mostly due to increasing warming of surface waters. On the other hand, at the other end of the copepod size spectra (i.e., large copepods) indicated an increasing presence of offshore species at stn MC. This could be pointing to a stronger coupling between offshore and coastal systems in the second part of the time series.

Chapter 6. Point B time series

6.1 Introduction

A recent study on the abundance of some copepod, jellyfish and siphonophore target species at Point B has reported important changes in the planktonic community during the period from 1967 to 1993 (Molinero et al. 2005a). The authors found a link between the observed changes and local environmental conditions, and between those local changes and the North Atlantic Oscilation (NAO). In a following study, Molinero et al. (2008b) included chaetognath abundance in their analyses and formulated an explanation for the observed changes as well as a scenario for the following decade. They pointed to a regime shift in 1987 to a more regenerated dominated system in which, due to temperature increase, jellyfish would outcompete chaetognaths and would reduce copepod populations in the 1990s. In their study, top-down control by jellyfish was pointed as the main forcing for the copepod community, whereas the detrimental effect of stronger thermal stratification and thus oligotrophy from the late 1980s was not much taken into account.

In the present thesis, the analyses of Point B ZooScan datasets from 1974 to 2003 were mainly conducted to test observations and predictions of earlier studies. Moreover, the new analyses allowed new explanations and predictions to be formulated based on observations on copepod size distribution. Firstly, interannual changes of copepod, chaetognath, decapod, siphonophore and jellyfish total abundances were analysed (1) to check if the reported changes in some target species were representing changes in broad taxa, and (2) to check if the main prediction of jellyfish top-down control of copepods from the early 1990s was maintained throughout the 1990s until the early 2000s. Secondly, the temporal variability of copepod size distribution was analysed to try to elucidate the main copepod community changes in the 30-year study

and their relationship to environmental changes. To help in the interpretation of results, six-year monthly samples (1979, 1985, 1995-1997, 2003) were semi-automatically recognised to study the abundance of certain copepod species and some efficient filter feeders (see section 2.4.3 for a detailed list of groups). The presence of *Calanus helgolandicus* at Point B was also tracked due to its oceanic character in the Mediterranean Sea (Bonnet et al. 2005).

6.2 Results

6.2.1 Environmental variability

Temperature at Point B, in the period from 1974 to 2003, ranged from 13-14 °C winter minimal to 22-24 °C summer maxima (18-20 °C annual maximum in autumn, at 50 m depth) (Fig.6.1 A, B). Annual mean temperature was mostly below the long-term average before 1983 (Fig.6.1C), it was generally above the average from 1983, and constantly above the long-term average from 1995.

Annual minimal temperature, in winter, was mostly below the long-term average before 1988 (Fig.6.1 D, E). From 1988, winters were milder. Annual maximal temperature, in summer, at 20 m depth showed a periodicity of 5-10 years from values above the long-term average to values below the long-term average. As a result, the 1980s showed the highest amplitude of annual temperature of the time series. In addition, summer thermal stratification occurred one month earlier from the mid-1980s as indicated by the 19°C isoline at 20 m depth (Fig.6.1D).

Each year, a typical seasonal cycle for temperate zones was observed (Fig.6.1D). Thermocline formation occurred at the beginning of summer (Fig.6.1D). Water-column mixing was observed at the beginning of autumn, reflected by the water warming at 50 m depth at about September (Fig.6.1E).

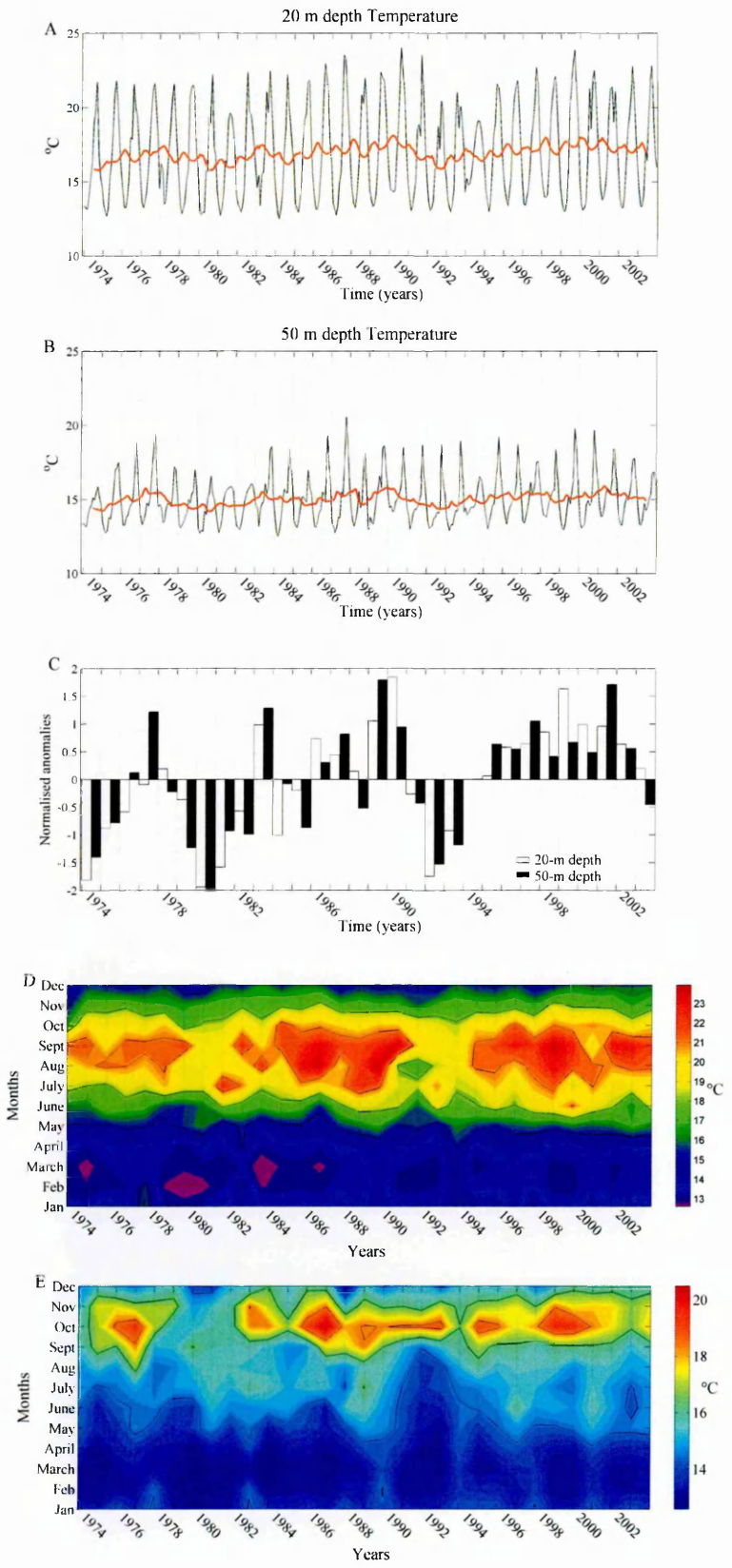

Figure 6.1 - Water temperature at Point B. A) Monthly time series (black line) and an annual (i.e., 12 points window) moving average to smooth the seasonal signal (red line) for values recorded at 20 m depth; B) same as in A for values at 50 m depth; C) annual normalised anomalies at 20 m (white) and 50 m (black) depths; D) seasonal and interannual variability at 20 m depth; E) same as in D for values at 50 m depth.

Salinity showed very similar patterns at 20 and 50 m depths (Fig.6.2 A, B). Generally, annual values ranged from 37.7-37.8 to 38.2-38.4. Before 1980, annual mean salinity was below the long-term average, except for the years 1975-1976 (Fig.6.2C). From 1980 to 1988 salinity was above the average and values were the highest of the time series. The period from 1989 to 1998 was characterised by values generally below the long-term average salinity. Finally, from 1999 annual mean salinity was again above the long-term average except in 2002. During the whole 1980s, annual maximal salinity was above the long-term average and occurred between October and March (Fig.6.2D).

At 20 m depth seasonality was quite marked. The annual minimum was generally recorded in spring and the maximum in autumn-winter (Fig.6.2D).

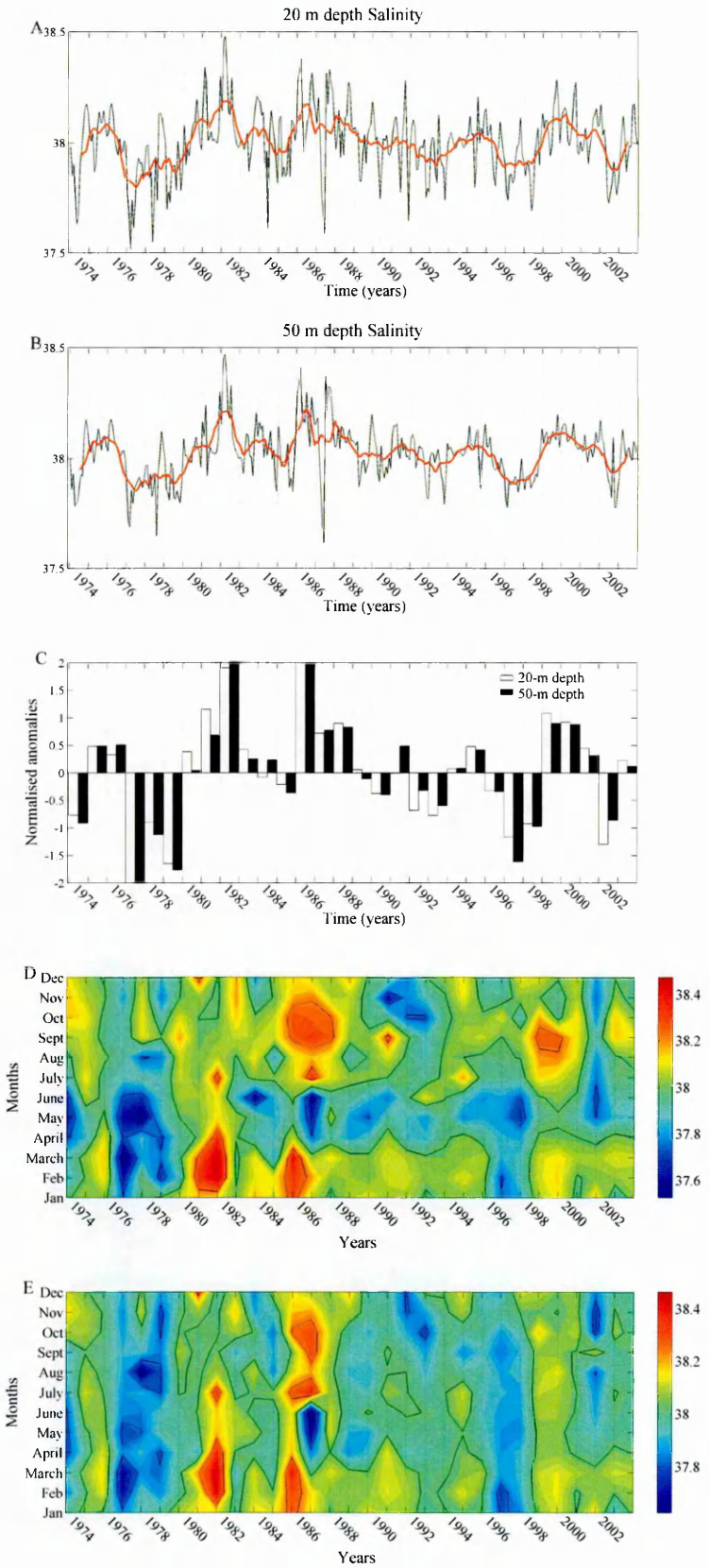

Figure 6.2 - Salinity at Point B. A) Monthly time series (black line) and an annual (i.e., 12 points window) moving average to smooth the seasonal signal (red line) for values recorded at 20 m depth; B) same as in A for values at 50 m depth; C) annual normalised anomalies at 20 m (white) and 50 m (black) depths; D) seasonal and interannual variability at 20 m depth; E) same as in D for values at 50 m depth.

Water density was calculated from salinity, temperature and sampling-depth (Millero et al., 1980; Fofonoff and Millard Jr., 1983) and thus it presented a combination of the temporal patterns of temperature and salinity (Fig.6.3A). The 30-year mean winter density (February-March mean) and its standard deviation were 28.75 ± 0.2 (kg m^{-3}) at 20 m depth, and 28.91 ± 0.16 (kg m^{-3}) at 50 m depth. From 1980 to 1988, winter water at 20 m depth was denser than in the rest of the time series (Fig.6.3B).

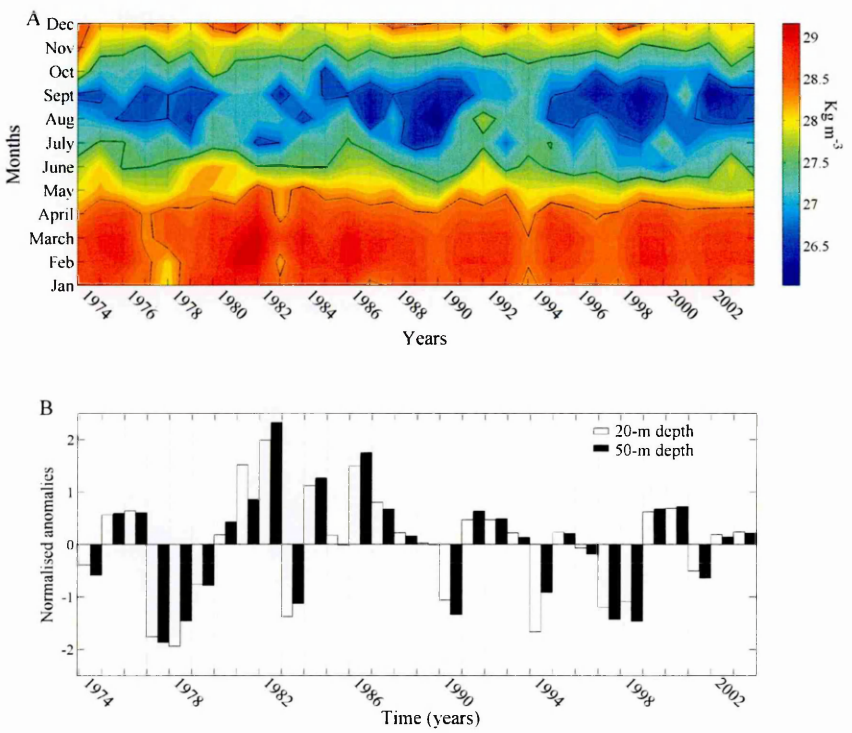

Figure 6.3 - A) Seasonal and interannual variability of water density at 20 m depth; B) winter (Feb.-March mean) normalised anomalies of density at 20 m (white) and 50 m (black) depths.

Changes in water temperature and salinity are related to local atmospheric changes forcing the water column. Temperature changes at 20 m depth were due to air-water heat exchange. Atmospheric pressure was below the long-term average in the 1970s and above it from 1982 to 1994, while after 1994 it was between the 1970s and 1980s values (Fig.6.4A). Interestingly, winter atmospheric pressure (Jan.-Feb.)

increased in 1989, whereas autumn atmospheric pressure decreased (Fig.6.4B). Late winter-spring irradiance increased from the early 1990s, and in that decade annual minimal irradiance was recorded in December instead of January-February (Fig.6.4 C, D). The observed changes of salinity were quite similar to changes in precipitation, which was below the long-term average in the 1980s and in 2001 and 2003 (Fig.6.4E). In the 1990s, annual mean precipitation increased due to higher autumn precipitation (Fig.6.4F) related to a decrease of autumn atmospheric pressure (Fig.6.4B).

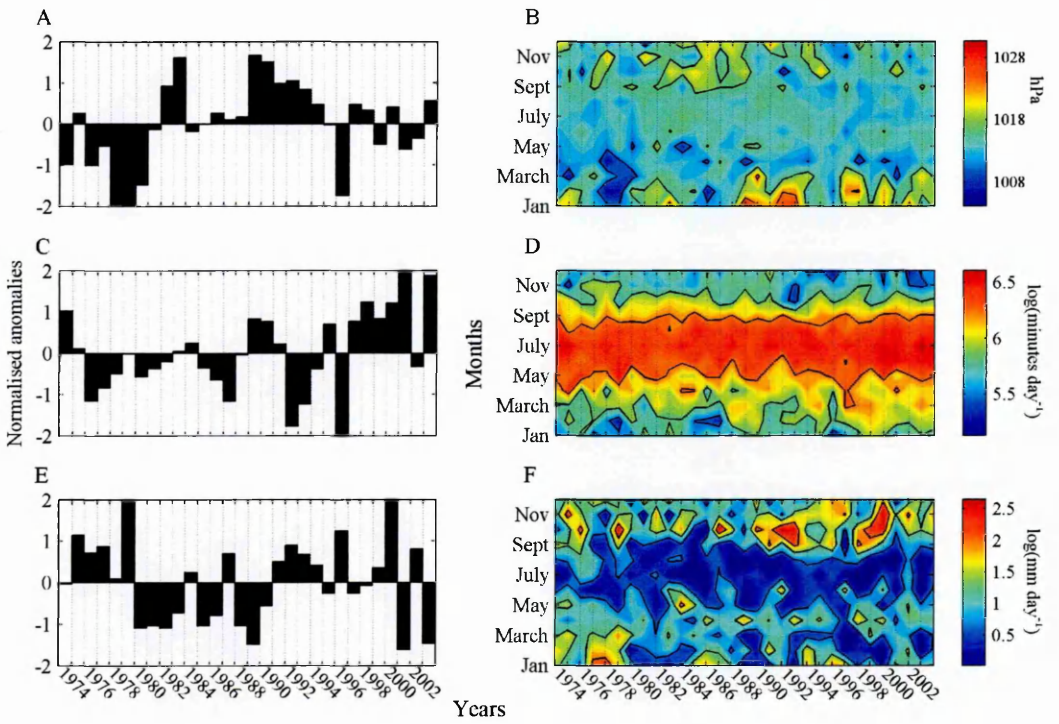

Figure 6.4 – Annual normalised anomalies of atmospheric pressure (A), irradiance (C) and precipitation (E); seasonal and interannual variability of atmospheric pressure (B), irradiance (D) and precipitation (F).

Wind is another atmospheric variable forcing the water column.The annual mean Ekman depth showed 4 alternate periods (Fig. 6.5 A, B). The periods from 1974 to 1978 and from 1985 to 1992 presented annual mean Ekman depth usually below the 30-year average. From 1979 to 1984, and from 1993 to 2003, years presented values above the

average or close to the average. Regarding seasonality, wind was weaker in summer and the strongest records were usually recorded in winter-spring (Fig.6.5C).

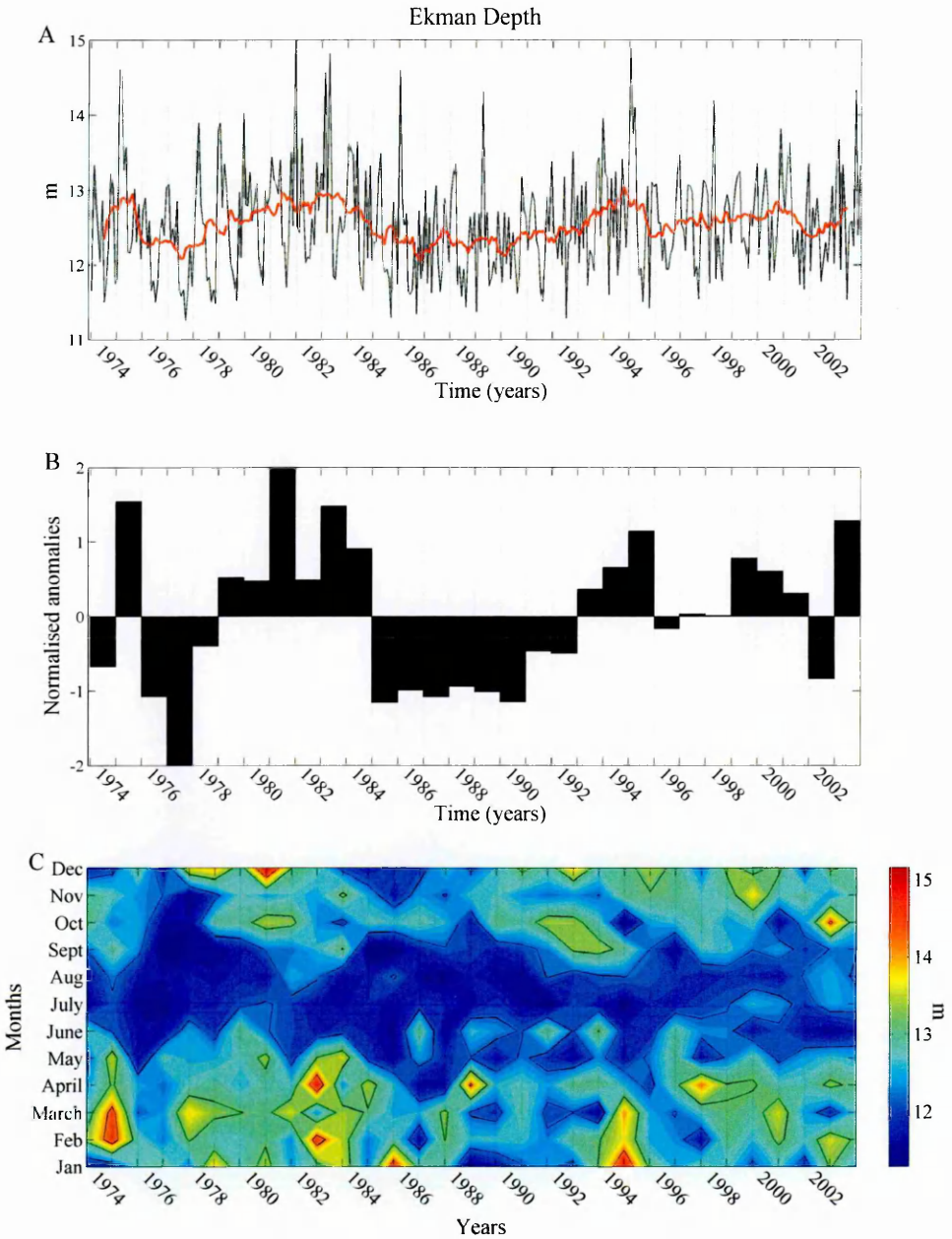

Figure 6.5 - Ekman depth at Point B. A) Monthly time series (black line) and an annual (i.e., 12 points window) moving average to smooth the seasonal signal (red line); B) annual normalised anomalies; C) seasonal and interannual variability.

Wind direction was expressed by the wind pattern ($\alpha \sin(\beta)$), in which wind speed was weighted by its direction (see 2.2.2 section for further explanation). Both

directions followed similar trends (Fig.6.6). No relevant changes occurred in wind direction over the 30-year time series.

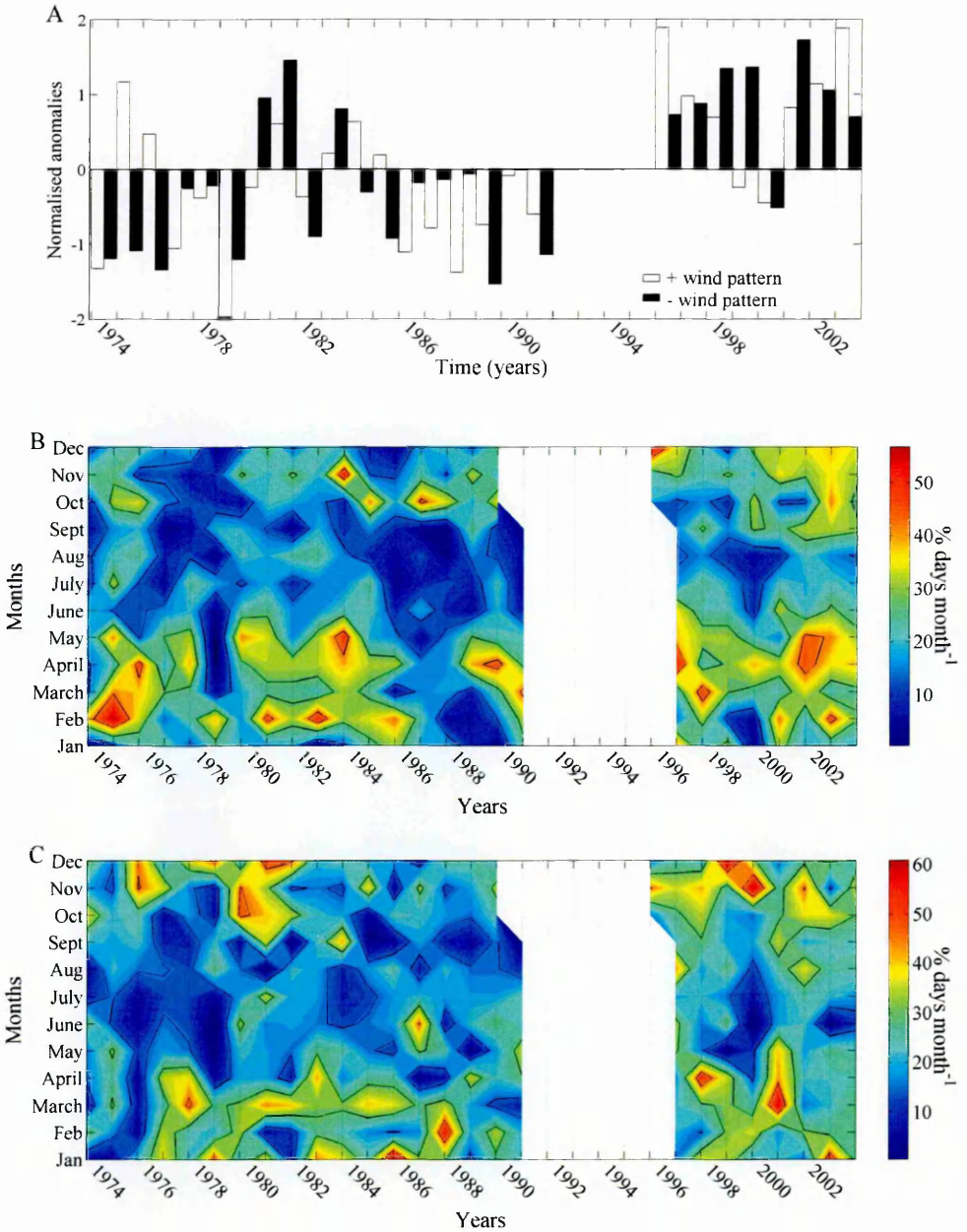

Figure 6.6 - Wind pattern at Point B. A) Annual normalised anomalies of + wind pattern (easterly winds) (white) and – wind pattern (westerly winds) (black) frequencies; B) seasonal and interannual variability of + wind pattern frequency; C) same as in B for – wind pattern frequency.

6.2.2 General environmental patterns

From the analysis of each environmental variable, some periods were identified. To define common interannual periods of environmental conditions, a PCA (see section 2.6.4 for explanation on the method) was performed on the annual mean values of all variables, except wind direction due to its five-year interruption. The three first synthetic axes (PCs) created by the PCA explained 73% of the environmental variability (Table 6.1). The 1st PC, which accounted for 33% of the general variability, was mainly driven by salinity (weighting 0.5), with precipitation in opposition (-0.38). The rest of original variables contributed less than salinity, but still in the same direction to the construction of this axis (range of contribution 0.20-0.36). The 2nd PC (26%) mainly reflected the temperature signal.

Table 6.1 - Contribution of the original environmental variables to the three first PCs of the PCA. Explained variances by each PC are indicated between brackets.

Variables	1st PC (33%)	2nd PC (26%)	3rd PC (14%)
Temperature 20 m	0.27	0.54	0.14
Temperature 50 m	0.22	0.57	0.14
Salinity 20 m	0.50	-0.33	0.24
Salinity 50 m	0.47	-0.32	0.36
At.Pressure	0.36	0.11	0.08
Precipitation	-0.38	0.03	0.20
Irradiance	0.31	0.24	-0.65
Ekman depth	0.20	-0.31	-0.57

The 1st PC of local environmental conditions was correlated with the winter North Atlantic Oscillation (NAO) (r = 0.44; p<0.05) (Fig.6.7A). Indeed, local atmospheric pressure was highly correlated with the winter NAO (r = 0.67; p<0.0001). Following Kirby and Beaugrand (2009), a sliding correlation analysis was applied to monitor the temporal stability of the relationship between both signals. Correlations were calculated on periods of 10 years by moving one year at a time from the first 10 years until completing the time series. The correlation between the 1st PC and the winter NAO was not stable over the years (Fig.6.7B) (similar results with 5 and 15 years). There was no significant correlation from the end of the 1980s, and the first half of the 1990s presented the lowest values.

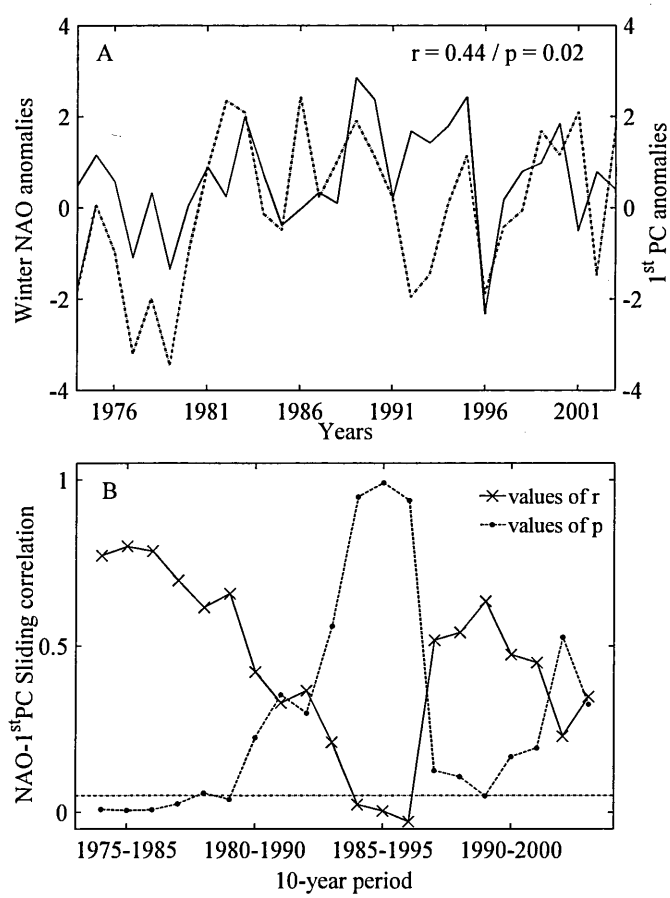

Figure 6.7 Correlation between the annual normalised anomalies of the winter NAO (continuous line) and the 1st PC of local environmental variables (dashed line), and (B) sliding correlation analysis of both variables using a 10-year window (the horizontal dashed line indicates the 0.05 floor of significance).

The cusum of the deviations from the mean of the1st PC reflected four quasi-decadal periods (Fig.6.8):

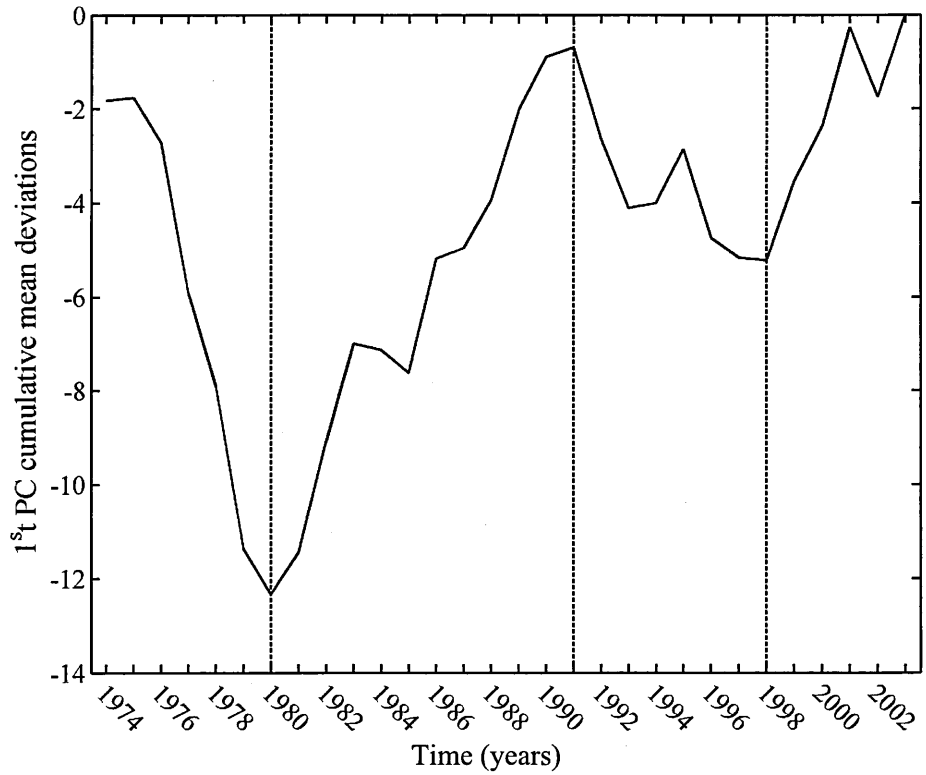

Figure 6.8 - Cusum of the deviations from the mean of the 1st PC of the annual mean environmental conditions.

The first period of the time series ranged from 1974 to 1980 (the 1970s). During those years the 1st PC reached its lowest values. This period was characterised by low winter and summer atmospheric pressure which led to increased precipitation and associated low salinity as well as low water temperature.

The 1980s (1981-1991) constituted a single period with constant high values of the 1st PC, except for 1985. It was mainly characterised by dry years and associated high salinity. Annual mean water temperature was above the average, although during most of the period the winter water at 20 m depth was colder than the long-term winter average.

The 1990s period ranged from 1991 to 1998. The common factor in those years was the record of cloudier autumns, entailing less irradiance and more precipitation which led to lower than average salinity records. During that period, summer and autumn seasons were windier than the previous decade. The year 1995 appeared different, with a higher value.

Finally, the last period extending from 1998 to 2003 (the end of the analysed time series, the 2000s) was characterised by an increase of winter and summer irradiance, whereas autumns continued to be cloudy. Salinity annual records were intermediate between the high 1980s and the low 1990s values.

6.2.3 Chlorophyll *a* and NO_3 concentration

Chlorophyll *a* (chl *a*) and NO_3 concentration have been measured at Point B from 1991. Chl *a* concentration varied from 0.1-0.3 mg m^{-3} minimal records to annual maximal values in the 0.5-0.8 mg m^{-3} range (0.4-0.6 mg m^{-3} at 50 m depth) (Fig.6.9 A, B). Concentration at 20 and 50 m depths showed a similar pattern, although in the deep layer the annual amplitude was lower. The period from 1992 to 1996 was characterised by annual mean chl *a* concentration above the long-term average (Fig.6.9C). Since then, the annual mean concentration decreased, attaining lowest mean values in the 2000s.

Maximal annual chl *a* concentration occurred in spring in the surface layer, and between spring and summer in the deep layer (Fig.6.9 D, E). The decrease of chl *a* concentration from 1996 occurred due to shortening of the spring bloom in surface layers and disappearance of a secondary autumn peak. In the 2000s, chl *a* concentration was depleted at surface in summer, and was very low in the deep layer all the year round.

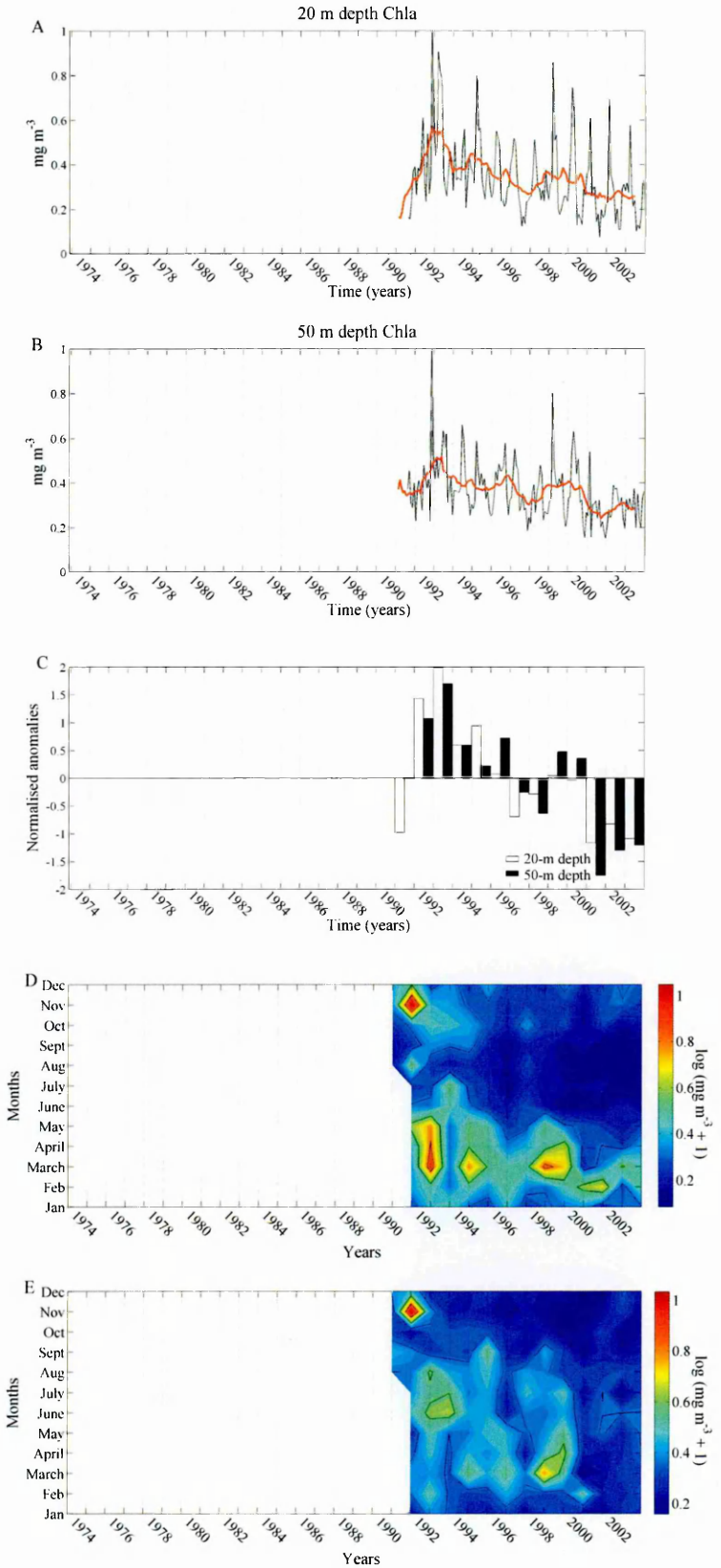

Figure 6.9 - Chl *a* at Point B. A) Monthly time series (black line) and an annual (i.e., 12 points window) moving average to smooth the seasonal signal (red line) for values recorded at 20 m depth; B) same as in A for values at 50 m depth; C) annual normalised anomalies at 20 m (white) and 50 m (black) depths; D) seasonal and interannual variability at 20 m depth; E) same as in D for values at 50 m depth.

The concentration of NO_3 at the surface showed a different interannual pattern from Chl *a*. It presented higher values at the end of the time series (Fig.6.10A), with a notable increase of winter concentration and a slight increase of the autumn peak (Fig.6.10B).

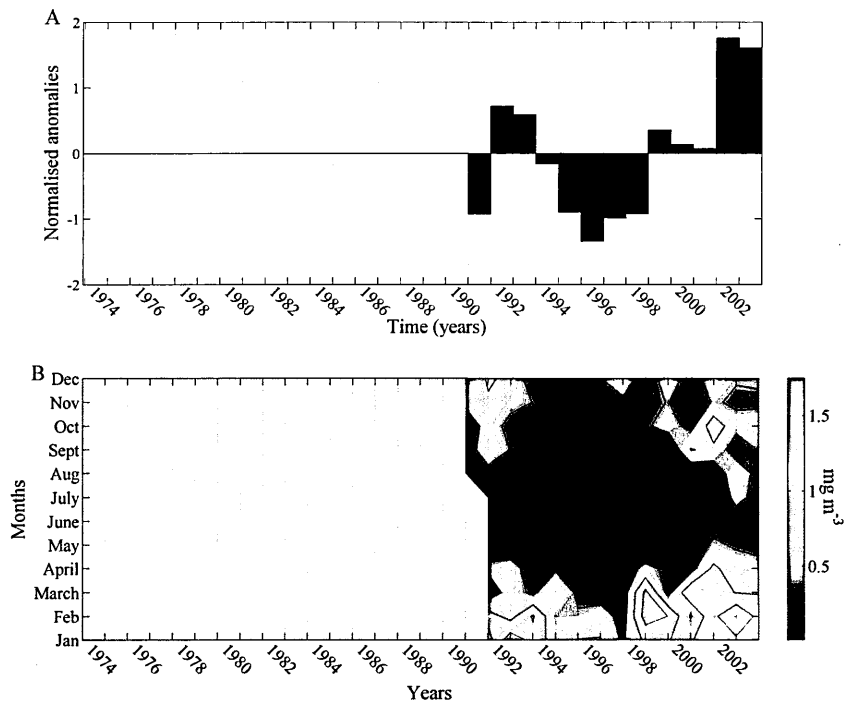

Figure 6.10 – Surface concentration of NO_3 at Point B. A) annual normalised anomalies; B) seasonal and interannual variability.

6.2.4 Zooplankton variability

Seasonal and interannual changes of the abundance of copepods, chaetognaths, jellyfish, siphonophores and decapod larvae were analyzed for the studied period. Interannual changes were quite similar among groups, with the 1980s characterised by standing stocks of each group above the 30-year average (Fig.6.11). At the beginning of the 1990s concentrations decreased, and during the 1990s annual values were below the long-term average. From 2000, the groups presented higher concentrations than in the near previous years. Despite the common long term pattern, while copepods and decapod larvae displayed high concentrations from 1982-1983 to 1991-1992

(Fig.6.11 A, B), the high concentration period of the other groups were more restricted. In the case of siphonophores and jellyfish, high abundances appeared one year late, in 1984 (Fig.6.11 D, E). For chaetognaths, siphonophores and jellyfish, the period of high concentration ended earlier, in 1989-1990 (Fig.6.11 C, D, E). In addition, copepods and chaetognaths showed a short period of concentration higher than the average in the mid 1970s (Fig.6.11 A, C) not recorded for the rest of the groups.

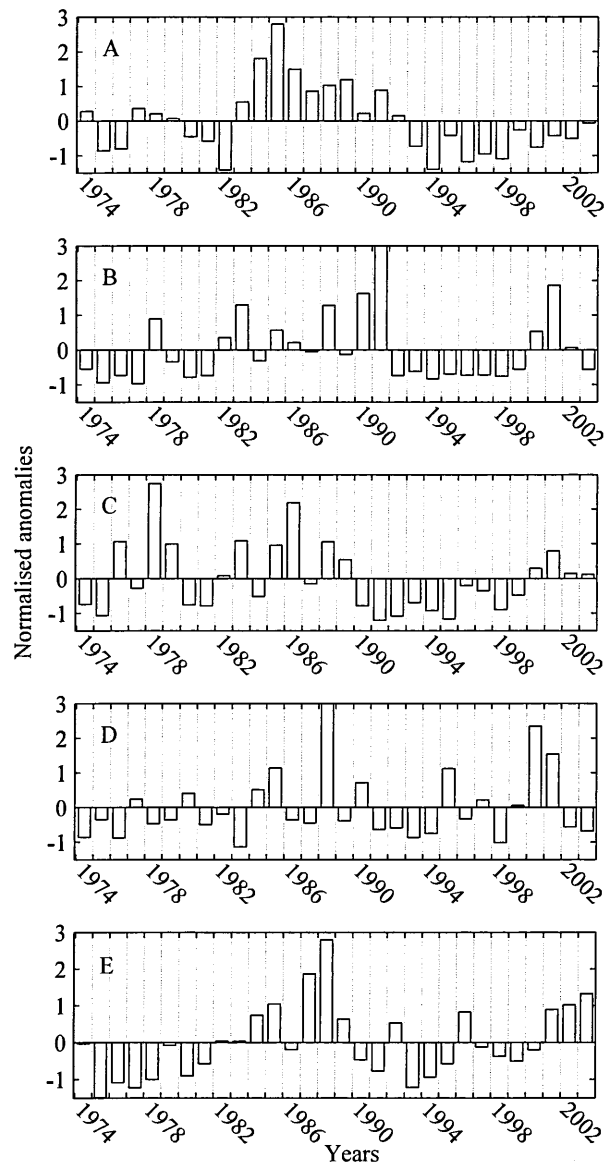

Figure 6.11 - Normalised annual anomalies of (A) copepods, (B) decapod larvae, (C) chaetognaths, (D) siphonophores and (E) jellyfish, at Point B from 1974 to 2003.

At a seasonal scale, the different groups did not show the same pattern. A common seasonal feature for Copepods was a recurrent spring peak over the whole time series (Fig.6.12A). Yet, there was a relatively high interannual variability in the seasonal cycle of this group. Indeed, the spring peak spread out from late winter to early summer depending on the period. From 1976 to 1979, a high annual peak was recorded in summer that was not present in the rest of the time series. Regarding the autumn season, a peak was recorded from 1983 to 1989; it disappeared in the 1990s and reappeared, less marked and more spread out, in the 2000s. Decapod larvae usually peaked in summer, from July to August, and were poorly represented in winter and late autumn (Fig.6.12B). The chaetognath seasonal cycle consisted of a single peak occurring between August and October and only in the mid-1970s high abundances were registered earlier in summer (Fig.6.12C). Compared to the other groups, the siphonophore seasonal cycle was quite constant during the 30-year time series, with narrow peaks taking place in spring, from April to June depending on the year (Fig.6.12D). Finally, jellyfish were usually rare in winter and early spring and sporadic peaks occurred from April to November (Fig.6.12E).

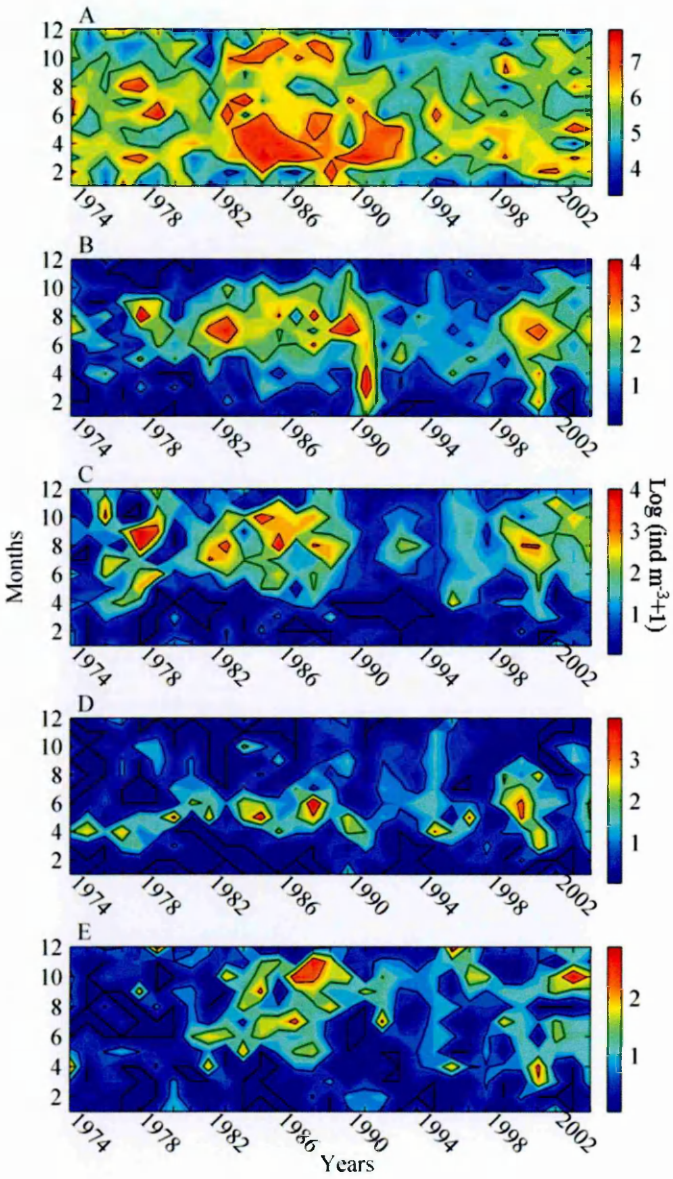

Figure 6.12 - Seasonal and interannual variability of log(abundance+1) of (A) copepods, (B) decapod larvae, (C) chaetognaths, (D) siphonophores and (E) jellyfish.

6.2.5 Zooplankton general pattern

The three PCs of the PCA, performed on the annual mean abundances of the groups mentioned above, gathered 78% of zooplankton variability. The 1st PC accounted for 44% of the total variance, and all zooplankton groups contributed with a similar weighting and direction to the creation of this axis (range of contributions 0.40-0.50) (Table 6.2). The 2nd PC (19%) reflected the opposition of copepods, decapod larvae and chaetognaths to siphonophores and jellyfish.

Table 6.2 - Contribution of each zooplankton group to the 3 first PCs of the PCA.

Variables	*1st PC (44%)*	*2nd PC (19%)*	*3rd PC (15%)*
Copepods	0.50	-0.24	-0.31
Decapod larvae	0.45	-0.13	0.71
Chaetognaths	0.40	-0.62	-0.04
Siphonophores	0.40	0.66	0.28
Jellyfish	0.47	0.33	-0.57

The cusum of the deviations from the mean of the 1st PC reflected 4 quasi-decadal periods (Fig.6.13):

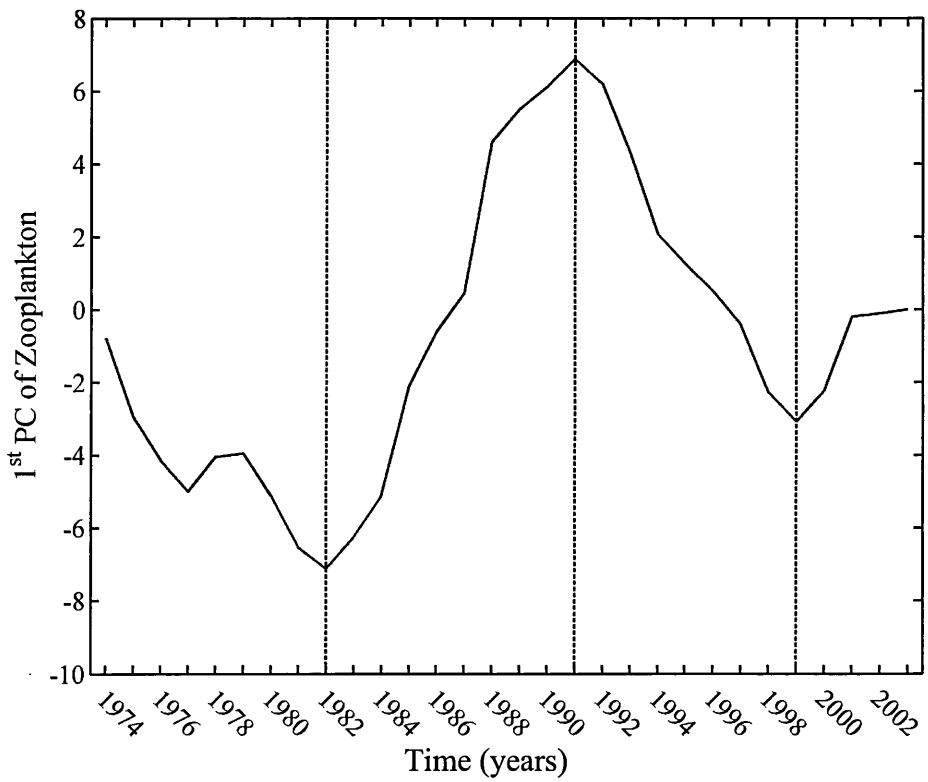

Figure 6.13 - Cusum of the deviations from the mean of the first principal component of the zooplankton interannual abundances.

The periodicity was similar to the 1st PC of environmental conditions (Fig.6.8). In the 1970s (1974-1982) zooplankton standing stocks were below the 30-year average. The change of slope in the middle of this period was due to an unusual high summer abundance of copepods and chaetognaths. The 1980s (1983-1991) showed a very steep positive cusum slope, reflecting the high abundance recorded in all groups during that

period. In the 1990s (1992-1999) there was an abrupt reduction in the abundance of copepods, decapods and chaetognaths, while the decrease of the gelatinous groups was less marked. From 1999 it seemed that all groups started to recover in terms of standing stocks.

6.2.6 Copepod size distribution

The copepod size distribution at Point B revealed a different long-term pattern than the almost decadal periodicity presented in abundance and environmental conditions (Fig.6.8; Fig.6.13). Copepod size-spectrum diversity increased from the mid-1980s and stabilized in the 1990s (Fig.6.14A). The year 1987 was the turning point of the change from lower to higher than average values (Fig.6.14B). Rather similar patterns were found in mean copepod body size and spectrum slope indexes (see Appendix V).

A common seasonal pattern was not depicted for the whole time series. However, annual minimum values were usually recorded in spring, especially from the mid-1980s to the mid-1990s. Very low values were recorded in summer during the 1970s.

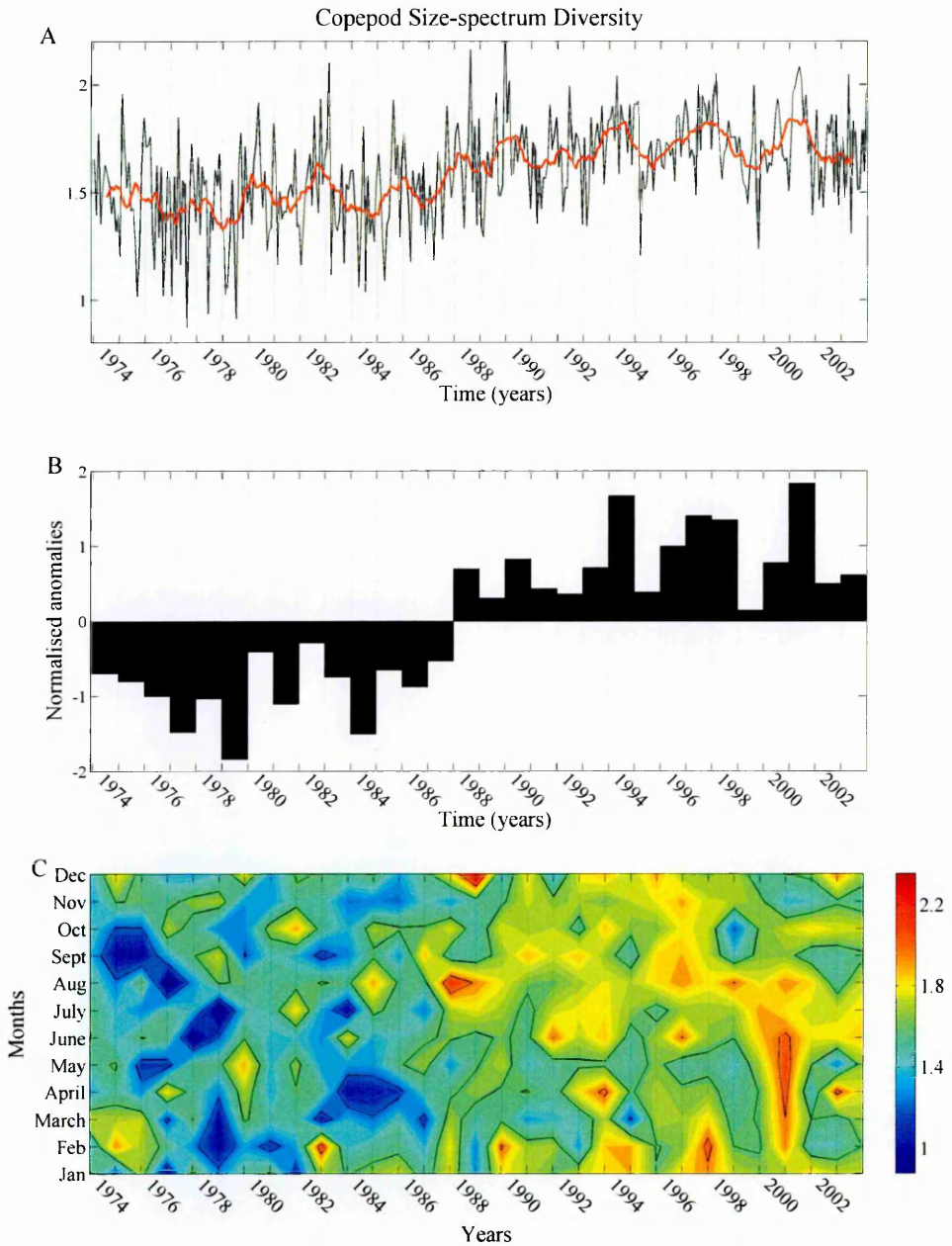

Figure 6.14 - Copepod size diversity at Point B. A) Monthly time series (black line) and an annual (i.e., 12 points window) moving average to smooth the seasonal signal (red line); B) annual normalised anomalies; C) seasonal and interannual variability;

To classify the spectra by their shapes, a cluster analysis was performed on their Kolmogorov distances (see section 2.4.4 for details on the method). The dendrogram (Fig.6.15) was cut at a distance of 70 to obtain five groups. Groups from 1 to 5 ranged from spectra containing the highest proportion of small copepods (group 1) to spectra containing the lowest proportion of small copepods (group 5) (Fig.6.16).

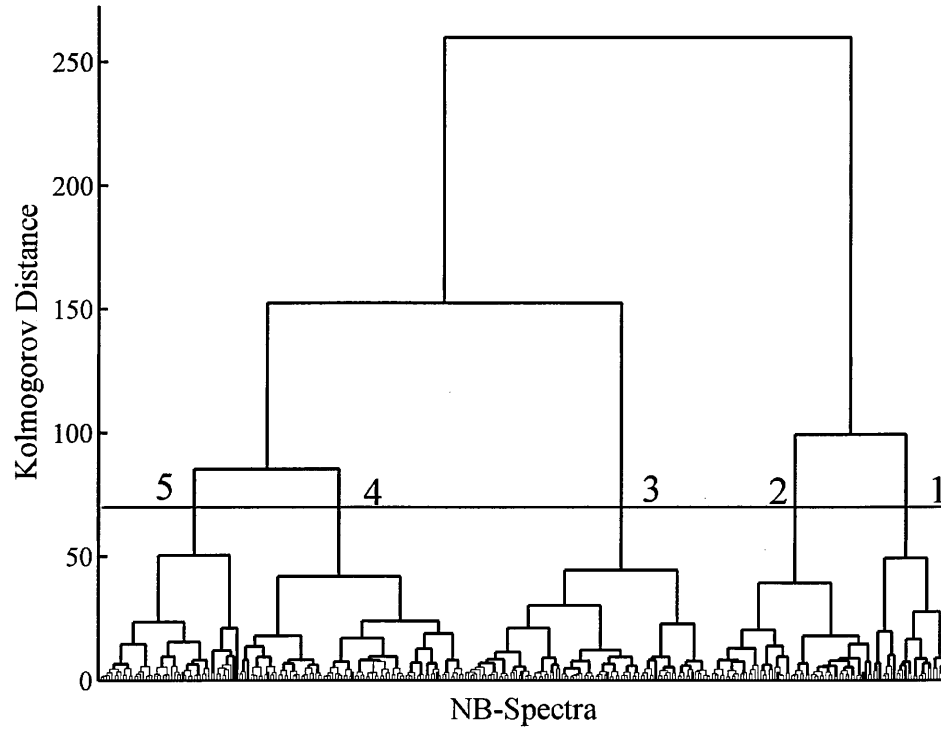

Figure 6.15 - Dendrogram obtained from a cluster analysis on the Kolmogorov distances of the cumulative sum of the Point B spectra size classes. Cut distance at 70 highlighted 5 groups.

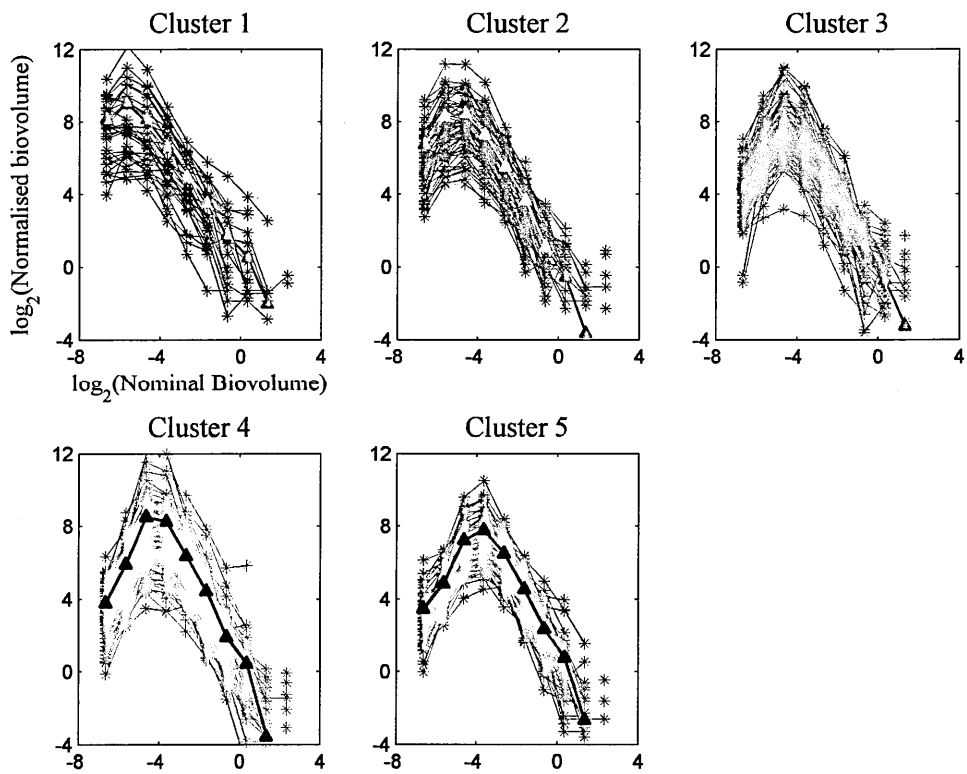

Figure 6.16 – Point B pectra constituting every cluster. The superposed line with triangle marks represents the average spectrum of each cluster.

The interannual variability of size spectra was much more pronounced than the seasonal one (Fig.6.17). The four periods already found in the 1st PC of zooplankton abundances could also be distinguished in the composition of copepod size spectra. In the 1970s (1974-1982), 70% of the spectra belonged to groups 2 and 3, and 16% belonged to group 1. The 1980s period (1983-1991) was a transition period. The presence of group 4 spectra increased from 9% in the 1970s, to 27% in the 1980s. On the contrary, the presence of group 2 spectra decreased from 30% to 20% in the 1980s. In the 1990s (1992-1999), 87% of the spectra belonged to the groups 4 and 5 (i.e., the flattest spectra). Spectra belonging to group 1 were not present in that period, and only one spectrum out of 120 belonged to group 2. Finally, in the 2000s (2000-2003), spectra belonging to group 4 dominated (45%), and while the presence of group 2 spectra increased, those belonging to group 5 decreased.

A seasonal pattern was not clearly depicted (Fig.6.17). Generally, the steepest spectra were recorded in winter although not throughout all the years. Increasing the number of groups did not highlight a clearer seasonal pattern.

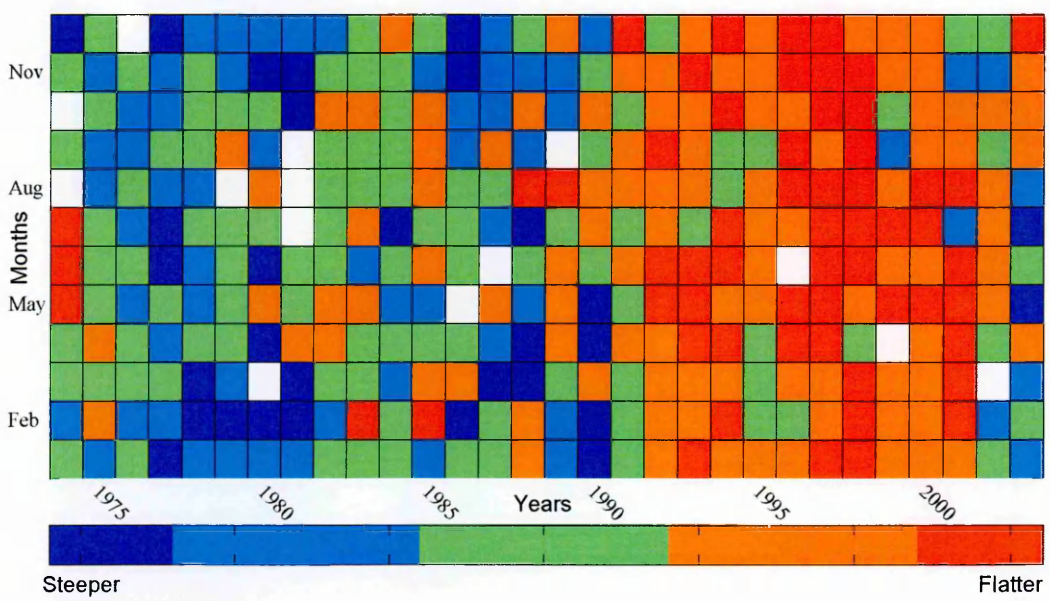

Figure 6.17 - Seasonality and interannual variability of the Point B spectra shape. Same colour codes as above; Group 1 gathers the steepest spectra and group 5 the flatest.

The size fraction containing copepods smaller than 0.04 mm^3 (~<700 μm length) represented, on average, less than 20% of total copepod abundance. The annual amplitude of contribution to total abundance ranged from 20-70% annual maxima to 3-10% minima. Their contribution was the highest during total abundance peaks. Relevant peaks of small copepods were recorded in 1978-1979 and from 1984 to 1989 (Fig.6.18 A, B). The abundance of small copepods presented a sharp decrease in the 1990s and later started a gradual recovery from 2000. Before the 1990s, the contribution of small copepods to the annual highest peak was in the 40-70% range. During the 1990s, they only accounted for 20-30% of the highest peaks of annual total copepod abundance.

Notable changes were recorded in the small copepod seasonal pattern throughout the time series (Fig.6.18C). From 1976 to 1979, three periods of high abundance occurred in late-winter spring, summer and late autumn. In the 1980s, the spring and autumn peaks were more evident, although at the end of the 1980s, the autumn peak disappeared. In the 1990s the spring and summer abundances were rather similar, with sparse small peaks, and low abundances were recorded in the autumn-winter period. Finally, from 2000, spring and autumn peaks reappeared, although less marked and narrower than in the 1980s.

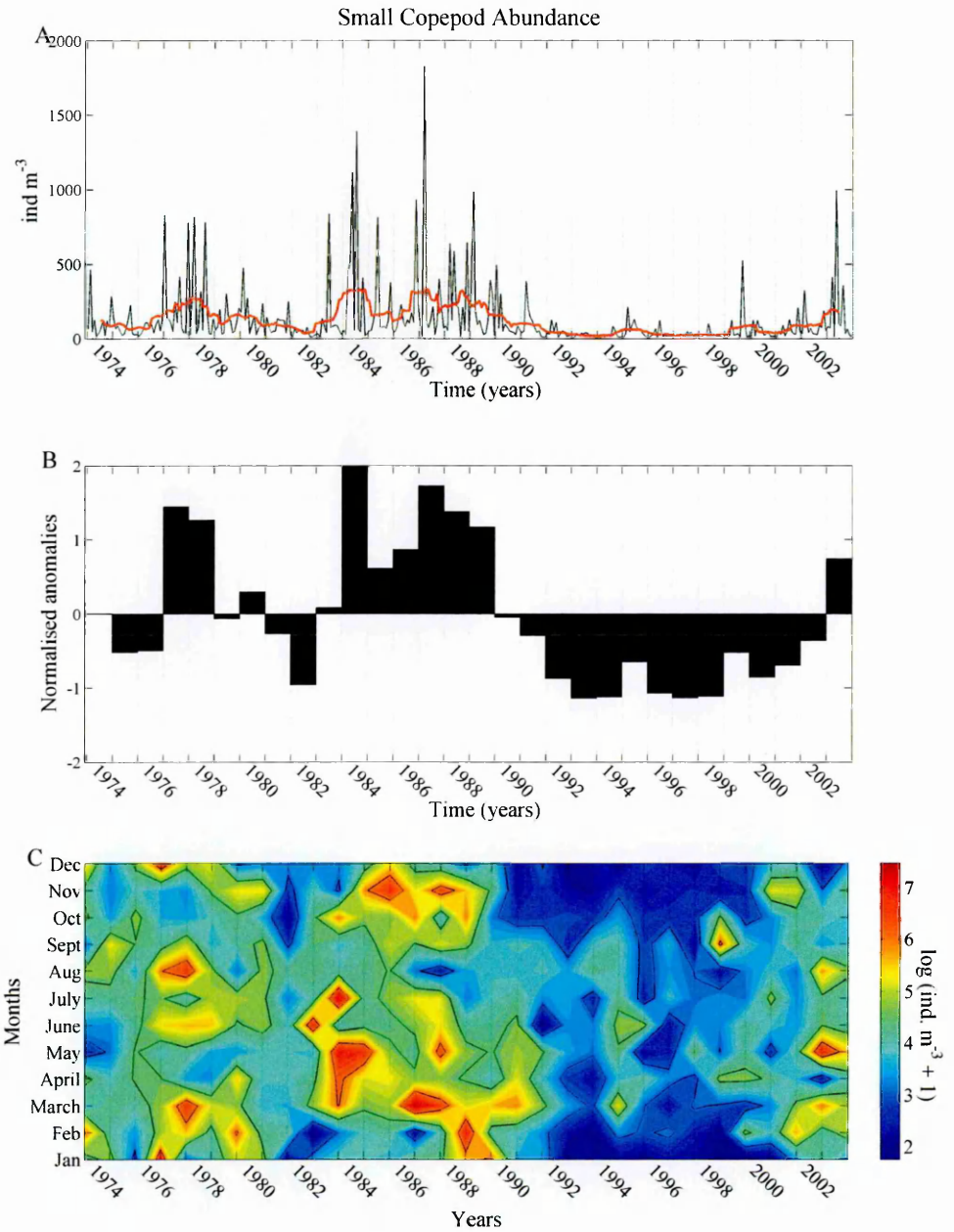

Figure 6.18 - Abundance of copepods smaller than 0.04 mm^3 at Point B. A) Monthly time series (black line) and an annual (i.e., 12 points window) moving average to smooth the seasonal signal (red line); B) annual normalised anomalies; C) seasonal and interannual variability of log (abundance+1).

Copepods larger than 0.32 mm^3 (~>1.5 μm length) represented, on average, less than 5% of the total copepod abundance. Four periods were distinguished in the time series. Before 1984, the lowest abundances were recorded (Fig.6.19 A, B). From 1985 to 1993, annual mean abundance was above the long-term average. From 1994 to 1999, abundance was below the average but values were greater than before the mid-1980s due to a raised baseline. From 2000 abundance increased and annual mean values were close to the long-term average. Their contribution to the total copepod bulk increased during the 1980s from an average 5% in the 1970s to an average 10% in the 1990s.

A common seasonal pattern could not be distinguished for the whole time series, although low abundances were recurrently recorded in early winter (Fig.6.19C). A spring peak was recorded from 1974-1977, 1984-1993 and from 2000. A late-summer-autumn peak was recorded from 1983 to 1989, and again from 2000. In the mid-1990s, no seasonal peak was recorded; relatively high abundances were recorded throughout spring and summer, and low abundance was recorded throughout late autumn and winter.

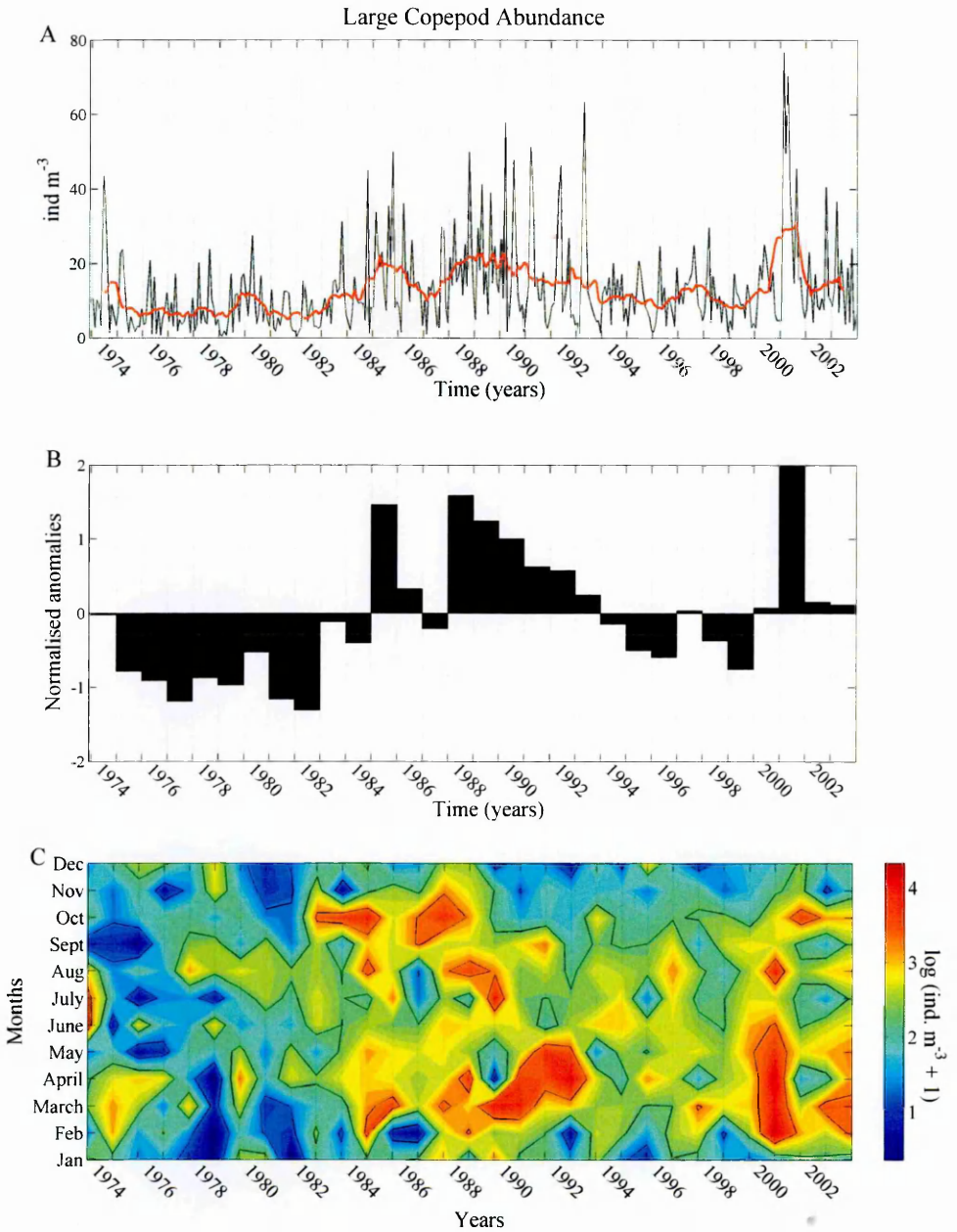

Figure 6.19 - Abundance of copepods larger than 0.32 mm^3 at Point B. A) Monthly time series (black line) and an annual (i.e., 12 points window) moving average to smooth the seasonal signal (red line); B) annual normalised anomalies; C) seasonal and interannual variability of log (abundance+1).

6.2.7 Regime shift in copepod size distribution

Copepod size distribution at Point B showed a clear pattern of increase in the mid-1980s and stabilization in the 1990s. To test if the size-distribution change could be defined as a regime shift, the exponential weighted moving average (EWMA) (see section 3.6.6 for details) was computed on the annual mean values of the copepod size-spectrum diversity. Smoothing was done by a λ value of 0.25; the control limits (UCL and LCL) were calculated with an L value of 1.96. The EWMA of the copepod-size diversity index revealed a regime shift from a copepod community characterised by dominance of small organisms between 1977 and 1987 to a new steady regime from 1997 and characterised by a higher proportion of large copepods (Fig.6.20).

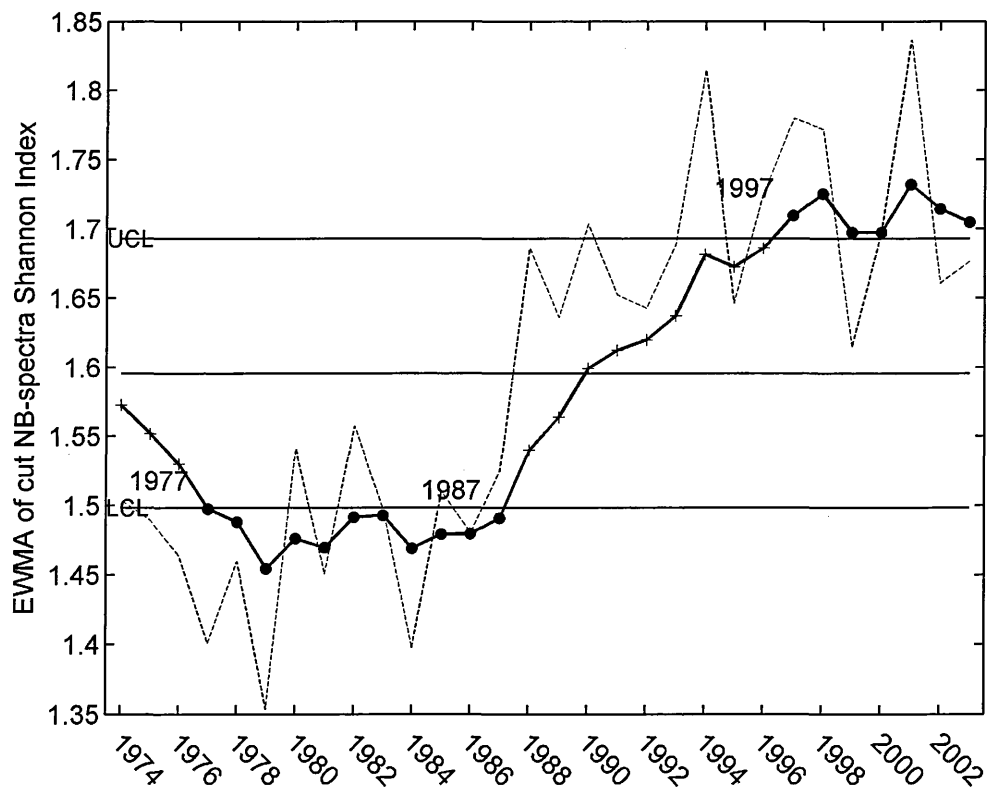

Figure 6.20 - Exponential weighted moving average (EWMA) of the annual mean values of the copepod size diversity at Point B. Black dots correspond to the out of control years (1977-1987; 1997-2003). This figure represents a regime-shift of copepod-size diversity from the 1980s to the 1990s, with a decadal transition period from 1987 to 1997.

6.2.8 Species composition changes

Abundance of several copepod species as well as cladocerans and appendicularians were analysed for six non-continuous years of the time series chosen before, within and after the size-spectrum diversity shift (see section 3.4.3 for details). Regarding copepods, only *Centropages* spp., poecilostomatoida and the group containing typical offshore calanoid species (i.e., genera belonging to the following families: Aetideidae, Augaptilidae, Calanidae, Candaciidae, Eucalanidae, Euchaetidae, Heterorhabdidae, Lucicutiidae, Scolecithricidae) did not present much lower abundances in the period 1995-1997 than in the rest of the years analysed (Fig.6.21). Appendicularians and cladocerans neither showed relevant lower abundances in the 1995-1997 period.

Seasonality was strong in *Centropages* spp. and *Acartia* spp., both with their annual peak in spring, in *Temora stylifera* with its annual peak in autumn, and in cladocerans with a narrow peak in summer. The rest of the copepod taxa and appendicularia did not present a clear seasonal pattern.

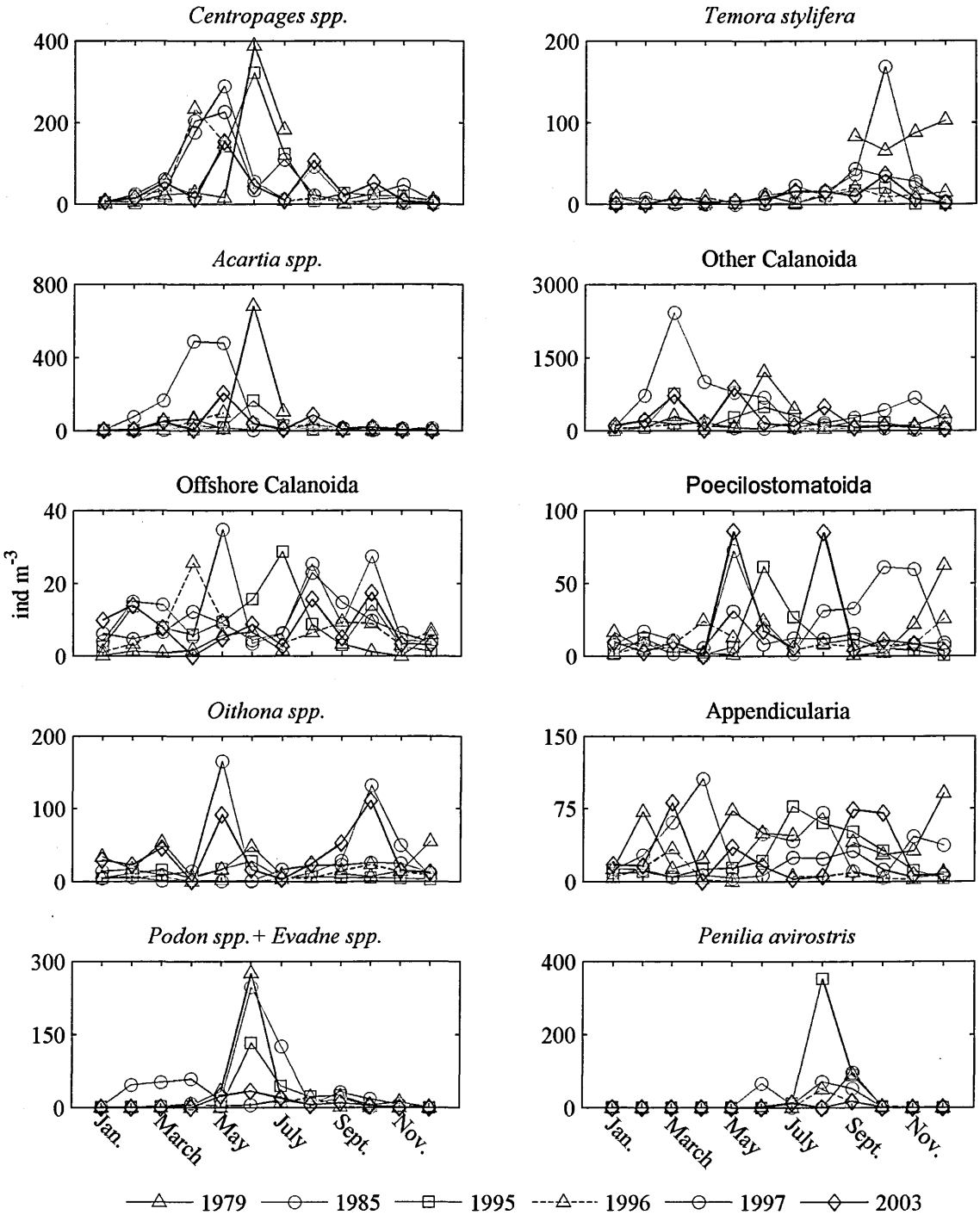

Figure 6.21 - Abundance of several taxonomic groups: *Centropages* spp., *Temora stylifera*, *Acartia* spp., other Calanoida (mostly *Paracalanus* spp. and *Clausocalanus* spp.), offshore Calanoida (i.e., genera belonging to the following families: Aetideidae, Augaptilidae, Calanidae, Candaciidae, Eucalanidae, Euchaetidae, Heterorhabdidae, Lucicutiidae, Scolecithricidae), Poecilostomatoida (i.e., oncaeids, corycaeids, *Farranula*) and *Oithona* spp., Appendicularia (i.e., *Oikopleura* spp. and *Fritillaria* spp.), the cladoceran *Penilia avirostris*, and other Cladocera (i.e., *Podon* spp. and *Evadne* spp.) sorted by semi-automatic recognition of the years 1979, 1985, 1995-1997, 2003 of the Point B time series.

6.2.9 *Calanus helgolandicus*

Copepodites CV and adults of *Calanus helgolandicus* were sorted from the monthly ZooScan samples of the Point B time series. *Calanus helgolandicus* was very scarce in 1976-1978 and presented its highest peaks in the 1980s (Fig.6.22A). Generally, an annual peak was recorded in late winter-early spring, and for some years a punctual second peak was recorded in August-September (Fig.6.22B).

An increasing trend was recorded in the presence of *C. helgolandicus* in the monthly samples (Fig.6.22C). While in the 1970s its presence in the samples did not exceed 50 % of the months of each year, in the 1980s its annual frequency oscillated between 50-80%, and in the 1990s it was always above 70 %. To verify the independence of these results from the number of daily tows contained in a sample (Fig.4.1), a general linear model (GLM) was built. In the model, the response variable was the presence/absence of *C. helgolandicus*, and the predictive variables were the number of tows per month, the date and the interaction of both. Only the date was significant in the model ($p = 0.07$), meaning that the occurrence of *C. helgolandicus* at Point B was independent of the number of tows in a sample.

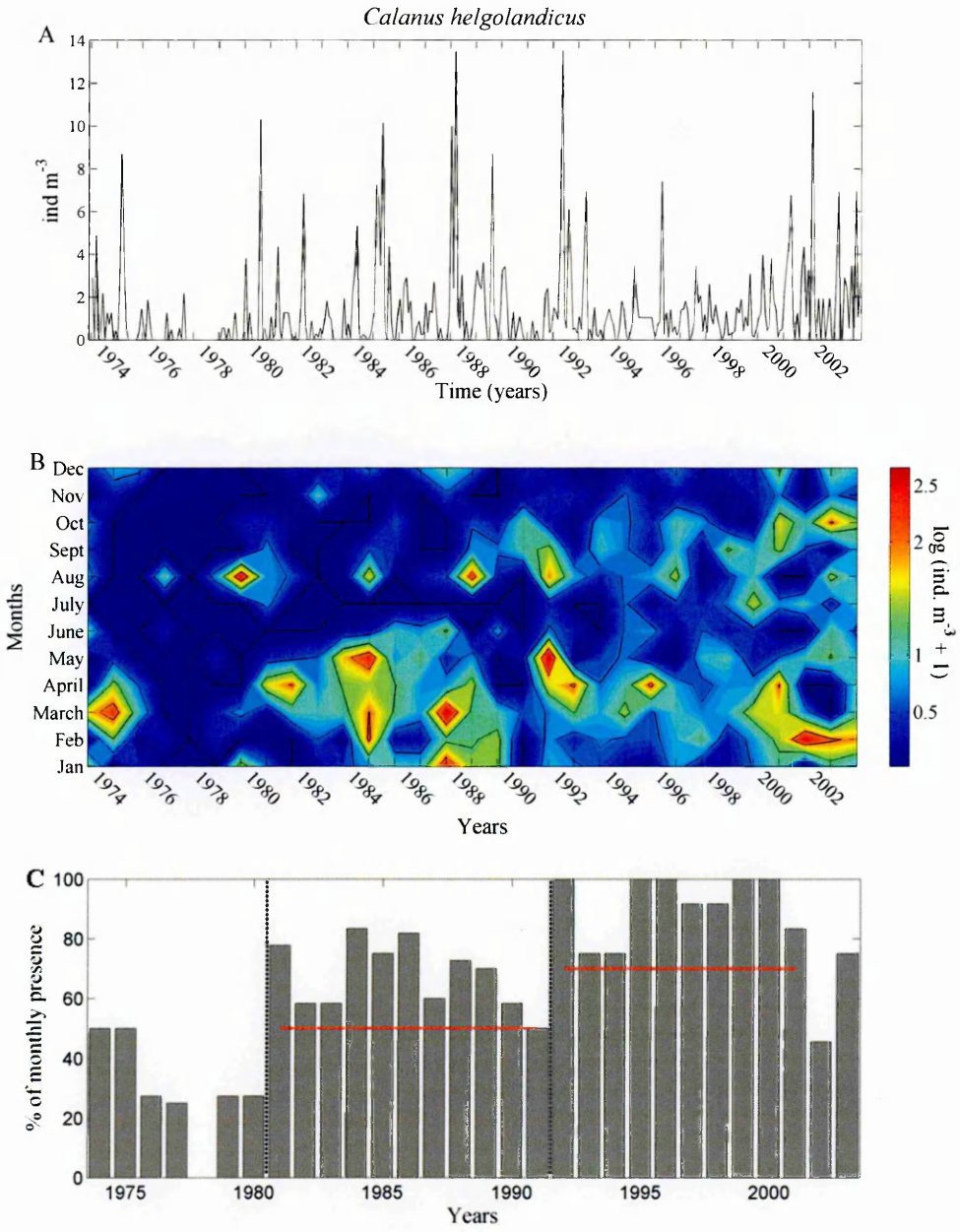

Figure 6.22 – Temporal patterns of *Calanus helgolandicus* at Point B. A) Monthly time series; B) seasonal and interannual changes of log (abundance+1); C) annual frequency of presence of specimens in the monthly samples.

6.3 Discussion

In previous studies on some target species of copepods, jellyfish, siphonophores and chaetognaths for the period 1967-1993, Molinero et al. (2005a; 2008b) proposed a mechanism based on top-down control by jellyfish to explain the copepod abundance decrease observed at Point B in the early 1990s. They predicted increasing concentrations of jellyfish in the following decade due to increasing temperature. By contrast, the present study on the abundance of broad groups (i.e., copepods, chaetognaths, siphonophores and jellyfish, as well as decapod larvae) for the period 1974-2003 revealed similar trends in the abundance of copepod, jellyfish and the other groups. Almost decadal changes appeared almost simultaneously in the environmental and zooplankton conditions, and annual environmental conditions seemed to be partially coupled with atmospheric alterations occurring over the Atlantic Ocean (i.e., 1st PC of environmental conditions correlated to the winter NAO). These results suggest that pelagic ecosystems in the Ligurian Sea may vary in response to large-scale climate changes, as already highlighted by Molinero et al. (2005a; 2008b). The novelty of this study is that i) the changes appear to occur periodically every 8-9 years rather than being long-term, ii) salinity seems to have a relevant role and iii) in general all the studied groups show a similar response, which may indicate bottom-up control instead of top-down control as the main trophic control shaping those zooplankton groups.

Abundance reflected a quasi-decadal periodicity, whereas copepod size distribution reflected a regime shift. Besides the difference of abundance between the 1980s and the 1990s, the size-spectrum diversity showed an increase in the relative abundance of large copepods from 1987 to 1997. During the 1980s, flatter spectra appeared at Point B, as reflected by the spectra clustering. Large copepods had their lowest annual mean abundance from 1975 to 1982. These results suggest that also other

processes, apart from the stratification-destratification dynamics controlling phytoplankton, notably affected the copepod community in the 30 years under study.

In the previous chapter, it was shown that at stn MC the abundance of the small-copepod size fraction was highly correlated with copepodite abundance and the large size fraction corresponded in part to changes in offshore copepod abundance. On the one hand, the observed reduction in the abundance of small copepods at Point B in the 1990s supports the hypothesis of a shift from an eutrophic period (i.e., the 1980s) to an oligotrophic period (i.e., the 1990s), and thus the bottom-up control mechanism as a relevant forcing of the copepod community at Point B. On the other hand, the fact that the large copepod abundance did not show such a drop between the 1980s and the 1990s, and that in contrast this size fraction was very rare in the 1970s, suggests that perhaps the dynamics of coastal-offshore water masses interaction at Point B varied in the 30-year period, with a temporal trend to more offshore conditions.

6.3.1 Species versus broad groups as climate change indicators

The first aim of the present work was to asses if the interannual zooplankton changes found in the Bay of Villefranche by Molinero et al. (2005a; 2008b), for the period 1967 to 1993, were also observed when studying broad zooplankton groups (i.e., total copepods) instead of studying several target species (i.e., *Centropages typicus*). The interannual changes observed in chaetognath and copepod stocks were similar, for the common period, to those reported by Molinero et al. (2008b). Concerning chaetognaths, this similarity is not surprising since in both studies individuals were counted without any species distinction. This observation confirms that the new methodology (i.e., ZooScan semi-automatic counts) gives results that can be compared with previous studies performed with traditional methodologies (i.e., counts under the microscope). In the case of copepods, both patterns were similar because although in the

former study the copepod signal was built with few species, those were key species of the seasonal succession of Mediterranean copepods (i.e., *Centropages typicus* and *Acartia clausi* peak in spring, *Oithona spp.* and *Oncaea spp.* peak between summer and autumn, and *Temora stylifera* represents the autumn community) and thus they may be representative of a wide range of physiological constrains. Contrary to the similar results for chaetognaths and copepods, the estimated abundance of the broad groups jellyfish and siphonophores showed a different interannual pattern to the one suggested by the 1st PC of the four medusae species (*Pelagia noctiluca*, *Liriope tetraphylla*, *Solmundella bitentaculata*, and *Rhopalonema velatum*), two siphonophores (*Abylopsis tetragona* and *Chelophyes appendiculata*) and one ctenophore species (*Pleurobrachia rhodopissome*) reported by Molinero et al. (2005a). Our datasets showed a decrease of jellyfish (medusae) stocks from 1989, coinciding with the disappearance of the copepod autumn peak, and a slight decrease of siphonophore abundance in the 1990s, whereas the 1st PC of jellyfish of the former study suggested a continuous increase from the beginning of the 1990s. Such contrasting results in the two studies highlight the difference between studying a few target species or the whole community. The relative magnitude of changes in species abundance/biomass, phenology, and physiological condition are often larger than the changes in total biomass or abundance of broader groups (Mackas and Beaugrand 2010). At a species level covariance with climate is often stronger than at a broader taxonomic level because each species has its particular requirements depending on the niche they occupy and, if their niche breadths are narrow, slight climatic changes can critically alter their population dynamics (Thuiller et al. 2005; Parmesan 2006). Yet, studies based on the relationship between individual species and climate have limited potential to infer changes at the whole plankton ecosystem level (Beaugrand and Ibanez 2004). Species diversity does not necessarily imply functional diversity, and effects in some species can be compensated at the

community level by other species with overlapping niches (Hooper et al. 2005). Thus, the analysis of broad groups does not substitute but efficiently complements the species level approach, and may act as an indicator of the total plankton production of an ecosystem.

6.3.2 Changes in mixing-stratification processes: The role of winter convection and salinity as a key forcing parameter for zooplankton

The results presented by Molinero et al. (2005a; 2008b) prompted the authors to propose thermal stratification as the main local forcing shaping the zooplankton ecosystem at Point B. They suggested that the rising abundance of jellyfish between 1987 and 1993 was due to increasing temperature, by means of greater water-column stability, that would have increased their survival and reproduction rates. According to the authors, stronger thermal stratification, predicted related dominance of small phytoplankton, and mainly a strong jellyfish predation pressure in the early 1990s would have been detrimental to copepod populations by affecting their physiological thresholds, life-history traits and recruitment. In addition, in their conceptual model chaetognaths were out-competed by jellyfish for their main prey, copepods (Molinero et al. 2008b; 2008c).

In the present study, although a constant trend to earlier stratification from the beginning of the 1980s is reported, the main modes of zooplankton and environmental conditions showed an almost decadal periodicity. The presence of jellyfish in the water column seems to be related to temperature, as reflected by their low records in the 1970s, when water was colder, and by their absence in the water column during the winter months. Nevertheless, although temperature continued to increase in the 1990s, jellyfish numbers decreased with respect to the 1980s. Consequently, another factor apart from temperature may have controlled jellyfish standing stocks. All five

zooplankton groups showed high abundances in the 1980s and lower in the 1990s. The 1980s have been named the dry period, characterised by high salinity records and water temperature above the average (Fromentin and Ibanez 1994; Menard et al. 1994; Menard et al. 1997). Although annual-mean temperature values were above the long-term average, winter water was colder than average at Point B during most of the 1980s. Contrary to the former studies that focused on thermal stratification, in the present study winter hydrology seems to be the main local forcing shaping the zooplankton ecosystem, and salinity might play a key role in the intensity of winter convection and nutrient enrichment at Point B.

A scenario of changes between the 1980s and the 1990s is suggested by the results presented here. The 1980s might have been more productive than the precedent and following decades due to stronger winter convection triggered by high salinity and low winter temperature, which in turn increased the input of nutrients into the photic zone. More nutrients would have entailed higher phytoplankton production and resources for grazers (i.e., copepods) and their predators (i.e., chaetognaths and jellyfish). The enhanced spring nutrient input may have set the biological production for the whole year including effects on the summer and autumn communities. Contrary to the 1980s situation, in the 1990s lower salinity may possibly have been detrimental for the vertical input of nutrients to surface waters and thus to the annual biological production. The salinity decrease in the 1990s was mainly due to increased precipitation in autumn. This would have affected the following winter convection, but also autumn destratification, which would have explained the disappearance of the autumn copepod peak during those years.

The scenario proposed above is speculative, as was also the case for that proposed by Molinero et al. (2005a; 2008b), because a time series of nutrient concentration and phytoplankton biomass is lacking at Point B for the whole studied period. Nevertheless, other studies at Point B and in central and southern areas of the Ligurian Sea seem to support this hypothetical scenario. Recently, data from monthly cruises performed between 1995 and 2007 50 km offshore from Point B, at a sampling station over a depth of ~2000 m in the central Ligurian Sea, revealed an increasing frequency of strong winter vertical mixing and the authors hypothesized as major cause a deficit in fresh water inputs since 2003 in the western Mediterranean basin (Marty and Chiaverini, 2010). The flow of rivers close to Point B was correlated to local precipitation, which decreased after 2000. The authors reported a salinity increase in surface waters during those years, enhancement of nutrient content in surface waters after the winter convection events, and consequent enhanced chl*a* biomass. Marty and Chiaverini (2010) stressed that salinity was a key parameter in winter convection, and thus precipitation and river inputs are important in dense water formation, as already highlighted in previous studies for the western Mediterranean basin (Bethoux and Gentili 1999; Somot et al. 2006; Skliris et al. 2007). The results presented by Marty and Chiaverini (2010) also support the possible almost-decadal periodicity of zooplankton and environmental modes presented in our study, as salinity and productivity are increasing again from the early 2000s in the central Ligurian Sea as at our coastal station, Point B. The authors concluded that, in the northwestern Mediterranean basin, the increasing frequency of mixing events related to decreasing fresh water inputs and evaporation due to warming, could go against the decrease of production due to enhanced stratification associated to warming that is predicted by models for temperate areas (Sarmiento et al. 2004b; Behrenfield et al. 2006). In the southern (off Calvi, northern Corsica coast) and central Ligurian Sea, silicic acid and nitrate concentrations

have been shown to increase with salinity (Goffart et al. 2002). Off Calvi, the phytoplankton winter-spring bloom was high from 1979 to 1986 due to nutrient replenishment by convection, whereas from 1988 the input of nutrients was lower, and consequently phytoplankton blooms were weaker. In addition, Gomez and Gorsky (2003) obtained similar results by compiling information about the spring-peak amplitude of single-year studies in the Bay of Villefranche. The spring peak was high from 1985 to 1988, whereas it was low in all the seven non-consecutive years of study from 1988 to 1999. Based on these results from different areas of the Ligurian Sea, it thus appears that the 1980s may have been productive years throughout the Ligurian Sea and were related to more saline and cold winter hydrological conditions.

6.3.3 Large scale mecanisms linking local environmental changes: The role of the winter NAO

Based on a reconstruction of salinity and temperature data on 0.2° by 0.2° grids covering the Mediterranean Sea and the 1950 to 2000 period, Rixen et al. (2005) observed that in the western Mediterranean basin the 1980s were characterized as a period of highest positive salinity anomalies in the upper layer (0-150m) whereas deep waters showed a monotonic increase from the 1950s. Cold winters during the 1980s (Hurrell and VanLoon 1997), and a quasi-decadal precipitation regime, with increased seawater salinity during low precipitation periods, have already been reported for the north and western areas of the Mediterranean regions (Xoplaki et al. 2004). The precipitation regime is related to storm formation, which in turn has been related to variations in sea surface temperature (SST) and atmospheric pressure, ultimately linked to the NAO in the northern Mediterranean region (Hurrell 1995; Trigo et al. 2000). Orfila et al. (2005) showed a negative correlation between sea level anomalies in the Ligurian Sea and the NAO index at monthly-scales.

In the present study, stronger winter convection in the 1980s might have been linked to the high winter NAO of that decade as supported by the significant correlation between the winter NAO and the 1st PC of local environmental conditions, to which the main variable contributing to its creation was salinity. The mechanism linking winter NAO and local winter convection in the 1980s would be as follows. During high winter NAO records, the atmospheric pressure is high at Villefranche. High atmospheric pressure leads to clearer skies that entail less precipitation. Precipitation decreases cause salinity to increase. And while in summer related enhanced irradiance entails more evaporation that contributes to salinity increases in surface waters, in winter clear skies increase sea surface heat losses, due to a lack of cloud albedo, with a consequent SST decrease (Cess et al. 1992). The consequent high sea surface water density enhances the strength of vertical convection in the northwestern Mediterranean Sea (Hurrell, 1995; Krahmann and Schott, 1998; Tsimplis and Josey, 2001). Nevertheless, mechanisms do not seem as clear and direct in the 30-year time series. The sliding correlation analysis between the winter NAO and 1st PC of environmental conditions at Point B was stronger in the first years of the time series, and the link between both signals was missing during the first half of the 1990s. The early 1990s, although presenting the highest winter NAO values of the time series, presented low annual salinity records at Point B in relation to enhanced precipitation in autumn. More detailed studies are necessary to better understand the links between atmospheric changes in the Atlantic sector and the Mediterranean hydroclimate. Research has been focused on the effect of the winter NAO on annual dynamics, but previous autumn climatic conditions may substantially force winter convection processes by altering the water column stability.

6.3.4 Bottom-up control as the main mechanism shaping the structure of the zooplankton communities at Point B

Instead of the top-down and competition control formerly stated (Molinero et al. 2005a; 2008b), the synchrony and same direction of changes of our data suggests bottom-up control forced by climate as the main factor altering the standing-stocks of the studied zooplankton groups. Zooplankton would depend on microplankton availability, which would be driven by nutrient availability related to winter convection. Bottom-up control can be inferred from the comparison of copepod and chaetognath temporal patterns. Copepods are the main prey of chaetognaths in the Mediterranean Sea (Duro and Saiz, 2000; Kehayias, 2003). The chaetognath peak occurs between August and October at Point B. Our results show that the chaetognath abundance increased when an unusual mid-summer copepod peak occurred in the mid-1970s, and it dropped in the 1990s following the disappearance of the autumn copepod peak.

The hypothesis proposed here to explain the observed abundance changes is based on a hypothetical increase of primary production in the 1980s followed by a strong decrease in the 1990s. Unfortunately, chl *a* time series started in 1991 and phytoplankton information at Point B is scattered. Gomez and Gorsky (2003) reported higher spring peaks in 1985-1988 than in 7 non-consecutive years of the period 1988-1999, in Villefranche Bay. Yet, if the mechanism proposed here is right, chl *a* would be expected to increase in the late 1990s due to increasing salinity. On the contrary, chl *a* concentration decreased in the late 1990s, with a narrower spring peak and disappearance of the autumn peak. Although chl *a* concentration decreased, surface levels of NO_3 concentration increased, mainly in spring but also in autumn. This increase of nitrates in the surface layer supports our hypothesis of stronger convection than preceding years at the end of the time series due to increasing salinity by means of stronger winter convection. The contrasting trends in chl *a* and nitrate concentration

could have been due to a change of phytoplankton composition due to earlier stratification driven by a temperature increase. In the previous chapter, changes in phytoplankton assemblages at stn MC that were probably linked to stratification conditions were presented. Earlier stratification seemed to favour the dominance of phytoflagellates and small diatoms over large diatoms, and in general, small-cell species over large cells. The observed environmental changes at Point B suggest that similar changes in phytoplankton composition could have taken place in the 1990s and lasted until the end of the studied period due to earlier stratification. The detrimental effect of enhanced thermal stratification on nutrient availability could be counteracted in the early 2000s due to stronger winter convection, but the effect of enhanced stratification on physical species constraints such as buoyancy would still persist.

Changes in predation and competition processes, driven by the observed environmental changes, might have also taken place at Point B. Predator pressure (i.e., prey size selection) as well as competition (i.e., size-dependent competition for resources) can modify the size distribution of the copepod community. Morphological and behavioural features suggest that predator avoidance has been a very significant factor in copepod evolution (Verity and Smetacek 1996; Kiørboe 1998). Predation accounts for 2/3 to 3/4 of total copepod mortality on average (Hirst and Kiørboe 2002), and thus it deserves attention for the tentative explanation of copepod size spectra changes at Point B.

Chaetognaths are copepod predators (Reeve 1980). The observed synchrony of chaetognath and copepod interannual variability points to bottom-up control of copepods on chaetognaths being more relevant than the opposite top-down control. Indeed, the impact of chaetognaths on copepod standing stock was <1% in a study conducted in the Catalan Sea, in the western Mediterranean basin (Duro and Saiz 2000).

Jellyfish were very rare in the 1960s and the 1970s at Point B as reported by Molinero et al. (2008b) and herein. The presence of jellyfish is related to warm water temperature, as reflected by their absence in winter and their lowest abundances in the 1970s and the early 1990s. Related to earlier stratification in the mid-1990s, jellyfish increased their numbers earlier in the year. Enhanced abundance of jellyfish in the water column could probably have contributed to the observed decline in small copepod abundance in the 1990s, by predating on them. Yet, the decrease of jellyfish when copepods decreased at the end of the 1980s instead of a continuous increase of jellyfish suggests a more important bottom-up control on jellyfish dependent on the trophic status of the system.

Thaliaceans (i.e., salps and doliolids) are known to have fast reproduction and growth rates and to be efficient filter feeders, and thus are strong competitors for the majority of copepods when water column conditions are favourable for them to product swarms (e.g., Harbison and Gilmer 1976; Deibel 1982). In addition, doliolids have been reported to capture copepod eggs and nauplii, and thus can also be considered as predators for copepods (Paffenhöfer et al. 1995). At Point B, the annual peak of salps occurs in late winter-spring coinciding with the spring phytoplankton bloom (Menard et al. 1994; Licandro et al. 2006), while doliolid peaks occur in summer-autumn in relation to the water column stratification (Menard et al. 1997). Licandro et al. (2006) studied changes of two salp species from 1984 to 1999 and did not find changes in their populations that could match the observed changes in the copepod community. Salp abundance neither decreased in the 1990s as was the case of the other studied groups. This might indicate better adaptation to the new conditions by salps than by the groups studied here.

Finally, appendicularian and cladoceran abundances estimated in this thesis for the years 1979, 1985, 1995-1997 and 2003 did not show lower abundances in the period 1995-1997 than in the rest of the years. Also in this case, this could indicate a better adaptation of these groups to the enhanced stratification conditions than the majority of copepods, which showed a reduced abundance in that period. Yet, the information available is not enough to support these suppositions.

The results presented in this chapter suggest that bottom-up control is the main mechanism shaping zooplankton standing stocks, although with the information available for this study, the effect of food availability, predation and competition pressure cannot be quantified. Nevertheless, a possible increase in predation and competition by the gelatinous zooplankton in the 1990s may have affected smaller size classes more than the rest of copepods. This would be due to predation on small copepods by carnivorous jellyfish, and by the more efficient feeding on small particles by gelatinous filter feeders. The effect of competition on the small copepod size-fraction would be enhanced by the stronger effect of food availability on reproduction than on somatic growth (Kiørboe 1998).

6.3.5 Changes in coastal-offshore hydrodynamics: The role of advection

To better understand the different changes recorded in total copepod abundance and copepod size distribution, several copepod genera/species for the years 1979, 1985, 1995-1997, 2003 were analysed. The general pattern observed was in accordance with the total copepod abundance signal: highest abundance in 1985, and lowest abundance of most groups in 1995-1997. Some species did not present a decrease in the 1995-1997 period, suggesting that other processes took place, apart from the assumption of high production in the 1980s and a likely associated increase of carrying capacity by the system. Differences among groups could be due to phenological differences and the effect of environmental changes associated to a certain season.

Acartia spp. and *Centropages* spp. presented a similar seasonal pattern, with their main peak in spring. Both groups presented earlier peaks in 1985, 1996 and 1997, and late peaks in 1979 and 1995. Yet, *Centropages* spp. abundance remained more or less in the same range for the six years, whereas *Acartia* spp. decreased in 1995-1997 like *Temora stylifera.*, the group containing the rest of calanoids (mostly *Paracalanus* spp. and *Clausocalanus* spp.) and *Oithona* spp. The non abundance decrease, from 1985 to the 1995-1997 period, observed in *Centropages* spp. was also present in the group gathering the typical offshore calanoid species as well as poecilostomatoids. The abundance of Poecilostomatoids may have not decreased because the appendicularian abundance did not decrease in the 1995-1997 period, and Poecilostomatoids have been appointed to feed on discarded appendicularian houses (Alldredge 1972). In the case of *Centropages* spp. and typical offshore calanoids, these might indicate hydrological changes.

While *Temora stylifera* populations are largely restricted to coastal waters (Boucher et al. 1987; Molinero et al. 2005b), *Centropages typicus* (the species contributing most to the *Centropages* spp. group) is abundant also offshore (Halsband-Lenk et al. 2001; Molinero et al. 2005b; Molinero et al. 2008a) and its coastal populations seem to be linked to high juvenile concentration in the Liguro-Provençal front, 13-19 miles offshore Nice (Boucher 1984; Ibanez and Boucher 1987; Molinero et al. 2005a; Molinero et al. 2008a). Molinero et al. (2008a) found a correlation between *C.typicus* abundance and inshore spring transport. In addition to the decrease in 1995-1997, the group gathering offshore calanoids was the least abundant in 1979 with respect to the other 5 studied years. Overall, these results suggest a change from a typical neritic Mediterranean community to a community more characterised by oceanic species in the 1990s. Most of the species constituting the typical offshore calanoids are large copepods. This could have been the main factor modifying the large copepod abundance. In the north-western Mediterranean, Fernandez de Puelles et al. (2007) observed an onshore-offshore gradient of decreasing zooplankton abundance without accompanied decrease of zooplankton biomass.

In the Ligurian Sea, the Ligurian Current presents a permanent cyclonic circulation, flowing south-eastward along the coast on a narrow continental shelf. The Ligurian Current is about 25 km wide, 300-400 deep and with a mean speed of 20-25 m s^{-1} (Bethoux et al. 1988) with seasonal variations due to seasonality in the contribution of flow from the Thyrrenian Sea through the Corsica Channel (Astraldi and Gasparini 1992). A density front delimitates the offshore path of the current and presents meanders (Prieur 1979; Boucher 1984; Boucher et al. 1987; Sournia et al. 1990; Pinca and Dallot 1995). The frontal zone is characterised by complex physical dynamics, and its cool and nutrient rich waters are related to mesoscale upwelling related to the near

continental slope (Bethoux et al. 1988; Sournia et al. 1990; Strass 1992). McGeehe et al. (2004) in a survey in August 1999 reported no strong physical or biological differences between the frontal zone and the coastal margin of the Ligurian Current. Zooplankton populations offshore the Villefranche Bay have been reported to be gathered in patches related to lenses of water masses which maintain the properties of the original water mass (i.e., the Ligurian Current) and flow across the shelf (Pinca and Dallot 1995; Gasparini et al. 1999; Molinero et al. 2008a). Other zooplankton patches observed during oceanographic surveys in the Ligurian Sea have not been related to hydrological structures, suggesting that behavioural patterns contribute to their formation (Mcgehee et al. 2004; Warren et al. 2004; Molinero et al. 2008a). Zooplankton patchiness may in fact derive from a complex interplay of various physical and biological processes that are difficult to discern (Mackas and Boyd 1979; Davis et al. 1991). In addition, diel vertical migration of large copepods (Mcgehee et al. 2004; Warren et al. 2004; Raybaud et al. 2008) as well as the residence time of surface waters for periods <1month in the peripheral zone (Bethoux et al. 1982) complicate the study of zooplankton distribution offshore the Villefranche Bay.

To test the hypothesis of an increase in offshore copepods at Point B, related to enhancement of offshore-coastal advection, the presence of *Calanus helgolandicus* at Point B was analysed. This species, although common in neritic zones of the Atlantic Sea, appears to be present in Mediterranean shelf waters only during winter, or occasionally in other periods associated with upwelling (Bonnet et al. 2005). From late spring to late autumn, *C. helgolandicus* is found in deep waters (500-1000 m in the Ligurian Sea) of the Mediterranean Sea, mostly as CV developmental stages (Hure and Scotto di Carlo 1969; Gasser et al. 1998; Andersen et al. 2001; Fernandez de Puelles et al. 2007). Commonly, *C.helgolandicus* in the Ligurian Sea has been related to the

frontal zone (Boucher 1984; Molinero et al. 2008a) and classified as an offshore species after analyzing 5 transects in 1982-1983, from the coast to the middle of the central zone, covering all the seasons (Boucher et al. 1987). In the study of Boucher et al. (1987), *C. helgolandicus* was most abundant in the frontal zone during early spring, to later be concentrated in the central zone and finally, was not found in the samples of November. In the present study, while the abundance of *C. helgolandicus* at Point B resembled the trend of total copepod abundance, the interannual pattern of *C. helgolandicus* frequency revealed an increasing trend of occurrence during the 30-year study. While the abundance might be dependent on the state of the pelagic ecosystem, the species presence at Point B could be related to the presence of waters of oceanic character in the coastal zone.

It could be hypothesized that changes in the wind pattern would have favoured the transport of offshore waters to the coast. Indeed, a study of the currents in Villefranche Bay from the 28th January to the 6th May 1959 showed that strong eastern winds accelerate the usual process of accumulation of offshore surface water coming inside the bay by its eastern side, and their exit at ~30 m depth by the western side. During strong westerly winds events, the pattern reverses, and deep water enters the bay towards the Point B location (Hentch 1959). Nevertheless, the wind interannual pattern does not show any trend, with both easterly and westerly wind frequencies covarying with time. Nor has wind speed increased in the last 30 years and so cannot explain the more common arrival of the species off the coast after the 1970s and the 1980s. No correlations have been found between wind properties and the presence of *C. helgolandicus*, neither with a lag between the two variables. Thus, either wind is not the cause for this observation or wind measured at Cap Ferrat, due to the orography of the area, is not representative of the wind blowing offshore. If wind is not the cause,

perhaps hydrological changes have occurred in response to the decreasing trend of the Ligurian Current transport related to the positive phase of the winter NAO (Vignudelli et al. 1999) or to the gradual increase of temperature and salinity of deep waters (Rixen et al. 2005).

Although, with the information currently available, a mechanism that ultimately explains the increase of large copepod abundance at Point B cannot be determined, the results suggest that it could be mainly related to physical changes, probably involving interactions with the slope of the continental shelf, close to the sampling site. An alternate hypothesis is that physical conditions at Point B changed to conditions usually found offshore allowing open ocean copepods to grow closer to the coast.

6.3.6 Conclusions

The changes identified in the copepod size distribution of Point B were probably due to several forcing factors, which in turn interacted among them, resulting in synergistic and not linear forcing on the copepod community. All the elements to resolve the causes of the observed increase of mean body size are lacking, although the results presented in this study point to two long-term variations superimposed due to two main different forcings. On the one hand, the productivity of the system could present an almost decadal variability due to changes in the intensity of winter convection related to atmospheric changes, and on the other hand, a trend of increasing presence of offshore species from the early 1980s may indicate mesoscale hydrological changes. In addition, a trend to earlier stratification was detected throughout the time series and could probably have influenced on the drop of small copepod abundance in the 1990s in addition to the weakness of winter convection.

It is worth stressing the role of salinity as an important factor affecting the water-column stability. Stratification-convection processes and nutrient supply to surface waters are not only driven by temperature but also by salinity changes. At a seasonal scale, winter-spring mixing in the Mediterranean Sea can trigger large blooms even if mean annual temperature is high. Although there is a general trend of sea water warming at an annual average scale, high-salinity conditions in surface layers and/or cool winters may still allow strong convection and nutrient input into the photic zone.

Results suggest that unidentified mesoscale hydrological changes may have occurred in the Ligurian Sea around the early 1980s and the early 1990s that led to changes in the copepod community composition. The copepod community sampled at Point B may have varied from a typical neritic community to a pelagic community with common offshore species that are usually characterised by large body size (~1.5 mm). An alternate hypothesis is that physical conditions at Point B changed to conditions usually found offshore.

Chapter 7. Comparison of MC and Point B time series

7.1 Introduction

In chapters five and six, each coastal time series was studied independently. From the results obtained, some similarities in their long term changes were observed. Regarding copepods, a common change was observed between the 1980s and the 1990s in both locations, with the copepod community being composed of fewer and larger individuals in recent decades.

In this chapter, seasonal and interannual patterns of local environmental conditions (temperature, salinity, water column stability, chl *a*), zooplankton composition and the abundance and size diversity of the copepod community were compared for common sampling periods to try to elucidate common forcing factors and mechanisms controlling both coastal ecosystems.

7.2 Results

7.2.1 Hydrology

Temperature and salinity were compared at 10 m depth to represent surface waters (instead of surface measurements, to avoid the immediate effect of local meteorological conditions), and at 50 m depth to represent the bottom waters of both coastal water columns. Chlorophyll *a* concentration was compared for the whole water column (column-integrated values) to avoid miscalculating concentrations if different vertical phytoplankton patterns occurred at the two locations. The seasonal pattern and interannual changes of environmental and copepod variables were compared. Seasonality was compared by means of monthly boxplots calculated on two separate periods of five years each, before (1986-1990) and after (1996-2000) the early 1990s, to represent a common sequence of years before and after the major change in the copepod

community. In the case of chl *a*, (where measurement only started at Point B in mid-1991) seasonality was calculated for two common four-year periods: 1996-1999 and 2000-2003. As shown in earlier chapters, for chl *a* the early 2000s showed a pattern that appears to have reversed to a community more similar to that of the 1980s. Interannual changes were compared by calculating the Pearson correlation (taking into account autocorrelation) between annual average values of complete common years in both time series.

Temperature

In both time series, temperature showed the typical seasonality of temperate ecosystems, with thermocline formation in May-June and water column mixing from October; a pattern that is reflected by the difference in monthly variation between temperatures in surface and bottom waters (Fig.7.1, Fig.7.2). Monthly surface temperatures and monthly interannual variability at stn MC were usually higher than at Point B (Fig.7.1). Summer temperatures at the surface were similar at both locations, although at stn MC the variability was much higher. In the case of bottom waters, the thermal difference between both locations was sharper. Especially during the warm period (June-September), temperature at stn MC was 2-3 °C higher than at Point B (Fig.7.2).

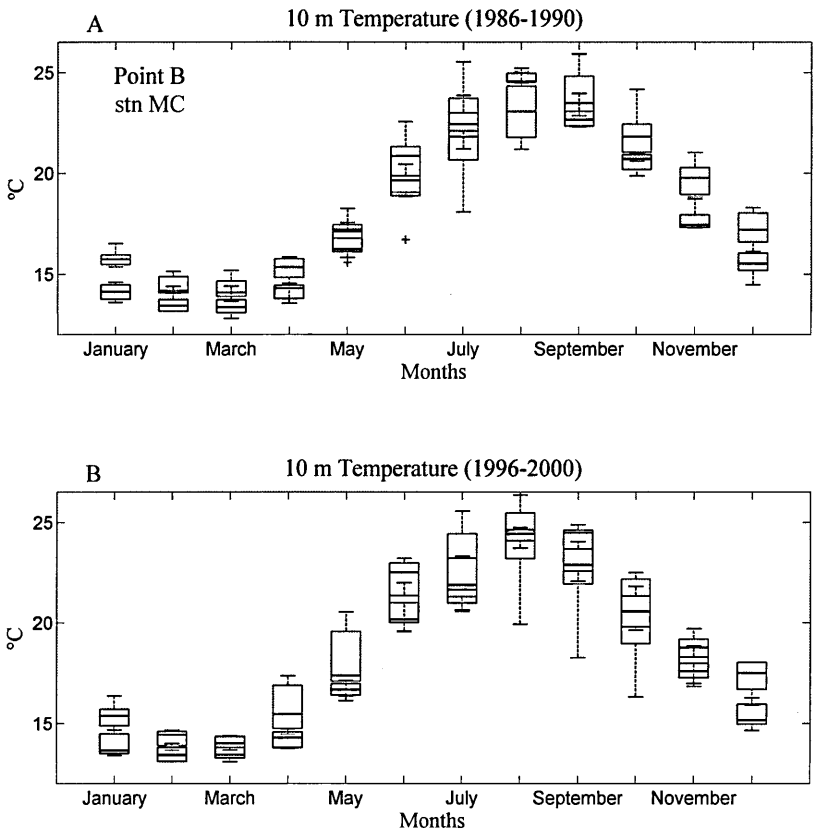

Figure 7.1 - Seasonality of water temperature at 10 m depth represented by boxplots for both Point B and stn MC. The central mark of each box represents the median of the monthly distribution, whiskers are 1.5 times the interquartile range and crosses indicate outliers. A) Monthly boxplots for the period 1986-1990; B) Monthly boxplots for the period 1996-2000.

During the second period, surface waters warmed up earlier in the year. At stn MC temperatures from April to June were above those of the first period, and at Point B only in June temperature was significantly higher during the second period (Fig.7.1 A, B). The thermal difference at 50 m depth, from June to September, increased at both locations in the second period due to less interannual variability (Fig.7.2).

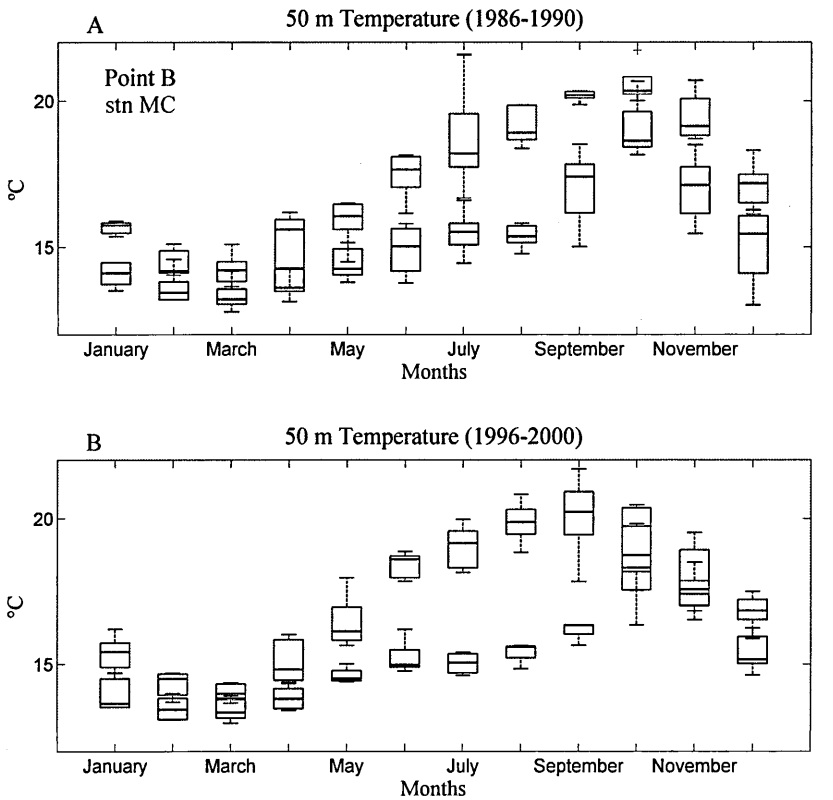

Figure 7.2 - Seasonality of water temperature at 50 m depth represented by boxplots for both Point B and stn MC. The central mark of each box represents the median of the monthly distribution, whiskers are 1.5 times the interquartile range and crosses indicate outliers. A) Monthly boxplots for the period 1986-1990; B) Monthly boxplots for the period 1996-2000.

Thermal interannual changes were not significantly correlated at either of the two depths compared for the 13 complete common years (Fig.7.3 A, B), although the pattern of SST changes were significantly correlated ($r = 0.61$; $p = 0.03$; $n = 13$). A positive trend of SST has been reported to occur over the entire western Mediterranean basin, as observed by its spatial PCA (see Fig.2.4). Average annual values of SST for common complete years at both locations were positively correlated to the 1st PC of basin SST ($r = 0.85$ and $r = 0.81$, for MC and Point B respectively, $p<0.005$, $n = 13$).

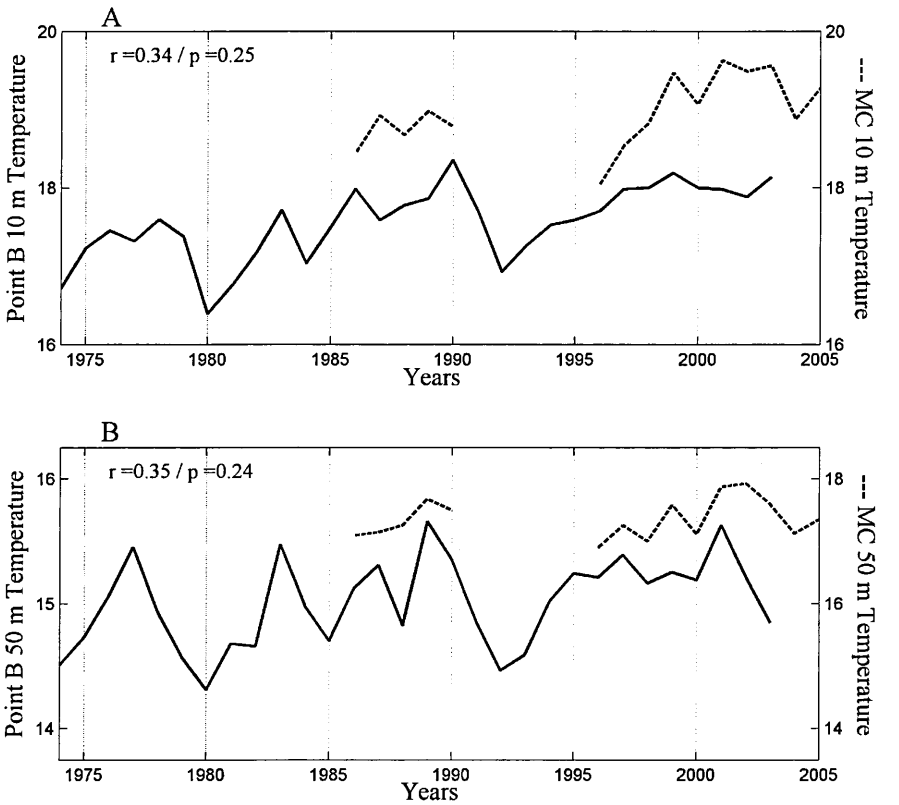

Figure 7.3 – Interannual changes of water temperature at A) 10 m depth and B) 50 m depth. The Pearson correlation of the annual average values at Point B (continuous) and stn MC (dashed line) was performed on 14 complete common years.

Salinity

In both locations, the salinity of surface waters decreased in spring in relation to increased fresh water input from precipitation and/or snow thaw (Fig.7.4). This seasonal pattern was still observed at 50 m depth although much less marked (Fig.7.5). Salinity at Point B was generally stronger than at stn MC throughout the whole annual cycle during the 10 years of comparison.

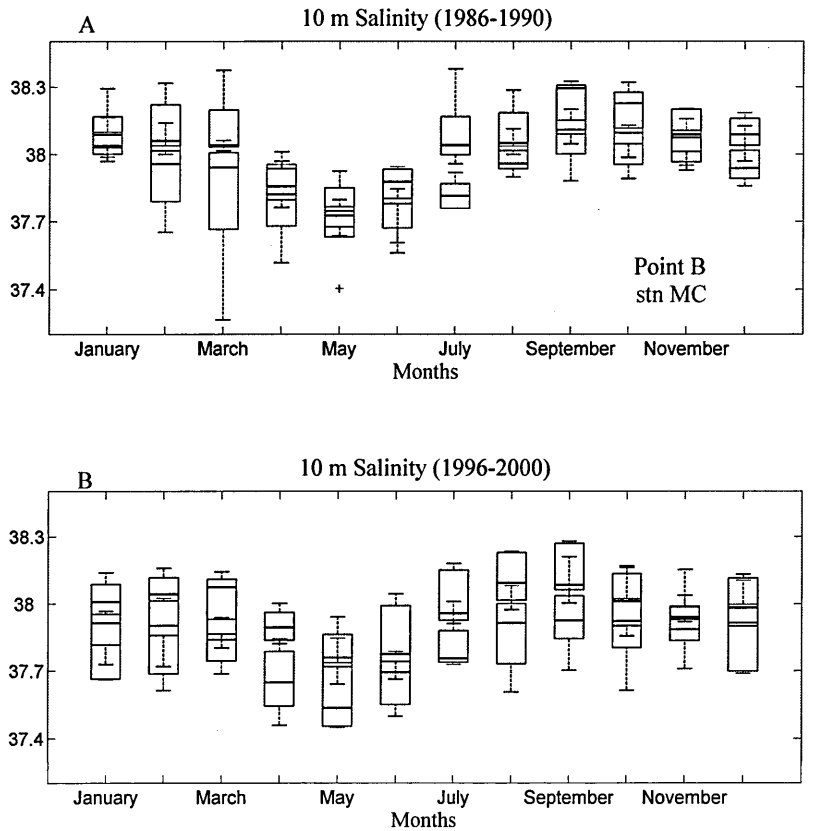

Figure 7.4 - Seasonality of salinity at 10 m depth represented by boxplots for both Point B and stn MC. The central mark of each box represents the median of the monthly distribution, whiskers are 1.5 times the interquartile range and crosses indicate outliers. A) Monthly boxplots for the period 1986-1990; B) Monthly boxplots for the period 1996-2000.

During the first period (Fig.7.4A and Fig.7.5A), salinity was generally higher than in the second period (Fig.7.4B and Fig.7.5B) in both locations. In the case of Point B, surface winter and late autumn values were generally higher in the first period, whereas summer values did not vary much between both periods, and thus the average seasonality at Point B was less marked in the second period (Fig.7.4, Fig.7.5). In addition, in the second period, the interannual variability increased for both time series except for March at stn MC.

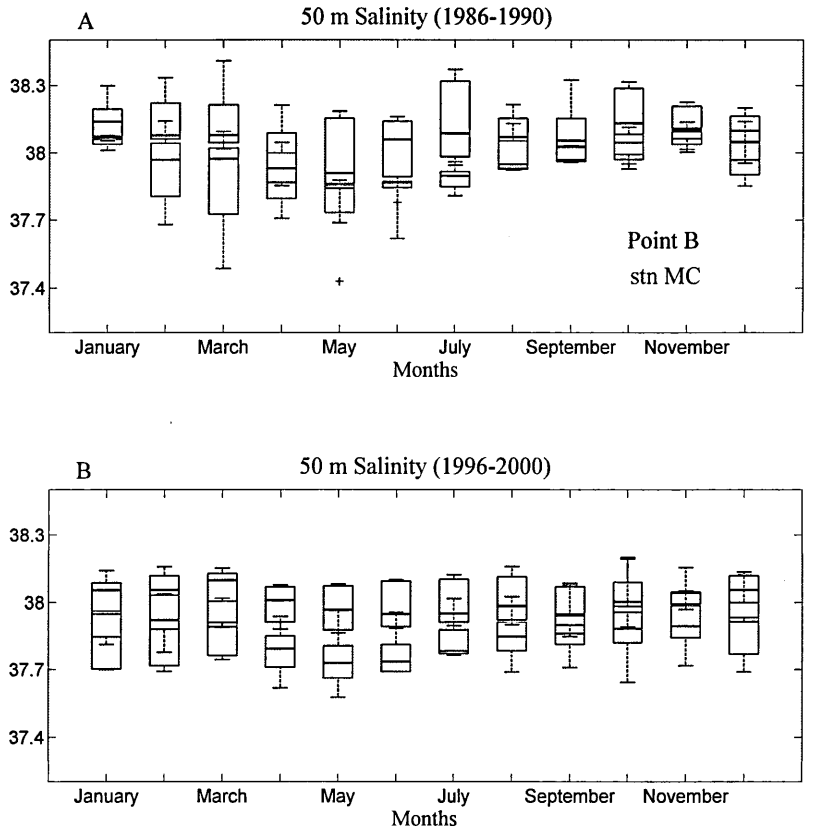

Figure 7.5 - Seasonality of salinity at 50 m depth represented by boxplots for both Point B and stn MC. The central mark of each box represents the median of the monthly distribution, whiskers are 1.5 times the interquartile range and crosses indicate outliers. A) Monthly boxplots for the period 1986-1990; B) Monthly boxplots for the period 1996-2000.

Although both locations had the same pattern of lower salinity in the second period (Fig.7.4, Fig.7.5), annual average values of salinity at both locations were not significantly correlated (Fig.7.6).

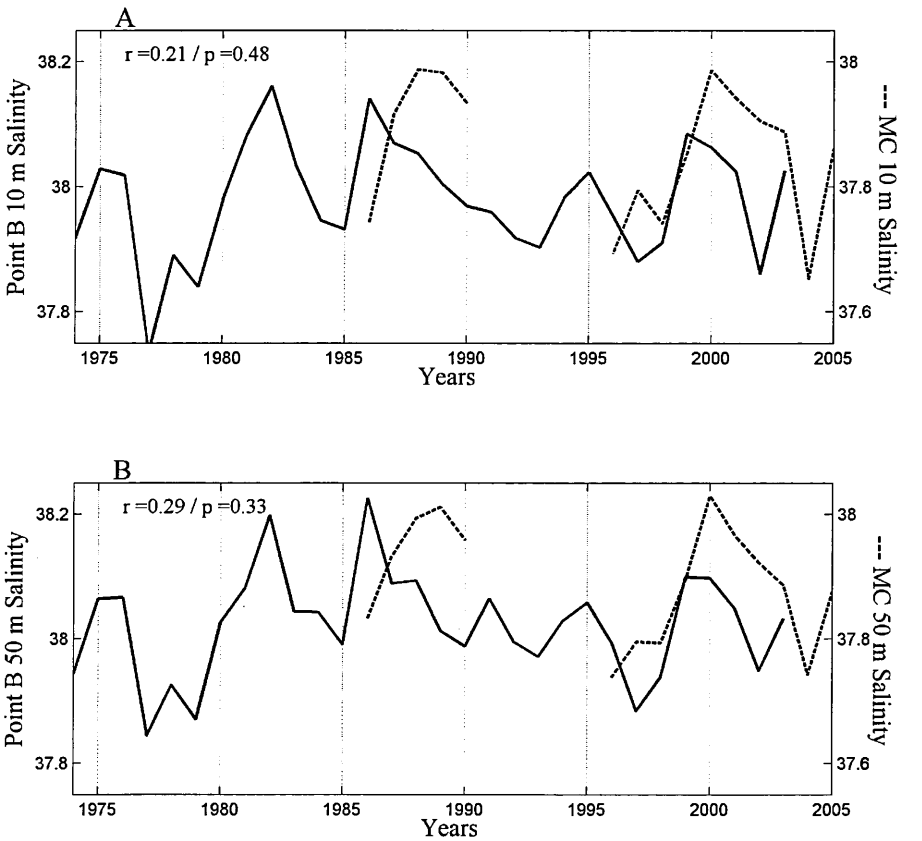

Figure 7.6 - Interannual changes of salinity at A) 10 m depth and B) 50 m depth. The Pearson correlation of the annual average values at Point B (continuous) and stn MC (dashed line) was performed on 14 complete common years.

Water-column stability

Water-column stability (WCS) was calculated as the difference of density at 50 m (D_{50}) and 10 m (D_{50}) depth (Lacroix and Nival, 1998) (see Fig. 5.3). The mean density was 27.65- 28.51 kg m^3 at Point B, and 27.26- 27.86 at stn MC at 10 m and 50 m depth respectively. Density was higher at Point B due to colder and saltier water. Thus, differences were standardised by the mean density at each site as follows:

$$WCS = 1000(50-10)\frac{D_{50} - D_{10}}{D_{50} + D_{10}}$$

The summer average (July-September) of standardised water-column stability was calculated to quantify the stratification of the water column at both sites. Higher water-column stability implies stronger stratification. In the first period of comparison

(1986-1990), minimal, mean and maximal values of standardised summer water-column stability were 1.723-1.833-1.958 m^{-1} at Point B, and 0.958-1.129-2.095 m^{-1} at stn MC. In the second period (1996-2000), minimal, mean and maximal summer stability were 1.793-1.927-2.095 m^{-1} at Point B, and 0.491-1.119-1.526 m^{-1} at stn MC. Thus, at Point B stratification was stronger than at stn MC, and it increased in the second period while at stn MC stratification was more variable in the second period. The non-parametric Spearman correlation coefficient (φ) was calculated between summer average density and time at both depths, and between summer water-column stability and time, to find significant interannual trends (Table 7.1). The density of surface waters tended to decrease at Point B from 1974 to 2003. At stn MC the whole water column tended to have lower density from 1986 to 2005, although the trend in surface waters was slightly steeper. As a result, at both sites a trend of increasing water column stratification in summer was recorded, although in the case of the MC time series this trend was not significant.

	Point B (n = 30)	Stn MC (n = 15)
D_{10}	φ = -0.40 ; p-val = 0.02	φ = -0.65 ; p-val = 0.01
D_{50}	φ = 0.002; p-val = 0.99	φ = -0.59 ; p-val = 0.02
WCS	φ = 0.50; p-val = 0.006	φ = 0.47; p-val = 0.07

Table 7.1 - Spearman correlation (φ) and level of significance (p-val) of density interannual changes at 10 m (D_{10}) and 50 m depth (D_{50}), and of water column stability (WCS); from 1974 to 2003 in the case of Point B time series, and from 1986 to 2005 in the case of MC.

The above results can be illustrated by comparing thermal vertical profiles at both stations for the two periods under comparisonFig.7.7). The strongest difference in the vertical profiles at both stations was recorded in August (Fig.7.7 A, B). The water column was more stratified at Point B than at stn MC (Fig.7.7 C, D). At Point B, deep water did not warm up until destratification, whereas at stn MC the water column warmed up after spring (Fig.7.7 A, B). In addition, in the second period, in May at stn MC, the water column was on average warmer, whereas in October it was colder. The envelopes of the average summer profiles show that the greater variability of WCS at stn MC in the second period was due to variability in surface waters (Fig.7.7 C, D). Deep water at stn MC warmed up in the second period. From the observation of the thermal vertical profiles it can be concluded that stratification-destratification seasonal processes were more abrupt at Point B than at stn MC. Actually, the difference between the standardised water-column stability in summer and winter (ΔWCS_{S-W}) is 1.6 m^{-1} (42.8 kgm^{-4},non-standardised value) and 0.7 m^{-1} (25.5 kgm^{-4}).

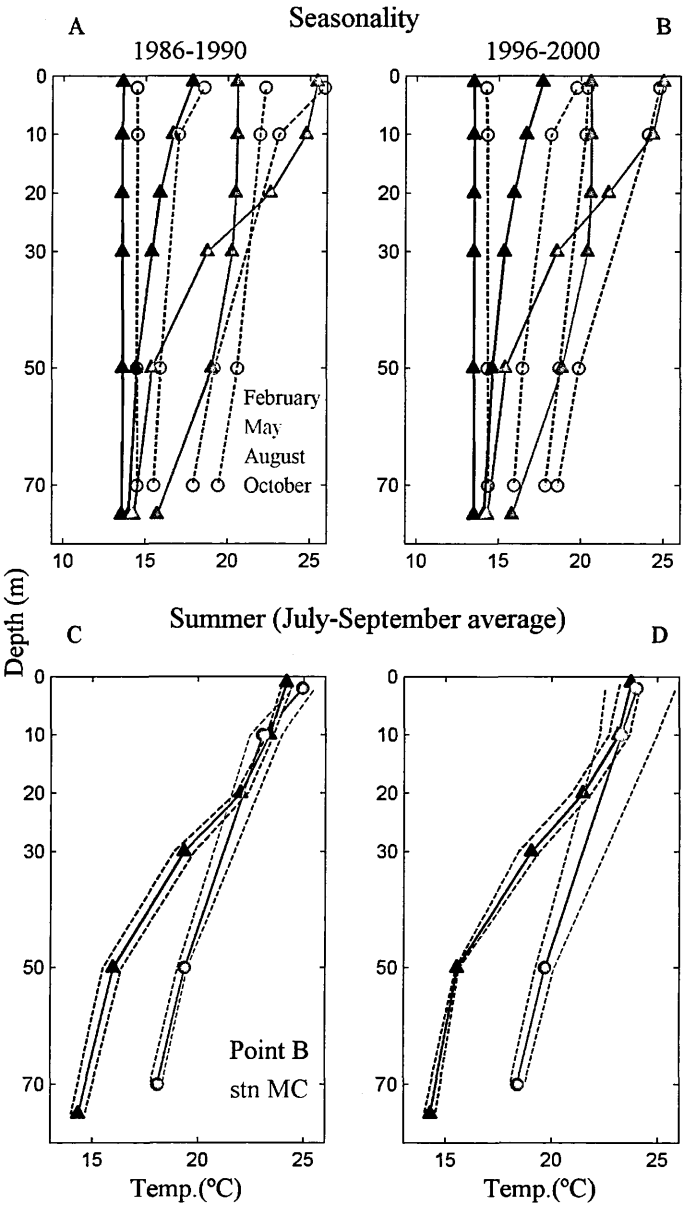

Figure 7.7 Average thermal vertical profiles at Point B (▲) and stn MC (○) for the 1986-1990 period (A, C) and the 1996-2000 period (B, D). In the upper panels, the seasonality of thermal stratification is represented by the average profiles of February (winter mixing), May (spring stratification onset), August (strongest summer stratification) and October (beginning of autumn destratification). In the lower panels, the summer average vertical profile (continuous line) and the 1st and 3rd quartiles of the 5-year profile distribution (dotted lines) are represented.

7.2.2 Chl *a*

At stn MC, chl *a* seasonality presented high interannual variability as reflected by the wide range of values in the monthly boxplots, more noticeable in the 1996-1999 period than in the second one (Fig.7.8). In the second period both time series presented an average seasonality composed of a main spring peak and a secondary autumn peak (Fig.7.8B).

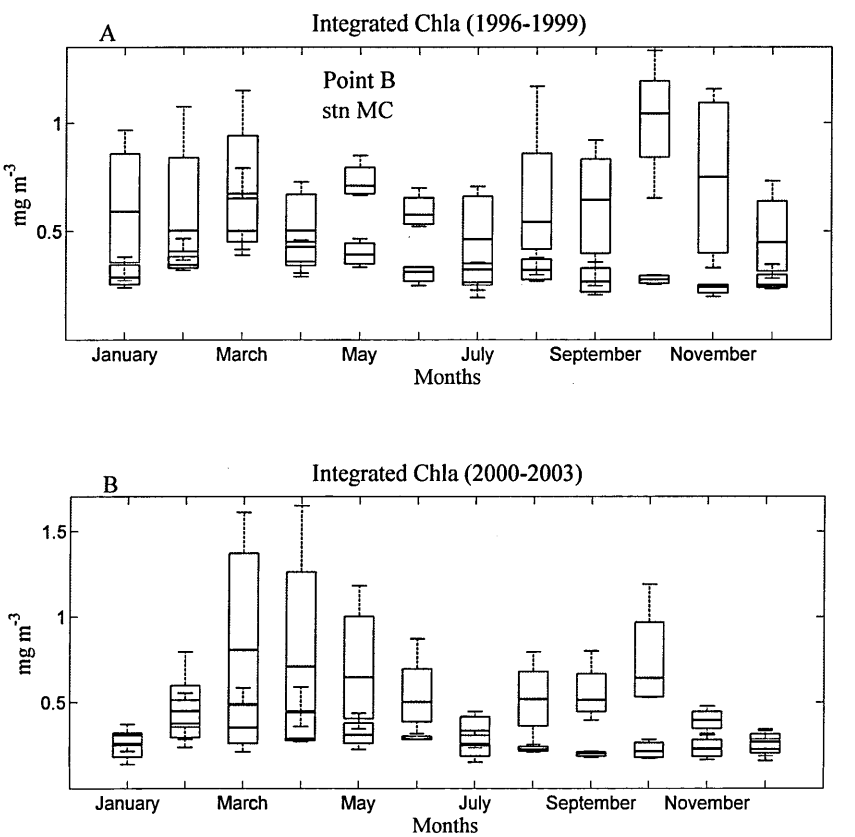

Figure 7.8 - Seasonality of integrated chl *a* represented by boxplots for both Point B and stn MC. The central mark of each box represents the median of the monthly distribution, whiskers are 1.5 times the interquartile range and crosses indicate outliers. A) Monthly boxplots for the period 1996-1999; B) Monthly boxplots for the period 2000-2003.

In the second period (200-2003) the chl *a* concentration was lower than in the first period at Point B, while at stn MC the autumn peak decreased and some years presented enhanced spring peaks (Fig.7.8B). Interannual changes were similar for the common period of both time series, eight years (Fig.7.9).

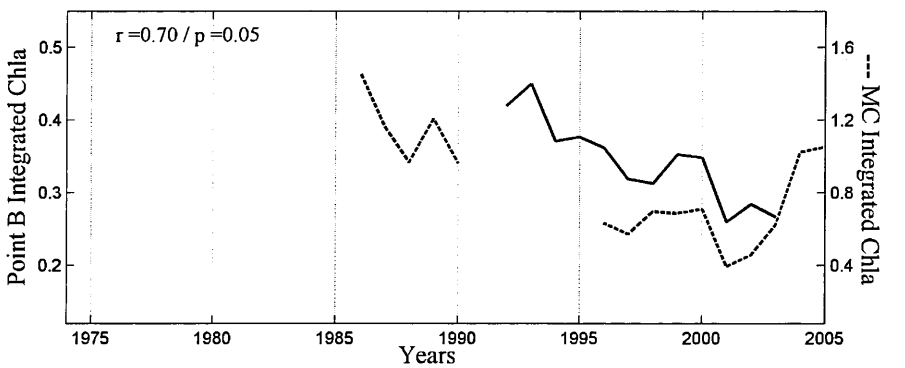

Figure 7.9 - Interannual changes of salinity integrated chl *a*. The Pearson correlation of the annual average values at Point B (continuous) and stn MC (dashed line) was performed on 8 complete common years.

7.2.3 Zooplankton composition

The abundance of 12 zooplankton groups (*Centropages* spp., *Temora stylifera*, *Acartia* spp., offshore Calanoida, other Calanoida, Poecilostomatioda, *Oithona* spp., *Penilia avirostris*, other cladocera, appendicularia, chaetognatha and jellyfish) was estimated by semi-automatic recognition of zooplankton samples from four years (1995-1997 and 2003) (see section 2.4.3 for details). Zooplankton composition was compared by contrasting boxplots representing the contribution of each zooplankton group to the total abundance of the 12 studied groups at each site, for the four common years of semi-automatic counts of ZooScan data (Fig.7.10). Average contributions of each taxon were contrasted by one-way Anova. The group 'other copepoda' (dominated by *Clausocalanus* spp. and *Paracalanus* spp.) is not represented in the figure as it shows a much higher contribution than the rest of the groups. It's contribution was higher at Point B (45.93% mean, 39.8-52.07% 1st and 3rd quartiles) than at stn MC

(35.33%, 29.47-41.19%), but the difference was not significant (p-val = 0.093). In this study, the notch occupies the whole boxplot indicating that the results of these analyses must be considered cautiously as distributions were calculated on only four years (n = 4). Interannual variability can be noticed by drawing seasonal patterns of each group for the four years (see Fig.6.21). Nevertheless, the consistency of the results obtained deserves attention.

Regarding copepods, only *Centropages* spp. and the group containing typical offshore calanoid species (i.e., genera belonging to the following families: Aetideidae, Augaptilidae, Calanidae, Candaciidae, Eucalanidae, Euchaetidae, Heterorhabdidae, Lucicutiidae, Scolecithricidae) presented significantly different contributions at both sites, with Point B characterised by a higher proportion of both groups than at stn MC. On the contrary, the contribution of *Temora stylifera* was higher at stn MC, although the difference was not significant (p-value = 0.058). Cladocera and appendicularia contributions at stn MC exceeded those at Point B, whereas chaetognatha and jellyfish (i.e., carnivorous medusae) contributions were lower than those at Point B.

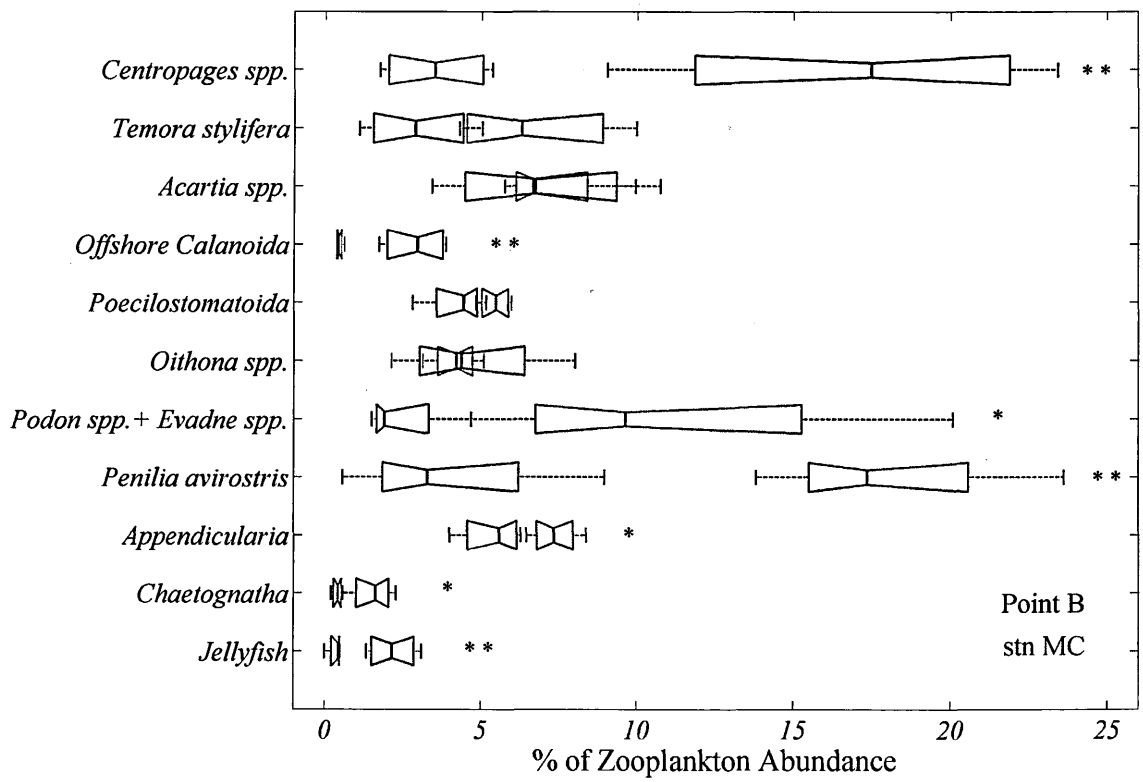

Figure 7.10 – Comparison of the contribution of each zooplankton group to the abundance of all the 12 groups compared at Point B (black boxplots) and at stn MC (red boxplots). The group 'other calanoida', with 45.93% and 35.33% mean values respectively and not significantly different, is not represented in the figure. The central mark of each box represents the median of the monthly distribution, and whiskers are 1.5 times the interquartile range. Boxplots are notched to represent a robust estimate of the uncertainty about the medians for box to box comparison. Results of a one-way Anova performed for each taxon are indicated by asterisks; a significantly different mean contribution of a taxon in the two locations is indicated for p-values <0.05 (*) and for p-values <0.01 (**).

7.2.4 Copepod abundance and size distribution

The copepod community at Point B presented two wide annual peaks, the main one around spring and the second one in autumn (Fig.7.11), whereas the annual copepod distribution at MC presented a bell shape, with highest annual values dispersed between April and October. Due to a different seasonality, although monthly copepod abundance at stn MC was generally higher than the one at Point B throughout the seasons, in late summer the difference increased (Fig.7.11). The same plots were performed with medium-copepod abundance (0.04 mm3-0.32 mm3 of body

biovolume), to try to avoid biases of abundance estimates produced by the different mesh used in both locations (330 μm at Point B and 200 μm at stn MC), and results were similar.

Abundances tended to decrease in the second period studied. In the case of MC it was clearly lower in December, January and April, while at Point B abundances decreased in the second period throughout the whole year.

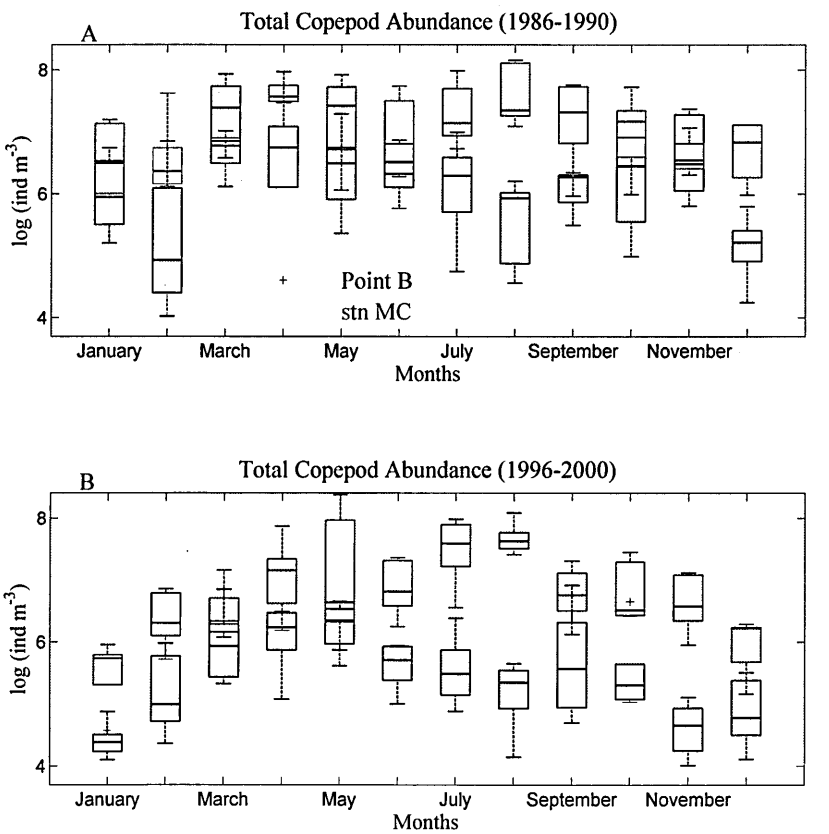

Figure 7.11 - Seasonality of total copepod abundance represented by boxplots for both Point B and stn MC. The horizontal line inside each box represents the median of the monthly distribution, whiskers are 1.5 times the interquartile range and crosses indicate outliers. A) Monthly boxplots for the period 1986-1990; B) Monthly boxplots for the period 1996-2000.

The size diversity of the copepod community at the two sampling sites showed an opposite pattern with respect to abundance due to the normal abundance-size inverse relationship. Thus, the copepod community at stn MC showed a higher proportion of

small organisms than the one at Point B as reflected by the lower size diversity of MC copepods throughout the year (Fig.7.12). And as in the case of abundance, the copepod size diversity in August was the highest of the annual cycle at Point B and the lowest at stn MC.

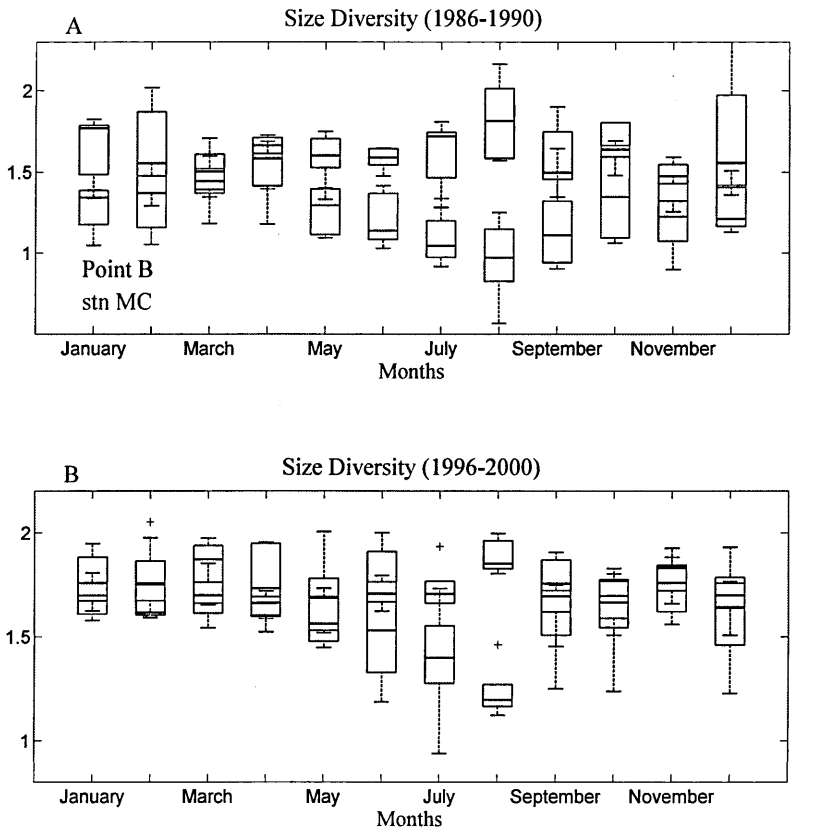

Figure 7.12 - Seasonality of copepod size diversity represented by boxplots for both Point B and stn MC. The horizontal line inside each box represents the median of the monthly distribution, whiskers are 1.5 times the interquartile range and crosses indicate outliers. A) Monthly boxplots for the period 1986-1990; B) Monthly boxplots for the period 1996-2000.

If the trend of annual average abundance and size diversity at both stations is compared, the long-term changes are seen to be relatively similar. In the 1980s the community was more abundant and with a smaller average body size, to then decrease their abundance and increase their size in the 1990s (Fig.7.13). In the 2000s at MC the situation started reversing, while at Point B only abundance showed a slight recovery. Despite these similar patterns, correlations were not significant.

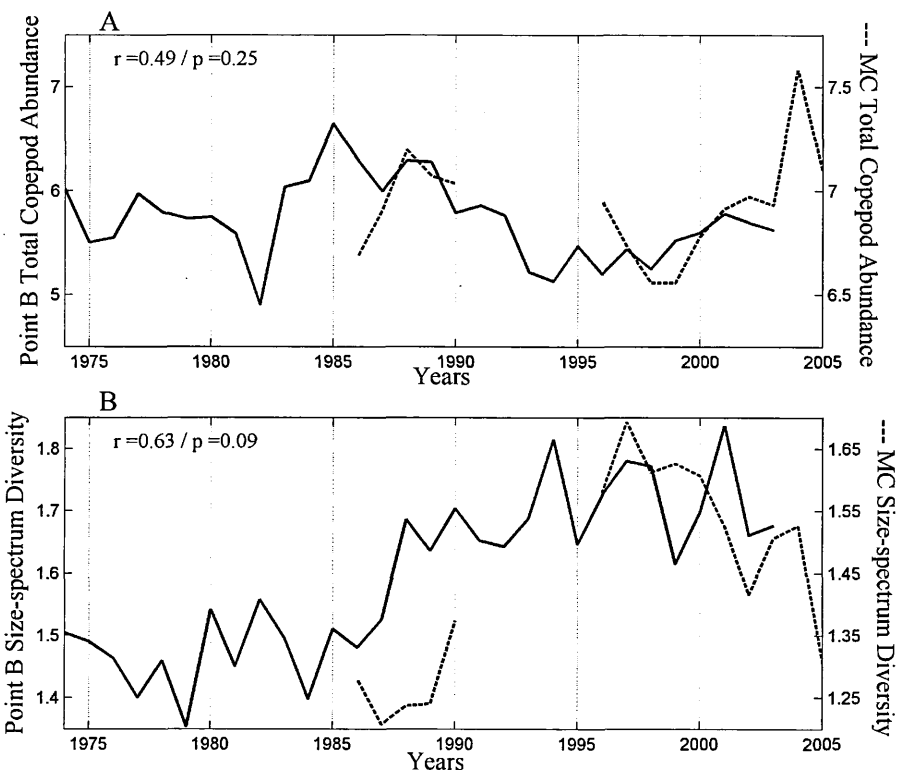

Figure 7.13 - Interannual changes of A) abundance and B) size diversity of copepods. The Pearson correlation of the annual average values at Point B (continuous) and stn MC (dashed line) was performed on 14 complete and common years.

7.3 Discussion

7.3.1 Methodological limitations of time series comparison

Before comparing time series, note should be taken of possible methodological biases, which usually are not possible to quantify but that at least must be kept in mind when interpreting results (Perry et al. 2004). Biases can be produced due to the use of different sampling techniques in the two time series. Among these biases, the most notable one is the net sampling. For copepods the issue has been previously tackled in this thesis (see section 3.4.4). Although at stn MC the 200 μm mesh catches more small organisms than the 330 μm mesh of Point B (Calbet et al. 2001), copepods with a body size larger than the mode of the spectra (the small copepod fraction, <0.004 μm^3 neglected) were still more abundant at stn MC than at Point B. Copepod size diversity was also independent from the net bias on the small size fraction because this fraction was not considered in its calculation. For jellyfish, the effect of the mesh would be the opposite (Molinero et al. 2008a); at Point B gelatinous zooplankton would be less damaged than at stn MC due to its coarser net. Another net bias is expected due to the different volume sampled. At stn MC the volume sampled by the Nansen net is greater compared to that at Point B, but at Point B the sample contains more replicates and thus more volume and temporal variability in a sample. Other biases could come from the measurements; the instruments used in both stations were not calibrated between them and thus hydrological data could be slightly biased. The advantage of this study is that we do not add the common bias issued from methodological differences in taxonomic recognition using the microscope. Taxonomic biases might occur between time series but also in the same time series due to the different parataxonomists/technicians that were used in the analyses during the years of sampling. In this comparative study, the ZooScan methodology minimised human error and/or allowed its detection and correction.

Despite all these difficulties in comparing the time series, such studies are important to help understand the processes underlying the synchronies and similarity of patterns found between distant locations (Mackas and Beaugrand 2010). Alheit and Bakun (2010) propose time series comparison in ecology as the equivalent of laboratory experiments in empirical biology. In the present study, with the comparison of overlapping periods of both time series the differences and similarities noticed during the parallel study of both time series are highlighted. Although they presented strikingly similar long-term changes the seasonal and year to year patterns tended to differ.

7.3.2 Coastal-Offshore distinction

The comparison of hydrological and biological records of both time series emphasises the more coastal character of stn MC with respect to Point B. The MC time series presented warmer and less saline waters than Point B. The plankton community at stn MC showed higher levels of chl *a* concentration and copepod abundance, as well as a copepod community characterised by smaller mean body size than at Point B. In addition, the chl *a* concentration at stn MC was very variable from month to month and between years, and thus the seasonality characteristic of temperate zones was not as clear as for the Point B time series, especially in the first period compared (1996-1999). The copepod seasonal pattern neither presented the typical spring peak and lowest summer records, instead, the highest annual peaks were usually recorded in that season. Finally, the zooplankton composition during four years of study support the more coastal character of stn MC due to a higher proportion of cladocerans and a lower proportion of typical offshore calanoid species than at Point B.

A large-scale classification of Mediterranean pelagic ecosystems based on diverse atmospheric factors, salinity, temperature and/or chl *a* shows a similar pattern, with regions formed following an East-West and North-South gradients (D'ortenzio and

Ribera D'alcalà 2009; Katara et al. 2008; Tsimplis and Josey 2001) (see section 2.2.1 for further explanation). Yet, a recent study of six Mediterranean coastal time series (including both Point B and MC) found that the coastal-offshore gradient was more important in sorting the stations than large-scale gradients (Berline et al. 2010). The authors found that the six stations were sorted by their chl *a* average concentration and variance in two groups, the more open sea oligotrophic stations (Stoncica, Balears and Point B) with low mean values and low ranges of chl *a*, and the more coastal mesotrophic stations (Athens, Trieste and stn MC) with high chl *a* average concentration and high ranges (Fig.2 in Berline et al 2010). In addition, in that study, the same distinction was found when contrasting chl *a* and abundance of broad taxonomic groups (Fig.2 in Berline et al 2010). They found more copepods and cladocerans in coastal stations following a linear relationship with chl *a* concentration, and higher abundance of jellyfish in offshore stations despite the higher chl *a* concentration in the latter. In addition, the cladoceran offshore-coastal gradient was clearer and steeper than that of copepods, and at stn MC chaetognaths were less abundant than at Point B for the whole series. These results fully match the results presented here on zooplankton during the four years of observations.

The higher proportion of jellyfish and chaetognaths at Point B than at stn MC despite the lower chl *a* concentration could be related to a higher trophism due to its more offshore character. In a global survey, Gasol et al. (1997) examined simultaneous reports of phytoplankton, bacteria and mesozooplankton biomass, and concluded that the heterotrophic-autotrophic ratio tended to decline with phytoplankton biomass and primary production, and that this trend was steeper in open-water communities. Thus, offshore communities may support more heterotrophic biomass than coastal ones for a

given autotrophic biomass, and this would be due to tighter and more efficient coupling between phytoplankton and heterotrophs.

The colder and more saline character of the water column at Point B may indicate also its more offshore character than stn MC. A coastal-offshore gradient of salinity (saltier), temperature (colder) and chl *a* (higher) is a common pattern in marine ecosystems due to river fresh water input, runoffs and shallow waters in the coastal areas. In both coastal sites, a local gradient of temperature and salinity has been found when performing coastal-offshore transects (Molinero et al. 2008a; Zingone et al. 1995). Yet, only in the case of the Gulf of Naples chl *a* and phytoplankton production increased coastward (Zingone et al., 1995). In the case of Point B, the existence of a frontal zone and associated upwelling offshore implied higher concentrations than inshore (Molinero et al., 2008a). Due to the coastal character of stn MC, phytoplankton blooms are rather intermittent and short, and have been mostly related to terrestrial runoff, sewage discharge, atmospheric nutrient input and lateral advection due to very dynamic mesoscale patterns (Zingone et al. 1995, Ribera d'Alcalá et al 2004, Zingone et al., 2010). In this site nutrients are seldom depleted and blooms depend on calm conditions that provide light and water column stability.

Regarding the higher size diversity recorded at Point B, this is related to different species composition and population structure in both sites. In chapter 5 the large-size fraction of the copepod community was significantly correlated to the group of typical offshore species. The large-size fraction at Point B represented around 5% of the total copepod abundance, whereas, at stn MC it represented around 2%. A coastal-offshore gradient has been reported for the size distribution of copepod communities in different basins (D'Elbée, 2001; Sourisseau and Carlotti 2006; Mackas and Coyle 2005) and is based on behavioural and life-history adaptations that favour survival and

retention of species in shallow near-shore areas or in deep offshore areas (Gasser et al. 1998; Mackas and Coyle 2005; Mazzocchi et al. 2010). Typical offshore species are usually large, strong swimmers that perform vertical migration, and carnivory or omnivory is more frequent that in neritic communities (Mackas and Coyle 2005). In addition, the higher concentration of chl *a* at stn MC related to its more coastal character could probably imply more copepod secondary production than at Point B, and thus more small copepodites constituting the copepod populations contributing to the observed lower size diversity at this location.

Finally, regarding this coastal-offshore gradient, in both stations the presence of typical offshore species has increased from the 1980s to the 1999s, and in the case of stn MC, in the 1980s chl *a* concentration was much higher and related to more frequent sporadic inputs of nutrients of terrestrial origin (Ribera d'Alcalá et al. 2004, Zingone et al. 2010). These results suggest a trend to a more offshore character in both stations that could be related to a more frequent intrusion of offshore waters in the study sites. This common pattern could indicate a common environmental forcing affecting hydrology at basin-scale dimensions.

7.3.3 Seasonality: Differences related to water-column dynamics

Different dynamics of water-column stability as well as seasonality of chl *a* and copepod abundance point to different mechanisms driving the biological production in both sites. Results of other studies at stn MC suggest that phytoplankton blooms are less dependent on nutrient input related to vertical stability compared to other temperate coastal systems like Point B, due to intermittent input from terrestrial and anthropogenic sources (Ribera D'alcalà et al. 2004; Zingone et al. 1995; Zingone et al. 2009). Phytoplankton at stn MC in winter has been analysed in detail, and chl *a* profiles from that season were sorted into groups by cluster analysis (Zingone et al. 2009). The

authors found that the highest surface concentrations related to diatom blooms occurred in association with low salinity. A surface layer of low salinity appeared and was generally characterised by heavy nutrient loads, yet in a mixed nutrient-replete water column the hypothesis of a higher chl *a* concentration related to nutrient input was not supported. Instead, they hypothesized that the enhancement of primary production was possibly due to water-column stratification, allowing diatoms to concentrate in the first few meters of the column, and if followed by calm weather a winter bloom occurred. In that study, stratified conditions in winter were reported to decrease in the 20-year time series at the same time as fresh water inputs reduced. In another study of phytoplankton blooms in autumn, the same authors proposed terrestrial runoff and stability of the water-column as the trigger to initiate blooms rather than higher nutrient concentrations due to vertical mixing (Zingone et al. 1995). Actually, the erosion of the thermocline, at least at the beginning of the time series, is unlikely to have caused an increase in the vertical flux of nutrients because the main nutricline was below the depth reached by the autumn mixing (Carrada et al. 1980; Ribera D'alcalà et al. 2004).

Observing figures 5.4 D and 6.9 D it is evident that at Point B a classical seasonal cycle representative of temperate areas is found, with one spring bloom and occasionally a second lower autumn bloom, whereas at stn MC high peaks were dispersed throughout the year. Yet, while at the beginning of the MC time series, peaks were very high throughout the year, at the end of the time series highest values were recorded in spring and autumn and were lower than peaks at the beginning. These patterns might be related on the one hand to the effect of terrestrial inputs at stn MC and its decrease after the 1980s as suggested in former publications, and on the other hand perhaps to water-column stability. In autumn, the erosion of the thermocline at Point B might liberate more energy and mix nutrients from the deeper waters to the photic zone.

At stn MC, the autumn erosion might be weaker than at Point B and may not play an important role in annual phytoplankton production, as pointed out by Carrada et al. (1980). Supporting the role of summer stability on annual primary production, at the end of the MC time series, when the summer-column stability was stronger and stratification started earlier, the autumn secondary and the spring primary peaks were the highest peaks of the year although these peaks were lower due to less terrestrial inputs and higher depletion of nutrients in summer than in the 1980s.

The strongest difference of copepod abundance and size in both time series was observed in summer, with August presenting the highest abundance and smallest size at stn MC and one of the lowest annual abundances and the highest size diversity at Point B. At Point B, the water-column stability in summer was stronger than at stn MC, the photic zone was nutrient depleted and thus copepod abundance presented the lowest values of the year (see figures 6.10 B and 6.12 A). At stn MC, nutrients were seldom depleted (Ribera d'Alcalà et al., 2004) and copepods presented their highest annual abundance in summer. Related to these very different conditions in summer, the zooplankton community of stn MC was characterised by a higher proportion of efficient filter feeders such as cladocerans and appendicularians, and a higher proportion of small copepods than at Point B. In Mediterranean coastal waters, the zooplankton community in summer shifts towards filter-feeding organisms such as the cladoceran *Penilia avirostris* and appendicularians (Calbet et al. 2001). As the summer progresses, the combination of warm and calm waters with a higher abundance of prokaryotic picoplankton may explain the dominance of fine particle filter feeders. The higher proportion of filter feeders at stn MC might be due to more nutrients being available for the summer zooplankton community, warmer conditions than at Point B, and warming of the whole water column in summer. While at Point B, only water above the

thermocline (~ 30 m depth) warmed up, at stn MC summer temperature increased throughout the water column, with temperature at 70 m depth similar to that at 30 m depth at Point B (~ 18-19 °C). It could be hypothesized that the microbial loop would be reinforced at stn MC due to higher temperatures that would accelerate metabolic rates, and to more nutrients being available than at Point B to support those metabolic increases, and that the asexual reproduction of cladocerans and appendicularians would be favoured by the same reasons. In addition, the warmer conditions in the whole water column in summer would favour the dispersion of plankton throughout the water column and not only in the first upper meters. The lack of data on vertical distribution in the two stations does not allow testing this hypothesis.

Summer copepods can coexist with cladocerans and other efficient filter feeders due to niche segregation; with copepods feeding mostly on small diatoms, ciliates and dinoflagellates and cladocerans on small bacteriophagus flagellates (Atienza et al. 2006; Katechakis et al. 2002; Turner et al. 1988). The abundance of typical-summer copepods at stn MC such as *Paracalanus parvus* has been reported to decrease in the 1990s (Mazzocchi et al. 2010), and this thesis also shows a decrease of copepodites during that season. This could be related to more stratified conditions and to less nutrients being available favouring smaller phytoplankton species that would escape from copepod predation. From the comparison of both time series presented here, it seems that in the 1980s the mechanisms controlling the pelagic ecosystem in both locations differed more than in the 1990s.

7.3.4 Long-term similarities

Despite the differences observed in the community composition, water-column dynamics and the different mechanisms that seem to control the pelagic communities at both time series, long term changes were quite similar: temperature increased in both locations and SST were significantly correlated, salinity was higher in the 1986-1990 than the 1996-2000 period and then increased again in the 2000s at both sites, chl *a* showed significant correlations for the overlapping period, copepod abundance decreased in the 1990s and increased again in the 2000s, and copepod size diversity was higher in the 1990s than in the 2000s.

Similar long term patterns that are not significant at a year to year level suggest that large scale atmospheric forcing might affect both locations in a similar fashion, although local environmental forcing may play a role in modulating hydrological changes and thus shaping the plankton communities at both sites. Local forcing may possibly be stronger at stn MC as it is in the inner part of the Gulf of Naples, around two nautical miles from the city of Naples. Anthropogenic forcing of a highly populated area and mesoscale variability might be the main factors affecting the hydrology and plankton variability recorded at stn MC. Perhaps the strong coastal character of stn MC and thus a higher frequency of environmental variability could in part explain the resilience of its plankton communities, and its less marked long-term patterns as stressed in previous studied of this time series (Mazzocchi and Ribera d'Alcalá 1995, Ribera d'Alcalá et al. 2004, Mazzocchi et al 2010).

It is worth highlighting that also off the coast of Trieste, in the Adriatic basin, a long-term change has been detected in copepod and phytoplankton communities in the late 1980s, and that the SST recorded at that location showed a significant correlation with the SST at Point B and stn MC (Berline et al. 2010). Conversi et al. (2010)

consider that the reason for the late-1980s shift at Point B and in the North Adriatic is a synchrony of local water temperature with the Northern Hemisphere temperature (NHT) variations. This would explain the parallel changes of zooplankton communities in the different basins (see review in chapter 2). The authors suggest that due to a continuous increase in warming, the late 1980s regime shift might not reverse to previous conditions in the near future. Our results suggest quasi-decadal changes, as the copepod abundance as well as salinity seem to reverse their trend in the early 2000s in both time series. Long-term changes in the Northern Hemisphere centres of pressure, as indicated by the NAO index, could have affected atmospheric pressure, SST, cloud coverage, precipitation and/or wind regimes in a similar fashion at both sites, and/or hydrological changes at a basin scale would have affected both sites in a similar fashion, as reflected by the more frequent appearance of typical offshore species. These suggestions are however, speculative, and it is essential that both time series are maintained into the future so that a greater insight can be gained of the possible links between both sites and the mechanisms shaping their pelagic ecosystems.

Chapter 8. Conclusions and perspectives

8.1 Main conclusions

This work has pioneered analysis of zooplankton time series with ZooScan, an image system to automatically count and size mesozooplankton. From the results presented here, on the one hand the ZooScan integrated system has been improved and on the other hand results from the analyses of copepod size spectra have given new insight on the mechanisms linking climate and plankton at stn MC and Point B. These results could help to understand large-scale climate forcing in the western Mediterranean basin. The most important results of this thesis are the following:

1 – *Significant relationships were found between copepods sorted manually and copepods sorted automatically with the ZooScan integrated system*

Manual and automatic recognition were not significantly different in 60 samples from Point B. In addition, the MC time series of manual counts under the microscope and the time series of automatic counts with the ZooScan integrated system were highly correlated.

In this thesis, it has been shown for the first time that copepod size spectra issued from automatic estimates were very similar to those of true copepods. The size-spectrum diversity calculated on automatic spectra was highly correlated to the true copepod size-spectrum diversity, and it was also significantly correlated to the species diversity of the MC time series. Moreover, it has been shown that the small size fraction of the copepod spectra can be used as a proxy for copepodites, and the large size fraction as a proxy for typical offshore species due to the significant correlations found with the MC time series of taxonomic counts under the microscope.

2 – *The copepod size spectrum is a useful synthetic index to detect changes in pelagic ecosystems*

Long-term changes, at both studied sites, have been described in this thesis. Those changes were not previously detected with the traditional taxonomic approach. Copepod size spectra revealed changes in population dynamics (i.e., less copepodites in the 1990s) and changes in community composition (i.e., a trend to an increasing proportion of typical offshore species from the late 1980s).

Computing copepod size spectra is much less time consuming than performing species taxonomic counts under the microscope, because copepods can be sorted by automatic recognition implemented in the ZooScan integrated system. The results presented in this thesis support the copepod size spectrum as a synthetic index to detect changes that could be more difficult to detect by studying the more complex species composition. Analyses of the taxonomic composition would be a second step after having detected temporal patterns in the community size distribution.

3 – *Analyses of MC time series suggest changes in the copepod community related to changes in the phytoplankton community*

Previous analyses on copepod taxonomic counts could not detect changes that may had reflected a response to the long-term changes previously reported in phytoplankton (i.e., lower chl *a*, higher abundance but smaller average cell size in the 1990s). With the ZooScan integrated system approach, copepod changes parallel to the long-term changes described for phytoplankton were detected. Lower copepod abundance and higher size-spectrum diversity were found in the 1990s. Significant correlations between phytoplankton and copepods were described: Chl *a* annual mean concentration and annual mean copepod size-spectrum diversity were highly anticorrelated; copepod size-spectrum diversity was weakly but significantly correlated to the small phytoflagellate abundance ratio measured one month earlier; and

phytoplankton mean-cell size and copepodite concentration a month later were also correlated. These results pointed to a decrease of copepod secondary production due to less prey available in the 1990s. In addition, phytoplankton seemed to be controlled by stratification dynamics. This hypothesis had not been suggested previous to this study.

4 – *Analyses of Point B time series suggest salinity and winter convection to be key factors shaping the zooplankton community*

Previous studies performed on some key zooplankton species had not detected a quasi-decadal zooplankton abundance oscillation. The most recent studies, pointed to a regime shift in 1987 due to water warming and suggested that, due to the thermal long-term trend, the zooplankton community would remain in the new state, a community dominated by gelatinous zooplankton. In our study, the quasi-decadal oscillation of environmental conditions and the studied zooplankton groups, as well as the salinity and winter density patterns suggested periodic changes related to atmospheric forcing altering stratification-destratification dynamics by means of salinity changes. Winter convection was hypothesized to be a key factor in controlling zooplankton stocks by bottom-up control.

5 – *Synchronous almost-decadal changes may have occurred at both sites due to large-scale forcing, although the underlying mechanisms seem to be rather different*

The results presented in this thesis suggest two possible scenarios of change at the studied sites, synthesized in the following paragraph:

In both time series, MC and Point B, the copepod community in the 1990s was characterised by less copepods and a community with a larger average body size than in the 1980s. In the early 2000s abundance seemed to start recovering. Stn MC presented a more coastal character than Point B, and although the apparent synchrony of long-term changes points to large-scale climate forcing, the mechanisms underlying the copepod

changes in both sites seem different. The results presented in this thesis suggest that at Point B, winter convection might have been the main factor controlling the copepod annual production by bottom-up control dependent on nutrient input into the photic zone. Whereas at stn MC, nutrients were rarely depleted due to terrestrial inputs, higher environmental variability was recorded due to its location inside the Gulf of Naples, and the water column stability in summer seemed to be the main factor controlling the copepod community in the studied period. In the 1990s, winters were warmer and less saltier than in the 1980s at Point B, and this might have provoked a decrease of zooplankton production. At stn MC, earlier stratification in the 1990s and a possible decrease of terrestrial inputs of nutrients seem to have favoured small phytoplankton species (i.e., small flagellates) over large species (i.e., large diatoms) and this in turn may have been detrimental to copepod secondary production. The concomitant increasing presence of typical offshore species in both coastal sites might indicate a common large-scale forcing, maybe related to changes in currents or sea level in the western Mediterranean.

6 – *The ZooScan integrated system is a powerful tool to monitor mesozooplankton ecosystems*

The main advantages of the ZooScan with respect to traditional counts under a microscope are: the rapidity of processing, standardisation of measurements, large-data output (i.e., ~1500 measurements of body size per sample) and the ability to produce an image database that can be shared for further analysis. Despite the advantages of using ZooScan, microscopic counts cannot be neglected. Depending on the difficulty of a given species recognition (i.e., sharpness of morphological characteristics) the automatic identification may or may not be satisfactory. Generally, the ZooScan integrated system is not able to identify organisms at a species level. Thus, it is recommended to perform the automatic-semiautomatic coupling system for an optimal result (Gorsky et al., 2010). In this thesis, the usefulness of studying broad groups (i.e., copepod, chaetognath, jellyfish, etc.) with the ZooScan to monitor the state of a pelagic ecosystem has been highlighted. After the changes in a long-time time series have been rapidly detected with the ZooScan integrated system, hypotheses can be made, and tested by analysing the abundance of key species. If those species cannot be sorted from the ZooScan images, the microscopic counts are essential.

8.2 Main perspectives

The results obtained in this thesis open new questions and point to new research topics:

- Performance of calibration experiments between body size obtained with the ZooScan and C and N content in broad taxonomic groups. These new datasets could be a great contribution to validate models on energy flux and C export to deep waters depending on the community composition.

- Study size spectra at species level to find physiological constrains (i.e., thermal effect on body size and secondary production) and to find patterns in population dynamics by studying the species size spectrum shape.

- The importance of continuing to monitor both time series to test the predictions, and to better understand the mechanisms underlying Mediterranean zooplankton changes.

- Initiate a global comparison of zooplankton time series with the ZooScan system.

- Coupling the ZooScan with flow cytometry and the FlowCam to obtain continuous biomass spectra from pico- to mesoplankton.

- Analysis of a global ZooScan database to search for general patterns of size spectra as the one proposed by the Metabolic Theory of Ecology.

References

Aebischer, N. J., J. C. Coulson, and J. M. Colebrook. 1990. Parallel Long-Term Trends across 4 Marine Trophic Levels and Weather. Nature 347: 753-755.

Ahlstrom, E. H., and J. R. Thrailkill. 1962. Plankton volume loss with time of preservation. Rapports et Procès-Verbaux des Reunions du Conseil International pour l'Exploration de la Mer 153.

Alcaraz, M., E. Saiz, A. Calbet, I. Trepat, and E. Broglio. 2003. Estimating zooplankton biomass through image analysis. Marine Biology 143: 307-315.

Alheit, J., and M. Niquen. 2004. Regime shifts in the Humboldt Current ecosystem. Progress in Oceanography 60: 201-222.

Alheit, J., C. Mollmann, J. Dutz, G. Kornilovs, P. Loewe, V. Mohrholz, and N. Wasmund. 2005. Synchronous ecological regime shifts in the central Baltic and the North Sea in the late 1980s. Ices Journal of Marine Science 62: 1205-1215.

Alheit, J., and A. Bakun. 2010. Population synchronies within and between ocean basins: Apparent teleconnections and implications as to physical-biological linkage mechanisms. Journal of Marine Systems 79: 267-285.

Alldredge, A. L. 1972. Abandoned larvacean houses: A unique food source in the pelagic environment. Science 177: 885-887.

Andersen, V., A. Gubanova, P. Nival, and T. Ruellet. 2001. Zooplankton community during the transition from spring bloom to oligotrophy in the open NW Mediterranean and effects of wind events. 2. Vertical distributions and migrations. Journal of Plankton Research 23: 243-261.

Astraldi, M., and G. P. Gasparini. 1992. The seasonal characteristics of the circulation in the North Mediterranean Basin and Their Relationship With the Atmospheric-Climatic Conditions. Journal of Geophysical Research-Oceans 97: 9531-9540.

Astraldi, M., and G. P. Gasparini. 1994. The seasonal characteristics of the circulation in the Tyrrhenian Sea. Coastal and estuarine studies 46: 115-134.

Astraldi, M., C. N. Bianchi, G. P. Gasparini, and C. Morri. 1995. Climatic fluctuations, current variability and marine species distribution - a case-study in the Ligurian Sea (north-west Mediterranean). Oceanologica Acta 18: 139-149.

Astraldi, M., G. P. Gasparini, A. Vetrano, and S. Vignudelli. 2002. Hydrographic characteristics and interannual variability of water masses in the central Mediterranean: A sensitivity test for long-term changes in the Mediterranean Sea. Deep-Sea Research Part I-Oceanographic Research Papers 49: 661-680.

Atienza, D., A. Calbet, E. Saiz, M. Alcaraz, and I. Trepat. 2006. Trophic impact, metabolism, and biogeochemical role of the marine cladoceran Penilia avirostris and the co-dominant copepod Oithona nana in NW Mediterranean coastal waters. Marine Biology 150: 221-235.

Bakun, A. 2006. Wasp-waist populations and marine ecosystem dynamics: Navigating the "predator pit" topographies. Progress in Oceanography 68: 271-288.

Bakun, A., and S. J. Weeks. 2006. Adverse feedback sequences in exploited marine systems: are deliberate interruptive actions warranted? Fish and Fisheries 7: 316-333.

Barale, V., J-M. Jaquet, and M. Ndiaye. 2008. Algal blooming patterns and anomalies in the Mediterranean Sea as derived from the SeaWiFS data set (1998-2003). Remote Sensing of Environment 112: 3300-3313.

Baum, J. K., and B. Worm. 2009. Cascading top-down effects of changing oceanic predator abundances. Journal of Animal Ecology 78: 699-714.

Beaugrand, G., F. Ibanez, J. A. Lindley, and P. C. Reid. 2002a. Diversity of calanoid copepods in the North Atlantic and adjacent seas: Species associations and biogeography. Marine Ecology-Progress Series 232: 179-195.

Beaugrand, G., P. C. Reid, F. Ibanez, J. A. Lindley, and M. Edwards. 2002b. Reorganization of North Atlantic marine copepod biodiversity and climate. Science 296: 1692-1694.

Beaugrand, G., and F. Ibanez. 2002c. Spatial dependence of calanoid copepod diversity in the North Atlantic Ocean. Marine Ecology-Progress Series 232: 197-211.

Beaugrand, G., K. M. Brander, J. A. Lindley, S. Souissi, and P. C. Reid. 2003. Plankton effect on cod recruitment in the North Sea. Nature 426: 661-664.

Beaugrand, G. 2004. The North Sea regime shift: Evidence, causes, mechanisms and consequences. Progress in Oceanography 60: 245-262.

Beaugrand, G. and F. Ibanez. 2004. Monitoring marine plankton ecosystems. II: Long-term changes in North Sea calanoid copepods in relation to hydro-climatic variability. Marine Ecology-Progress Series 284: 35-47.

Beaugrand, G., M. Edwards, K. Brander, C. Luczak and F. Ibanez, 2008. Causes and projections of abrupt climate driven ecosystem shifts in the North Atlantic. Ecology Letters 11: 1157-1168.

Beaugrand, G., C. Luczak, and M. Edwards. 2009. Rapid biogeographical plankton shifts in the North Atlantic Ocean. Global Change Biology 15: 1790-1803.

Beaulieu, S. E., M. M. Mullin, V. T. Tang, S. M. Pyne, A. L. King, and B. S. Twining. 1999. Using an optical plankton counter to determine the size distributions of preserved zooplankton samples. Journal of Plankton Research 21: 1939-1956.

Behrenfeld, M. J., R.T. O'Malley, D.A. Siegel, C.R. McClain, J.L. Sarmiento, G.C. Feldman, A. J. Milligan, P.G. Falkowski, R.M. Leterier, and E. S. Boss. 2006. Climate-driven trends in contemporary ocean productivity. Nature 444: 752-755.

Bell, J. L., and R. R. Hopcroft. 2008. Assessment of Zooimage as a tool for the classification of zooplankton. Journal of Plankton Research 30: 1351-1367.

Benfield, M. C., P. Grosjean, P. F. Culverhouse, X. Irigoien, M. E. Sieracki, A. Lopez-Urrutia, H. Dam, G., Q. Hu, C. S. Davis, A. Hansen, C. H. Pilskaln, M. R. Edward, H. Schultz, P. E. Utgoff, and G. Gorsky. 2007. RAPID: Research on automated plankton identification. Oceanography 20: 172-187.

Béranger, K., L. Mortier, and M. Crépon. 2005. Seasonal variability of water transport through the Straits of Gibraltar, Sicily and Corsica, derived from a high-resolution model of the Mediterranean circulation. Progress in Oceanography 66: 341-364.

Berggreen, U., B. Hansen, and T. Kiørboe. 1988. Food size spectra, ingestion and growth of the copepod *Acartia tonsa* during development: Implications for determination of copepod production. Marine Biology 99: 341-352.

Berline, L., I. Siokou-Frangou, I. Marasovićc, O. Vidjakc, M. L. Fernández de Puelles, M. G. Mazzocchi, G. Assimakopoulou, S. Zervoudakib, S. Fonda Umani, A. Conversi, C. Garcia-Comas, F. Ibanez, S. Gasparini, L. Stemmann, and G. Gorsky. 2010 in revision. Intercomparison of six Mediterranean zooplankton time series. Progress in Oceanography. Ms. Ref. PROOCE-D-09-00018R1.

Bertram, D. F., D. L. Mackas, and S. M. McKinnell. 2001. The seasonal cycle revisited: Interannual variation and ecosystem consequences. Progress in Oceanography 49: 283-307.

Bethoux, J. P., L. Prieur, and F. Nyffeler. 1982. The water circulation in the North Western Mediterranean Sea, its relations with wind and atmospheric pressure. Elsevier Oceanography Series 34: 129-142.

Bethoux, J. P., L. Prieur, and J. H. Bong. 1988. Le Courante Ligure au large de Nice. Oceanologica Acta 9: 59-67.

Bethoux, J. P., B. Gentili, J. Raunet, and D. Tailliez. 1990. Warming trend in the Western Mediterranean deep-water. Nature 347: 660-662.

Bethoux, J. P., B. Gentili, and D. Tailliez. 1998. Warming and freshwater budget change in the Mediterranean since the 1940s, their possible relation to the greenhouse effect. Geophysical Research Letters 25: 1023-1026.

Bethoux, J. P., and B. Gentili. 1999. Functioning of the Mediterranean Sea: past and present changes related to freshwater input and climate changes. Journal of Marine Systems 20: 33-47.

Bethoux, J. P., B. Gentili, P. Morin, E. Nicolas, C. Pierre, and D. Ruiz-Pino. 1999. The Mediterranean Sea: A miniature ocean for climatic and environmental studies and a key for the climatic functioning of the North Atlantic. Progress in Oceanography 44: 131-146.

Bianchi, C. N., and C. Morri. 2000. Marine biodiversity of the Mediterranean Sea: Situation, problems and prospects for future research. Marine Pollution Bulletin 40: 367-376.

Bianchi, C. N. 2007. Biodiversity issues for the forthcoming tropical Mediterranean Sea. Hydrobiologia 580: 7-21.

Blanco, J. M., F. Echevarria, and C. M. Garcia. 1994. Dealing with size spectra: Some conceptual and mathematical problems. Scientia Marina 58: 17-29.

Bombace, G. 2001. Influence of climatic changes on stocks, fish species and marine ecosystems in the Mediterranean Sea. Archo Oceanogr. Limnol. 22: 67-72.

Bonnet, D., A. Richardson, R. Harris, A. Hirst, G. Beaugrand, M. Edwards, S. Ceballos, R. Diekman, A. Lopez-Urrutia, L. Valdes, F. Carlotti, J. C. Molinero, H. Weikert, W. Greve, K. Lucic, A. Albaina, N. Daly Yahia, S. Fonda Umani, A. Miranda, A. dos Santos, K. Cook, S. Robinson, and M. L. Fernandez de Puelles. 2005. An overview of *Calanus helgolandicus* ecology in European waters. Progress in Oceanography 65: 1-53.

Bopp, L., O. Aumont, P. Cadule, S. Alvain, and M. Gehlen. 2005. Response of diatom distribution to global warming and potential implications: A global model study. Geophysical Research Letters 32 , L19606, doi:10.1029/2005GL023653.

Boucher, J. 1984. Localization of zooplankton populations in the Ligurian Marine Front - Role of ontogenic migration. Deep-Sea Research 31: 469-484.

Boucher, J., F. Ibanez, and L. Prieur. 1987. Daily and seasonal-variations in the spatial-distribution of zooplankton populations in relation to the physical structure in the Ligurian Sea Front. Journal of Marine Research 45: 133-173.

Boudreau, P. R., L. M. Dickie, and S. R. Kerr. 1991. Body-size spectra of production and biomass as system-level indicators of ecological dynamics. Journal of Theoretical Biology 152: 329-339.

Boudreau, P. R., and L. M. Dickie. 1992. Biomass spectra of acquatic ecosystems in relation with fisheries yield. Canadian Journal of Fisheries and Acquatic Sciences 49: 1528-1538.

Breiman, L. 2001. Random forests. Machine Learning 45: 5-32.

Brodeur, R. D., H. Sugisaki, and G. L. Hunt. 2002. Increases in jellyfish biomass in the Bering Sea: implications for the ecosystem. Marine Ecology-Progress Series 233: 89-103.

Broglio, E., S. H. Jonasdottir, A. Calbet, H. H. Jakobsen, and E. Saiz. 2003. Effect of heterotrophic versus autotrophic food on feeding and reproduction of the calanoid copepod *Acartia tonsa*: Relationship with prey fatty acid composition. Aquatic Microbial Ecology 31: 267-278.

Broglio, E., E. Saiz, A. Calbet, I. Trepat, and M. Alcaraz. 2004. Trophic impact and prey selection by crustacean zooplankton on the microbial communities of an oligotrophic coastal area (NW Mediterranean Sea). Aquatic Microbial Ecology 35: 65-78.

Brooks, J. L., and S. I. Dodson. 1965. Predation, body size, and composition of plankton. Science 150: 28-35.

Brown, J. H. 2004. Toward a Metabolic Theory of Ecology. Ecology 85: 1771-1789.

Brucet, S., D. Boix, R. Lopez-Flores, A. Badosa, and X. D. Quintana. 2006. Size and species diversity of zooplankton communities in fluctuating Mediterranean salt marshes. Estuarine Coastal and Shelf Science 67: 424-432.

Buitenhuis, E., C. Le Quere, O. Aumont, G. Beaugrand, A. Bunker, A. Hirst, T. Ikeda, T. O'Brien, S. Piontkovski, and D. Straile. 2006. Biogeochemical fluxes through mesozooplankton. Global Biogeochemical Cycles 20, GB 2003, doi: 10.1026/2005GB002511.

Calbet, A. 2008. The trophic roles of microzooplankton in marine systems. ICES Journal of Marine Science 65: 325–331.

Calbet, A., S. Garrido, E. Saiz, M. Alcaraz, and M. Duarte. 2001. Annual zooplankton succession in coastal NW Mediterranean waters: The importance of the smaller size franctions. Journal of Plankton research 23: 319-331.

Calder, W. A. 1984. Size, function and life history. Cambridge, Harvard University press. 373 pp. ISBN-0-486-69191-8.

Carrada, G. C., T. S. Hopkins, G. Bonaduce, A. Ianora, D. Marino, M. Modigh, M. Ribera d'Alcalá, and B. Scotto di Carlo. 1980. Variability in the hydrographic and biological features of the Gulf of Naples. P.S.Z.N.I. Marine Ecology 1: 105-120.

Cess, R.D., E.F. Harrison, P. Minnis, B.R. Barkstrom, V. Ramanathan and T.Y. Kwon. 1992. Interpretation of seasonal cloud-climate interactions using Earth Radiation Budget Experiment data. Journal of Geophysical Research 97(D7): 7613-7617.

Christou, E. D. 1998. Interannual variability of copepods in a Mediterranean coastal area (Saronikos Gulf, Aegean Sea). Journal of Marine Systems 15: 523-532.

Colebrook, J. M. 1978. Continuous plankton records - zooplankton and environment, Northeast Atlantic and North-Sea, 1948-1975. Oceanologica Acta 1: 9-23.

Conversi, A., T. Peluso, and S. Fonda-Umani. 2009. Gulf of Trieste: A changing ecosystem. Journal of Geophysical Research-Oceans 114, C03S90, doi:10.1029/2008JC004763.

Conversi, A., S. Fonda Umani, T. Peluso, J.C. Molinero, A. Santojanni and M. Edwards, 2010. The Mediterranean Sea Regime Shift at the End of the 1980s, and intriguing Parallelisms with Other European Basins. PLoS ONE 5(5): e10633. doi:10.1371/journal.pone.0010633.

Costello, J. H., B. K. Sullivan, and D. J. Gifford. 2006. A physical-biological interaction underlying variable phenological responses to climate change by coastal zooplankton. Journal of Plankton Research 28: 1099-1105.

Coulter, W. H. 1953. Means for counting particles suspended in a fluid. United States Patent 2656508.

Cousins, S. H. 1987. The trophic continuum in marine ecosystems: Structure and equations for a predictive model. in R. E. Ulanowicz and T. Platt, editors. Ecosystem theory for biological oceanography. Department of Fisheries and Oceans, Ottawa, Canada.: 76-93.

Crame, J. A. 1993. Latitudinal Range Fluctuations in the Marine Realm through Geological Time. Trends in Ecology & Evolution 8: 162-166.

Cury, P., A. Bakun, R. J. M. Crawford, A. Jarre, R. A. Quiñones, L. J. Shannon, and H. M. Verheye. 2000. Small pelagics in upwelling systems: patterns of interaction and structural changes in "wasp-waist" ecosystems. Ices Journal of Marine Science 57: 603-618.

Cushing, D. H., G. F. Humphrey, and K. L. Banse, T. 1958. Report of the committee on terms and equivalents. . Rapp. P.-v. Réun. Cons. int. Explor. Mer 144: 15–16.

Cushman-Roisin, B. 1994. Introduction to geophysical fluid dynamics. Prentice Hall, Englewood Cliffs, NJ, 320 pp.

d'Elbée. 2001. Distribution et diversité des copépodes planctoniques dans le Golfe de Gascogne, in Océanographie du Golfe de Gascogne. Ifremer Actes Colloq. 31: 147–156.

D'Ortenzio, F., and M. Ribera d'Alcalà. 2009. On the trophic regimes of the Mediterranean Sea: A satellite analysis. Biogeosciences 6: 139–148.

Dam, H. G., and W. T. Peterson. 1991. In situ feeding-behavior of the copepod *Temora-longicornis* - effects of seasonal-changes in chlorophyll size fractions and female size. Marine Ecology-Progress Series 71: 113-123.

Davis, C. S., G. R. Flierl, P. H. Wiebe, and P. J. S. Franks. 1991. Micropatchiness, turbulence and recruitment in plankton. Journal of Marine Research 49: 109-151.

Deibel, D. 1982. Laboratory-measured grazing and ingestion rates of the salp, *Thalia-democratica* Forskal, and the doliolid, *Dolioletta-gegenbauri* Uljanin (tunicata, thaliacea). Journal of Plankton Research 4: 189-201.

deYoung, B., M. Barange, G. Beaugrand, R. Harris, R. I. Perry, M. Scheffer, and F. Werner. 2008. Regime shifts in marine ecosystems: Detection, prediction and management. Trends in Ecology & Evolution 23: 402-409.

Dickie, L. M., S. R. Kerr, and P. R. Boudreau. 1987. Size-dependent processes underlying regularities in ecosystem structure. Ecological Monographs 57: 233-250.

Drinkwater, K. F. G. Beaugrand, M. Kaeriyama, S. Kim, G. Ottersen, R. I. Perry, H. Pörtner, J. J. Polovina, and A. Takasuka. 2010. On the processes linking climate to ecosystem changes. Journal of Marine Systems 79: 374-388.

Duarte, C. M., S. Agustí, and H. Peters. 1987. An upper limit to the abundance of aquatic organisms. Oecologia 74: 272-276.

Duarte, C. M., S. Agustí, H. Kennedy and D. Vaque1999. The Mediterranean climate as a template for Mediterranean marine ecosystems: The example of the northeast spanish littoral. Progress in Oceanography 44: 245-270.

Dundar, M., G. Fung, L. Bogoni, M. Macari, A. Megibow, and B. Rao. 2004. A methodology for training and validating a CAD system and potential pitfalls. International Congress Series 1268: 1010-1014.

Dupuis, H., Taylor, P. K., Weill, A., Katarasos, K. 1997. Inertial dissipation method applied to derive turbulent fluxes over the ocean during the SOFIArESTEX and SEMAPHORE experiments with low to moderate wind speeds. Journal of Geophysical Research 102: 21.115-121.129.

Durant, J. M., D. O. Hjermann, T. Anker-Nilssen, G. Beaugrand, A. Mysterud, N. Pettorelli, and N. C. Stenseth. 2005. Timing and abundance as key mechanisms affecting trophic interactions in variable environments. Ecology Letters 8: 952-958.

Duro, A., and E. Saiz. 2000. Distribution and trophic ecology of chaetognaths in the Western Mediterranean in relation to an inshore-offshore gradient. Journal of Plankton Research 22: 339-361.

Echevarria, F., P. Carrillo, F. Jimenez, P. Sanchez-Castillo, L. Cruz-Pizarro, and J. Rodriguez. 1990. The size-abundance distribution and taxonomic composition of plankton in an oligotrophic, high mountain lake (La Caldera, Sierra Nevada, Spain). Journal of Plankton Research 12: 415-422.

Edvardsen, A., M. Zhou, K. S. Tande, and Y. W. Zhu. 2002. Zooplankton population dynamics: Measuring in situ growth and mortality rates using an Optical Plankton Counter. Marine Ecology-Progress Series 227: 205-219.

Edwards, M., and A. J. Richardson. 2004. Impact of climate change on marine pelagic phenology and trophic mismatch. Nature 430: 881-884.

Edwards, M., D. G. Johns, S. C. Leterme, E. Svendsen, and A. J. Richardson. 2006. Regional climate change and harmful algal blooms in the northeast Atlantic. Limnology and Oceanography 51: 820-829.

Elton, C. S. 1927. Animal Ecology. Sidgwick & Jackson, London, 296 pp. ISBN 9780226206394.

Escoufier, Y. 1973. Treatment of vector variables. Biometrics 29: 751-760.

Etienne, M., M. C. Corre, S. Dallot, and P. Nival. 1991. Observations hydrologiques à une station cotiere Méditerraneénne. Point B- Rade de Villefranche sur Mer. Campagnes Oceanogr.Françaises IFREMER 14: 89.

Fenchel, T. 1974. Intrinsic rate of natural increase: The relationship with body size. Oecologia 14 (4): 317-326.

Fernandes, J. A., X. Irigoien, G. Boyra, J. A. Lozano, and I. Inza. 2009. Optimizing the number of classes in automated zooplankton classification. Journal of Plankton Research 31: 19-29.

Fernandez de Puelles, M. L., J. Valencia, and L. Vicente. 2004. Zooplankton variability and climatic anomalies from 1994 to 2001 in the Balearic Sea (Western Mediterranean). ICES Journal of Marine Science, 61: 492-500.

Fernandez de Puelles, M. L., F. Alemany, and J. Jansa. 2007. Zooplankton time-series in the Balearic Sea (Western Mediterranean): Variability during the decade 1994-2003. Progress in Oceanography 74: 329-354.

Fernandez de Puelles, M. L. F., and J. C. Molinero. 2007. North Atlantic climate control on plankton variability in the Balearic Sea, Western Mediterranean. Geophysical Research Letters 34, L04608, doi:10.1029/2006GL028354.

Fernandez de Puelles, M. L., and J. C. Molinero. 2008. Decadal changes in hydrographic and ecological time-series in the Balearic Sea (Western Mediterranean), identifying links between climate and zooplankton. Ices Journal of Marine Science 65: 311-317.

Field, J. C., R. C. Francis, and K. Aydin. 2006. Top-down modeling and bottom-up dynamics: Linking a fisheries-based ecosystem model with climate. Progress in Oceanography 68: 238-270.

Finke, D. L., and R. F. Denno. 2004. Predator diversity dampens trophic cascades. Nature 429: 407-410.

Fofonoff, N. P., and R. C. Millard Jr. 1983. Algorithms for computation of fundamental properties of seawater. Unesco Technical Papers in Marine Science 44: 53.

Folke, C. , S. Carpenter, B. Walker, M. Schefer, T. Elmqvist, L. Gunderson, and C. S. Holling. 2004. Regime shifts, resilience, and biodiversity in ecosystem management. Annual Revue of Ecology Evolution and Systematics 35: 557-581.

Fonselius, S., and J. Valderrama. 2003. One hundred years of hydrographic measurements in the Baltic Sea. Journal of Sea Research 49: 229-241.

Francour, P., C. F. Boudouresque, J. G. Harmelin, M. L. Harmelinvivien, and J. P. Quignard. 1994. Are the Mediterranean Waters Becoming Warmer - Information from Biological Indicators. Marine Pollution Bulletin 28: 523-526.

Frank, K. T., B. Petrie, and N. L. Shackell. 2007. The ups and downs of trophic control in continental shelf ecosystems. Trends in Ecology and Evolution 22: 236-242.

Frederiksen, M., M. Edwards, A. J. Richardson, N. C. Halliday, and S. Wanless. 2006. From plankton to top predators: bottom-up control of a marine food web across four trophic levels. Journal of Animal Ecology 75: 1259-1268.

Fromentin, J. M., and F. Ibanez. 1994. Year-to-year changes in meteorological features of the French coast area during the last half-century - examples of 2 biological responses. Oceanologica Acta 17: 285-296.

Fromentin, J. M., and B. Planque. 1996. Calanus and environment in the eastern North Atlantic .2. Influence of the North Atlantic Oscillation on C-finmarchicus and C-helgolandicus. Marine Ecology-Progress Series 134: 111-118.

Frost, B. W. 1972. Effects of size and concentration of food particles on feeding behavior of marine planktonic copepod *Calanus pacificus*. Limnology and Oceanography 17: 805-815.

Frost, B. W. 1977. Feeding-behaviour of *Calanus pacificus* in mixtures of food particles. Limnology and Oceanography 22: 472-491.

Gaedke, U. 1995. A comparison of whole-community and ecosystem approaches (biomass size distributions, food-web analysis, network analysis, simulation-models) to study the structure, function and regulation of pelagic food webs. Journal of Plankton Research 17: 1273-1305.

Gaedke, U., and N. Kamjunke. 2006. Structural and functional properties of low- and high-diversity planktonic food webs. Journal Of Plankton Research 28: 707-718.

Garcia, C. M., F. Jimenez-Gomez, J. Rodriguez, B. Bautista, M. Estrada, J. Garcia Braun, J. M. Gasol, F. Gomez Figueiras, F. Guerrero, F. Jimenez Montes, W. K. W. Li, J. M. Lopez Diaz, G. Santiago, and M. Varela. 1994. The size structure and functional composition of ultraplankton and nanoplankton at a frontal station in the Alboran Sea. Working groups 2 and 3 report. Scientia Marina 58: 43-52.

Gasol, J. M., P. A. D. Giorgio, and C. M. Duarte. 1997. Biomass Distribution in Marine Planktonic Communities. Limnology and Oceanography 42: 1353-1363.

Gasparini, G. P., G. Zodiatis, M. Astraldi, C. Galli, and S. Sparnocchia. 1999. Winter intermediate water lenses in the Ligurian Sea. Journal of Marine Systems 20: 319-332.

Gasser, B., G. Payet, J. Sardou, and P. Nival. 1998. Community structure of mesopelagic copepods (> 500 mu m) in the Ligurian Sea (Western Mediterranean). Journal of Marine Systems 15: 511-522.

Gladan, Z. N., I. Marasović, B. Grbec, S. Skejić, M. Bužančić, G. Kušpilić, S. Matijević, and F. Matić. 2010. Inter-decadal Variability in Phytoplankton Community in the Middle Adriatic (Kaštela Bay) in Relation to the North Atlantic Oscillation. Estuaries and Coasts 33: 376-383.

Glantz, M. H., R. W. Katz, and N. Nicholls. 1991. Teleconnections linking worldwide climate anomalies: Scientific basis and societal impact. Cambridge University Press, 535 pp.

Goffart, A., J.-H. Hecq, and L. Legendre. 2002. Changes in the development of the winter-spring phytoplankton bloom in the Bay of Calvi (NW Mediterranean) over the last two decades: A response to changing climate? Marine Ecology-Progress Series 236: 45-60.

Gomez, F., and G. Gorsky. 2003. Annual microplankton cycles in Villefranche Bay, Ligurian Sea, NW Mediterranean. Journal of Plankton Research 25: 323-339.

Gorsky, G., C. Aldorf, M. Kage, M. Picheral, G. Y., and J. Favole. 1992. Vertical distribution of suspended aggregates determined by a new Underwater Video Profiler. Annales de l'Institut Océanographique 68: 275–280.

Gorsky, G., and R. Fenaux. 1998. The role of Appendicularia in marine food webs. In Bone, Q. (ed.) The Biology of Pelagic Tunicates. Oxford University Press, Oxford, pp. 161-169.

Gorsky, G., M. D. Ohman, M. Picheral, G. P. Gasparini, L. Stemmann, J.-B. Romagnan, A. Cawood, S. Pesant, and F. Prejger. 2010. Digital zooplankton image analysis using the zooscan integrated system. Journal of Plankton Research 32 (3): 285-303.

Gregg, W. W., M. E. Conkright, P. Ginoux, P. O'Reilly, and N. W. Casey. 2003. Ocean primary production and climate: Global decadal changes. Geophysical Research Letters 30 (15), 1809, doi: 10.1029/2003GL016889.

Grosjean, P., M. Picheral, C. Warembourg, and G. Gorsky. 2004. Enumeration, measurement, and identification of net zooplankton samples using the ZooScan digital imaging system. Ices Journal of Marine Science 61: 518-525.

Hall, D. J. S. T. Thelkeld, Burns, C. W. and Crowley, P. H. 1976. The Size-Efficiency Hypothesis and the size structure of zooplankton communities. Annual Review of Ecology and Systematics 7: 177-208.

Halsband-Lenk, C., S. Nival, F. Carlotti, and H. J. Hirche. 2001. Seasonal cycles of egg production of two planktonic copepods, *Centropages typicus* and *Temora stylifera*, in the North-Western Mediterranean Sea. Journal of Plankton Research 23: 597-609.

Harbison, G. R., and R. W. Gilmer. 1976. Feeding rates of pelagic tunicate *Pegea-confederata* and 2 other salps. Limnology and Oceanography 21: 517-528.

Hare, S. R., and N. J. Mantua. 2000. Empirical evidence for North Pacific regime shifts in 1977 and 1989. Progress in Oceanography 47: 103-145.

Harris, R. P., P. H. Wiebe, J. Lenz, H. R. Skjoldal, and M. Huntley. 2000. ICES Zooplankton methodology manual. Academic Press. 684 pp. ISBN 10: 0-12-327645-4.

Hays, G. C., A. J. Richardson, and C. Robinson. 2005. Climate change and marine plankton. Trends in Ecology & Evolution 20: 337-344.

Heath, M. R. 1995. Size spectrum dynamics and the planktonic ecosystem of Loch-Linnhe. Ices Journal Of Marine Science 52: 627-642.

Helaouet, P., and G. Beaugrand. 2007. Macroecology of Calanus finmarchicus and C-helgolandicus in the North Atlantic Ocean and adjacent seas. Marine Ecology-Progress Series 345: 147-165.

Heier, S. 2005. Grid Integration of Wind Energy Conversion Systems. Chichester: John Wiley & Sons. pp. 45. ISBN 0470868996.

Hentch, J. M. 1959. Etude des courants de la Baie de Villefranche, p. 1-40. D.E.S.

Herbaut, C., F. Martel, and M. Crepon. 1997. A sensitivity study of the general circulation of the Western Mediterranean Sea .2. The response to atmospheric forcing. Journal of Physical Oceanography 27: 2126-2145.

Herman, A. W. 1988. Simultaneous measurement of zooplankton and light attenuance with a new Optical Plankton Counter. Continental Shelf Research 8: 205-221.

Herman, A. W. 1992. Design and calibration of a new Optical Plankton Counter capable of sizing small zooplankton. Deep-Sea Research 39: 395-415.

Hirst, A. G., and R. S. Lampitt. 1998. Towards a global model of in situ weight-specific growth in marine planktonic copepods. Marine Biology 132: 247-257.

Hirst, A. G., and T. Kiørboe. 2002. Mortality of marine planktonic copepods: Global rates and patterns. Marine Ecology-Progress Series 230: 195-209.

Hirst, A. G., and A. J. Bunker. 2003. Growth of marine planktonic copepods: Global rates and patterns in relation to chlorophyll a, temperature, and body weight. Limnology and Oceanography 48: 1988-2010.

Holling, C. S. 1973. Resilience and stability in ecological systems. Annual Revue of Ecological Systems 4: 1-23.

Holm-Hansen, O., C. J. Lorenzen, R. W. Holmes, and J. D. H. Strickland. 1965. Fluorimetric determination of chlorophyll. J.Cons.Perm.Int.Explor.Mer 30: 3-15.

Hooper, D. U., F. S. Chapin III, J.J. Ewel, A. Hector, P. Inchausti, S. Lavorel, J.H. Lawton, D.M. Lodge, M. Loreau, S. Naeem, B. Schmid, H. Setälä, A.J. Symstad, J. Vandermeer, and D. A. Wardle 2005. Effects of biodiversity on ecosystem functioning: A consensus of current knowledge. Ecological Monographs, 75(1): 3-35.

Hunt, G. L., P. Stabeno, G. Walters, E. Snclair, R. D. Brodeur, J.M. Napp, and N. A. Bond. 2002. Climate change and control of the southeastern Bering Sea pelagic ecosystem. Deep-Sea Research Part IITopical Studies in Oceanography 49: 5821-5853.

Hunt, G. L., and S. Mckinnell. 2006. Interplay between top-down, bottom-up, and wasp-waist control in marine ecosystems. Progress in Oceanography 68: 115-124.

Huntley, M. E., M. Zhou, and W. Nordhausen. 1995. Mesoscale distribution of zooplankton in the California Current in late spring, observed by Optical Plankton Counter. Journal of Marine Research 53: 647-674.

Hure, J., and B. Scotto di Carlo. 1969. Ripartizione quantitativa e distribuzione verticale dei copepodi pelagici di profondità su una stazione nel Mar Tirreno ed una nell'Adriatico meridionale. Pubblicazioni della Stazione Zoologica di Napoli 37: 51-83.

Hurrell, J. W. 1995. Decadal trends in the North-Atlantic Oscillation - regional temperatures and precipitation. Science 269: 676-679.

Hurrell, J. W., and H. VanLoon. 1997. Decadal variations in climate associated with the North Atlantic Oscillation. Climatic Change 36: 301-326.

Hurrell, J. W., and C. Deser. 2010. North Atlantic climate variability: The role of the North Atlantic Oscillation. Journal of Marine Systems 79: 231-244.

Huxley, J. S. 1932. Problems of relative growth. Johns Hopkins University press. 276 pp.

Ianora, A., S. A. Poulet, and A. Miralto. 2003. The effects of diatoms on copepod reproduction: A review. Phycologia 42: 351-363.

Ibanez, F., and J. Boucher. 1987. Anisotropy of zooplankton populations in the Ligurian Sea front. Oceanologica Acta 10: 205-216.

Ibanez, F. 1991. Treatment of the data derived from the cost 647 project on coastal benthic ecology: The within-site analysis. In B. Keegan, Space and time series data anlysis in coastal benthic ecology. , pp. 5-43.

Ibanez, F., and M. Etienne. 1992. Le filtrage des séries chronologiques par l'Analyse en Composantes Principales des Processus (ACPP). Journal de Recherches Océanographiques 16: 66-72.

Ibanez, F., J. M. Fromentin, and J. Castel. 1993. Application of the cumulated function to the processing of chronological data in oceanography. Comptes Rendus De L'Academie Des Sciences Serie III-Sciences De La Vie-Life Sciences 316: 745-748.

Ibanez, F., and A. Conversi. 2002. Prediction of missing values and detection of 'exceptional events' in a chronological planktonic series: A single algorithm. Ecological Modelling 154: 9-23.

IPCC. 2007. Climate change 2007: Synthesis report. Contribution of working groups I, II and III to the fourth assessment. Report of the Intergovernmental Panel on Climate Change p. 104 Pachauri, R.K, and A. Reisinger. IPCC, Geneva, Switzerland.

Irigoien, X., R. P. Harris, H. M. Verheye, P. Joly, J. Runge, M. Starr, D. Pond, R. Campbell, R. Shreeve, P. Ward, A. N. Smith, H. G. Dam, W. Peterson, V. Tirelli, M. Koski, T. Smith, D. Harbour, and R. Davidson. 2002. Copepod hatching success in marine ecosystems with high diatom concentrations. Nature 419: 387-389.

Irigoien, X., J. Huisman, and R. P. Harris. 2004. Global biodiversity patterns of marine phytoplankton and zooplankton. Nature 429: 863-867.

Jennings, B. R., and K. Parlslow. 1988. Particle size measurement: The Equivalent Spherical Diameter. Proceeding of the Royal Society of London- Series A 419: 137-149.

Jimenez, F., J. Rodriguez, F. Jimenez-Gomez, and B. Bautista. 1989. Bottlenecks in the propagation of a fluctuation up the planktonic sizespectrum in Mediterranean coastal waters. Scientia Marina 53: 269-275.

Jollife, I. T. 2002. Principal Component Analysis, 2 ed.

Johns, D. G., M. Edwards, and S. D. Batten. 2001. Arctic boreal plankton species in the Northwest Atlantic. Canadian Journal of Fisheries and Aquatic Sciences 58: 2121-2124.

Jones, R. H., and K. J. Flynn. 2005. Nutritional status and diet composition affect the value of diatoms as copepod prey. Science 307: 1457-1459.

Jonsson, P. R., and P. Tiselius. 1990. Feeding behaviour, prey detection and capture efficiency of the copepod *Acartia tonsa* feeding on planktonic ciliates. Marine Ecology Progress Series 60: 35-44.

Kamburska, L., and S. Fonda-Umani. 2006. Long-term copepod dynamics in the Gulf of Trieste (Northern Adriatic Sea): Recent changes and trends. Climate Research 31: 195-203.

Kamykowski, D., and S. Zentara. 1986. Predicting plant nutrient concentrations from temperature and sigma-*t* in the upper kilometer of the world ocean. Deep-Sea Research 33: 89-105.

Karl, D. M., R. R. Bidigare, and R. M. Letelier. 2001. Long-term changes in plankton community structure and productivity in the North Pacific Subtropical Gyre: The Domain Shift Hypothesis. Deep-Sea Research Part II, Topical Studies in Oceanography 48: 1449.

Katara, I., J. Illian, G. J. Pierce, B. Scott, and J. J. Wang. 2008. Atmospheric forcing on chlorophyll concentration in the Mediterranean. Hydrobiologia 612: 33-48.

Katechakis, A., H. Stibor, U. Sommer, and T. Hansen. 2002. Changes in the phytoplankton community and microbial food web of Blanes Bay (Catalan Sea, NW Mediterranean) under prolonged grazing pressure by doliolids (Tunicata), cladocerans or copepods (Crustacea). Marine Ecology-Progress Series 234: 55-69.

Kehayias, G. 2003. Quantitative aspects of feeding of chaetognaths in the eastern Mediterranean pelagic waters. Journal of the Marine Biological Association of the UK 83(03): 559-569.

Kerr, S. R. 1974. Theory of size distribution on ecological communities. Journal of Fisheries Research Board of Canada 31: 1859-1862.

Kimmel, D. G., M. R. Roman, and X. Zhang. 2006. Spatial and temporal variability in factors affecting mesozooplankton dynamics in Chesapeake Bay: Evidence from biomass size spectra. Limnology and Oceanography 51(1): 131-141.

Kiørboe, T., E. Saiz, and M. Viitasalo. 1996. Prey switching behaviour in the planktonic copepod *Acartia tonsa*. Marine Ecology-Progress Series 143: 65-75.

Kiørboe, T. 1998. Population regulation and role of mesozooplankton in shaping marine pelagic food webs. Hydrobiologia 363: 13-27.

Kirby, R. R., and G. Beaugrand. 2009. Trophic amplification of climate warming. Proceedings of the Royal Society B-Biological Sciences 276: 4095-4103.

Kleiber, M. 1932. Body size and metabolism. Hilgardia 6: 315-356.

Kleppel, G. S. 1993. On the diets of calanoid copepods. Marine Ecology-Progress Series 99: 183-195.

Kotsiantis, S. B. 2007. Supervised machine learning: A review of classification techniques. Informatica 31: 249-268.

Kouwenberg, J., and C. Razouls. 1990. The Incidence of Environmental-Factors on the Evolution of Copepod Populations in the Golfe-Du-Lion during the Period 1986-88 - in Comparison with the Period 1957-64. Bulletin de la Société Zoologique de France 115: 23-36.

Krahmann, G., and F. Schott. 1998. Long term increases in Western Mediterranean salinities and temperatures: Anthropogenic and climatic sources. Geophysical Research Letters 25: 4209-4212.

Krom, M. D., N. Kress, S. Brenner, and L. I. Gordon. 1991. Phosphorus limitation of primary productivity in the Eastern Mediterranean Sea. Limnology and Oceanography 36 (3): 424-432.

Lacroix, G., and P. Nival. 1998. Influence of meteorological variability on primary production dynamics in the Ligurian Sea (NW Mediterranean Sea) with a 1D hydrodynamic/biological model. Journal of Marine Systems 16: 23-50.

Lascaratos, A., W. Roether, K. Nittis, and B. Klein. 1999. Recent changes in deep water formation and spreading in the Eastern Mediterranean Sea: A review. Progress in Oceanography 44: 5-36.

Legendre, P., and L. Legendre. 1979. Numerical Ecology. Second English edition, 1998: Elsevier Science B. V., Amsterdam. ISBN: 0-444-89250-8 (Paperback edition).

Lehman, J. T. 1976. Filter-feeder as an optimai forager, and predicted shapes of feeding curves. Limnology and Oceanography 21: 501-516.

Levitus, S., J. I. Antonov, T. P. Boyer, and C. Stephens. 2000. Warming of the world ocean. Science 287: 2225–2229.

Licandro, P., and F. Ibanez. 2000. Changes of zooplankton communities in the Gulf of Tigullio (Ligurian Sea, Western Mediterranean) from 1985 to 1995. Influence of hydroclimatic factors. Journal of Plankton Research 22: 2225-2253.

Licandro, P., F. Ibanez, and M. Etienne. 2006. Long-term fluctuations (1974-1999) of the salps *Thalia democratica* and *Salpa fusiformis* in the Northwestern Mediterranean Sea: Relationships with hydroclimatic variability. Limnology and Oceanography 51: 1832-1848.

Lindeman. 1942. Trophic-dynamic aspect of ecology. Ecology 23: 399-418.

Lindley, J. A., and S. Daykin. 2005. Variations in the distributions of Centropages chierchiae and Temora stylifera (Copepoda : Calanoida) in the north-eastern Atlantic Ocean and western European shelf waters. Ices Journal of Marine Science 62: 869-877.

Link, J. 2002. Does food web theory work for marine ecosystems? Marine Ecology-Progress Series 230: 1-9.

Litzow, M. A., and L. Ciannelli. 2007. Oscillating trophic control induces community reorganization in a marine ecosystem. Ecology Letters 10: 1124-1134.

Longhurst, A. R. 1998. Ecological Geography of The Sea. Academic. Press, San Diego, 398 pp. ISBN 10: 0-12-455521-7.

Lopez-Urrutia, A., E. San Martin, R. P. Harris, and X. Irigoien. 2006. Scaling the metabolic balance of the oceans. Proceedings of the National Academy of Sciences of the United States of America 103: 8739-8744.

Loreau, M., S. Naeem, P. Inchausti, J. Bengtsson, J. P. Grime, A. Hector, D. U. Hooper, M. A. Huston, D. Raffaelli, B. Schmid, D. Tilman, and D. A. Wardle. 2001. Ecology - Biodiversity and ecosystem functioning: Current knowledge and future challenges. Science 294: 804-808.

Lorenzen, C. J. 1966. A method for the continous measurement of in vivo chlorophyll concentration. Deep Sea Research 13: 223-227.

Louw, G. G., C. D. Van Der Lingen, and M. J. Gibbons. 1998. Differential feeding by sardine Sardinops sagax and anchovy Engraulis capensis recruits in mixed shoals. South African Journal of Marine Science 19: 227-232.

Lozier, M. S., and L. Sindlinger. 2009. On the Source of Mediterranean Overflow Water Property Changes. Journal of Physical Oceanography 39: 1800-1817.

Mackas, D. L., and C. M. Boyd. 1979. Spectral analysis of zooplankton spatial heterogeneity. Science 204: 62-64.

Mackas, D., K. Denman, and M. R. Abbott. 1985. Plankton patchiness: Biology in the physical vernacular. Bulletin of Marine Science 37: 652-674.

Mackas, D. L., R. Goldblatt, and A. G. Lewis. 1998. Interdecadal variation in developmental timing of Neocalanus plumchrus populations at Ocean Station P in the subarctic North Pacific. Canadian Journal of Fisheries and Aquatic Sciences 55: 1878-1893.

Mackas, D. L., and K. O. Coyle. 2005. Shelf-offshore exchange processes, and their effects on mesozooplankton biomass and community composition patterns in the northeast Pacific. Deep-Sea Research Part Ii-Topical Studies in Oceanography 52: 707-725.

Mackas, D. L., S. Batten, and M. Trudel. 2007. Effects on zooplankton of a warmer ocean: Recent evidence from the Northeast Pacific. Progress in Oceanography 75: 223-252.

Mackas, D. L., and G. Beaugrand. 2010. Comparisons of zooplankton time series. Journal of Marine Systems 79: 286-304.

Mantua, N. J., S. R. Hare, Y. Zhang, J. M. Wallace, and R. C. Francis. 1997. A Pacific interdecadal climate oscillation with impacts on salmon production. B Am Meteorol Soc 78: 1069-1079.

Maranon, E., P. Cermeno, J. Rodriguez, M. V. Zubkov, and R. P. Harris. 2007. Scaling of phytoplankton photosynthesis and cell size in the ocean. Limnology and Oceanography 52: 2190-2198.

Marasović, I., B. Grbec, and M. Morović. 1995. Long-term production changes in the Adriatic. Netherlands Journal Sea Research 34: 267-273.

Margalef, R. 1961. Communication of structure in planktonic populations. Limnology and Oceanography 6: 124-128.

Margalef, R. 1963. On certain unifying principles in ecology. The American Naturalist 97: 357-374.

Mariotti, A., N. Zeng, and K. M. Lau. 2002. Euro-Mediterranean rainfall and ENSO - a seasonally varying relationship. Geophysical Research Letters 29: 1621, doi:10.1029/2001GL014248.

Marty, J.C. and J. Chiaverini. in open review. Hydrological changes in the Ligurian Sea (NW Mediterranean, DYFAMED site) during 1995-2007 and biogeochemical consequences. Biogeosciences Discussions, 7, 1377-1406, 2010.

Mazzocchi, M., and M. Ribera d'Alcalà. 1995. Recurrent patterns in zooplankton structure and succession in a variable coastal environment. ICES Journal of Marine Science. 52: 679-691.

Mazzocchi, M. G., D. Nervegna, G. D'elia, I. Di Capua, L. Aguzzi, and A. Boldrin. 2003. Spring mesozooplankton communities in the epipelagic Ionian Sea in relation to the Eastern Mediterranean Transient. Journal of Geophysical Research 108, 8114, 12 pp. doi:10.1029/2002JC001640.

Mazzocchi, M. G., G. Buffoni, Y. Carotenuto, S. Pasquali, and M. Ribera d'Alcalà. 2006. Effects of food conditions on the development of the population of *Temora stylifera*: A modeling approach. Journal of Marine Systems 62: 71-84.

Mazzocchi, M. G., L. Dubroca, M. Ribera d'Alcalà, C. Garcia-Comas, and I. Di Capua. Submitted. Stability and resilience in coastal copepod assemblages: The case of the Mediterranean LTER-MC Progress in Oceanography Ms. Ref. No.: PROOCE-D-09-00045.

Mccartney, M. S., and C. Mauritzen. 2001. On the origin of the warm inflow to the Nordic Seas. Progress in Oceanography 51: 125-214.

Mcgehee, D. E., D. A. Demer, and J. D. Warren. 2004. Zooplankton in the Ligurian Sea: Part I. Characterization of their dispersion, relative abundance and environment during summer 1999. Journal of Plankton Research 26: 1409-1418.

Menard, F., S. Dallot, G. Thomas, and J. C. Braconnot. 1994. Temporal fluctuations of 2 mediterranean salp populations from 1967 to 1990 - Analysis of the influence of environmental variables using a Markov-chain model. Marine Ecology-Progress Series 104: 139-152.

Menard, F., J.-M. Fromentin, J. Goy, and S. Dallot. 1997. Temporal fluctuatuions of doliodids abundance in the Bay of Villefranche-sur-Mer (Northwestern Mediterranean Sea) from 1967 to 1990. Oceanologica Acta 20: 733-742.

Millero, F. J., C. T. Chen, K. Schleicher, and A. Bradshaw. 1980. A new high-pressure equation of state for seawater. Deep-Sea Research 27: 255-264.

Millot, C. 1999. Circulation in the Western Mediterranean Sea. Journal of Marine Systems 20: 423-442.

Millot, C. 2005. Circulation in the Mediterranean Sea: Evidences, debates and unanswered questions. Scientia Marina 69: 5-21.

Millot, C., J. Candela, J. L. Fuda, and Y. Tber. 2006. Large warming and salinification of the Mediterranean outflow due to changes in its composition. Deep-Sea Research Part I-Oceanographic Research Papers 53: 656-666.

Molinero, J. C., F. Ibanez, P. Nival, E. Buecher, and S. Souissi. 2005a. North Atlantic climate and Northwestern Mediterranean plankton variability. Limnology and Oceanography 50: 1213-1220.

Molinero, J. C., F. Ibanez, S. Souissi, M. Chifflet, and P. Nival. 2005b. Phenological changes in the Northwestern Mediterranean copepods *Centropages typicus* and *Temora stylifera* linked to climate forcing. Oecologia 145: 640-649.

Molinero, J. C., F. Ibanez, S. Souissi, E. Bosc, and P. Nival. 2008a. Surface patterns of zooplankton spatial variability detected by high frequency sampling in the NW Mediterranean. Role of density fronts. Journal of Marine Systems 69: 271-282.

Molinero, J. C., F. Ibanez, S. Souissi, E. Buecher, S. Dallot, and P. Nival. 2008b. Climate control on the long-term anomalous changes of zooplankton communities in the Northwestern Mediterranean. Global Change Biology 14: 11-26.

Molinero, J. C., M. Casini, and E. Buecher. 2008c. The influence of the Atlantic and regional climate variability on the long-term changes in gelatinous carnivore

populations in the northwestern Mediterranean. Limnology and Oceanography 53: 1456-1467.

Mollmann, C., R. Diekmann, B. Muller-Karulis, G. Kornilovs, M. Plikshs, and P. Axe. 2009. Reorganization of a large marine ecosystem due to atmospheric and anthropogenic pressure: a discontinuous regime shift in the Central Baltic Sea. Global Change Biology 15: 1377-1393.

Motoda, S. 1959. Motoda, devices of simple plankton apparatus. Memoirs, Faculty of Fisheries: Hokkaido University 7: 73-94.

Neveux, J., and M. Panouse. 1987. Spectrofluorometric determination of chlorophylls and pheophytins. Archiv Fur Hydrobiologie 109: 567-581.

Nival, P., and M. C. Corre. 1976. Annual variation of surface hydrology in Bay of Villefranche-sur-Mer. Annales De L'Institut Oceanographique 52: 57-78.

O'brien, C. M., C. J. Fox, B. Planque, and J. Casey. 2000. Fisheries - Climate variability and North Sea cod. Nature 404: 142-142.

Odum, H. T. 1956. Efficiencies, size of organims, and community structure. Ecology 37: 592-597.

Ohman, M. D. 1988. Behavioral-Responses of Zooplankton to Predation. B Marine Science 43: 530-550.

Omori, M. 1978. Some factors affecting on dry-weight, organic weight and concentrations of carbon and nitrogen in freshly prepared and in preserved zooplankton. Internationale Revue Der Gesamten Hydrobiologie 63: 261-269.

Orfila, A., A. Álvarez, J. Tintoré, A. Jordi, and G. Basterretxea. 2005. Climate teleconnections at monthly time scales in the Ligurian Sea inferred from satellite data. Progress in Oceanography 66: 157-170.

Ortner, P. B., S. R. Cummings, R. P. Aftring, and H. E. Edgerton. 1979. Silhouette photography of oceanic zooplankton. Nature 277: 50–51.

Osborn, T. J. 2004. Simulating the winter North Atlantic Oscillation: the roles of internal variability and greenhouse gas forcing. Clim Dynam 22: 605-623.

Ottersen, G., S. Kim, G. Huse, J. J. Polovina, and N. C. Stenseth. 2010. Major pathways by which climate may force marine fish populations. Journal of Marine Systems 79: 343-360.

Paffenhöfer, G.-A. 1984. Food ingestion by the marine planktonic copepod *Paracalanus* in relation to abundance and size distribution of food. Marine Biology 80: 323-333.

Paffenhöfer, G.-A. 1988. Feeding rates and behavior of zooplankton. Bulletin of Marine Science 43: 430-445.

Paffenhöfer, G.-A., L. P. Atkinson, T. N. Lee, P. G. Verity, and L. R. Bulluck. 1995. Distribution and abundance of thaliaceans and copepods off the Southeastern USA during winter. Continental Shelf Research 15: 255-280.

Paffenhöfer, G.-A., A. Ianora, A. Miralto, J. T. Turner, G. S. Kleppel, M. R. d'Alcala, R. Casotti, G. S. Caldwell, G. Pohnert, A. Fontana, D. Muller-Navarra, S. Jonasdottir, V. Armbrust, U. Bamstedt, S. Ban, M. G. Bentley, M. Boersma, M. Bundy, I. Buttino, A. Calbet, F. Carlotti, Y. Carotenuto, G. d'Ippolito, B. Frost, C. Guisande, W. Lampert, R. F. Lee, S. Mazza, M. G. Mazzocchi, J. C. Nejstgaard, S. A. Poulet, G. Romano, V. Smetacek, S. Uye, S. Wakeham, S. Watson, and T. Wichard. 2005. Colloquium on diatom-copepod interactions. Marine Ecology-Progress Series 286: 293-305.

Parmesan, C., and G. Yohe. 2003. A globally coherent fingerprint of climate change impacts across natural systems. Nature 421: 37-42.

Parmesan, C. 2006. Ecological and evolutionary responses to recent climate change. Annual Review of Ecological Systems 37: 637-669.

Parsons, T. R., and J. D. H. Strickland. 1963. Discussion of spectrophotometric determination of marine plants pigments, with revised equations for ascertaining chlorophylls and carotenoids. Journal of Marine Research 21: 155-163.

Parsons, T. R. 1969. The use of particle size spectra in determining the structure of plankton community. Journal of Oceanographic society of Japan 25: 172-181.

Perry, R. I., H. P. Batchelder, D. L. Mackas, S. Chiba, E. Durbin, W. Greve, and H. M. Verheye. 2004. Identifying global synchronies in marine zooplankton populations: Issues and opportunities. Ices Journal of Marine Science 61: 445-456.

Perry, A. L., P. J. Low, J. R. Ellis, and J. D. Reynolds. 2005. Climate change and distribution shifts in marine fishes. Science 308: 1912-1915.

Persson, L. 1999. Trophic cascades: abiding heterogeneity and the trophic level concept at the end of the road. Oikos 85: 385-397.

Peters, R. H. 1976. Tautology in evolution and ecology. The American Naturalist 110: 1-12.

Peters, R. H. 1983. The ecological implications of body size. Cambridge University press. ISBN 0-521-28886-X paperback.

Peterson, W. T., and F. B. Schwing. 2003. A new climate regime in northeast pacific ecosystems. Geophysical Research Letters 30: doi:10.1029/2003GL017528.

Pielou, E. C. 1975. Ecological diversity. New York: Wiley InterScience.

Pierini, S., and A. Simioli. 1998. A wind-driven circulation model of the Tyrrhenian Sea area. Journal of Marine Systems 18: 161-178.

Pinca, S., and S. Dallot. 1995. Mesozooplankton and macrozooplankton composition patterns related to hydrodynamic structures in the Ligurian Sea (Trophos-2 experiment, April-June-1986). Marine Ecology-Progress Series 126: 49-65.

Planque, B., and J. M. Fromentin. 1996. Calanus and environment in the eastern North Atlantic .1. Spatial and temporal patterns of *C.finmarchicus* and *C.helgolandicus*. Marine Ecology-Progress Series 134: 101-109.

Platt, T., and K. Denman. 1977. The organisation of pelagic marine ecosystems. Helgonalder Wissenschaftliche Meeresuntersuchungen 30: 575-581.

Platt, T. a. D., K. 1978. The structure of pelagic marine ecosystems. Rapports et Procès-Verbaux des Reunions du Conseil International pour l'Exploration de la Mer 173: 60-65.

Price, H. J., G.-A. Paffenhöfer, and J. R. Strickler. 1983. Modes of cell capture in calanoid copepods. Limnology and Oceanography 28: 116-123.

Prieur, L. 1979. Structures hydrologiques, chimiques, biologiques dans le Bassin Liguro-Provençal. Rapports et Procès-verbaux des Réunions. Comission internationale pour l'exploration Scientifique de la Mer Mediterranée 25/26: 75-76.

Prieur, L., J. P. Bethoux, J. H. Bong, and D. Tailliez. 1983. Particularités hydrologiques et formation d'eau profonde dans le Basin Liguro-Provençal en 1981-1982. Rapp.Comm.int.Mer Medit. 28: 51-53.

Purcell, J. E., S. Uye, and W. T. Lo. 2007. Anthropogenic causes of jellyfish blooms and their direct consequences for humans: a review. Marine Ecology-Progress Series 350: 153-174.

Quinones, R. A., T. Platt, and J. Rodriguez. 2003. Patterns of biomass-size spectra from oligotrophic waters of the Northwest Atlantic. Progress in Oceanography 57: 405-427.

Quintana, X. D., S. Brucet, D. Boix, R. Lopez-Flores, S. Gascon, A. Badosa, J. Sala, R. Moreno-Amich, and J. J. Egozcue. 2008. A nonparametric method for the

measurement of size diversity with emphasis on data standardization. Limnology and Oceanography-Methods 6: 75-86.

Rakotomalala, R. 2005. Tanagra: A free software for research and academic purposes. Proceedings of EGC'2005, RNTI-E-3, 2: 697-702.

Raybaud, V., P. Nival, L. Mousseau, A. Gubanova, D. Altukhov, S. Khvorov, F. Ibanez, and V. Andersen. 2008. Short term changes in zooplankton community during the summer-autumn transition in the open NW Mediterranean Sea: Species composition, abundance and diversity. Biogeosciences 5: 1765-1782.

Reeve, M. R. 1980. Comparative experimental studies on the feeding of chaetognaths and ctenophores. Journal of Plankton Research 2: 381–393.

Reid, J. L. 1979. On the contribution of the Mediterranean Sea outflow to the Norwegian-Greenland Sea. Deep Sea Research Part A. Oceanographic Research Papers 26: 1199-1223.

Reid, J. L. 1994. On the total geostrophic circulation of the North Atlantic Ocean: Flow patterns, tracers, and transports. Progress in Oceanography 33: 1-92.

Reid, P. C., M. Edwards, H. G. Hunt, and A. J. Warner. 1998. Phytoplankton change in the North Atlantic. Nature 391: 546-546.

Reid, P. C., M. D. Borges, and E. Svendsen. 2001. A regime shift in the North Sea circa 1988 linked to changes in the North Sea horse mackerel fishery. Fisheries Research 50: 163-171.

Reid, P. C., J. M. Colebrook, J. B. L. Matthews, and J. Aiken. 2003a. The Continuous Plankton Recorder: Concepts and history, from plankton indicators to undulating recorders. Progress in Oceanography 58: 117-173.

Reid, P. C., M. Edwards, G. Beaugrand, M. Skogen, and D. Stevens. 2003b. Periodic changes in the zooplankton of the North Sea during the twentieth century linked to oceanic inflow. Fisheries Oceanography 12: 260-269.

Reynolds, C. S. 2001. Emergence in pelagic communities. Scientia Marina 65: 5-30.

Ribera d'Alcalà, M., F. Conversano, F. Corato, P. Licandro, O. Mangoni, D. Marino, M. G. Mazzocchi, M. Modigh, M. Montresor, M. Nardella, V. Saggiomo, D. Sarno, and A. Zingone. 2004. Seasonal patterns in plankton communities in the pluriannual time series at a coastal Mediterranean site (Gulf of Naples): An attempt to discern recurrences and trends. Scientia Marina 68: 65-83.

Richardson, A. J., and S. Schoeman. 2004. Climate impact on plankton ecosystems in the Northeast Atlantic. Science 305: 1609-1612.

Richardson, A. J. 2008. In hot water: Zooplankton and climate change. Ices Journal of Marine Science 65: 279-295.

Rixen, M., J. M. Beckers, S. Levitus, J. Antonov, T. Boyer, C. Maillard, M. Fichaut, E. Balopoulos, S. Iona, H. Dooley, M. J. Garcia, B. Manca, A. Giorgetti, G. Manzella, N. Mikhailov, N. Pinardi, and M. Zavatarelli. 2005. The Western Mediterranean Deep Water: A proxy for climate change. Geophysical Research Letters 32: L12608.

Robert, P., and Y. Escoufier. 1976. Unifying tool for linear multivariate statistical-methods - RV-coefficient. Jounal of the Royal Statistical Society, Series C (Applied Statistics) 25: 257-265.

Rodriguez, J., and M. M. Mullin. 1986. Relation between biomass and body-weight of plankton in a steady-state oceanic ecosystem. Limnology and Oceanography 31: 361-370.

Rodriguez, J., F. Jimenez, B. Bautista, and V. Rodriguez. 1987. Planktonic biomass spectra dynamics during a winter production pulse in Mediterranean coastal waters. Journal of Plankton Research 9: 1183-1194.

Rodriguez, J. 1994. Some comments on the size-based structural analysis of the pelagic ecosystem. Scientia Marina 58: 1-10.

Roemmich, D., and J. Mcgowan. 1995. Climatic Warming and the Decline of Zooplankton in the California Current. Science 267: 1324-1326.

Roether, W., B. B. Manca, B. Klein, D. Bregant, D. Georgopoulos, V. Beitzel, V. Kovacevic, and A. Luchetta. 1996. Recent changes in Eastern Mediterranean deep waters. Science 271: 333-335.

Ruiz, J. 1994. The measurement of size diversity in the pelagic ecosystem. Scientia Marina 58: 103-107.

Samuel, S., K. Haines, S. Josey, and P. G. Myers. 1999. Response of the Mediterranean Sea thermohaline circulation to observed changes in the winter wind stress field in the period 1980-1993. Journal of Geophysical Research-Oceans 104: 7771-7784.

San Martin, E., R. P. Harris, and X. Irigoien. 2006. Latitudinal variation in plankton size spectra in the Atlantic Ocean. Deep-Sea Research Part II-Topical Studies In Oceanography 53: 1560-1572.

Sarmiento, J. L., T. M. C. Hughes, R. J. Stouffer, and S. Manabe. 1998. Simulated response of the ocean carbon cycle to anthropogenic climate warming. Nature 393: 245-249.

Sarmiento, J. L., N. Gruber, M. A. Brzezinski, and J. P. Dunne. 2004a. High-latitude controls of thermocline nutrients and low latitude biological productivity. Nature 427: 56-60.

Sarmiento, J. L., R. Slater, R. Barber, L. Bopp, S. C. Doney, A. C. Hirst, J. Kleypas, R. Matear, U. Mikolajewicz, P. Monfray, V. Soldatov, S. A. Spall,and R. Stouffer. 2004b. Response of ocean ecosystems to climate warming. Global Biogeochemical Cycles 18, GB3003, doi:10.1029/2003GB002134.

Scheffer, M., S. Carpenter, and B. De Young. 2005. Cascading effects of overfishing marine systems. Trends in Ecology & Evolution 20: 579-581.

Scheffer, M., S. Carpenter, J. A. Foley, C. Folke, and B. Walker. 2001. Catastrophic shifts in ecosystems. Nature 413: 591-596.

Schmidt-Nielsen, K. 1984. Why is animal size so important? Cambridge University press. ISBN: 0-521-31987-0 Paperback.

Shannon, C. E., and W. Weaver. 1948. A mathematical theory of communication. Bell System Technical Journal 27: 379-423.

Sheldon, R. W., A. Prakash, and J. Sutcliffe, W.H. 1972. The size distribution of particles in the ocean. Limnology and Oceanography 17: 327-340.

Sheldon, R. W., W. H. J. Sutcliffe, and M. A. Paranjape. 1977. Structure of pelagic food chain and relationship between plankton and fish production. Journal of Fisheries Research Board Canada 34: 2344-2353.

Sherr, E. B., and B. F. Sherr. 2007. Heterotrophic dinoflagellates: A significant component of microzooplankton biomass and major grazers of diatoms in the sea. Marine Ecology Progress Series 352: 187-197.

Sieracki, C. K., M. E. Sieracki, and C. S. Yentsch. 1998. An imaging-in-flow system for automated analysis of marine microplankton. Marine Ecology Progress Series 168: 285–296.

Silvert, W., and T. Platt. 1978. Energy flux in pelagic ecosystem - time-dependent equation. Limnology and Oceanography 23: 813-816.

Skliris, N., S. Sofianos and A. Lascaratos. 2007. Hydrological changes in the Mediterranean Sea in relation to changes in the freshwater budget: A numerical modelling study. Journal of Marine Systems 65(1-4): 400-416.

Sommer, U. 1996. Plankton ecology: The past two decades of progress. Naturwissenschaften 83: 293-301.

Somot, S., F. Sevault and M. Déqué. 2006. Transient climate scenario simulation of the Mediterranean Sea for the twenty-first century using a high-resolution circulation model. Climate Dynamics 27: 851-879.

Sourisseau, M., and F. Carlotti. 2006a. Spatial distribution of zooplankton size spectra on the French continental shelf of the Bay of Biscay during spring 2000 and 2001. Journal of Geophysical Research-Oceans 111, C05S09, doi: 10.1029/2005JC003063.

Sournia, A., J. M. Brylinski, S. Dallot, P. Lecorre, M. Leveau, L. Prieur, and C. Froget. 1990. Hydrological fronts off the coasts of France - a review. Oceanologica Acta 13: 413-438.

Southward, A. J., S. J. Hawkins, and M. T. Burrows. 1995. 70 Years Observations of Changes in Distribution and Abundance of Zooplankton and Intertidal Organisms in the Western English-Channel in Relation to Rising Sea Temperature. J Therm Biol 20: 127-155.

Sprules, W. G. 2008. Ecological change in Great Lakes communities - a matter of perspective. Canadian Journal of Fisheries and Aquatic Sciences 65: 1-9.

Sprules, W. G., and A. P. Goyke. 1994. Size-based structure and production in the pelagia of lakes Ontario and Michigan. Canadian Journal of Fisheries and Aquatic Sciences 51: 2603-2611.

Sprules, W. G., E. H. Jin, A. W. Herman, and J. D. Stockwell. 1998. Calibration of an Optical Plankton Counter for use in fresh water. Limnology and Oceanography 43: 726-733.

Sprules, W. G., and M. Munawar. 1986. Plankton size spectra in relation to ecosystem productivity, size, and perturbation. Canadian Journal of Fisheries and Aquatic Sciences 43: 1789-1794.

Sprules, W. G., M. Munawar, and E. H. Jin. 1988. Plankton community structure and size spectra in the Georgian Bay and North Channel ecosystems. Hydrobiologia 163: 135-140.

Stenseth, N. C., A. Mysterud, G. Ottersen, J. W. Hurrell, K. S. Chan, and M. Lima. 2002. Ecological effects of climate fluctuations. Science 297: 1292-1296.

Strass, V. H. 1992. Chlorophyll patchiness caused by mesoscale upwelling at fronts. Deep-Sea Research 39: 75-96.

Strickland, J. D. H., and T. R. Parsons. 1972. A practical handbook of sea water analysis. Bulletin of Fisheries Research Board Canada 167: 1-310.

Strong, D. R. 1992. Are Trophic Cascades All Wet - Differentiation and Donor-Control in Speciose Ecosystems. Ecology 73: 747-754.

Swain, D. P., and A. F. Sinclair. 2000. Pelagic fishes and the cod recruitment dilemma in the Northwest Atlantic. Canadian Journal of Fisheries and Aquatic Sciences 57: 1321-1325.

Sydeman, W. J., and S. J. Bograd. 2009. Marine ecosystems, climate and phenology: introduction. Marine Ecology-Progress Series 393: 185-188.

Taylor, A. H., J. I. Allen, and P. A. Clark. 2002. Extraction of a weak climatic signal by an ecosystem. Nature 416: 629-632.

Thingstad, T. F., U. L. Zweifel, and F. Rassoulzadegan. 1998. P limitation of heterotrophic bacteria and phytoplankton in the Northwest Mediterranean. Limnology and Oceanography 43: 88-94.

Thuiller, W., S. Lavorel and M.B. Araújo, 2005. Niche properties and geographical extent as predictors of species sens.tivity to climate change. Global Ecology & Biogeography 14(4): 347-357.

Trigo, I. F., T. D. Davies, and G. R. Bigg. 2000. Decline in Mediterranean rainfall caused by weakening of Mediterranean cyclones. Geophysical Research Letters 27: 2913-2916.

Tsimplis, M. N., A. F. Velegrakis, A. Theocharis, and M. B. Collins. 1997. Low-frequency current variability at the straits of Crete, Eastern Mediterranean. Journal of Geophysical Research 102 (C11), 25,005-25,020, doi: 10.1029/97JC01011.

Tsimplis, M. N., and T. F. Baker. 2000. Sea Level Drop in the Mediterranean Sea: An Indicator of Deep Water Salinity and Temperature Changes? Geophysical Research Letters 27 (12): 1731–1734, doi: 10.1029/1999GL007004.

Tsimplis, M. N., and S. A. Josey. 2001. Forcing of the Mediterranean Sea by atmospheric oscillations over the North Atlantic. Geophysical Research Letters 28: 803-806.

Turley, C. M. 1999. The changing Mediterranean Sea - A sensitive ecosystem? Progress in Oceanography 44: 387-400.

Turner, J. T., P. A. Tester, and R. L. Ferguson. 1988. The marine cladoceran Penilia avirostris and the "microbial loop" of pelagic food webs. Limnology and Oceanography 33: 245-255.

Van Guelpen, L., D. F. Markle, and D. J. Duggan. 1982. An evaluation of accuracy, precision, and speed of several zooplankton subsample techniques. Journal du Conseil pour L'Exploration de la Mer 161: 45-47.

Vargas-Yáñez, M., M. J. García, J. Salat, M. C. García-Martínez, J. Pascual, and F. Moya. 2008. Warming trends and decadal variability in the Western Mediterranean shelf. Global Planet Change 63: 177-184.

Verity, P. G., and V. Smetacek. 1996. Organism life cycles, predation, and the structure of marine pelagic ecosystems. Marine Ecology-Progress Series 130: 277-293.

Vidondo, B., Y. T. Prairie, J. M. Blanco, and C. M. Duarte. 1997. Some aspects of the analysis of size spectra in aquatic ecology. Limnology and Oceanography 42: 184-192.

Vignudelli, S., G. P. Gasparini, M. Astraldi, and M. E. Schiano. 1999. A possible influence of the North Atlantic Oscillation on the circulation of the Western Mediterranean Sea. Geophysical Research Letters 26: 623-626.

Walther, G. R., L. Hughes, P. Vitousek, and N. C. Stenseth. 2005. Consensus on climate change. Trends in Ecology & Evolution 20: 648-649.

Ward, J. H. 1963. Hierarchical grouping to optimize an objetive function. Journal of the American Statistical Association 58: 236-244.

Warren, J. D., D. A. Demer, D. E. Mcgehee, R. Di Ment, and J. F. Borsani. 2004. Zooplankton in the Ligurian Sea: Part II. Exploration of their physical and biological forcing functions during summer 2000. Journal of Plankton Research 26: 1419-1427.

Wasmund, N., G. Nausch, and W. Matthaus. 1998. Phytoplankton spring blooms in the southern Baltic Sea - spatio-temporal development and long-term trends. Journal of Plankton Research 20: 1099-1117.

Wiebe, P. H. 1975. Relationships between zooplankton displacement volume, wet weight, dry weight and carbon. Fishery Bulletin 73: 777-786.

Wiebe, P. H. 1988. Functional regression equations for zooplankton displacement volume, wet weight, dry weight and carbon, a correction. Fishery Bulletin 86: 833-835.

Wieland, K., D. Petersen, and D. Schnack. 1997. Estimates of zooplankton abundance and size distribution with the Optical Plankton Counter (OPC). Archive of Fishery and Marine Research 45: 271-280.

Worm, B., and J. E. Duffy. 2003. Biodiversity, productivity and stability in real food webs. Trends in Ecology & Evolution 18: 628-632.

Worm, B., H. K. Lotze, H. Hillebrand, and U. Sommer. 2002. Consumer versus resource control of species diversity and ecosystem functioning. Nature 417: 848-851.

Xoplaki, E., J. F. Gonzalez-Rouco, J. Luterbacher, and H. Wanner. 2004. Wet season Mediterranean precipitation variability: Influence of large-scale dynamics and trends. Climate Dynamics 23: 63-78.

Zhou, M. 2006. What determines the slope of a plankton biomass spectrum? Journal of Plankton Research 28: 437-448.

Zhou, M., and M. E. Huntley. 1997. Population dynamics theory of plankton based on biomass spectra. Marine Ecology-Progress Series 159: 61-73.

Zingone, A., R. Casotti, M. R. D'alcalà, M. Scardi, and D. Marino. 1995. 'St Martin's Summer': the case of an autumn phytoplankton bloom in the Gulf of Naples (Mediterranean Sea). Journal of Plankton Research 17: 575-593.

Zingone, A., L. Dubroca, D. Iudicone, F. Margiotta, F. Corato, M. Ribera d'Alcalà, V. Saggiomo, and D. Sarno. 2009. Coastal phytoplankton do not rest in winter. Estuaries and Coasts 33 (2): 342-361.

Appendix I

Table 1 - Variables measured by Zooplocess on the scanned objects. For more information on the on the parameters refer to http://www.obs-vlfr.fr/~gaspari/Plankton_Identifier/faq.html

Variable	Description of the variable
Area	Surface of the object in square pixel.
Mean	Average grey value within the object
StdDev	Standard deviation of the grey value within the object
Mode	Modal grey value within the object
Min	Minimum grey value within the object (0 = black)
Max	Maximum grey value within the object (255 = white)
X	X position of the centre of gravity of the object
Y	Y position of the centre of gravity of the object
XM	X position of the centre of gravity of the grey level in the object
YM	Y position of the centre of gravity of the grey level in the object
Perim	Length of the outside boundary of the object
BX	X coordinate of the top left point of the smallest rectangle delimiting the object
BY	Y coordinate of the top left point of the smallest rectangle enclosing the object
Width	Width of the smallest rectangle enclosing the object
Height	Height of the smallest rectangle enclosing the object
Major	Primary axis of the best fitting ellipse to the object
Minor	Secondary axis of the best fitting ellipse to the object
Angle	Angle between the primary axis and a line parallel to the x-axis of the image

Circ	Circularity = (4 * Pi * Area) / Perim^2
Feret	The longest distance between any two points along the object boundary
IntDen	Sum of the grey values of the pixels in the object
Median	Median of the grey value used to generate the mean grey value
Skew	The skewness being the third order moment about the mean
Kurt	Kurtosis, the fourth order moment about the mean
%area	Surface of holes in percentage
XStart	X coordinate of the top left point of the image
YStart	Y coordinate of the top left point of the image
Area_exc	Surface of the object excluding holes in square pixel (=Area*(1-(%area/100))
Mean_exc	Average grey value excluding holes within the object (= IntDen /Area_exc)
Fractal	Fractal dimension of object boundary
Skelarea	:Surface of skeleton in square pixel

Table 2 - Variables of Plankton identifier calculated from the Zooprocess original variables.

Variable	Description of the variable
ESD	Equivalent Spherical Diameter
Elongation	Major / Minor
Range	Max – Min
MeanPos	(Max – Mean) / Range
CentroidsD	Square root of $((XM - X)^2 + (YM - Y)^2)$
CV	100 * (StdDev / Mean)
SR	100 * (StdDec / (Max-Min)
PerimAreaexc	Perim / Area_exc
FeretAreaexc	Feret/Area_exc
PerimFeret	Perim / Feret
PerimMaj	Perim / Major
Circexc	$(4 * Pi * Area\_exc) / Perim^2$
CDexc	$(CentroidsD)^2 / Area\_exc$

Table 3 - Confusion matrix of the first cross-validation performed on the 45 original categories; the total error rate was 0.41 with the Random Forest algorithm.

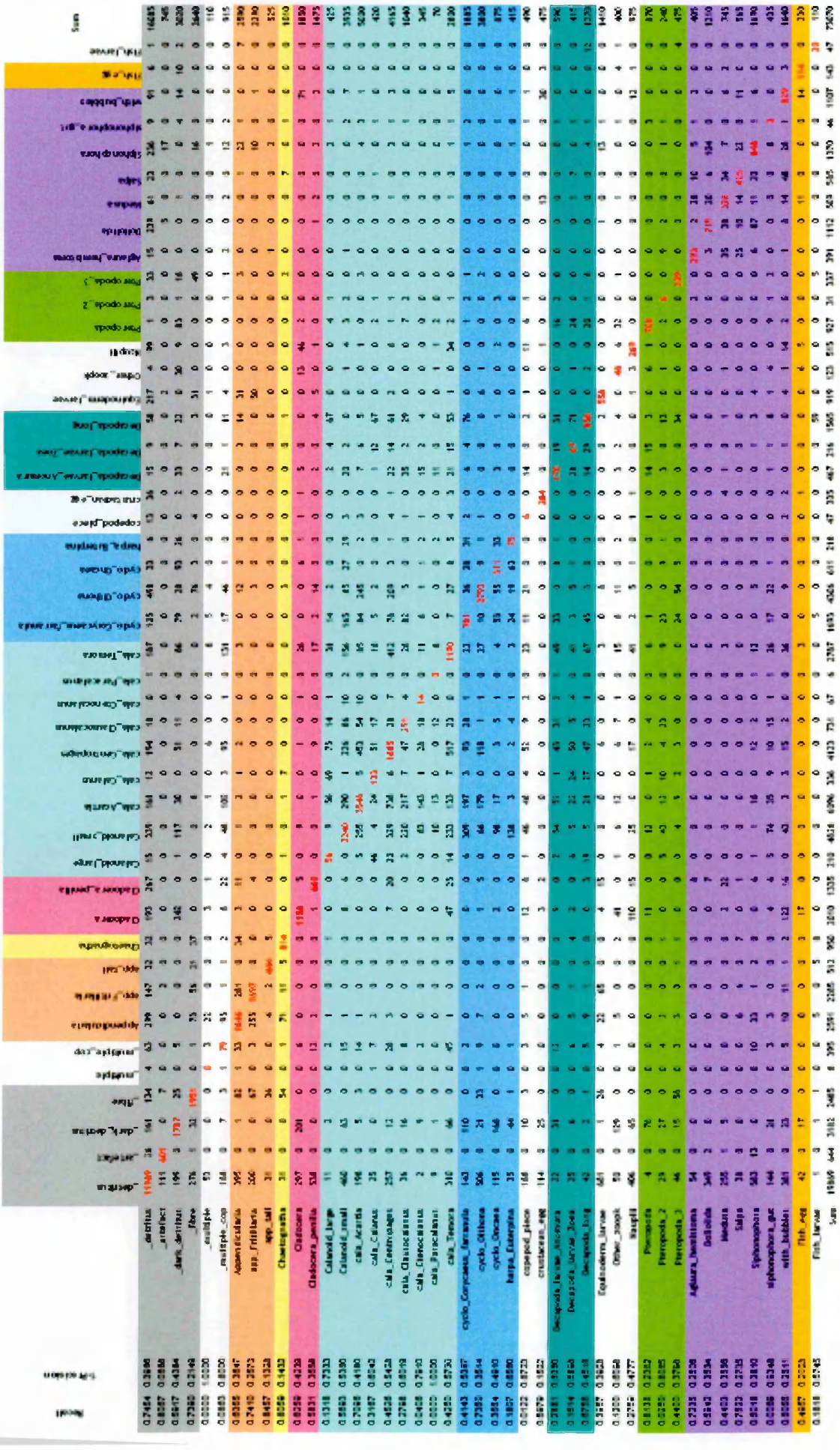

Table 4 - Confusion matrix of the definitive learning set's cross-validation; 26 categories and 0.23 total error rate with the Random Forest algorithm.

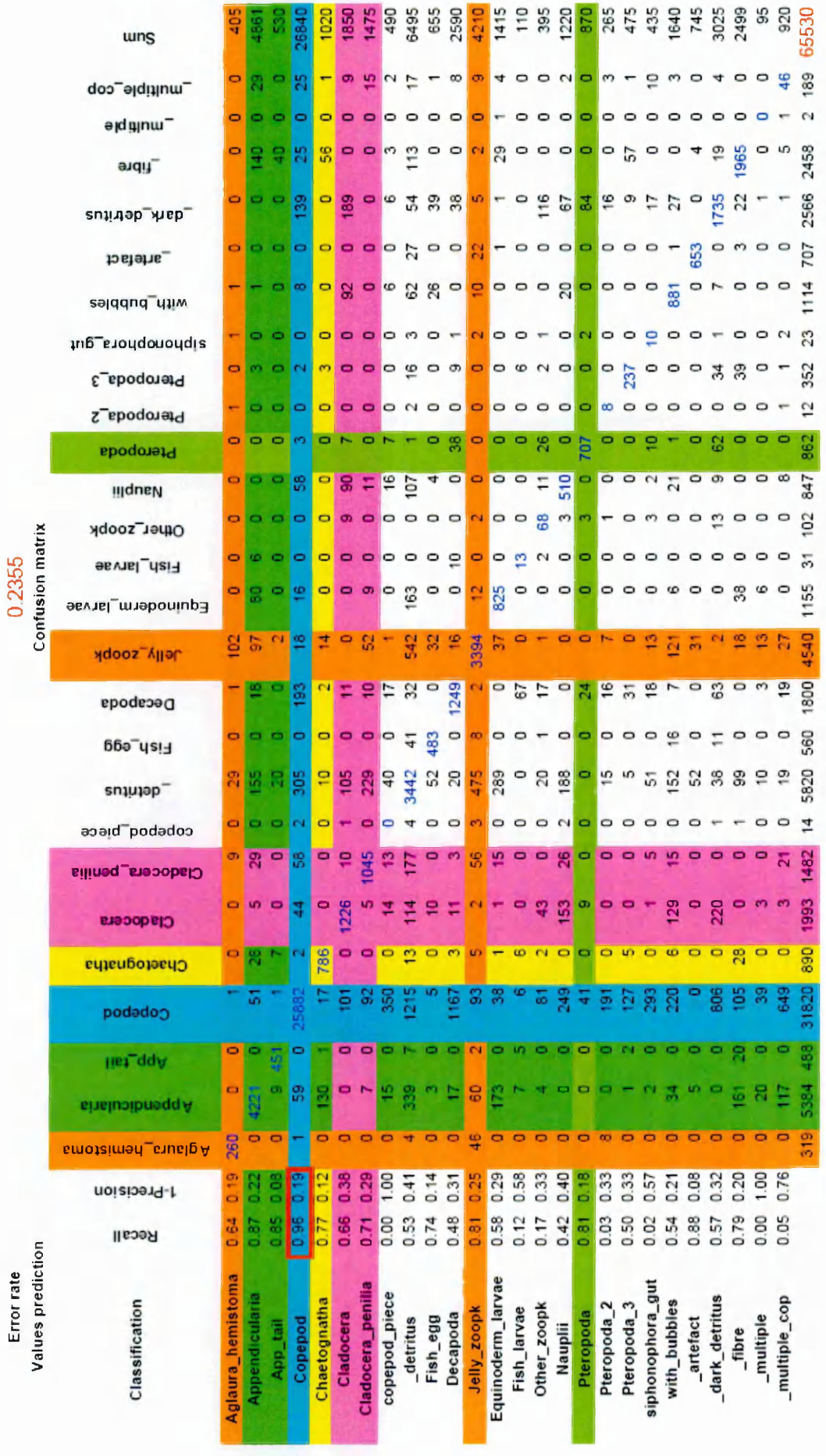

Table 5 - Confusion matrix of learning set validation with the testset.

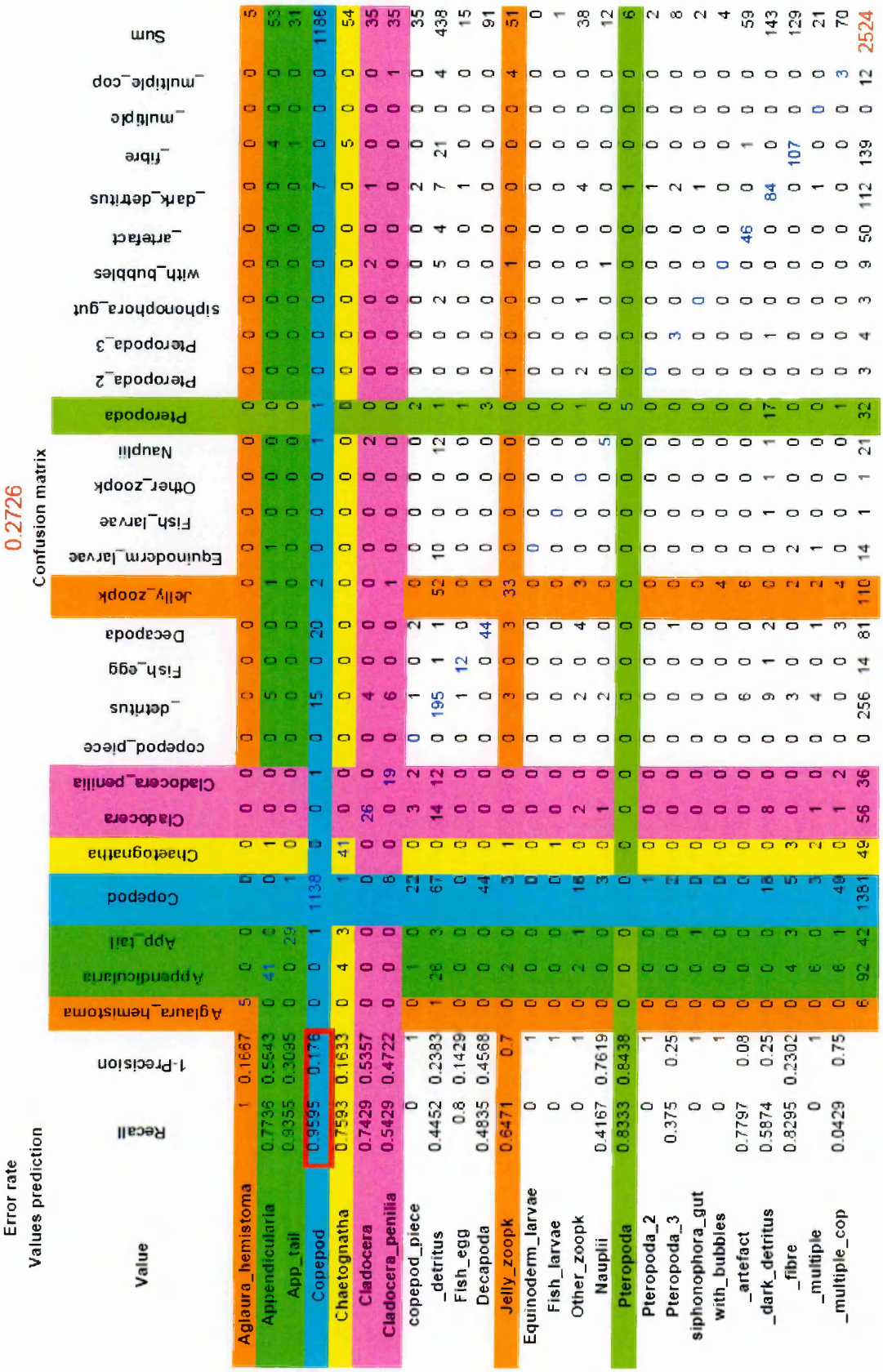

Appendix II

Carmen Garcia-Comas
Written for Zooprocess version 6.16
Hydroptic & LOV

SHORT MANUAL TO WORK WITH THE ZOOSCAN

Please use the following "tools" to learn how to use the ZooScan:

ZooScan Manual (v.6.16) to download in www.zooscan.com
ZooScan Users Forum: http://zooscan.forumakers.com/
Gorsky et al. (2010) ZooScan methodological paper.
Open access link in www.zooscan.com
http://plankt.oxfordjournals.org/cgi/reprint/fbp124?ijkey=gJnvV9AjR20gITg&keytype=ref

ZOOSCAN WORKING PROTOCOL

Morning:

Turn on the ZooScan and rinse the scan tray.

Eliminate marks on the glass and frame and check from time to time if the glass of the ZooScan cover has not marks.

Put some water to cover the tray (it avoids scratching the tray with the frame).
Place the frame of your project.

Fill with water until the step of the frame is covered.

Do a background scan (2scans) in the project you will work on (check that there is not dust on the OD, dark circle, position and that the tray and water are clean).
DON'T FORGET TO PRESS THE TEMP GREEN LIGHT BUTTON before scanning.

Day:

Scan samples (while one sample is being scanned you can recondition the previous one or prepare the next one if you want to).
COVER THE STEP OF THE FRAME WITH EXTRA WATER!
PRESS THE TEMP GREEN LIGHT BUTTON before scanning!
(if your ZooScan has also a blue light button and it's on, turn it off before scanning)

End of the day:

Launch "Convert and process images in batch mode" in ImageJ, Z, (All images in the Raw folder will be processed during the night). If in your project you already have processed images, you can select to process the converted images (in the subfolders of the Work folder) to spare conversion time.

Once a week:

You can dedicate 1/5 days to creating your Learning set at the beginning (at the end of the first week of scanning) (we recommend not investing too much time in building it) and to validate your samples (check automatic recognition by extracting vignettes according to prediction and resorting them if wrongly recognized).

We recommend using a small Learning set (about 200 objects/group) to accelerate organism recognition, and to validate all the samples to have a robust dataset at the end.

ZOOSCAN PROTOCOL FOR SCANNING

DO NOT FORGET TO DO A BACKGROUND (2 scans) every morning before a day of scanning.

If it is the first time that you will use your ZooScan:

1. Check that your ZooScan is on a bench without vibrations and that the instrument is horizontal.

Check first that the top-left corner of the ZooScan is stable (push on it). If not, you should lift that leg a bit until it does not sink under the pressure of your hand. If the ZooScan is not horizontal, level it by screwing or unscrewing the legs.

2. The height of your ZooScan legs must be enough to place below the mouth of the zooscan a receptacle to recover your sample when pouring it from the scanning tray.

3. The receptacle to recover your sample should be wide enough to not miss the mouth of the tray when elevated, and deep enough (although lower than the ZooScan height) to recover all the water of the sample+ the extra-water poured to rinse the tray.

First time working with ZooProcess:
Read section 12.9 in page 90-91 of Zooprocess_manual_v6.16

If you have just installed Zooprocess for the first time or also if you installed it but it is the very first time that you create a project for your new ZooScan, you need to change the default sampling settings. Check the version of your ZooScan and dimensions of your frames in the Qualification Report that Hydroptic delivered to you with your instrument.

Choose the option "CHANGE/CHECK Zooscan version & parameters" in Zooprocess.

- Select your ZooScan version to the one corresponding to your model (if delivered by Hydroptic check if it is v1 or v2 in the qualification report).
- Check if the OD position and frame X-Y dimensions correspond to those noted in the Qualification report and if not change them in the computer according to the values delivered by the company.

Now the standard .ini files are modified according to your machine, and your ZooScan is ready to scan.

Create a Project:
Read section 12.9 in pages 90-91 of Zooprocess_manual_v6.16

Open Image J, click on Z icon and choose the option "create a new project" which is on the bottom of the options' list. Click OK.
Choose the drive. We recommend to create your projects in a drive root were you just can store them and you just keep the ZooScan projects (clean) (i.e., Zooscan root folder in C:, and zooscan projects in D: drive).

We recommend that each project has only one scanning configuration file (vuescan.ini file). So choose just the one you will always be using in that project.
It is recommended to use the large frame and highest resolution image: "vuescan_zooscan_2400dpi_frame2_large.ini" (although you need at least 2G RAM to be able to process those images!).
Untick the other options (other .ini files). Only the ticked .ini file will be copied to your Zooscan_config folder in the created project.

Before scanning:

We recommend keeping bottles with water to have litres of water at environmental temperature to work with your zooscan. If not, you will probably have condensation, bubbles, etc, due to temperature differences between the tap pipes and the zooscan room.

Treat the ZooScan gently and maintain it (e.g., clean it at the end of the day; hold always the tray when you lift it to remove the water! It could fall). Use only wooden sticks to separate organisms in the tray (it avoids scratches). We use dried cactus spines stuck with scotch taper on a thin pipette in the Laboratory of Villefranche.

Check the performance of the ZooScan by doing a background scan (2 replicates) every morning. This is also important for image processing, as the process will be done with the latest background (if it was done a long time ago it could maybe not represent the present background of your ZooScan).

4. Turn on your ZooScan if it's the first sample in the morning (it needs to warm up). Then you leave it on all the day if you are passing samples. Turn the zooscan off during the night.

5. Prepare your sample. Here, I explain the procedure followed in Villefranche (for 200 and 330 µm sampling nets):

    1) Sieve your sample to take out the formol and sea water (you can keep it to recondition the sample afterwards). We sieve each sample through a 1mm mesh and 200µm mesh to have 2 size fractions (this is to avoid missing the rare large organisms while splitting the sample to scan a subsample). Rinse the sample with tap water to properly eliminate the sea water. Place each fraction (subsample) in tap water.
    2) Now you have 2 size fractions. The large one (>1mm) is called d1; the small one is called d2 (200µm-1mm) (d1 and d2 will be added at the end of the sample name to distinguish them during the data processing).
    3) Take one of the fractions (e.g., d2) and split it until there are ~1000-1500 individuals (experience will give you the good eye for dilution to have a good scan: not too crowded and not poor).

Scanning (we scan during the day, and process them later during the night):

1. Pour some water on the scanning tray until you have covered it.

2. Place the frame (the one defined in your Zooscan Project; preferably the large one). Control that the frame is well placed on the foremost left-bottom side of

the scanning tray (this is very important because the area of scan is fixed to cover the frame when well positioned)!

3. Clean drops or marks on the frame.

4. Pour the sample and add tap water until all the perimeter of the frame's step is covered with water. When you pour the sample and add the extra water you can already accelerate the separation of organisms by pouring the sample homogeneously on the tray and by pouring the extra water on conglomerated areas of the tray (i.e., high density of organisms and thus touching) to "dissolve" them.

6. Take 5-15 minutes to properly separate the organisms. Move to the tray the organisms placed on the step of the frame or touching the frame (if not, they will not be considered in the scan as the image is cropped on the borders of the frame). Also, if some organisms are floating, try to sink them with the wood peak (otherwise their size measurements are wrong and their image captions are blurred). If it's difficult to sink the floating organisms and they are very few, the best is to take them out of the image (e.g. placing them on the step of the frame). This step (organisms' separation) is critical to have good data quality. Thus, please pay attention and try that none object is touching another one. Nevertheless, some samples can be difficult to separate. Make a compromise between the time expended separating and the quality of the image. You can, after the process of the image, separate touching objects with the separation tool in zooprocess.

7. Launch Zooprocess, select your project and click on SCAN sample with Zooscan (for archive, no process). Then, follow the instructions on zooprocess window.

If you would like to use our matlab files to read and treat your data "par default" you must write the date of sampling and fraction as follows in this example:

Mc19980530d1 (this is the large size fraction of a sample from the 30th May 1998 at mc station in Naples).
If you do not need to divide your samples in two size classes, please add d1 at the end of the
name anyway. The matlab program will search for it, and if there is not d2 subsample it will work anyway.

8. IMPORTANT! Do not forget to turn on the green light of the ZooScan before launching the scan in Vuescan. WAIT 30 seconds between the preview and pressing scan (if you don't wait, the light-tempo can bug!).

After scanning:

Be very careful writing your sample meta data file. The first time you do a sample in a project you write in all the boxes of the meta file. Then, in the case of a time series of a fixed station, you will need to change the volume sampled (if the net changes) and the subpart (i.e., the fraction that has been scanned...16 if you have split the sample 4 times). Do not leave any boxes empty.

When you have written the sample meta file and pressed OK, Image J has finished. Your sample raw image + log.txt file + meta.txt file will be created in your project folder:
e.g., E:\Zooscan_largeframe2400\Zooscan_scan_raw

The log file gives information on the scanning method (parameters).

The meta file gives information on the sampling method (sampling site, sampling methodology, e.g., net size, volume...etc, and on the sampling preparation for the zooscan, e.g., pre-filtering and splitting rate).

The image will be treated when you process the scan with those of the day "Convert and process image in batch mode" (during the night). Anyway you have other options as scanning and processing one image or converting and then processing one image.

PROCESSING SAMPLES
Read section 9, pages 30-41, of Zooprocess_manual_v6.16.

(Recommended to launch the batch mode during the night)

If it is the first time that you process samples with your project, before doing it maybe you want to arrange the size limits of the organisms you want to measure. You can change the ESD thresholds (equivalent spherical diameter) of particles to be considered in the scan (0.3-4 mm by default which is good for the mesozooplankton bulk).

To change the configuration for processing scans, open ImageJ, click on Z as usual, select your project if you were in a different one the last time you used the program, and click on the option "Edit Configuration File". All the options will be displayed in a box. To know about these options (which I recommend to not change if you are not confident with the changes) *go to section 12.7, pages 85-88, of Zooprocess_manual_v6.16.*

Open Image J, click on Z icon and select "CONVERT PROCESS IMAGES in batch mode".

It is recommended to leave the configuration by default. If you tick the option "Save thumbnail images of organisms" the image process will take much longer. It might be faster to extract the vignettes afterwards with the option "Extract vignettes for plankton identifier"; or much faster with the option "Extract vignettes in folder according to prediction" once the objects have been automatically recognized by a created Learning set.

At the end of the sample processing you will obtain a new subfolder named as the sample and placed in Zooscan_scan_work\ of your project. In the subfolder you will have a new file which is the .pid file. The .PID FILE is a single file that concatenates the log.txt, the meta.txt, the processing functions applied and at the end the meas.txt which is the table containing all objects (rows) and their measurements (columns). The measurements that you might use to compute size for data analysis are Area, Major (longest axis of the object) and Minor (minor axis of a perfect ellipse of the same area of the object measured). Other measurements correspond to variables of shape and texture for automatic recognition, and of position in the tray. To see what each variable is, please check the "IJ_variables.txt" file.

CHECKING IMAGE QUALITY AND SEPARATING TOUCHING OBJECTS

Read sections 11 and at least 12.1, pages 59; 70-71, of Zooprocess_manual_v6.16

(Recommended to do it every morning on the batch launched during the previous night)

Every morning, after a night of processing in batch, you select on Zooprocess to "CHECK process by viewing segmented images". You select the first image of the batch you performed the previous night and you pass to the next one when you close it. If you want to finish you press the space bar (if any image stays opened on the screen, select the option "close all opened images" on the bottom of Z menu). The opened images are the _msk1.gif and they allow you to see if the background was well extracted from your image, i.e., no areas with many dots. You can also check on this image if the organisms are not aggregating.

If you have doubts on the quality of your image, to better check if organisms are well separated you can use the "view image with outlines" or also "view vignettes". These tools allow you to see if more than one object were considered as a single object by the system.

Whenever you are not satisfied with the manual separation that you performed on the scanning tray (many objects touching in the image), you can separate them by drawing lines between the touching objects. Select the option "Separation from B/W msk image". A line will cut the single object that was actually composed of two organisms (or more organisms, and in that case more lines to be drawn). When you have finished drawing lines, you press cancel and Zooprocess rewrites on your datatable of the .pid file to correct the modified objects. You can do the same using the "Separation using vignettes" option. We recommend leaving ticked the sort vignettes by decreasing surface as the conglomerates of organisms might create large objects. Then, if the organisms have already been recognized, you can also tick the second option to see vignettes by group (i.e., you see all the copepods to "clean them").

ZOOSCAN PROTOCOL FOR AUTO- & SEMIAUTOMATIC RECOGNITION

Read section 13, pages 91-98, of Zooprocess_manual_v6.16

Creating a first Learning set:

Learning set: Objects arranged in groups; it acts as reference to sort sample objects.
Programs used: ImageJ (Zooprocess) + Plankton Identifier.

Once you have some samples and you have checked their quality (perhaps you have also applied the separation mask). You are ready to build your first learning set that will help to automatically sort all the objects in the scanned samples.

1. Enter your project folder and go to "Pid_process" and into "Pid_results". COPY the .pid files that you want to use to build your Learning set (a representative subset of all your set, e.g., seasons represented…) and paste them in "Unsorted_vignettes_pid".

2. Open ImageJ and click on Z icon; then choose the menu "Extract vignettes for Plankton Identifier".

3. Leave "extract all vignettes" option. If the resolution of your images is not 2400 (we recommend 2400dpi though), please change Resolution to the one you have used. If not leave it at 2400 par default.

   The Gamma value can increase if you think the contrast of the vignettes is not enough (e.g., 1.2), but we usually leave it at 1.1 par default. Leave by default ticked boxes and press OK.

4. If you don't want to sort all objects (e.g, you prefer to create a learningset with subsets of many samples instead of all the objects of a few samples), you can click on the first option: Extract all vignettes and select "Random extraction of vignettes", (change resolution and gamma if necessary: see point 3) and click OK. Then choose the number of vignettes you would like to extract (e.g., 200 by sample, and so 200 raws of each pid table in the list). Click OK.

5. Your vignettes are now with the related .pid files in "Unsorted_vignettes_pid".

To be organized, please create a new folder inside the "Unsorted_vignettes_pid" and name it as "unsorted_date" to keep track of it. Then move all the vignettes and .pids there.

6. Your learning set will be built sorting all those vignettes in groups defined by you in "Pid process" "sorted vignettes". Go in sorted vignettes folder and create a new folder

(i.e., Learningset_date). Then, COPY all the pid files in this new folder. You need the pid files to build the table constituting the learning set!

7. Close Image J and open Plankton Identifier. Click on Learning. And select "Learningset_date" in sorted vignettes. The new window has the Learningset_date on the right (i.e., sorted thumbs). Click on the folders icon up on he right to create groups (i.e., categories as copepoda, cladocera, etc). Then, on the left (i.e., Unsorted thumbs) select your folder in "unsorted vignettes" (i.e., unsorted_date). Select vignettes (no more than 50 each time as because they are copied and not moved you could have windows memory problems) and move them to the group they belong to.

8. Once you have finished sorting ALL the vignettes, click on the icon on the right bottom, "create learning file". We recommend naming it as Learningset_date to keep track of it. Save it in the Learningset_date folder (notice that this file is a concatenation of all the files used to build it, and that a last column has been added with the recognition of each object). Job completed, continue sorting....Say No and click on Data Analysis.

9. Usually, this first Learning set is very crowded but not all groups are well represented. What we recommend is to create a subset of this learningset to be created in the "Learning_set" folder of Pid_process. We recommend to randomly sort 200 vignettes of each category. To do so, open Image J, Z and select "create subset of a learning set from identified vignettes (random)" option. Select your source folder which is the complete learning set created in the sorted_vignettes folder, and then you select to save the new subset on the "learning_set" folder. Select 200 vignettes per category, OK. The subset new folder is named by the datehour of creation and number of random vignettes.

10. Close Image J and open Plankton Identifier. Enter the Learning box to create a new learningset .pid concatenation. Select the Learnset1_random200 with its folders and original .pid files and create a learningset.txt. Click on learning and select the date_random_200 folder (it needs to have the .pid files of all the samples included in it to be accepted).

11. Before using the Learningset (subset), you can check its performance by testing the recognition on itself (i.e., cross validation). You click on Data Analysis on PkId. On the learning set box, select as Learning file your Learnset1_random200 in the "daterandom200"subfolder of "learning_set" folder of pid_process in your project, and on the left bottom of the main box select the method Cross-validation4 (Rndm tree). The method consists on one part (random) of the learning set recognizing another (2 folds), and this is repeated x times (5 trials in this case) to obtain strong statistical values. Once you have unticked some variables and created some other customised variables following what recommended at the IJ_variables.txt file you

launch the analysis that will produce a confusion matrix (true classification (rows) versus automatic classification (columns)).

You can click on "Start Analysis". Include in the name of the analysis the date to keep track. Select to SAVE RESULTS IN "Prediction" folder of PID_process folder of your project.
After analysis is completed, quit data analysis and click on show report, to then select the Analysis_name.txt you have created. There, clicking on cross-validation, you can see true classification (rows) versus automatic classification (columns).
The recall is the % of organisms belonging to a group that were automatically well recognised, whereas the 1-precision is the % of organisms classified by the algorithm as a group that they do not belong to (contamination in a group).

Validating object recognition and improving your Learning set:

1. Now, with the lerningset_date_subset we can recognize samples in the project (if you want to improve your learning set you can select samples that you think could implement it, i.e. other seasons, like summer to add a cladocera folder to the learning set, or special samples with rare groups). The scope is to do a pre-automatic sorting to then validate the recognition by resorting the vignettes manually. At the end of the process, we will have our final datasets, and if we want we can have some new vignettes to implement the Learning set.

We strongly recommend to spend very short time in implementing your learning set and to rather validate all your samples after automatic recognition.

In this procedure, automatic recognition is a mean to sort organisms faster. But human eye is who finally decides the classification.

2. In Plankton Identifier you click on Data Analysis and select on the left top box the Learning set (i.e., Learnset1_random200). Bellow, you select in Pid_results folder the samples .pid than you want to automatically recognize (recommended max 20-30 at a time to not have memory issues). Check the variables that will be used to classify the objects (you should have them as in the doc "IJ_variables.txt", if it's the first time you use PkId you will have to select the valiables as the list in the last line of the .txt file).

3. Select the SpvLearning4 (Random forest) method. TICK "save detailed results for each sample" option. A file will be created for each sample (if not it will give you just a concatenation of results in one single file!). SAVE RESULTS, as Analysis_yyyymmdd to keep track of the date, in the "Prediction" subfolder of your project's Pid_process folder.

Each Analysissamplename_dat1.txt file will be the table of objects in the .pid file with a last added column containing the automatic classification (Prediction) of each object (line). When PkId has finished you can close it.

In Prediction folder you can now find the Analysis_samplename_dat1.txt files of your samples. These are the original .pid files with an added last column in the data table which says the group predicted by your learningset (i.e., copepod).

4. Now, the samples have to be validated to create your final datasets, and if you want you can take some vignettes to implement the learning set (don't forget to also copy the related .pid files to the learningset folder).

5. Before validation! COPY the Analysis.txt files of the samples you are interested in from the "Prediction" folder to the root of "Pid_results".

6. To validate the automatic recognition of the selected samples, we extract the vignettes in the predicted groups: in ImageJ, Z select "extract vignettes in folders according to prediction"(zooprocess will read the last column and sort the objects' vignettes in the different groups).

The menu of this function allows you the random extraction of vignettes (as is the case of extract vignettes for PkId). You just need to select it in the select method box. This option will be ticked just to implement the Learning set, if not we extract all vignettes to validate the whole sample and obtain the definitive datasets. Leave the rest by default (only if your scans have been done with a resolution other than 2400 you need to change it in the vignettes) and press OK. Leave the name of the folder by default (date_hour_tovalidate).

If any of the samples has already been extracted, zooprocess will tell you. It helps to avoid using a sample twice to create a learning set and also to avoid validating the same sample more than once when you are creating your definitive dataset. The folder_tovalidate with the objects automatically classified is in sorted_vignettes in the Pid_process folder. The .txt used have been copied to Dat1_extracted in Pid_results.

7. Now, validate the samples. That is, check the automatic sorting and correct it when necessary. To accelerate this process, we recommend using XnView (free software). Instead of copying vignettes to one folder to another as PkId, it moves the vignettes and thus, you can move many more vignettes in one selection and no problems of windows memory are encountered. Yet, check well your work as you move vignettes and you don't have a reference folder as when working with PkId.

8. Open XnView and select the folder you want to validate (i.e., datehour_tovalidate). Go through each of the subfolders (groups) and check the vignettes. If classification is wrong move the vignette to the right folder (sometimes it will be necessary to create new folders that were not present in the learning set to classify your samples).

9. Once you have finished, close XnView and open Image J:Z. Select "Load identifications from sorted vignettes". The folder is in sorted_vignettes and you select the _tovalidate folder. Then, leave ticks par default. You could untick "Process detailed statistics" if the samples you have validated are not to implement the learningset but to create your definitive dataset. It's up to you. A results table is created if you left it ticked. In it you can see the performance of the automatic algorithm (random forest) by calculating the vignettes corrected and thus recall and 1-pred rates as well as the global error rate (N of vignettes moved).

10. The .txt files have been renamed by deleting the Analysis_ beginning of the name (final data name) and copied in the Dat1_validated of Pid_results. These new tables have a new last column which contains the true classification of each object.

11. Now in the folder "datehour_tovalidate" some .txt files have been added. A part from the statistics file, there is a .txt file per sample included in the vignettes' set. The .txt files without the "Analysis_date_" are the ones used to compute size spectra. These files have been automatically copied to Pid_results Dat1_validated. So each time you will perform the automatic recognition of your samples+validation by manual sorting, the new dat1.txt files created will be stored with the previous ones in Pid_results. Once your project is finished, you can take all of these data and compute abundance and size spectra to analyse.

12. To add new sorted vignettes to the old learning set, you just have to copy the vignettes in each group to the same group in the learning set. Do not forget to then add the .pid files of the last samples you have used to the completed learningset (in the main root of the learning set to be able to compute the new learningset table). Then you just have to load the new learning set in PkId Learning and create the learningset.txt.

We recommend that you re-do step 8 of the previous section (you obtain a new learningset with 200 vignettes for each category, but now some rare categories will be fuller and maybe you have been able to create new categories during the process).

While with automatic recognition we try to recognize very fast a few well distinguished groups. When we validate data, we can add new groups or separate vignettes of a group in more specific ones (e.g., copepod transformed in three groups: cop_calanoid, cop_oithona, cop_oncaea). Do not create new subfolders in the original single folder (e.g.,

calanus and temora folders inside copepod forder NO), but create parallel new folder and then move the corresponding vignettes to those.

Finally, we will treat the data samplename_a_1_dat1.txt (which have the two columns of recognition), stored in Pid_results.

COMPUTING AND ANALYZING SIZE SPECTRA (some tips)

Datasets are in the form of a table in the "dat1.txt" files. We can provide you with matlab scripts to read these data and to compute the size spectra, calculate abundance and to calculate some variables on the spectra. If you do not want to use the matlab scripts, you can do your calculations with excel. You just import your data in excel and select the ";" separator to recognize the columns of the table.

Converting pixels to milimeters

You need the "Resolution" in the [Info] field of the first part of the _dat1.txt. The resolution is used to calculate the dimension of 1 pixel as follows:

Milimeter/1pixel=25.4/Resol*1000)*10^{-3} (if Resol=2400; 10.5833 microns/pixel);

So the values of "Area" column have to be transformed by multiplying it (e.g. for 2400 resolution: Area*10.5833^2 (because the area is in 2 D), and Major=Major*10.5833.

Calculating sampled abundance/m^3 from abundance in the scanning tray

You need to know the volume sampled with the net and the splitting ratio (subpart scanned) to calculate the abundance/m^3. You will calculate the real abundance as follows:

N = Number of raws with same prediction (e.g., in last column written "copepod").
Subpart = splitting ratio.
Vol = net volume.
Townb = number of net tows in a sample.

N of organisms/m^3= N*Subpart/(Vol*Townb);

You can calculate the abundance of each of your groups by just sorting your organisms by their classification in the last column of your data table.

Calculating ESD (equivalent spherical diameter) and Ellipsoidal Biovolume

From the Area, Major and Minor parameters we can compute the Spherical (SBv) and ellipsoidal biovolume (EBv) with the following equations:

$SBv = 4/3\ \pi\ (Area / \pi)^{3/4}$
$EBv = 4/3\ \pi\ (Mayor / 2)\ (Minor / 2)^2$

Creating the size spectra

Size spectra are just histograms computed on size classes. To create your spectrum you need to define your size classes and then sort the organisms (all, or of each group) by their size (ESD or ellipsoidal volume). You can just sort them (i.e., you add the body volume of each organism to the size class in which this body volume falls).

It is better to have size classes of geometrical-scale (each size class is wider than the previous one) than equal size classes (all size classes have he same width). Larger organisms are less abundant and have larger mean size; therefore we need wider size classes to better represent their size distribution. In particle size-spectrum analysis the use of the octaves-scale (a geometric 2^n series) has been applied since first description of particles-size distribution in the ocean. This scale allows size classes to be defined by the entire base of the logarithmical scale, and the amplitude of the bin is the same as its low limit.

In the matlab scripts we provide you with, size classes have an scale of $k=2^{1/4}$ with the lowest and largest size limit:

smin = 0.001; lower limit of the biovolume spectra that will be calculated
smax = 10000; upper limit of the biovolume spectra that will be calculated

(in this case 94 size classes to characterize the whole zooplankton spectrum)

Size classes are defined by their average size = (maxLim-minLim)/2.

Once you have computed your spectra, you need to multiply the value in each size class by the conversion factor we used to compute abundance/m^3:

spectrum*Subpart/(Vol*Townb);

At this step, the spectrum units are mm^3/m^3.
If you have more than one image per sample (d1 and d2 fractions). After converting the spectra you can add them together.

Spectra are then normalised by dividing the biovolume in each size class by the width of each size class. Finally, spectra are converted to logarithmical scale to obtain a linear spectrum.

Units are on the *y*-axis in log (mm^3 m^{-3} mm^{-3}) and the *x*-axis shows individual biovolume in log(mm^3).

Computing some parameters to describe the spectra

Spectra can be represented by the slope of their linear regression (of the whole spectrum or from their mode):

Y=bx+a

In which b is the slope.

The slope can be computed in the whole spectrum or from the mode of it (size classes with the maximum biovolume). The average mode for a study is computed as the mode frequency of the modes of all your spectra of your project. This mode is due to net sampling underestimation of small organisms of similar ESD or a bit higher than the net mesh.

The Shannon index on the size classes (size diversity) can also be used as an indicator:

Vi=vol in each size class;
Vol= Vol total spectrum;
pi=Vi/Vol;

$$H' = \sum_{i}^{S} p_i \log_2 p_i$$

The slope is around –1. The more negative the slope is (and the lower the Sh index is) it indicates that the spectra has a higher proportion of small organisms (and viceversa).

You could also calculate an abundance spectrum (number of organisms instead of volume in each size class) and then cut the spectra to observe the abundance changes in the smallest and largest size classes.

Appendix III

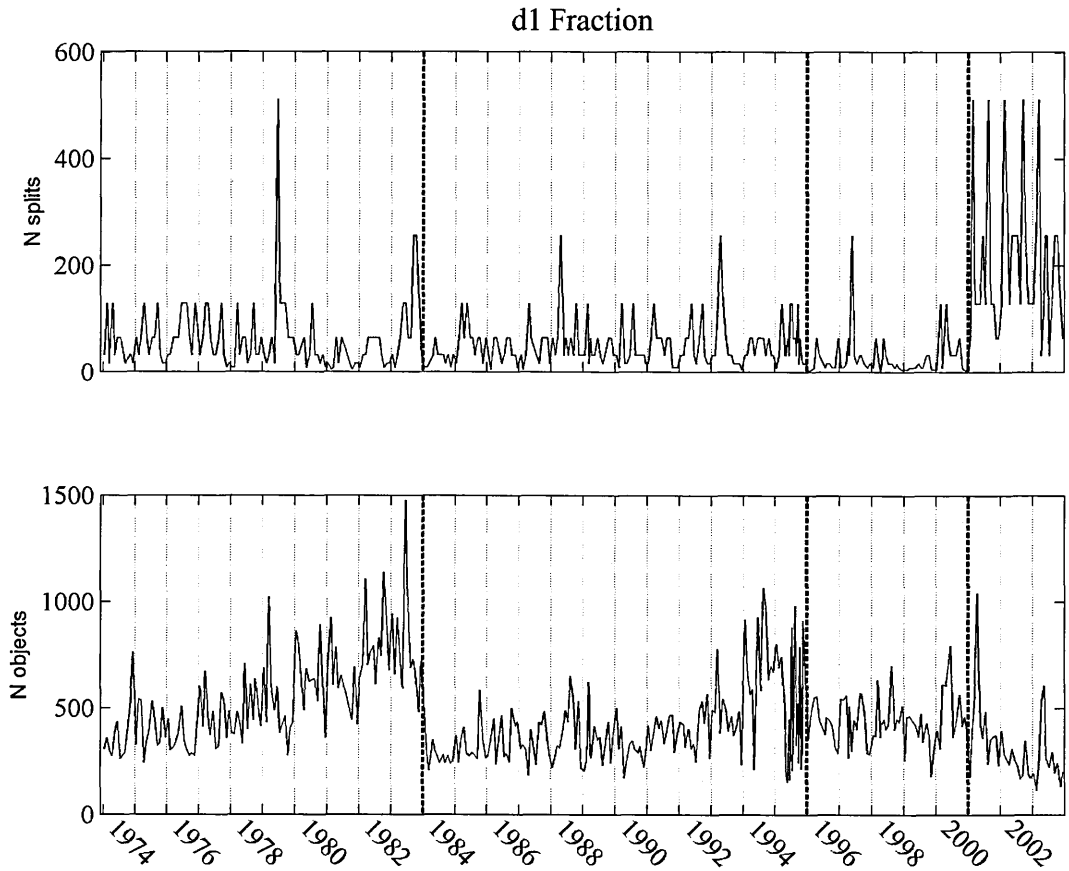

Figure 1 - Point B time series of d1-fraction sampling (objects>500μm). In the upper panel, number of splits performed with the Motoda box (dilution rate). In the lower panel, number of objects retained for scanning after splitting. Dashed lines correspond to change in operator processing the samples.

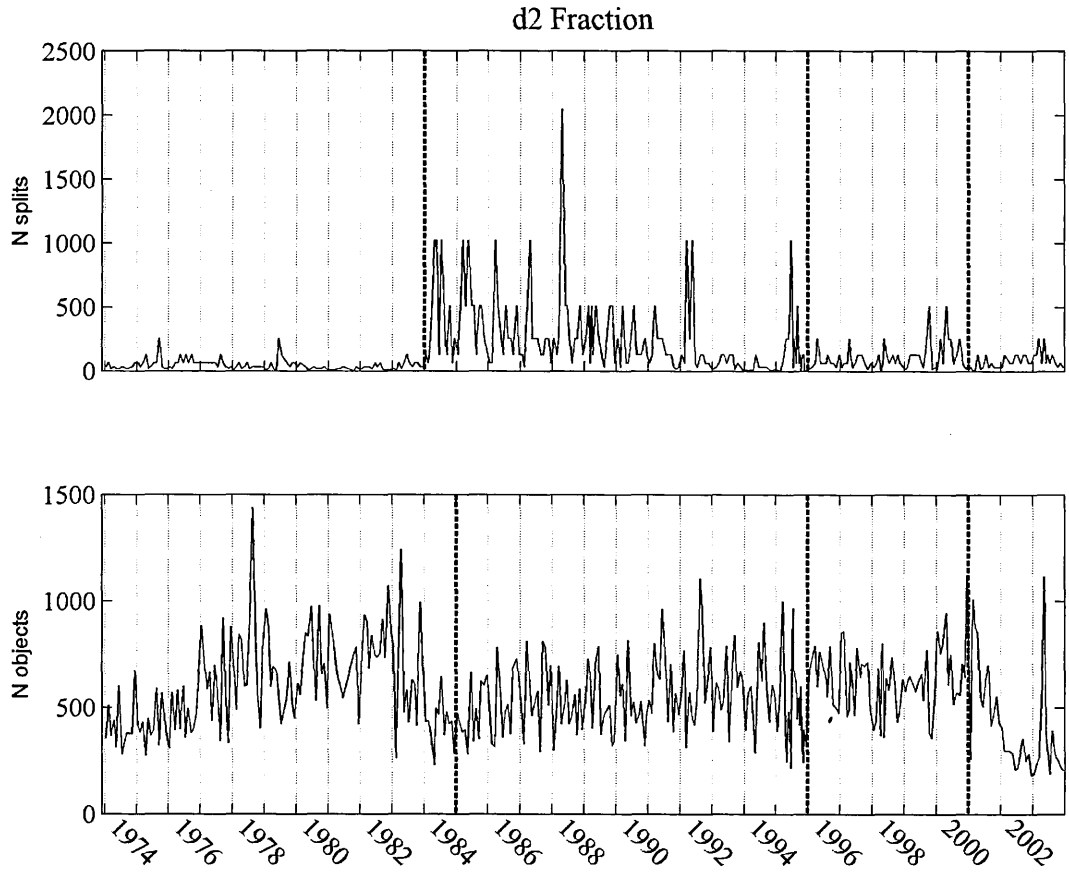

Figure 2 - Point B time series of d2-fraction sampling (objects<500μm). In the upper panel, number of splits performed with the Motoda box (dilution rate). In the lower panel, number of objects retained for scanning after splitting. Dashed lines correspond to change in operator processing the samples.

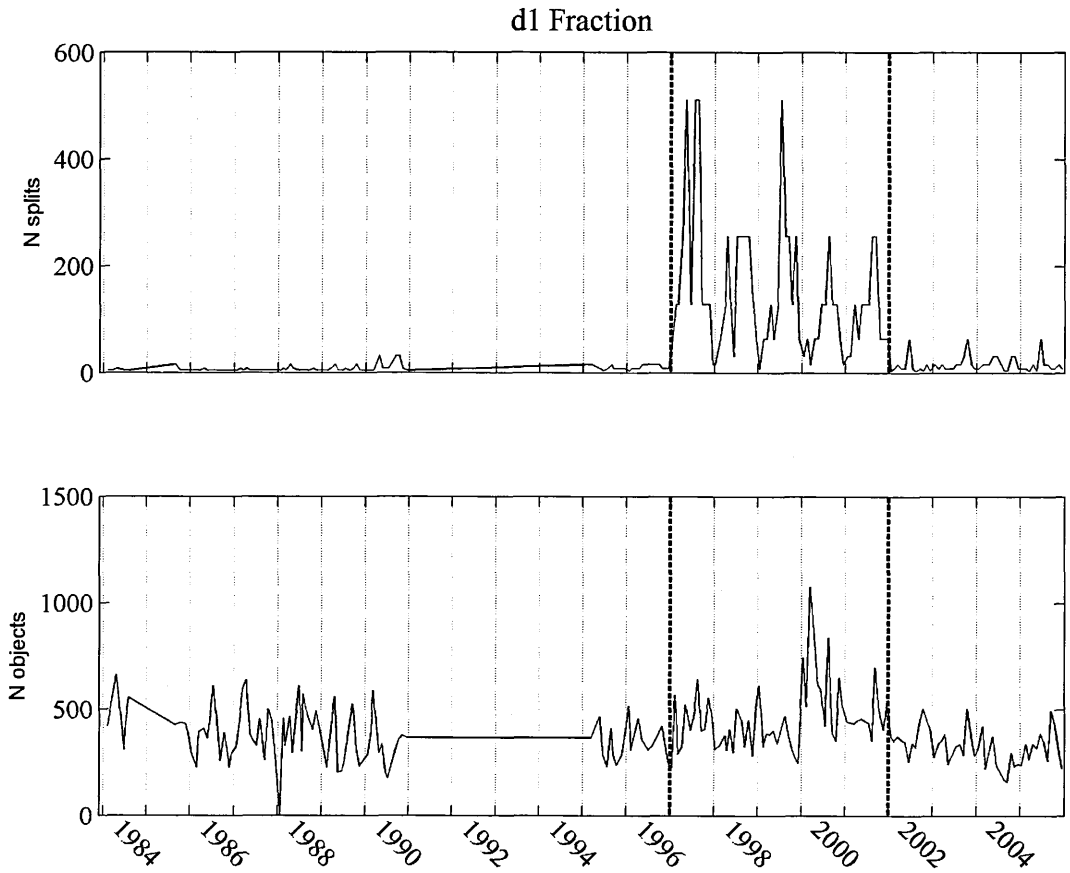

Figure 4 - Stn MC time series of d1-fraction sampling (objects>500µm). In the upper panel, number of splits performed with the Motoda box (dilution rate). In the lower panel, number of objects retained for scanning after splitting. Dashed lines correspond to change in operator processing the samples. The first and third periods where performed by the same operator.

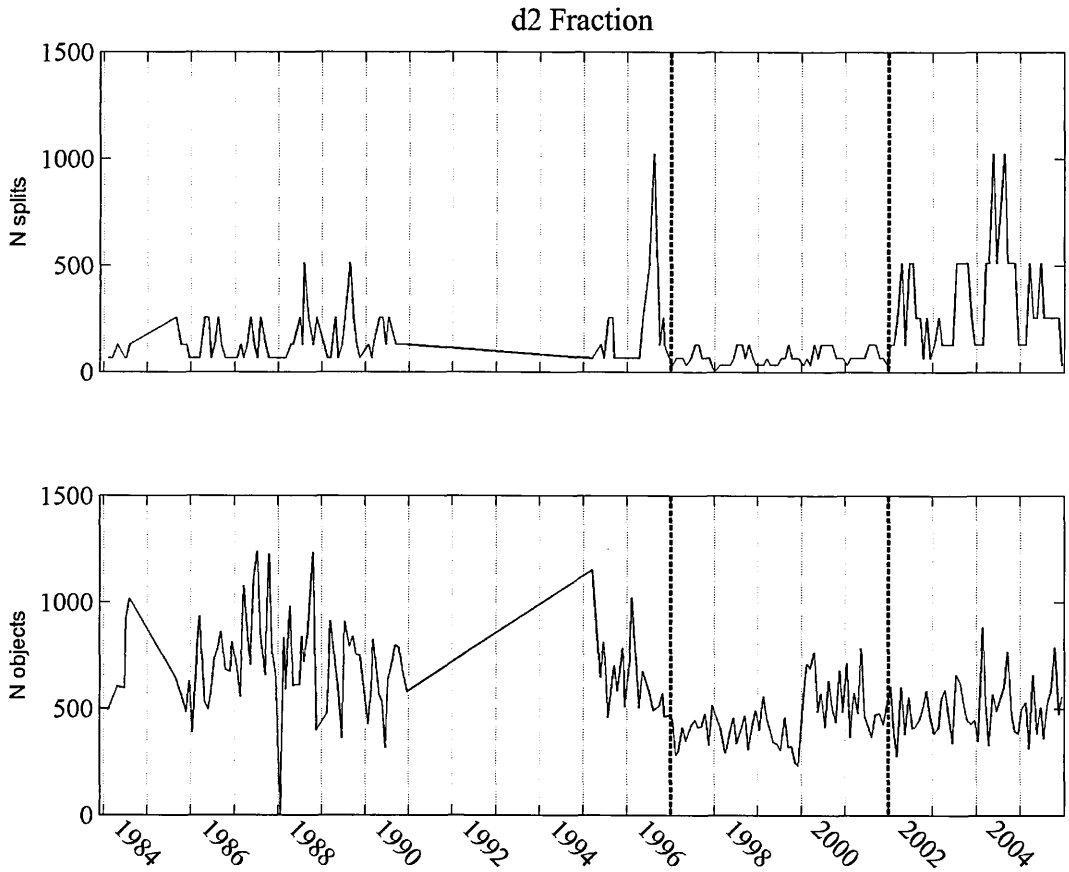

Figure 5 - Stn MC time series of d2-fraction sampling (objects<500µm). In the upper panel, number of splits performed with the Motoda box (dilution rate). In the lower panel, number of objects retained for scanning after splitting. Dashed lines correspond to change in operator processing the samples. The first and third periods where performed by the same operator.

Appendix IV

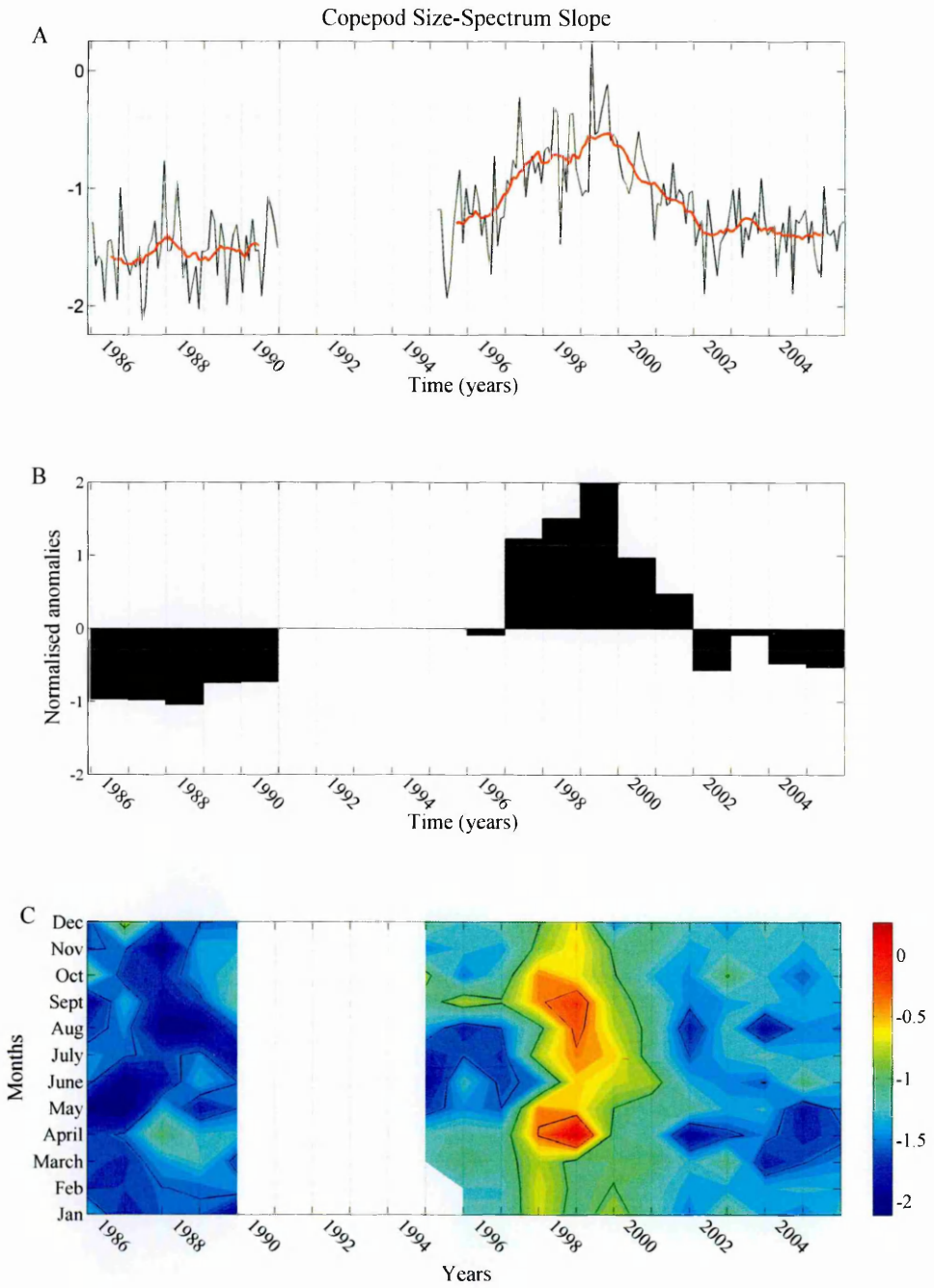

Figure 1 - Copepod size-spectrum slope at stn MC. In panel A, the monthly time series (black line) and an annual (i.e., 12 points window) moving average to smooth the seasonal signal (red line). Panel B represents the annual normalised anomalies. Panel C represents the seasonality of size-spectrum slope.

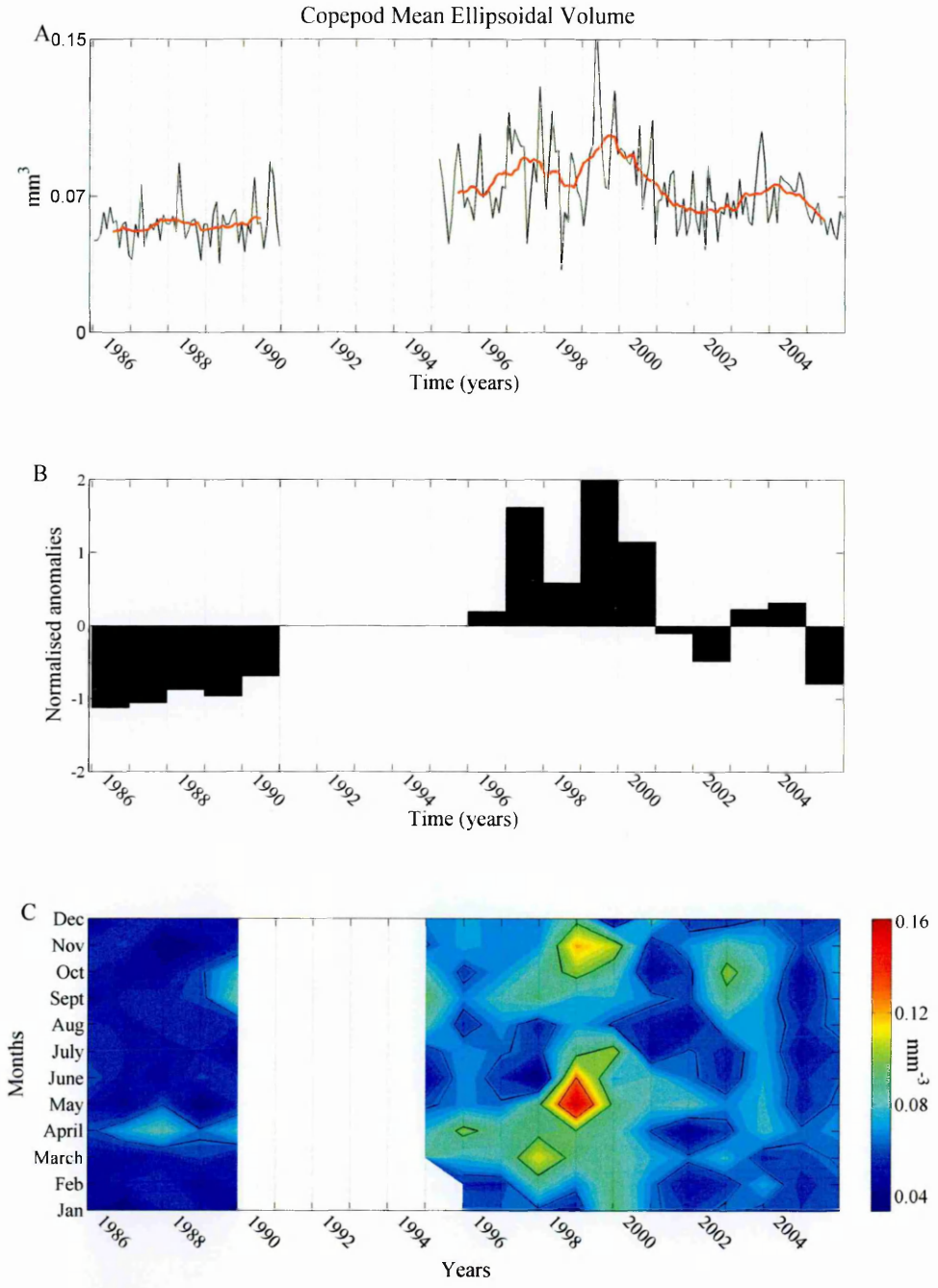

Figure 2 - Copepod mean biovolume at stn MC. In panel A, the monthly time series (black line) and an annual (i.e., 12 points window) moving average to smooth the seasonal signal (red line). Panel B represents the annual normalised anomalies. Panel C represents the seasonality of copepod mean biovolume.

Appendix V

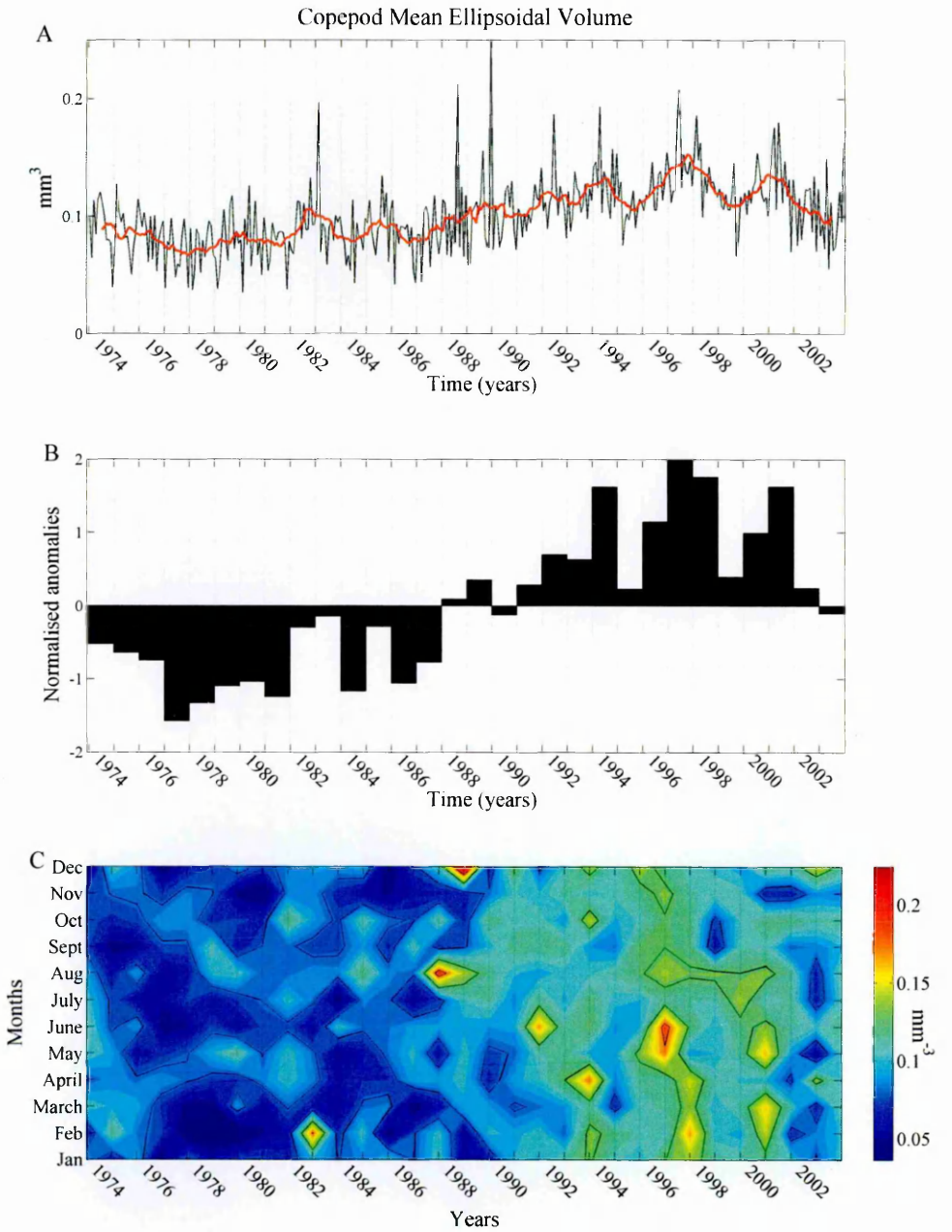

Figure 1 – Copepod mean body volume at Point B. A) Monthly time series (black line) and an annual (i.e., 12 points window) moving average to smooth the seasonal signal (red line); B) annual normalised anomalies; C) seasonal and interannual variability.

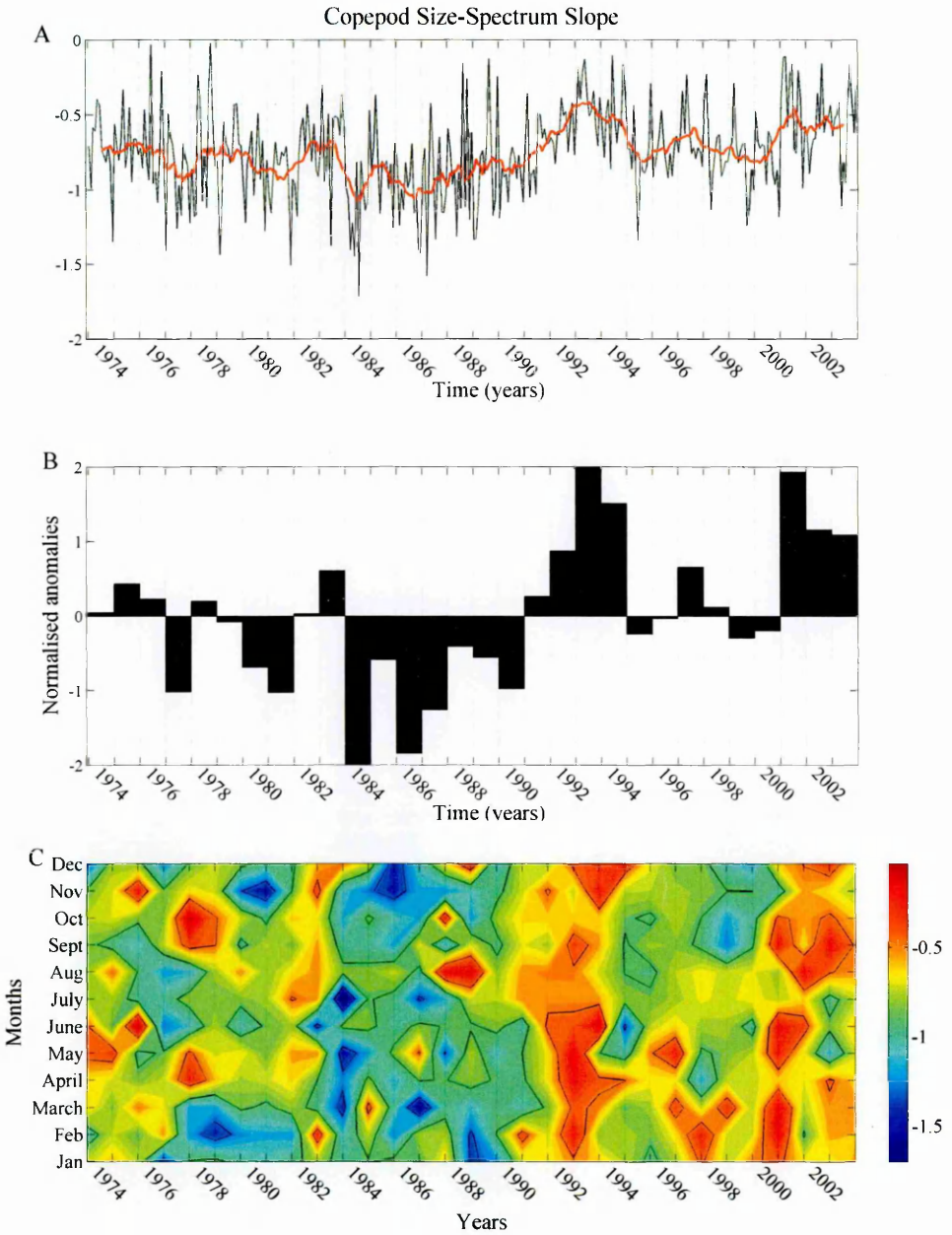

Figure 2 – Copepod size-spectrum slope at Point B. A) Monthly time series (black line) and an annual (i.e., 12 points window) moving average to smooth the seasonal signal (red line); B) annual normalised anomalies; C) seasonal and interannual variability.